University of California
Santa Barbara

Quantum Criticality and Non-locality: A Field Theoretical Study

A dissertation submitted in partial satisfaction
of the requirements for the degree

Doctor of Philosophy
in
Physics

by

Yichen Xu

Committee in charge:

Professor Cenke Xu, Chair
Professor Matthew Fisher
Professor Mark Sherwin

June 2023

The Dissertation of Yichen Xu is approved.

Professor Matthew Fisher

Professor Mark Sherwin

Professor Cenke Xu, Committee Chair

June 2023

Quantum Criticality and Non-locality: A Field Theoretical Study

by

Yichen Xu

To my parents

Acknowledgements

I would like to express my heartfelt gratitude to the countless individuals who have contributed to my journey, as I stand on the threshold of completing my PhD thesis. The passage of time has been nothing short of astonishing, whisking me away on a whirlwind of growth, discovery, and profound experiences.

Amidst the rapid pace at which moments have unfolded, memories have piled up like treasures, each one etching a lasting impression in the tapestry of my academic pursuit. From the very first day I set foot on the breathtakingly beautiful campus of UCSB, I was captivated by its serene charm and enchanting vistas. The scenic surroundings have served as a constant source of inspiration, fueling my determination to delve deeper into the realms of physics. Within the physics department, I have been fortunate to find an academic environment brimming with intellect, passion, and collaboration. The exceptional faculty members, whose expertise knows no bounds, have been instrumental in shaping my research path and fostering an unwavering commitment to scientific inquiry.

I am profoundly grateful for the guidance and support of my advisor, Prof. Cenke Xu, throughout the past four and a half years. It is with immense appreciation that I reflect on his pivotal role in introducing me to the captivating field of condensed matter theory, effortlessly navigating me through abstract concepts and mesmerizing theories. Under his tutelage, I have been fortunate to witness a mind with boundless creativity as he continually unveils inspiring research topics. In moments when I found myself entangled in the labyrinth of complicated analytical derivations, Feynman diagrams, or numerical calculations, Prof. Xu always emerged as a guiding light, leading me towards clarity by reminding me of our ultimate goal within the broader tapestry of physics. His ability to illuminate the bigger picture and infuse purpose into my scientific endeavors has been invaluable. Furthermore, I express my sincere gratitude to Prof. Xu for his

generous financial and mental support, which has been especially meaningful during the challenging times of the COVID-19 pandemic, allowing me to focus wholeheartedly on my research. It is with deep respect and admiration that I acknowledge Prof. Cenke Xu's profound impact on my academic journey. His mentorship, intellectual guidance, and belief in my potential have left an indelible mark on my scientific growth and personal development. I consider myself incredibly fortunate to have had the privilege of working under his guidance, and I am confident that the lessons learned and the insights gained will continue to shape my future career in physics.

I extend my heartfelt appreciation to Prof. Matthew P. A. Fisher and Prof. Mark Sherwin for being members of my advising committee. Their constant support, guidance, and diverse perspectives, encompassing quantum information theory and experimental research, have left their imprint on me as a physicist. Their consistent feedback and check-ins have ensured my progress through the PhD program.

I will always cherish the invaluable time I spent with Prof. Chao-Ming Jian of Cornell University during his tenure as a postdoc at UCSB. When I initially joined Prof. Xu's group in 2019, my understanding of the concepts and methodologies in condensed matter theory was limited. Chao-Ming's extensive knowledge and expertise played a pivotal role in jump-starting my involvement in numerous research projects. His unique perspective on physics and his ability to explain complex ideas with clarity and ease have been instrumental in my academic growth. I would also like to thank his support in my postdoc applications in such a highly competitive year.

I am immensely grateful for the incredible privilege of collaborating with the other members of Prof. Xu's group, as well as the vibrant community within the physics department and the Kavli Institute for Theoretical Physics (KITP). I would like to express my gratitude to my former group-mate and dear friend, Dr. Xiao-Chuan Wu, whose support and collaboration have been invaluable throughout our four years together in

Prof. Xu's group. Beyond our research endeavors, Xiao-Chuan has provided crucial mental support for me to recover from the hardness of my personal relationship, and his mentorship has greatly influenced my career aspirations as a physicist. Additionally, I have had the pleasure of fruitful collaborations with Dr. Zhu-Xi Luo, Dr. Mengxing Ye, and Dr. Kasra Hejazi. In particular, Zhu-Xi had always impressed me with her remarkable proficiency in carrying out complex calculations and theoretical arguments, and also provided me with indispensable support during my postdoc applications. Their contributions have enriched my research journey and broadened my understanding of physics. I also enjoyed discussions with my current group-mates Kaixiang Su and Nayan Myerson-Jain, and other current or former members of the theoretical physics community at UCSB, including Chun-Xiao Liu, Zhehao Zhang, Adolfo Holguin, Sean McBride, Jiu-Ci Xu, Shang Liu, Wenjie Ji, Ryan Lanzetta, Yi-Hsien Du, Umang Mehta, Jong Yeon Lee, Alex Meiburg, Zhenhao Song and many more. Sorry if I have missed a few names!

I would also like to extend my gratitude to my long-time friend, both within and beyond physics, Dr. Haoyu Guo. The time we spent together in 2022, when he served as a graduate fellow at KITP, hold a special place in my heart. Oh right, we are becoming colleagues soon at Cornell!

I thank Prof. Zhen Bi, Dr. Jian-Hao Zhang and Prof. Chong Wang for discussion and collaboration when they visited KITP during the program, "A Quantum Universe in a Crystal: Symmetry and Topology across the Correlation Spectrum". That was a lot of fun to be part of the fascinating project that they have just started.

In addition to my pursuit of physics, I want to express my appreciation to Prof. Robert Koenig from the Department of Music at UCSB. Prof. Koenig's guidance and expertise in piano techniques and collaborative skills have been invaluable during my involvement in the chamber music program. His mentorship not only enhanced my musical abilities but also provided opportunities for me to collaborate with exceptionally talented

musicians within the music department and perform at the Karl Geiringer Hall. I would also like to thank the members of the UCSB Cycling Team, whose shared experiences have been a source of immense joy and respite from the demands of study and research. The countless hours spent riding and racing together have not only invigorated my spirit but have also allowed me to explore the captivating city of Santa Barbara in its entirety.

Finally, I wish to express my deepest gratitude to my parents, Hongqin Xu and Yongqing Li, for their unwavering love and support. Despite the challenges posed by the COVID-19 pandemic and the inability to meet in person for nearly four years, I have felt their presence across the Pacific Ocean and their encouragement through numerous video chats. Their boundless love and understanding have been a source of strength, guiding me through the ups and downs of my academic journey. I acknowledge their sacrifices and the profound impact they have had on my personal and academic growth. Their endless mental and financial support remains an invaluable gift that I treasure deeply. With great respect, I dedicate this thesis to them.

Curriculum Vitæ

Yichen Xu

Education

2023	Ph.D. in Physics (Expected), University of California, Santa Barbara.
2021	M.A. in Physics, University of California, Santa Barbara.
2018	B.Sc. in Physics with honorary rank, University of Science and Technology of China

Publications

1. Yichen Xu, Xiao-Chuan Wu, Mengxing Ye, Zhu-Xi Luo, Chao-Ming Jian, and Cenke Xu. Interaction-driven metal-insulator transition with charge fractionalization. *Physical Review X*, 12(2):021067, 2022
2. Yichen Xu, Xiao-Chuan Wu, and Cenke Xu. Deconfined quantum critical point with nonlocality. *Phys. Rev. B*, 106:155131, Oct 2022
3. Xiao-Chuan Wu, Yichen Xu, Mengxing Ye, Zhu-Xi Luo, and Cenke Xu. A construction of exotic metallic states. In *A Festschrift in Honor of the CN Yang Centenary: Scientific Papers*, pages 517–533. World Scientific, 2022
4. Yichen Xu and Cenke Xu. Green's function zero and symmetric mass generation. *arXiv preprint arXiv:2103.15865*, 2021
5. Chao-Ming Jian, Xiao-Chuan Wu, Yichen Xu, and Cenke Xu. Physics of symmetry protected topological phases involving higher symmetries and its applications. *Physical Review B*, 103(6):064426, 2021
6. Chao-Ming Jian, Yichen Xu, Xiao-Chuan Wu, and Cenke Xu. Continuous néel-vbs quantum phase transition in non-local one-dimensional systems with $so(3)$ symmetry. *SciPost Physics*, 10(2):033, 2021
7. Yichen Xu, Hao Geng, Xiao-Chuan Wu, Chao-Ming Jian, and Cenke Xu. Non-landau quantum phase transitions and nearly-marginal non-fermi liquid. *Journal of Statistical Mechanics: Theory and Experiment*, 2020(7):073102, 2020
8. Yichen Xu, Xiao-Chuan Wu, Chao-Ming Jian, and Cenke Xu. Orbital order and possible non-fermi liquid in moiré systems. *Physical Review B*, 101(20):205426, 2020
9. Yichen Xu, Xiao-Chuan Wu, Chao-Ming Jian, and Cenke Xu. Topological edge and interface states at bulk disorder-to-order quantum critical points. *Physical Review B*, 101(18):184419, 2020
10. Xiao-Chuan Wu, Yichen Xu, Hao Geng, Chao-Ming Jian, and Cenke Xu. Boundary criticality of topological quantum phase transitions in two-dimensional systems. *Physical Review B*, 101(17):174406, 2020

11. Xiao-Chuan Wu, Yichen Xu, Chao-Ming Jian, and Cenke Xu. Interacting valley chern insulator and its topological imprint on moiré superconductors. *Physical Review B*, 100(15):155138, 2019

Abstract

Quantum Criticality and Non-locality: A Field Theoretical Study

by

Yichen Xu

Quantum field theory(QFT), although initially developed nearly a century ago to describe interactions between elementary particles, has proven to be a powerful tool in condensed matter systems, where there are naturally huge collections of degrees of freedom. It enables one to describe collective excitations, such as phonons and magnons, understand phase transitions, predict transport properties, and more recently, study topological phases. After a survey of QFT methodology in modern theoretical condensed matter physics in Chapter 1, the dissertation covers four sets of exotic scenarios to which quantum field theoretical methods can be applied:

In Chapter 2, we study boundary properties of several exotic quantum criticalities, including phase transition between symmetry protected topological(SPT) state, topologically orders and states with spontaneous symmetry breaking. Renormalization group(RG) studies show that in each case the bulk criticality can possibly give rise to new boundary phases and phase transitions.

In Chapter 3, we discuss quantum phase transitions beyond Landau's paradigm and its interaction with Fermi surfaces. In particular, we constructed their underlying field theories that can be studied using controlled perturbative RG approach. We found interesting new fixed points with non-fermi liquid(NFL) behaviors and unusual dynamical critical exponent.

In Chapter 4, field theoretical methods are applied to study strongly correlated physics in Moiré materials, namely, various orbital orders, Chern insulators and NFLs. We also

propose new mechanisms for interaction driven metal-to-insulator transitions in transition metal dichalcogenides(TMD) Moiré bilayers that can explain its large critical resistivity.

And finally in Chapter 5, we study an "avoided" phase transition between a trivially gapped fermionic state and an interaction trivialized fermionic SPT state. We point out that the latter state can still be distinguished from the former one by zeroes of its Green's function.

Contents

Chapter 1

Introduction

1.1 From Lattices to Fields: The Entry of Quantum Field Theory in Condensed Matter

Quantum field theory (QFT), initially developed almost a century ago in the 1920s and 30s, has been highly successful in describing the behavior of subatomic elementary particles and their interactions. These developments have ultimately led to the Standard Model of particle physics, which contains both the building blocks of matter, i.e. quarks and leptons, and also the mechanism of their interaction through gauge bosons. Nevertheless, the past few decades have seen QFT making a major inroad into theoretical studies of condensed matter. Given their huge numbers of microscopic particles, usually of order 10^{23}, condensed matters provide an ideal playground for QFT: Instead of performing extremely time-consuming quantum mechanical calculations for individual particles, we can instead regard the constituent particles as local degrees of freedom of a quantum field, while their interactions can also be translated into interactions between fields. This viewpoint facilitates our theoretical treatment of condensed matter systems,

especially at low temperatures and with strong interactions.

The modern-day application of QFT in condensed matter can be roughly summarized as follows:

1. Describe collective excitations or quasiparticles that arise in condensed matter systems. This includes phonons, magnons, and also electron modes in metals.

2. Predict transport properties of condensed matter systems, such as electrical conductivity and thermal conductivity. These properties can be calculated using field theoretical techniques such as the Kubo formula, which relates transport coefficients to correlation functions of the excitations due to the applied external fields.

3. Study topological phases of matter, which are usually characterized by nontrivial topological invariants that cannot be changed by local perturbations. These phases can be described by field theoretical models such as the Chern-Simons theory. QFT is also able to link topological invariants to the behavior of the excitations at the edge of the material.

4. Understand phase transitions and critical phenomena in condensed matter systems, such as the transition from a liquid to a solid or from a ferromagnetic to a paramagnetic state. In QFT, phase transitions can be understood as a change in the symmetry of the underlying field theory, which can lead to the appearance of new quasiparticles or the breakdown of existing ones. For a condensed matter system at criticality, QFT methods help one calculate the critical exponents.

In the rest of this section, we will demonstrate how QFT methods can be used to describe microscopic models of condensed matter and their phase transitions. We will also touch on the topology in QFT from a condensed matter point of view, which gives rise to exotic phase transitions that do not have classical counterparts.

1.1.1 Landau-Ginzburg Theory: A View From Field Theory

Statistical mechanics tells us that most of the macroscopic properties of a system can be calculated once we obtain the partition function. For models of condensed matter, which usually contain various degrees of freedom on lattices, this amounts to summing over all possible local configurations of the system (or in a quantum model, tracing over local Hilbert spaces). However, if the correlation length of the system, ξ, is much larger than the lattice spacing a, it is then possible to approximately describe all the degrees of freedom using a continuous field. The partition function will thus become a functional integral (or functional path integral) of this field.

To achieve a faithful description of the system using fields, one needs to identify the order parameter $\phi(\mathbf{x})$ of the system. In plain language, the order parameter $\phi(\mathbf{x})$ at some spatial position should look like some local degrees of freedom on the lattice. More precisely, if the system has certain global symmetries G, like $\mathbb{Z}_2$ or $SO(n)$ symmetry for various spin models, the field $\phi(\mathbf{x})$ should transform under the same representation of the group G as the lattice degrees of freedom. After that, one can write down the **Landau-Ginzburg (LG) theory**, which reflects the energy, and thus the statistical weight, of a certain field configuration of $\phi(\mathbf{x})$. In doing so, we obtain the partition functional

$$\mathcal{Z} = \int \mathcal{D}[\phi(\mathbf{x})] e^{-S[\phi(\mathbf{x}),\{g\}]} \tag{1.1}$$

and the LG action has the form

$$S[\phi(\mathbf{x}),\{g\}] = \int d^d\mathbf{x} (\partial_\mu \phi(\mathbf{x}))^2 + g_1\phi(\mathbf{x}) + g_2\phi^2(\mathbf{x}) + \dots \tag{1.2}$$

Here, d is the dimension of space and $\{g\} = \{g_1, g_2, \dots\}$ represents the set of coupling constants that reflect the various physical conditions of the system, such as temperature

or pressure. Some of the coupling constants can be argued to vanish to preserve the symmetry of the system. For example, if the system has an Ising symmetry that acts as $\phi(\mathbf{x}) \to -\phi(\mathbf{x})$, all the odd power terms of $\phi(\mathbf{x})$ should vanish. In other words, only terms that are invariant under G action can appear in the LG action.

Let us showcase the logic above using the example of classical Heisenberg model in d dimensions. The Hamiltonian of the model is given by

$$H = -J \sum_{\langle i,j \rangle} \mathbf{S}_i \cdot \mathbf{S}_j \tag{1.3}$$

where J is the coupling constant between nearest neighbor sites i and j, multiplied by $1/(k_B T)$ in the exponent of the partition function. $\mathbf{S}_i$ are classical $O(3)$ spins on a d-dimensional hypercubic lattice that satisfies $\mathbf{S}_i^2 = 1$, and S is the classical spin. The partition function is thus

$$\mathcal{Z} = \int \prod_i D\mathbf{S}_i \; e^{J \sum_{\langle i,j \rangle} \mathbf{S}_i \cdot \mathbf{S}_j} \tag{1.4}$$

The integral measure of the spins is $D\mathbf{S}_i \equiv d^3\mathbf{S}_i \; \delta(\mathbf{S}_i^2 - 1)$. We now introduce the **Hubbard-Stratonovich transformation** to decouple the Hamiltonian:

$$\mathcal{Z} = \int \prod_i D\mathbf{S}_i d\mathbf{\Phi_i} \; e^{-\frac{1}{4J} \sum_{\langle i,j \rangle} \mathbf{\Phi}_i \cdot \mathbf{\Phi}_j + \sum_i \mathbf{\Phi}_i \cdot \mathbf{S}_i} = \int \prod_i d\mathbf{\Phi_i} \; e^{-\frac{1}{4J} \sum_{\langle i,j \rangle} \mathbf{\Phi}_i \cdot \mathbf{\Phi}_j - \sum_i V(\mathbf{\Phi}_i)} \tag{1.5}$$

Here we introduced an auxiliary vector $\mathbf{\Phi}_i$ on each lattice site that is not restricted to a unit sphere in 3D. Nevertheless, in order to still preserve $O(3)$ symmetry, Φ_i needs to transform under $O(3)$ in the same way as $\mathbf{S}_i$. In the final equivalence, $D\mathbf{S}_i$ has been formally carried out, and we are left with an on-site effective potential $V(\mathbf{\Phi}_i)$. One can further perform a Fourier transformation to diagonalize the exponent:

$$H_{\text{eff}}(\mathbf{\Phi}) = \frac{1}{4J}\sum_{\langle i,j\rangle}\mathbf{\Phi}_i\cdot\mathbf{\Phi}_j + \sum_i V(\mathbf{\Phi}_i) = \frac{1}{J}\sum_{\mathbf{k}}\left(\sum_{\mu=1}^{d}\cos(ak_\mu)\right)\mathbf{\Phi}(\mathbf{k})\cdot\mathbf{\Phi}(-\mathbf{k}) + \tilde{V}(\mathbf{\Phi}(\mathbf{k})) \tag{1.6}$$

Here, $\tilde{V}(\mathbf{\Phi}(\mathbf{k}))$ consists of the Fourier transformation of the terms in $V(\mathbf{\Phi}_i)$. Now comes the important step towards field theory: one assumes that the spatial variation of $\{\mathbf{S}_i\}$ is much slower compared to the lattice scale, i.e., the correlation length ξ is much larger than the lattice constant a. It is then possible to take the continuum limit of $\mathbf{k}$ and focus on the small $\mathbf{k}$ part of the theory. Keeping the expansion of $\cos(ak_\mu)$ up to the quadratic order, taking the continuum limit of momentum and Fourier transforming the whole theory back to coordinate space, we arrive at (1.2) with the vector order parameter $\mathbf{\Phi}$.

1.1.2 Phase Transitions in Landau Paradigm

From the perspective of Landau-Ginzburg (LG) theory, a phase transition between a G-ordered and disordered phase can be characterized by the expectation value $\langle\phi(\mathbf{x})\rangle$ and its correlation function $\langle\phi(0)\phi(\mathbf{x})\rangle$. In the disordered phase, $\langle\phi(\mathbf{x})\rangle = 0$, and the correlation function exhibits short-ranged behavior with exponential decay as a function of distance: $\langle\phi(0)\phi(\mathbf{x})\rangle \sim e^{-\frac{|\mathbf{x}|}{\xi}}$, where ξ is the correlation length. In the ordered phase, $\langle\phi(\mathbf{x})\rangle \neq 0$, and the correlation function displays long-range behavior, approaching a constant value even as $|\mathbf{x}| \to \infty$. By tuning the parameters g_i from the disordered phase, the system reaches criticality when $\langle\phi(\mathbf{x})\rangle$ is on the verge of becoming nonzero, or when the correlation length ξ diverges. The divergence behavior can be described by $\xi \sim |g - g_*|^{-\nu}$ for a single tuning parameter g. For most common types of phase transitions, the correlation function decays algebraically at the critical point, following

a power law: $\langle\phi(0)\phi(\mathbf{x})\rangle \sim \frac{1}{|\mathbf{x}|^{2\Delta_\phi}}$, where Δ_ϕ is known as the critical dimension of $\phi(\mathbf{x})$. However, it is worth noting that in systems in two dimensions (2D) or in quantum systems in $1+1$ dimensions, such as the 2D boundary of a 3D system, the correlation function can potentially exhibit logarithmic decay with respect to $|\mathbf{x}|$.

It is widely accepted that the nature of a phase transition can be characterized by a small set of critical exponents and the symmetry of the system. Consequently, systems with different symmetry groups and critical exponents can be classified into **universality classes**. For instance, the 2D Ising model exhibits $\mathbb{Z}_2$ symmetry and has critical exponents $\nu = 1$ and $\eta \equiv \Delta_\phi - d + 2 = 1/4$. The concept of universality class plays a crucial role in condensed matter physics and statistical mechanics as it enables us to make general predictions about the behavior of systems near a critical point, even in the absence of detailed knowledge about the system's microscopic properties. Moreover, it provides a framework for classifying and comparing different types of phase transitions, as well as studying their underlying symmetries and properties.

Conversely, given the microscopic model of a system, the use of **renormalization group (RG)** techniques, developed by Kadanoff, Wilson, and many others in the 1960s and 70s, allows for the systematic removal of microscopic details near the critical point, enabling the calculation of corresponding critical exponents. RG provides a means to investigate the properties of a system at different length scales by identifying the relevant degrees of freedom at each scale and studying how their interactions change as the system approaches the critical point.

1.1.3 Quantum Phase Transitions

It is well-known that, using the path integral formalism, the partition function of a d-dimensional quantum system at temperature T can be connected to a $(d+1)$-dimensional

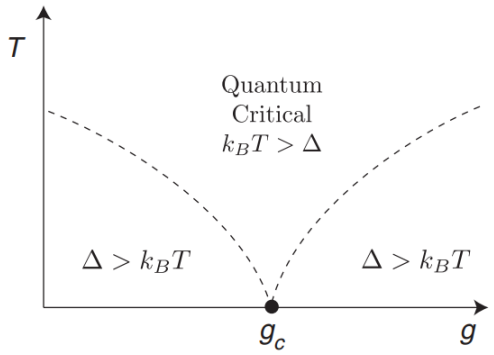

Figure 1.1: A schematic phase diagram near the quantum critical point, from [13].

classical system, and the inverse temperature $\beta \equiv 1/(k_BT)$ serves as the length of the periodic imaginary temporal direction of the quantum system. The main difference is that a quantum phase transition is driven by quantum fluctuations at zero temperature, instead of thermal fluctuations. When the coupling g is tuned to its **quantum critical point (QCP)** g_*, the energy gap Δ of the quantum spectrum closes with the scaling $\Delta \sim |g - g_*|^{\nu z}$ [12], and z is called the dynamical critical exponent. z is defined this way so that the characteristic time of the quantum fluctuation $\tau_q \sim 1/\Delta \sim \xi^z$, in which ξ is the correlation length.

For a quantum system at finite temperature, there are two energy scales in the system: the energy gap Δ and k_BT. In the regime of $\Delta > k_BT$, thermal fluctuations play a less significant role. The thermal equilibrium time τ_{eq} is much longer than τ_q, and classical dynamical equations can be used to describe its thermal equilibrium process. However, when the temperature reaches $\Delta < k_BT$, quantum and thermal fluctuations are equally important. One can depict this **quantum critical regime** in a "phase diagram" of g and T as a fan above the QCP. See Figure 1.1.

In principle, one may write down the field theory for a **quantum phase transition** at zero temperature in a similar fashion as classical statistical mechanics. However, this task is not an easy one. The main difference for quantum criticality is the inclusion of

Berry phases of different field configurations, which do not have classical equivalence. These phases contribute to the imaginary part of the statistical weight and can give rise to exotic quantum phase transitions that go beyond the Landau-Ginzburg paradigm. A famous example is the path integral of the quantum Heisenberg model, which yields [14]

$$\mathcal{Z} = \int D[\mathbf{n}_i(t)] e^{-S[\mathbf{n}_i(\tau)]}, \quad S[\mathbf{n}_i(\tau)] = -\mathrm{i}S \sum_i S_{WZ}[\mathbf{n}_i(\tau)] + J \int_0^\beta d\tau \sum_{\langle i,j \rangle} \mathbf{n}_i(\tau) \cdot \mathbf{n}_j(\tau), \tag{1.7}$$

in which J is the Heisenberg coupling.The Weiss-Zumino(WZ) term $S_{WZ}[\mathbf{n}(\tau)]$ is the Berry phase of each lattice spin accumulated from the spin evolution along imaginary time:

$$S_{WZ}[\mathbf{n}(\tau)] = \int_0^1 du \int_0^\beta d\tau \ \mathbf{n}(\tau, u) \cdot (\partial_\tau \mathbf{n}(\tau, u) \times \partial_u \mathbf{n}(\tau, u)) \,. \tag{1.8}$$

$\mathbf{n}(\tau, u)$, which satisfies $\mathbf{n}(\tau, 0) = (0, 0, 1)$ and $\mathbf{n}(\tau, 1) = \mathbf{n}(\tau)$, is the interpolation between $\mathbf{n}(\tau)$ and the north pole of the Bloch sphere.

There are several import applications of the theory. For anti-ferromagnetic Heisenberg model in 1d, one can further take the continuous limit and obtain an effective action [14]

$$\mathcal{L} = \frac{1}{2g} \left(\frac{1}{v_s} (\partial_\tau \mathbf{m})^2 - v_s (\partial_x \mathbf{m})^2 \right) + \mathrm{i} \frac{\theta}{8\pi} \epsilon_{\mu\nu} \mathbf{m} \cdot (\partial_\mu \mathbf{m} \times \partial_\nu \mathbf{m}), \tag{1.9}$$

in which $\mathbf{m}(x, \tau) \sim (-1)^i \mathbf{n}_i(\tau)$ is the anti-ferromagnetic order parameter, $g = 2/S$, $v_s = 2aJS$(a is the 1d lattice constant) and $\theta = 2\pi S$. The imaginary θ term captures the winding number(or skyrmion number) of $\mathbf{m}$ configuration around the whole $\tau - x$ plane:

$$Q = \frac{1}{8\pi} \epsilon_{\mu\nu} \mathbf{m} \cdot (\partial_\mu \mathbf{m} \times \partial_\nu \mathbf{m}) \in \mathbb{Z}. \tag{1.10}$$

Thus, for half-integer spin S, the winding number of $\mathbf{m}(\tau, x)$ along each path in the

path integral contributes $(-1)^Q$ phase factor in the overall partition function, while for integer spin there is no such effect. This ultimately leads to different universality class of half-integer spin and integer spins, which is known as the Haldane's conjecture. It has hence been confirmed numerically later that the integer spin case are found to be massive, with a gap of spin excitations, and the half-integer spin case is gapless.

A more relevant case to this thesis is the 2D $S = 1/2$ Heisenberg antiferromagnet on a square lattice. In two spatial dimensions, the analogue of the θ term is related to the hedgehog (or monopole) configuration of the antiferromagnetic Néel order parameter $\mathbf{N}(\mathbf{x})$. The hedgehog configuration again changes Q by 1. In the disordered phase of $\mathbf{N}$, we can alternatively view it as a condensate of monopoles of $\mathbf{N}$. However, due to the non-trivial Berry phase carried by the monopoles from the topological term of $\mathbf{N}$, we find that the path integral again contains phase factors for different Q. This factor is 1 only if Q is a multiple of 4. In other words, the four-fold lattice rotation symmetry of the square lattice is spontaneously broken in the monopole condensate, resulting in the so-called **valence bond solid (VBS)** order. A schematic phase diagram and a sketch of Néel and VBS orders are shown in Fig. 1.2. As conjectured by Senthil et al. [15, 16] and further supported by numerics [17, 18, 19, 20], there should be a direct second-order phase transition between Néel and VBS orders based on the fact that the monopole tunneling operator is suppressed near the critical point of the transition, leading to the notion of deconfinement. Such a critical point is thus dubbed a **deconfined quantum critical point (DQCP)**, and it is an example of quantum criticality that does not have classical counterparts, as both the Néel and VBS states break certain symmetries of the entire Hamiltonian.

The field theoretical description of the Néel-to-VBS transition is the non-compact

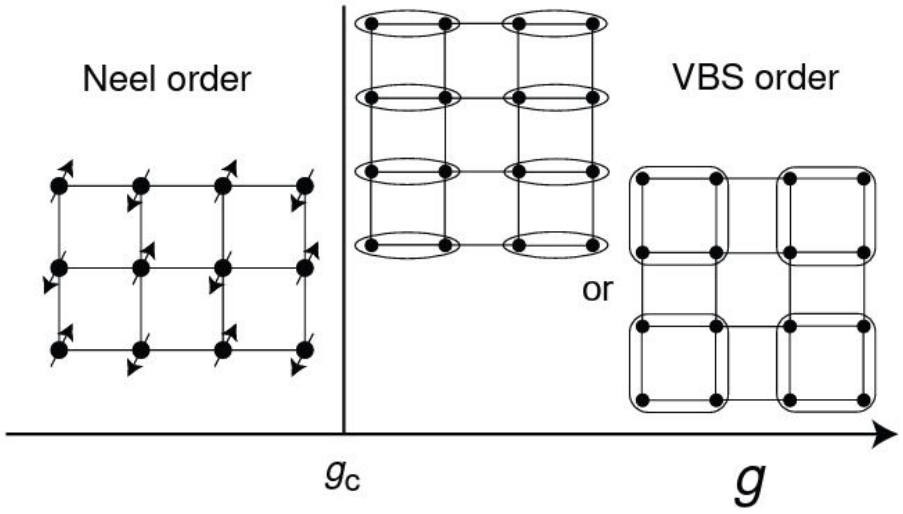

Figure 1.2: A schematic phase diagram and lattice configurations of the Néel and VBS orders, from [21]. $g = g_c$ is conjectured to be a deconfined quantum critical point.

CP^1 model:

$$\mathcal{L}_{NCCP^1} = \sum_{\alpha=1,2} |(\partial_\mu - \mathrm{i}a_\mu)z_\alpha|^2 + r|z_\alpha|^2 + u(|z_1|^2 + |z_2|^2)^2 + \dots . \tag{1.11}$$

Here the two component complex bosonic field z_α is the CP^1 representation of Néel order parameter:

$$N_i = z^*_\alpha \sigma^i_{\alpha\beta} z_\beta, \tag{1.12}$$

and the phase transition is driven by r. The two components are coupled to a dynamical $U(1)$ gauge field a_μ, hence the monopole tunneling operator of $\mathbf{N}$ now becomes the monopole operator $\mathcal{M}$ of a_μ. The monopoles are suppressed at the critical point, meaning a_μ is then a non-compact gauge field. The ellipse here consists of the Maxwell term that provides the dynamics of a_μ and other symmetry allowed interactions. For example, the four-vortex tunneling operator $\lambda_4 \mathcal{M}^4$ is allowed for square lattice. Even though the scaling dimension of $\mathcal{M}$ is likely to make λ_4 irrelevant at the critical point, it will quickly become relevant once one enters the disordered phase of $\mathbf{N}$, which condenses

the monopoles, breaking four-fold lattice rotation symmetry as we enter the VBS phase. Such operator is thus dubbed a "dangerously irrelevant" operator.

There is also a simpler case of the DQCP if one breaks the $SO(3)$ rotation symmetry of $\mathbf{N}$ down to $U(1)$ by introducing easy-plane anisotropies like $J'N_z^2$. The residual $U(1)$ is the rotation symmetry of N_x and N_y in the xy plane, and terms like $|z_1|^2|z_2|^2$ in the ellipse of (1.11) will be allowed. The field theory in the easy-plane case is

$$\mathcal{L}_{EP-NCCP^1} = \sum_{\alpha=1,2} |(\partial_\mu - \mathrm{i}a_\mu)z_\alpha|^2 + r|z_\alpha|^2 + u(|z_1|^4 + |z_2|^4) + \dots . \tag{1.13}$$

We note that the theory is self-dual, in the sense that one can rewrite the theory using vortex of (N_x, N_y) as order parameters:

$$\mathcal{L}^d_{EP-NCCP^1} = \sum_{\alpha=1,2} |(\partial_\mu - \mathrm{i}\tilde{a}_\mu)\psi_\alpha|^2 - r|\psi_\alpha|^2 + \tilde{u}(|\psi_1|^4 + |\psi_2|^4) + \dots . \tag{1.14}$$

The monopole operator is now identified as $\mathcal{M} \sim \psi^*(\sigma^x + i\sigma^y)\psi$. In the VBS phase, $r > 0$, ψ is condensed, giving $\mathcal{M}$ a non-zero expectation value.

Recently it has been shown that the 2+1d $NCCP^1$ theory is in a so-called "duality web" along with several other theories, including fermionic ones, meaning that even these set of theories have different mathematical forms and describe phase transitions with different physical nature, they share same universal features near the quantum critical points [22, 23]. In Chapter 3 of this thesis, we will utilize these dualities and study the fate of DQCPs that exist with other degrees freedom in the system that posses long-range interaction.

1.2 Boundary Critical Phenomena and Field Theories

We know move on to the boundary of a critical system. Experimentally, the boundary of a sample is much easier to probe, as the bulk is usually encapsulated in a fabricated device. The theoretical study of boundary physics is important in its own right, especially when the bulk is tuned to criticality. As we reviewed in the last section, a system at criticality exhibits scale invariance capitulated by various critical exponents, and such system can usually be studied using a **conformal field theory (CFT)**. However, the presence of a boundary introduces additional degrees of freedom and boundary conditions that need to be taken into account. These boundary conditions determine how the fields in the bulk CFT behave near the boundary. The study of CFT with a boundary is known as **boundary CFT (BCFT)**[24, 25].

One of the earliest rigorous field-theoretical study of boundary critical phenomena was done by Diehl and Dietrich[26, 27]. Quite remarkably, they found that the surface of D-dimensional $O(n)$ spin model at bulk order-to-disorder transition can exhibit several boundary universality classes. To study the surface criticality using field theory, the authors considered the following action

$$S = \int d^{D-1}x_{\parallel} \int_0^{\infty} dx_{\perp} \left[\frac{1}{2}(\partial\vec{\phi})^2 + \frac{\tau}{2}\vec{\phi}^2 + \frac{g}{24}(\vec{\phi}^2)^2 \right] + \int d^{D-1}x_{\parallel} \frac{c}{2}\vec{\phi}^2(x_{\parallel}, x_{\perp} = 0). \quad (1.15)$$

The final term above is a surface term that describes an enhancement of interactions near the surface. Using RG with $D = 4-\epsilon$ dimensional regularization, the authors found three distinct types of surface phase transitions near bulk criticality: the ordinary, the special and the extraordinary, when d exceeds the surface lower critical dimension. From Mermin-Wagner theorem, the surface can only be ordered if $D - 1 > 2 - \delta_{n,1}$. Thus

for $D = 3$, we would expect only ordinary surface transition, i.e. the surface develops order simultaneously with the bulk. Nevertheless, the surface criticality will have very different critical exponent, comparing to the bulk counterparts. A study of $O(n)$ model using BCFT is done by Cardy in [25, 24]. A important message from the work is that the fluctuation of the order parameter on the boundary near the ordinary transition can be effectively captured by $\vec{\Phi}(x_\parallel) = \partial_{x_\perp}\phi(x_\parallel, x_\perp)|_{x\perp=0}$. As we will see in Chapter 2, this result is a useful starting point of modelling various surface and interface criticality.

As recently revisited by Metlitski, el al., the $O(n)$ model in $D = 3$ with $n < n_c$ is still able to support a quasi long-range order[28, 29, 30], whose order parameter has logarithmic correlations:

$$\langle\vec{\phi}(0)\vec{\phi}(\mathbf{x})\rangle \sim \frac{1}{(\log|\mathbf{x}|)^q}. \tag{1.16}$$

Hence such surface transition is dubbed "extraordinary-log" universality class. These field-theoretical and numerical results opens the door to a new series of exotic criticalities, which could have deep implications in quantum magnetism. In Sec. 2.3, we show that for a 2+1d system with $SO(3)$ and translation symmetry, the 1+1d boundary can support a Néel-to-VBS transition similar to the one reviewed in the last subsection.

1.3 Field Theories in Fermionic Matters

1.3.1 Landau's Theory of Fermi Liquid

Landau's Fermi liquid theory, developed by the Soviet physicist Lev Landau in the 1950s, is a theoretical framework that is able to describe the behavior of weakly interacting fermions, such as electrons in a metal, at low temperatures. The key idea of the theory is that in a Fermi liquid, the interactions between the fermions are weak enough that the quasiparticles, which are essentially the electrons dressed with their interactions

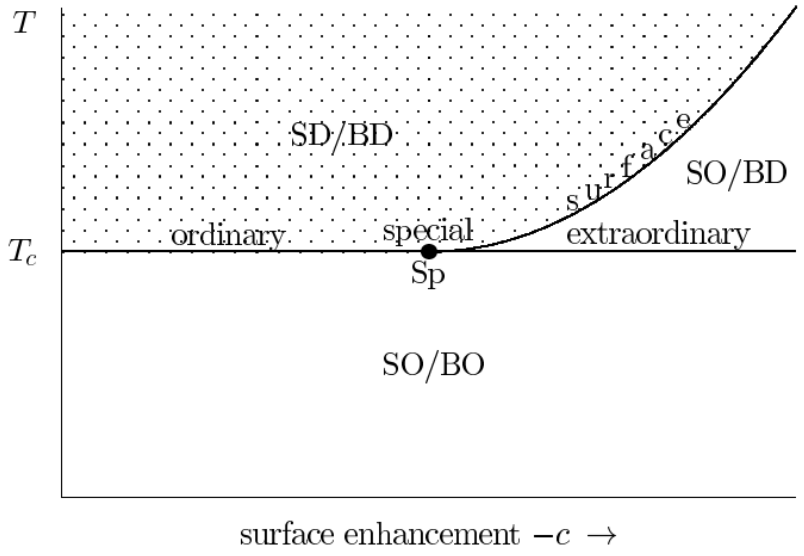

Figure 1.3: The phase diagram of surface near bulk critical point, from [31]. Here SO(BO) stands for surface (bulk) ordered, and SD(BD) stands for surface (bulk) disordered. The x axis is the negative surface-enhancement $-c$, and y axis is temperature $T \sim \tau$.

with other electrons, behave in many respects as if they were non-interacting, although physical parameters like the effective mass of the electron might be modified. This allows the Fermi liquid to be treated as a collection of nearly free particles, each with a well-defined momentum and energy. The quasiparticles in a Fermi liquid obey the same statistics as the underlying fermions, and they fill up the available energy states up to the chemical potential of the system.

Due to their weakly interacting nature, we can use momentum $\mathbf{k}$ as a good quantum number to label the electrons in a Fermi liquid, along with the electron spin. If we use the imaginary time path integral approach of a second-quantized Hamiltonian of the electron, we have the following field theory:

$$\mathcal{L}_f = c^\dagger_{\mathbf{k}\alpha}(\partial_\tau + \epsilon(\mathbf{k}) - \mu)c_{\mathbf{k}\alpha}, \tag{1.17}$$

where μ is the chemical potential. At low temperatures, one is mostly interested in the physics around the energy μ. In d-dimensional space, the solution of $\epsilon(\mathbf{k})-\mu=0$ gives us a **Fermi surface** of dimension $d-1$. The low energy physics of the Fermi liquid is then effectively one-dimensional: on each point of the Fermi surface, the electron is excited in the direction perpendicular to the Fermi surface. Expanding the theory near the Fermi surface, we obtain the following low-energy effective theory:

$$\mathcal{L}_{\text{patch}}=\sum_{\theta} c^{\dagger}_{\theta\mathbf{k}\alpha}(\partial\tau+\mathbf{v}_f(\theta)\cdot(\mathbf{k}-\mathbf{k}_f(\theta))+\dots)c_{\theta\mathbf{k}\alpha}, \tag{1.18}$$

where θ is a set of $d-1$ generalized coordinates that parameterize the Fermi surface, $\mathbf{v}_f(\theta)=\partial_{\mathbf{k}}\epsilon(\mathbf{k})|_{\mathbf{k}=\mathbf{k}_f(\theta)}$ is the local Fermi velocity, and the ellipsis consists of higher-order terms from the Taylor expansion of $\mathbf{k}-\mathbf{k}_f(\theta)$.

The Fermi liquid theory is able to explain many of the observed properties of metals, including the low-temperature behavior of the electrical resistivity $\rho-rho_0\sim T^2$ and the specific heat $C_V\sim T$. It has also been used to describe the behavior of other interacting fermion systems, such as neutron stars and quark-gluon plasma. From the Fermi liquid theory, it is possible to reach other fermionic phases when strong interactions are added, as we will see in the next subsection.

1.3.2 Theories of Non-Fermi Liquid and Phase Transitions of Fermions

In gapless fermionic systems with strong enough interactions between fermions, the properties of the system will deviate from the prediction by Landau's Fermi liquid theory. In these systems, dubbed **non-Fermi liquids**(NFL), interactions between fermions are strong enough to significantly alter the properties of the Landau quasiparticles, leading to

unconventional behaviors at low temperatures. For example, the **strange metal** phase in the phase diagram of high-temperature superconductor near quantum criticality has resistivity that increases linearly with temperature, and such relation persists to high temperatures. In strange metals, the concept of well-defined quasiparticles, which are characteristic excitations in Landau's theory, breaks down. The interactions between particles are strong, and the system lacks a clear Fermi surface. Instead, the electronic excitations are believed to be highly entangled and non-local.

From the low energy effective theory of the fermi surface, one famous way of obtaining non-Fermi liquid is through the Hertz-Millis theory[32, 33]. Starting from (1.18), one couples the bilinear mass to bosonic degress of freedom at criticality:

$$\mathcal{L} = \mathcal{L}_{\text{patch}} + g\Phi_{\alpha\beta} c^{\dagger}_{\theta\mathbf{k}\alpha} c_{\theta\mathbf{k}\beta} + \mathcal{L}_B, \tag{1.19}$$

in which $\mathcal{L}_B = |\partial\Phi_{\alpha\beta}|^2 + V(\Phi_{\alpha\beta})$ is a bosonic theory whose potential is tuned to criticality. The g term couples the bosonic field to a fermionic bilinear. If g is a relevant coupling, then when we tune the bosonic criticality from an disordered phase $\langle\Phi_{ab}\rangle = 0$ to an disordered phase $\langle\Phi_{\alpha\beta}\rangle \neq 0$, the term induces a phase transition of the fermions from a metal phase to certain fermionic ordered phase, depending on the actual form of the interaction. The above model is a useful starting point for field-theoretical studying of novel fermionic phases like quantum spin liquids, and interaction driven fermionic transitions, including **metal-to-insulator transition**(MIT) or Ising-nematic transition.

In the $U(1)$ spin liquid state, a candidate ground state for $2d$ frustrated magnets, the fermionic degree of freedom carries spin-$\frac{1}{2}$ but is charge neutral. The fermion forms a spinon Fermi surface and is coupled to an emergent $U(1)$ gauge field. Such theory can be studied using a similar theory as (1.19), in which g describes the minimal coupling between fermion and the gauge field, and $\mathcal{L}_B$ generates the dynamics of the gauge field.

In order to perform a RG analysis of the coupling constant, Sung-Sik Lee considered the large-N scheme by writing $g = \frac{e}{\sqrt{N}}$. However, such theory is strong coupled even in the infrared, because the vertex correction and fermion self-energy involves infinite number of Feynmann diagrams. This is ultimately caused by strong quantum fluctuations caused by the large collection of low energy excitations. Similar problem is encountered in the study of Fermi liquid near the onset of Ising-nematic and spin density wave order by Metlitski and Sachdev[34, 35], whose RG corrections contain singular contributions that cannot be controlled. A controlled perturbative expansion study is pioneered by Nayak and Wilczek, who studied fermions with a quartic interaction $\frac{1}{|\mathbf{k}|^x}$, and $(1-x)$ is a small parameter can be used to control the RG equation[36]. Mross, McGreevy, Liu and Senthil proposed a similar modified bosonic action[37]:

$$\mathcal{L}_B = \int \frac{d\mathbf{k}d\omega}{(2\pi)^3}|\mathbf{k}|^{z_b-1}|\Phi(\mathbf{k},\omega)|^2. \tag{1.20}$$

Such expansion is shown to be controlled in the limit of small $\epsilon = z_b - 2$. However, in most of the physical scenarios, $z_b = 3$ (or $\epsilon = 1$), so the validity of such perturbation is limited in these situations to recover actual physical properties like various scaling behaviors. Nevertheless, as will see in Chapter 3 and 4, the critical bosonic theory can be replaced by more exotic bosonic criticalities, in which the Φ correlation function can be effectively reproduced by such term with z_b around 2. In such cases the perturbative RG results will be more realistic in a considerable energy window.

Another important application of such theory is the interaction driven continuous **metal-to-insulator transition(MIT)**[38]. The physical picture of such transition is that the electron c_α in the system fractionalizes into a bosonic charge carrier b and neutral fermionic spinon f_α. Both b and f_α are coupled to an emergent $U(1)$ gauge field. The MIT is driven by an order-to-disorder transition of b. In the disordered phase of b, the

system is gapped with large resistance and a hidden spinon fermi surface, while in the ordered phase we recover the physical electron $c_\alpha \sim \langle b \rangle f_\alpha$, and the system is conductive. In $2d$, the electrical resistance is a dimensionless quantity multiplied by $\frac{h}{e^2}$. Thus, when the transition is tuned from the metallic side to the critical point, the resistivity should jump by $\rho_b = R\frac{h}{e^2}$, in which R is the dimensionless critical resistance of boson at the $2{+}1d$ XY universality class. In Chapter 4, we propose several alternative candidate theories of MIT that can potentially explain recently observed large critical resistance of MIT in Moiré transition metal dichalcogenides[39, 40].

1.4 Permissions and Attributions

1. The content of Sec. 2.1 is the result of a collaboration with Xiao-Chuan Wu, Hao Geng, Chao-Ming Jian, and Cenke Xu, and has previously published (on 5 May 2020) in Phys. Rev. B 101, 174406 (2020).

2. The content of Sec. 2.2 is the result of a collaboration with Xiao-Chuan Wu, Chao-Ming Jian, and Cenke Xu , and has previously published (on 18 May 2020) in Phys. Rev. B 101, 184419 (2020).

3. The content of Sec. 2.3 is the result of a collaboration with Chao-Ming Jian, Xiao-Chuan Wu, and Cenke Xu, and has previously published (on 12 February 2021) in SciPost Phys. 10, 033 (2021), licensed under the Creative Commons Attribution 4.0 License together with an author copyright.

4. The content of Sec. 3.1 is the result of a collaboration with Xiao-Chuan Wu, Hao Geng, Chao-Ming Jian, and Cenke Xu, and is from a preprint of the article

before peer review or editing, as submitted (on 5 March 2020) by an author to Journal of Statistical Mechanics: Theory and Experiment. IOP Publishing Ltd is not responsible for any errors or omissions in this version of the manuscript or any version derived from it. The version of record is available online at J. Stat. Mech. 073102 (2020).

5. The content of Sec. 3.2 is the result of a collaboration with Xiao-Chuan Wu and Cenke Xu , and has previously published (on 18 October 2022) in hys. Rev. B 106, 155131 (2022).

6. The content of Sec. 4.1 is the result of a collaboration with Xiao-Chuan Wu and Cenke Xu , and has previously published (on 22 May 2020) in hys. Rev. B 101, 2054261 (2020).

7. The content of Sec. 4.2 and App. A.1 is the result of a collaboration with Xiao-Chuan Wu, Mengxing Ye, Zhu-Xi Luo, Chao-Ming Jian, and Cenke Xu, and has previously published (on 28 June 2022) in Phys. Rev. X 12, 021067 (2022).

8. The content of Sec. 5 is the result of a collaboration with Cenke Xu, and has previously appeared in arXiv:2103.15865.

Chapter 2

Boundary Criticalities

2.1 Boundary Criticality of Deconfined Quantum Phase Transitions in $2d$ systems

2.1.1 Introduction

Two dimensional quantum many body systems at zero temperature gave us a plethora of exotic phenomena beyond the classical wisdom of phases of matter. These phenomena include topological orders [41, 42], symmetry protected topological orders [43, 44] (generalization of topological insulators), and unconventional quantum phase transitions beyond the Landau's paradigm [15, 16, 45, 46, 47, 48]. The unconventional quantum phase transitions usually have very distinct universal scalings compared with the ordinary $(2+1)d$ Landau's transitions. These unconventional quantum phase transitions, or unconventional quantum critical points (QCP), could happen between two ordinary Landau's phases with different patterns of spontaneous symmetry breaking [15, 16], they can also happen between a topological order and an ordered phase [45, 46, 47]. Although many appealing numerical evidences of these unconventional QCPs have been

found [49, 50, 51, 52], direct clear experimental observation of these unconventional QCPs is still demanded.

To identify an unconventional QCP in an experimental system, we need to measure the correlation functions and scaling dimensions of various operators at this QCP, and compare the results with analytical predictions. In this section we do not attempt to propose a particular experimental system that realizes one of the unconventional QCPs, instead we try to address one general issue that many experimental platforms would face, platforms where potentially these unconventional QCPs can be found. In numerical simulations of a QCP, correlation functions and scalings in the bulk can be directly computed. But experimentally many purely $2d$ systems of interests are sandwiched between other auxiliary layers in a Van der Waals heterostructure [53]. Hence the bulk of the $2d$ system is often not exposed for probing for many experimental techniques. Instead, the $1d$ boundary of the $2d$ system is exposed and can often be probed directly. Based on the early studies of the boundary of Wilson-Fisher fixed points [54, 27, 26, 55] and the boundary of two dimensional conformal field theories [25], we learned that the scaling of operators at the boundary of a system can be very different from the bulk, hence the previous calculations about unconventional QCPs in the bulk may not be so relevant to many experimental platforms. We need to restudy the critical exponents at the $1d$ boundary of the system in order to compare with future experimental observations.

2.1.2 Boundary Criticality of Z_2 topological quantum phase transitions

In this section we discuss the boundary critical behaviors of a $2d$ topological quantum phase transition between a fully gapped Z_2 topological order, and an ordered phase which spontaneously breaks the global symmetry of the system and has no topological order.

We assume that the "electric gauge particle" (the so called $e-$anyon) of the Z_2 topological order is an $N-$component complex boson b_a. This topological transition is described by the following field theory:

$$\mathcal{S} = \int d\tau d^2x \ \sum_{a=1}^{N} |\partial\phi_a|^2 + r|\phi_a|^2 + g(\sum_{a=1}^{N} |\phi|_a^2)^2, \tag{2.1}$$

where the complex scalar ϕ_a is the low energy field of anyon b_a, and it is coupled to a Z_2 gauge field which is not written explicitly. Because a Z_2 gauge field does not have gapless gauge boson, it does not contribute any infrared corrections to gauge invariant operators. When $r > r_c$, ϕ_a is disordered and the system is a Z_2 topological order which is also the deconfined phase of the Z_2 gauge field; when $r < r_c$, ϕ_a condenses and destroy the Z_2 topological order through the Higgs mechanism, and the condensate of ϕ_a has ground state manifold S^{2N-1}/Z_2, where S^{2N-1} is a $2N-1$ dimensional sphere.

This theory Eq. 4.8 with different N can be realized in various scenarios. For $N = 1$, this theory can be realized as the transition between a $2d$ superconductor and a Z_2 spin liquid. Similar unconventional topological transitions have been observed in numerical simulations in lattice spin (or quantum boson) models [45, 46], and theoretical predictions of the bulk critical exponents have been confirmed quantitatively. In this realization the boson b can be introduced by formally fractionalizing the electron operator on the lattice as

$$c_{j,\alpha} = f_{j,\alpha} b_j, \tag{2.2}$$

where b_j is a charge-carrying bosonic "rotor", $f_{j,\alpha}$ is the fermionic parton that carries the spin quantum number. $f_{j,\alpha}$ and b_j share a U(1) gauge symmetry, and the Z_2 topological order is constructed by assuming that b_j has a finite mass gap, while $f_{j,\alpha}$ forms a

superconductor at the mean field level, which breaks the U(1) gauge symmetry down to Z_2. The quantum phase transition between the superconductor and the Z_2 topological is described by Eq. 4.8 with $N = 1$. In the condensate of ϕ ($r < r_c$), the physical pairing symmetry of the superconductor is inherited from the mean field band structure of f_α. The long range Coulomb interaction between charge carriers is often screened by auxiliary layers such as metallic gages in experimental systems, hence in Eq. 4.8 there is only a short range interaction. Eq. 4.8 with $N = 1$ is often referred to as the "XY*" transition. In the dual picture, starting from the superconducing phase, the XY* transition can also be viewed as the condensation of double vortices of the superconductor.

Eq. 4.8 with even N and $N \geq 2$ can be realized in Sp(N) spin systems, as the Z_2 spin liquid can be naturally constructed in Sp(N) spin systems. $b_a \sim \phi_a$ is introduced as the fractionalized Schwinger boson of the spin system, and the Z_2 topological order emerges when a pair of b_a (which forms a Sp(N) singlet) condenses on the lattice [56, 57]. In particular, when $N = 2$, the theory Eq. 4.8 can be realized as the quantum phase transition between a Z_2 topological order and a noncollinear spin density wave of spin-1/2 systems on a frustrated lattice, for example the so-called 120° antiferromagnetic state on the triangular lattice [47]. The order parameter of the noncollinear spin order of a fully SU(2) invariant Hamiltonian will form a ground state manifold SO(3), which is equivalent to $\mathrm{SU}(2)/Z_2 = S^3/Z_2$, where the Z_2 is identified as the Z_2 gauge group, and also the center of the spin SU(2) group. The gauge invariant order parameter can be constructed with the low energy field ϕ_a as

$$\vec{N}_1 = \mathrm{Re}[\phi^t \mathrm{i}\sigma^2 \vec{\sigma} \phi], \quad \vec{N}_2 = \mathrm{Im}[\phi^t \mathrm{i}\sigma^2 \vec{\sigma} \phi], \quad \vec{N}_3 = \phi^\dagger \vec{\sigma} \phi, \tag{2.3}$$

and one can show that $\vec{N}_i$ are three orthogonal vectors. In this case theory Eq. 4.8 is referred to as the O(4)* transition, because there is an emergent O(4) symmetry that

rotates between the four component real vector $(\mathrm{Re}[\phi_1], \mathrm{Im}[\phi_1], \mathrm{Re}[\phi_2], \mathrm{Im}[\phi_2])$. Other systems can potentially realize the theory with larger$-N$, for instance spin systems with Sp(4) symmetry can be realized in spin-3/2 cold atom systems [58].

We are most interested in the composite operator $\sum_a \phi_a^2$, which is invariant under the Z_2 gauge symmetry, but transforms nontrivially under the physical symmetry, hence it is a physical order parameter. When $N = 1$, in the condensate of ϕ (or b_j), the electron operator has a finite overlap with the fermionic parton operator $c_{j,\alpha} \sim f_{j,\alpha}\langle\phi\rangle$, hence the superconductor order parameter $\Delta \sim \langle\phi^2\rangle$. In the bulk the scaling dimension of ϕ^2 can be extracted through the standard ϵ expansion or numerical simulation [59]. Near the critical point the superconductor order parameter should scale as $\Delta \sim |r|^\beta$, where $\beta = [\phi^2]\nu$ and $[\phi^2]$ is the scaling dimension of operator ϕ^2. At the XY* critical point the exponent $\nu \sim 2/3$. When $N = 2$, the composite operator $\sum_a \phi_a^2$ is one component of the spin order parameter of the noncollinear spin density wave.

All the results above are only valid in the $2d$ bulk. But in experiments on the boundary (as we discussed previously, it is the boundary that is exposed and hence can be probed conveniently), many of the critical exponents are modified. We now consider a system whose $2d$ bulk is in the semi-infinite xz plane with $z > 0$, with a $1d$ boundary at $z = 0$. For simplicity, let us tentatively ignore the Z_2 gauge field, and view ϕ_a as a physical order parameter. The most natural boundary condition is the Dirichlet boundary condition, *i.e.* the field vanishes at the boundary and also outside of the system $z \leq 0$. The boundary condition of the system can be imposed by turning on a large $c|\phi_a|^2$ term along the boundary, which fixes $\phi_a(\mathbf{x}, z = 0) = 0$, where $\mathbf{x} = (\tau, x)$.

At the mean field level, the correlation function of the ϕ_a field near the boundary can be computed using the "image method" [54]:

$$G(\mathbf{x}_1 - \mathbf{x}_2, z_1, z_2) = \langle\phi_a(\mathbf{x}_1, z_1)\phi_a^*(\mathbf{x}_2, z_2)\rangle =$$

$$G(\mathbf{x}_1 - \mathbf{x}_2, z_1 - z_2)_{\text{bulk}} - G(\mathbf{x}_1 - \mathbf{x}_2, z_1 + z_2)_{\text{bulk}}. \tag{2.4}$$

$G_{\text{bulk}} = \langle \phi_a(\mathbf{x}_1, z_1)\phi_a^*(\mathbf{x}_2, z_2)\rangle_{\text{bulk}}$ is the bulk correlation function far from the boundary. Notice that the boundary breaks the translation symmetry along the z direction, hence the full expression of the correlation function near the boundary is no longer a function of $z_1 - z_2$. The expression in Eq. 2.4 guarantees that the correlation function satisfies $G(\mathbf{x}_1 - \mathbf{x}_2, 0, z_2) = G(\mathbf{x}_1 - \mathbf{x}_2, z_1, 0) = 0$, which is consistent with the boundary condition. The fact that the correlation function of the ϕ_a field vanishes at the boundary means that ϕ_a itself is no longer the leading representation of the field at the boundary $z = 0$. Instead, another field with the same symmetry and quantum number at the boundary,

$$\Phi_{1,a} = \partial_z \phi_a, \tag{2.5}$$

should be viewed as the leading representation of the field near the boundary. In fact, since $\Phi_{1,a}$ and ϕ_a have the same symmetry transformation near the boundary, an external field that couples to ϕ_a should also couple to $\partial_z\phi_a$. At the mean field level, a typical configuration of ϕ_a scales as $\phi_a(\mathbf{x}, z) \sim z$ near the boundary, hence $\Phi_{1,a} = \partial_z\phi_a$ is not suppressed by the boundary condition. Also, the correlation function of $\Phi_{1,a}$ at the boundary does not vanish, and at the mean field level it has scaling dimension $[\Phi_{1,a}] = [\phi_a] + 1 = D/2$, where D is the total space-time dimension of the bulk.

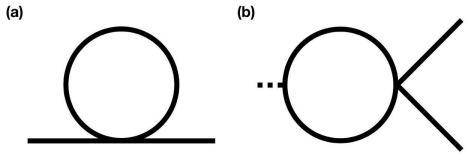

Figure 2.1: The diagrams that renormalize Φ_2 at the first order of ϵ. In the bulk the first diagram only shifts the mass of ϕ_a, but at the boundary it makes a nontrivial contribution to the wave function renormalization.

The gauge invariant order parameter $\sum_a \phi_a^2$ we are interested in reduces to $\Phi_2 = \sum_a \Phi_{1,a}^2$ at the boundary, and it has scaling dimension $[\Phi_2] = D$ at the mean field level. If the Z_2 gauge field is ignored, the correlation function of $\Phi_{1,a}$ at the boundary reads

$$\langle \Phi_{1,a}(\mathbf{x}_1)\Phi_{1,a}^*(\mathbf{x}_2)\rangle = \lim_{z_1,z_2\to 0} \partial_{z_1}\partial_{z_2} G(\mathbf{x}_1 - \mathbf{x}_2, z_1, z_2), \tag{2.6}$$

where $G(\mathbf{x}_1 - \mathbf{x}_2, z_1, z_2)$ is still given by the image method Eq. 2.4. If we assume that G_{bulk} takes the standard form at the Gaussian fixed point

$$\begin{aligned} &\langle \phi_a(\mathbf{x}_1, z_1)\phi_a^*(\mathbf{x}_2, z_2)\rangle_{\text{bulk}} \\ = \;& \frac{1}{(|\mathbf{x}_1 - \mathbf{x}_2|^2 + (z_1 - z_2)^2)^{\frac{D-2}{2}}}, \end{aligned} \tag{2.7}$$

the boundary correlation function of $\Phi_{1,a}$ at the mean field level reads

$$\langle \Phi_{1,a}(\mathbf{x}_1)\Phi_{1,a}^*(\mathbf{x}_2)\rangle = \frac{2(D-2)}{|\mathbf{x}_1 - \mathbf{x}_2|^D}. \tag{2.8}$$

At the Gaussian fixed point, the correlation function of Φ_2 can be derived using the Wick theorem:

$$\begin{aligned} \langle \Phi_2(\mathbf{x}_1)\Phi_2^*(\mathbf{x}_2)\rangle &= \sum_a \langle \Phi_{1,a}(\mathbf{x}_1)\Phi_{1,a}^*(\mathbf{x}_2)\rangle^2 \\ &\sim \frac{1}{|\mathbf{x}_1 - \mathbf{x}_2|^{2D}}. \end{aligned} \tag{2.9}$$

The scaling dimension of Φ_2 will acquire further correction from interaction, which can be computed through the $\epsilon = (4 - D)$ expansion. Interestingly, at the leading ϵ order, $[\Phi_2]$ will receive corrections from both wave function renormalization and vertex

corrections:

$$[\Phi_2] = D + 2\delta_{wf} + \delta_v. \tag{2.10}$$

The wave function renormalization δ_{wf} can be extracted from the previously calculated $\epsilon-$expansion of the anomalous dimension at the boundary of the Wilson-Fisher fixed points, *i.e.*

$$[\Phi_{1,a}] = \frac{D}{2} + \delta_{wf} = \frac{D}{2} - \frac{N+1}{2(N+4)}\epsilon. \tag{2.11}$$

In contrast, in the bulk renormalization group (RG) analysis of the Wilson-Fisher fixed point, the wave function renormalization only appears at the second and higher order of ϵ expansion.

The vertex correction is most conveniently computed using the standard real-space RG, since now the momentum along the $\hat{z}$ direction is no longer conserved. We will use the following operator-product-expansion (OPE) between $\Phi_2(\mathbf{x}, 0)$ and the interaction term in Eq. 4.8 (Fig. 2.1*b*), where $\Phi_2(\mathbf{x}, 0)$ is defined as $\Phi_2(\mathbf{x}, 0) = \lim_{z\to 0} (\partial_z \phi(\mathbf{x}, z))^2$:

$$\begin{aligned} & \Phi_2(\mathbf{x}, 0) g \left(\sum_a \phi_a^*(\mathbf{x}', z') \phi_a(\mathbf{x}', z') \right)^2 \\ = \;& 2g \lim_{z\to 0} (\partial_z G(\mathbf{x} - \mathbf{x}', z, z'))^2 \sum_a \phi_a^2(\mathbf{x}', z') \\ \sim \;& \frac{32 z'^4 g}{\left((\mathbf{x} - \mathbf{x}')^2 + z'^2\right)^4} \lim_{z\to 0} (\partial_z \phi(\mathbf{x}, z))^2 . \end{aligned} \tag{2.12}$$

Notice that like all the $4 - \epsilon$ expansions, the OPE and loop integrals were performed by assuming the bulk system is in a four dimensional space-time. Under rescaling $\mathbf{x} \to \mathbf{x}/b$,

through the vertex correction the operator Φ_2 will acquire a correction

$$\begin{aligned} \delta\Phi_2 &= -\Phi_2 \int_{a/b}^{a} 4\pi r^2 dr \int_0^{+\infty} dz' \, \frac{32 z'^4 g}{\left(r^2 + z'^2\right)^4} \\ &= -4g\pi^2 \left(\ln b\right) \Phi_2. \end{aligned} \tag{2.13}$$

The integral of z' is within the upper semi-infinite plane $z' > 0$.

Using epsilon expansion, g will flow from the noninteracting Gaussian fixed point to an interacting fixed point $g_* = \epsilon/(4(N+4)\pi^2)$. Plugging the fixed point value of g into Eq. 2.13, we obtain the vertex correction

$$\delta_v = \frac{\epsilon}{N+4}. \tag{2.14}$$

The wave function renormalization δ_{wf} can be reproduced in the same way through OPE (Fig. 2.1a). Eventually the scaling dimension of the gauge invariant order parameter Φ_2 at the boundary is

$$[\Phi_2] = D - \frac{N\epsilon}{N+4}. \tag{2.15}$$

We have also confirmed these calculations through direct computation of the correlation function of Φ_2 near the boundary (with diagrams in Fig. 2.2).

As we discussed before, the case with $N = 1$ can be realized as the transition between a Z_2 topological order and a superconductor. If the system is probed from the boundary, in the ordered phase but close to the critical point, the superconductor order parameter should scale with the tuning parameter r as

$$\Delta \sim |r|^{[\Phi_2]\nu} \sim |r|^{1.87}, \tag{2.16}$$

and we have taken $\nu \sim 2/3$ for the XY* fixed point [59].

For $N = 2$, the Φ_2 operator is one component of the noncollinear spin order of a SU(2) spin system, which scales as

$$\langle \vec{S} \rangle \sim \Phi_2 \sim |r|^{[\Phi_2]\nu} = |r|^{1.97} \tag{2.17}$$

Again, we have taken $\nu = 0.74$ for the O(4)* fixed point [59]. As a comparison, in the $2d$ bulk Φ_2 should scale with r as $\Phi_2 \sim |r|^{0.82}(N = 1)$ and $\Phi_2 \sim |r|^{0.87}(N = 2)$ respectively, which is significantly different from the boundary scaling.

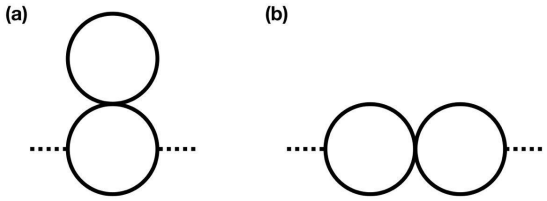

Figure 2.2: The renormalization of operator Φ_2 at the leading order of ϵ can also be computed directly using the correlation functions in this figure.

When $N = 1$, the action Eq. 4.8 may or may not allow an extra chemical potential term $\mu\phi^*\partial_\tau\phi$, depending on whether the system has a (emergent) particle-hole symmetry $\phi \to \phi^*$ or not. With nonzero μ the system has the same scaling as a mean field transition (with logarithmic corrections) as the total space-time dimension is effectively $D = 2 + d = 4$, and g is marginally irrelevant. In this case the scaling dimension of the Cooper pair at the boundary becomes $[\Phi^2]_{\mu\neq 0} = D = 4$, and $\nu = 1/2$ as in the mean field transition.

The boundary scaling is valid as long as we consider correlation function $G(\mathbf{x}_1 - \mathbf{x}_2, z_1, z_2)$ with $|\mathbf{x}_1 - \mathbf{x}_2| \gg z_1, z_2$. Right at the boundary of a $2d$ Z_2 topological order, the gauge field is confined, due to the condensation of the $m-$anyons of the Z_2 topological order at the boundary (the boundary of a Z_2 topological order can also have $e-$anyon

condensate, but since in our case the $e-$anyons carry nontrivial symmetry transformations, we assume our boundary always has $m-$anyon condensate). Near the boundary, the system still has a finite confinement length $\xi(z)$ as a function of z, *i.e.* the distance from the boundary, due to the "proximity effect" of the $m-$condensation at the boundary. In order to guarantee that we can approximately assume a deconfined Z_2 gauge field near the boundary, we need $\xi(z) \gg z$.

The most convenient way to estimate the confinement length $\xi(z)$ close to the boundary, is to evaluate the energy cost of two gauge charged particles separated with distance x near the boundary. This energy cost can be estimated in the "dual" Hamiltonian of a Z_2 gauge theory, which is a $(2+1)d$ quantum Ising model: $H_{\text{dual}} = \sum_{\bar{j}} -h\tau^x_{\bar{j}} - \sum_{\mu=x,y} J_{\bar{j},\mu}\tau^z_{\bar{j}}\tau^z_{\bar{j}+\mu}$, where $\tau^x_{\bar{j}}$, $\tau^z_{\bar{j}}$ are a pair of Pauli operators defined on the dual lattice sites $\bar{j}$. The dual Ising operator $\tau^z_{\bar{j}}$ is a creation/annihilation operator of the Z_2 gauge flux. A confined (and deconfined) phase of the Z_2 gauge field corresponds to the ordered (and disordered) phase of the dual quantum Ising model with nonzero (and zero) expectation value $\langle\tau^z\rangle$ [60]. If there is a pair of static $e-$particles with Z_2 gauge charges separated with distance x, this system is dual to a frustrated Ising model with $J_{\bar{j},\mu} = -J$ on the links along the branch-cut that connects the two particles, while $J_{\bar{j},\mu} = +J$ everywhere else. The energy cost of the two separated static particles corresponds to the energy difference between this frustrated Ising model nonuniform $J_{\bar{j},\mu}$, and the case with uniform $J_{\bar{j},\mu}$. Then if $\tau^z_{\bar{j}}$ has a nonzero expectation value $\langle\tau^z\rangle$, the pair of Z_2-gauge charges will approximately cost energy $E \sim J\langle\tau^z\rangle^2 x$, *i.e.* the system is in a confined phase with a linear confining potential between the two Z_2 gauge charges, and the confinement length is roughly $\xi \sim 1/(J\langle\tau^z\rangle^2)$. In our system with a boundary at $z = 0$, although $\langle\tau^z\rangle$ is nonzero at the boundary, its expectation value decays exponentially with z because the Z_2 gauge field is in a deconfined phase deep in the bulk with $\langle\tau^z\rangle = 0$. Hence the confinement length $\xi(z)$ also increases with z exponentially, and we can safely

assume that the Z_2 gauge field is still approximately deconfined near the boundary.

2.1.3 Continuous Metal-Insulator transition

Another unconventional quantum phase transition that can happen in $2d$ systems is the continuous metal-insulator transition, where the insulator is a U(1) liquid phase with a fermi surface of the fermionic parton $f_{j,\alpha}$. Both $f_{j,\alpha}$ and b_j are coupled to an emergent U(1) gauge field, which is presumably deconfined in the $2d$ bulk due to the existence of the Fermi surface and finite density of states of the matter fields. The critical behavior of this transition in the bulk was studied in Ref. [38], and it is again described by the condensation of b_j, but in this case b_j is coupled to an dynamic U(1) gauge field a_μ.

Although there is a gapless gauge field a_μ in the bulk, the gauge field dynamics is over-damped by the fermi surface of f_α through a term $\mathcal{S}_{\text{damp}} \sim \frac{1}{e^2}\sum_{\omega,\vec{q}} |a^t_{\omega,q}|^2 \frac{|\omega|}{|q|}$ based on the standard Hertz-Millis formalism [32, 33], where a^t is the transverse mode of the gauge field. A simple power-counting would suggest that the gauge coupling e^2 becomes irrelevant at the transition where b_j condenses, for both $\mu = 0$ and $\mu \neq 0$. Hence the universality class of this transition does not receive relevant infrared corrections from the gauge field. Moreover, the direct density-density interaction between the bosonic and fermionic partons also does not lead to relevant effects [38]. Hence the metal-insulator transition can still be described by Eq. 4.8. The quasiparticle residue is proportional to $|\langle b\rangle|$, and the electron Green's function is proportional to $|\langle b\rangle|^2$. Hence if one probes from the boundary, the local density of states of electrons at low energy, which is proportional to the electron Green's function, scales with the tuning parameter r as

$$\rho \sim |\langle \Phi_1 \rangle^2| \sim |r|^{2[\Phi_1]\nu}. \tag{2.18}$$

For $\mu = 0$, $[\Phi_1]$ is calculated in Eq. 2.11, and $\nu \sim 2/3$; for $\mu \neq 0$, $[\Phi_1] = 2$ and $\nu = 1/2$.

Again we need to address the question of confinement length near the boundary, and demonstrate that $\xi(z) \gg z$. A pure U(1) gauge field in $(2+1)d$ is dual to a scalar boson $\varphi \sim \exp(\mathrm{i}\theta)$ which physically is the Dirac monopole operator, and the confined phase of a U(1) gauge field corresponds to a phase with a pinned nonzero expectation value of φ. A U(1) gauged particle becomes a vortex of θ in the dual formalism, and in a deconfined phase a vortex costs logarithmically divergent energy; but if φ has a pinned nonzero expectation value, a vortex will cost linearly diverging energy and hence confined. Now suppose we consider a pair of gauge charged particles separated at distance x, the energy cost will be roughly $x\langle\varphi\rangle^2$. Hence we need to evaluate $\langle\varphi(z)\rangle$ as a function of z away from the boundary, assuming a nonzero expectation value of φ at the boundary $\varphi_0 = \langle\varphi(z=0)\rangle$. $\langle\varphi(z)\rangle$ can be inferred from the correlation function $\langle\varphi(z)\rangle \sim \langle\varphi(z)\varphi(0)^*\rangle \sim \exp(\langle\theta(z)\theta(0)\rangle)$.

A $(2+1)d$ pure U(1) gauge field without the matter field is dual to a scalar boson model with an ordinary action $\mathcal{S} \sim \int d^2x d\tau \rho_s(\partial_\mu\theta)^2$, then θ has a positive scaling dimension $[\theta] = 1/2$. The correlation function of θ reads $\langle\theta(r)\theta(0)\rangle \sim 1/r$, which makes the correlation function of the monopole operator saturates to a nonzero value as $r \to \infty$. Hence a positive scaling dimension of θ in the dual action renders the confinement of the compact gauge field in $(2+1)d$. If θ has a negative scaling dimension in its (dual) action, the correlation function of φ will decay exponentially. Then the confinement length $\xi(z) \sim 1/\langle\varphi(z)\rangle^2 \sim 1/\langle\varphi(z)\varphi(0)^*\rangle^2$ will grow exponentially with z in the bulk away from the boundary. And since $\xi(z) \gg z$, the boundary scaling behavior calculated in this section can be applied under the assumption that the gauge field is sufficiently deconfined near the boundary since the confinement length is long enough in the vicinity of the boundary.

Now we need to derive the dual action for θ more carefully. Schematically the action

for the transverse gauge field is

$$\mathcal{S} = \sum_{\omega,\vec{q}} \frac{1}{2} \left(\frac{1}{e^2} \frac{|\omega|}{q} + c^2 q^2 \right) |a^t|^2. \tag{2.19}$$

The canonical conjugate field of $\vec{a}$, *i.e.* the electric field of the gauge field is defined as $\vec{E} = \delta\mathcal{L}/\delta\dot{\vec{a}}$, hence $\vec{E}_{\omega,\vec{q}} \sim \vec{a}_{\omega,\vec{q}}/(e^2 q)$, hence the action can also be written as

$$\mathcal{S} = \sum_{\omega,\vec{q}} \frac{e^2}{2} |\omega||\vec{q}||\vec{E}_{\omega,\vec{q}}|^2 + \frac{c^2}{2} q^2 |a^t_{\omega,\vec{q}}|^2. \tag{2.20}$$

Then we can use the standard duality transformation that preserves the commutation relation between the canonical conjugate variables $\vec{E}$ and $\vec{A}$: $\vec{E} = \vec{\nabla}\theta$, $\vec{\nabla} \times \vec{a} = n$, where n is the flux density, or the particle density conjugate to θ. Eventually the dual action reads

$$\mathcal{S}_d = \sum_{\omega,\vec{q}} \frac{1}{2} \left(e^2 |\omega| q^3 + \frac{1}{c^2} \omega^2 \right) |\theta_{\omega,\vec{q}}|^2. \tag{2.21}$$

Indeed, $\theta(\mathbf{x}, \tau)$ has a negative scaling dimension in this dual action, which is consistent with our expectation that $\langle \varphi(z) \rangle$ decays exponentially in the bulk, hence the gauge field is still approximately deconfined in the vicinity of the boundary.

2.1.4 Discussion

In this section we computed the boundary universal scaling behaviors of a class of deconfined quantum phase transitions, which is relevant to future realization of these exotic transitions in experimental systems. From the perspective of the pure Laudau's paradigm, the cases we study correspond to the "ordinary transitions" of boundary CFT [54], meaning the bulk will enter an ordered phase before the boundary, which

we believe is the most natural case in real systems. Measurement of the scaling laws we calculated depends on the specific realization of the theory Eq. 4.8. For example, if the $N = 1$ theory is realized (as we proposed in this section) as the transition between the Z_2 spin liquid to superconductor, the amplitude of the Cooper pair at the boundary predicted in our calculation can be measured through the Josephson effect by building a junction between the boundary of the system and another ordinary bulk superconductor, as the Josephson current is proportional to the amplitude of the superconductor order parameter near the boundary. The Josephson current should follow the same scaling law as Eq. 4.9.

The studies in this section can be naturally generalized to higher dimensions. If there is a deconfined QCP between the Z_2 topological order and an ordered phase in the $(3+1)d$ bulk, at its $(2+1)d$ boundary the gauge invariant order parameter Φ_2 has precise scaling dimension $[\Phi_2] = 4$, since in the bulk this transition is described by a mean field theory and received no extra corrections.

The direct transition between the Néel and valance bond solid (VBS) order is another type of deconfined QCP that has attracted a great deal of attentions. The boundary effect of this deconfined QCP is more complex than the situations we have considered because the boundary breaks the lattice symmetry, hence the boundary condition would couple to the VBS order parameter. Another interesting scenario worth studying is the boundary scaling of a bulk transition between a symmetry protected topological (SPT) states and an ordered phase which spontaneously breaks part of the defining symmetries of the SPT phase. Although the bulk transition should belong to the same universality class as the ordinary Ginzburg-Landau transition, its boundary is expected to be very different due to the existence of symmetry protected nontrivial boundary states even in the SPT phase. Efforts have been made along this direction including numerical simulation [61] and construction of exactly soluble models [62]. We will leave these subjects to future

studies.

2.2 Topological Edge and Interface states at Bulk disorder-to-order Quantum Critical Points

2.2.1 Introduction

The most prominent feature of topological insulators (TI) [63, 64, 65, 66, 67, 68, 69] and more generally symmetry protected topological (SPT) states [43, 44] is the contrast between the boundary and the bulk of the system. In particular the $2d$ edge of $3d$ SPT states hosts the most diverse zoo of exotic phenomena that keep attracting attentions and efforts from theoretical physics. It has been shown that many exotic phenomena such as anomalous topological order [70, 71, 72, 73, 74, 75, 76], deconfined quantum critical points [77], self-dual field theories [78, 79, 80, 81] can all occur on the $2d$ edge of $3d$ SPT stats. Sometimes the symmetry of the system is secretly realized as a self-dual transformation of the field theories at the boundary [82, 22]. All these suggest that the $2d$ boundary of a $3d$ system is an ideal platform of studying physics beyond the standard frameworks of condensed matter theory.

On the other hand, even the boundary of an ordinary Landau-Ginzburg type of quantum phase transition can have nontrivial behaviors. It was studied and understood in the past that the boundary of a bulk conformal field theory (CFT) follows a very different critical behavior from the bulk [24, 25, 27, 26, 55, 31], due to the strong boundary condition imposed on the CFT. The boundary fluctuations (or the boundary CFT) of the Landau-Ginzburg phase transitions were studied through the standard $\epsilon-$expansion, and it was shown that the critical exponents are very different from the bulk. Hence if experiments are performed at the boundary of the system, one should refer to the

predictions of the boundary instead of the bulk CFT. These two different boundary effects were studied separately in the past. In this section we will study the interplay of these two distinct boundary effects. Our goal is to seek for new physics, ideally new fixed points under renormalization group (RG) flow due to the coupling of the two boundary effects.

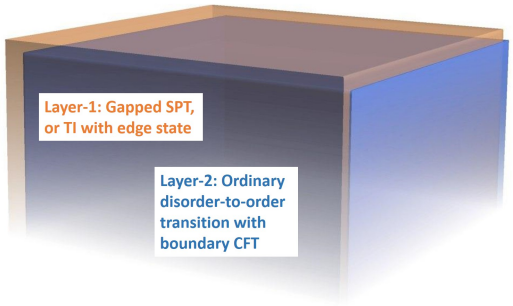

Figure 2.3: We view the system under study as a two layer system. Layer-1 is a SPT or TI with nontrivial edge states; layer-2 is an ordinary disorder-to-order phase transition whose order parameter at the boundary follows the scaling of boundary CFT. The boundary of the entire system may flow to new fixed points due to the coupling between the two layers.

For our purpose we give the system under study a virtual two-layer structure Fig. 2.3: layer-1 is a SPT state with nontrivial edge states, and it is not tuned to a bulk phase transition; layer-2 is a topological trivial system which undergoes an ordinary Landau-Ginzburg disorder-to-order phase transition. Then as a starting point we assume a weak coupling between the boundary of the two layers, and study the RG flow of the coupling. Besides the edge state localized at the boundary of a SPT state, we will also consider symmetry protected gapless states localized at a $2d$ interface embedded in a $3d$ bulk. We will demonstrate that in several cases, including the edge state of a prototype bosonic SPT state, the $2d$ boundary or interface will flow to a new fixed point due to the bulk quantum phase transition.

Previous works have explored related ideas with different approaches. Exactly soluble

$1d$ and $2d$ Hamiltonians have been constructed for gapless systems with protected edge states [83]; fate of edge states was also studied for $1d$ and $2d$ SPT states [84, 85, 86, 87, 88]. But the $2d$ edge of $3d$ bosonic SPT systems coupled with boundary modes which originate from bulk quantum critical points, *i.e.* the situation that potentially hosts the richest and most exotic phenomena, have not been studied to our knowledge. We note that the interaction between bulk quantum critical modes and the boundary of free or weakly interacting fermion topological insulator (or topological superconductor) was studied in Ref. [89], but the coupling in that case was strongly irrelevant hence will not lead to new physics in the infrared (we will review the interplay between the bulk quantum critical modes and the edge states of free fermion topological insulator in the next section). We will focus on bosonic SPT state with intrinsic strong interaction in this section. We use the generic long wavelength field theory description of both the bulk bosonic SPT states and the edge states. Due to the lack of exact results of strongly interacting $(2+1)d$ field theories, we seek for a controlled calculation procedure that allows us to identify new fixed points under RG flow. Indeed, in several scenarios we will explore in this section, new fixed points are identified based on controlled calculations.

2.2.2 Edge States of $3d$ SPT at Bulk QCP

Edge states of noninteracting $3d$ TIs

We first consider the edge state of $3d$ topological insulator (TI) and symmetry protected topological states. The edge state of free fermion TI is described by the action

$$\mathcal{S} = \int d^2x d\tau \sum_{\alpha=1}^{N_f} \bar{\psi}_\alpha \gamma_\mu \partial_\mu \psi_\alpha, \tag{2.22}$$

with $\gamma^1 = \sigma^2$, $\gamma^2 = -\sigma^1$, $\gamma^0 = \sigma^3$, $\bar{\psi} = \psi^\dagger \gamma^0$. Based on the "ten-fold way classification" [67, 68, 69], for the AIII class, at the noninteracting level the TI is always nontrivial and topologically different from each other for arbitrary integer$-N_f$; while for the AII class the TI is nontrivial only for odd integer N_f, and they are all topologically equivalent to the simplest case with $N_f = 1$. In both cases the fermion mass term $\sum_\alpha \bar{\psi}_\alpha \psi_\alpha$ is forbidden by the time-reversal symmetry. Hence let us consider the disorder-to-order phase transition in the $3d$ bulk associated with a spontaneous time-reversal symmetry breaking, which is described by an ordinary $(3+1)d$ Landau-Ginzburg quantum Ising theory:

$$\mathcal{S}_b = \int d^3x d\tau \ (\partial\phi)^2 + u\phi^4. \tag{2.23}$$

Because u is a marginally irrelevant coupling at the $(3+1)d$ noninteracting Gaussian fixed point, the scaling dimension of ϕ in the bulk is precisely $[\phi] = 1$.

Here we stress that the disorder-to-order transition is driven by the physics in the bulk. Without the bulk, the boundary alone does not support an ordered phase. To study the fate of the edge state when the bulk is tuned to the quantum critical point, we view the bulk as a "two layer" system (Fig. 2.3): layer-1 is a $3d$ TI which is not tuned to the quantum phase transition; while layer-2 is at the disorder-to-order bulk quantum phase transition between a time-reversal invariant trivial insulator and a spontaneous time-reversal symmetry breaking phase. Now both layers have nontrivial physics at the edge. The quantum critical fluctuation (from layer-2) at the $2d$ boundary must satisfy the boundary scaling law. When we impose the most natural boundary condition $\phi(z \geq 0) = 0$, the leading field at the boundary which carries the same quantum number as ϕ is $\Phi \sim \partial_z \phi$. Since ϕ has scaling dimension 1, Φ should have scaling dimension

$[\Phi] = 2$, *i.e.*

$$\langle \Phi(\mathbf{x}, z=0)\Phi(0, z=0)\rangle \sim 1/|\mathbf{x}|^4, \tag{2.24}$$

where $\mathbf{x} = (\tau, x, y)$. Eq. 2.74 is a much weaker correlation than ϕ in the bulk (more detailed derivation of boundary correlation functions can be found in Ref. [24, 27, 26, 55]).

Now we turn on coupling between the $2d$ boundaries of the two layers. The edge state of the TI in layer-1 is affected by the boundary fluctuations of layer-2 through the "proximity effect". The coupling between the two layers at the $2d$ boundary is described by the following term in the action:

$$\mathcal{S}_c = \int d^2x d\tau \ \sum_\alpha g\Phi\bar{\psi}_\alpha\psi_\alpha. \tag{2.25}$$

Since $\Phi \sim \partial_z\phi$ has scaling dimension 2, g will have scaling dimension $[g] = -1$, *i.e.* it is strongly irrelevant. This conclusion is consistent with previous study Ref. [89]. A negative "mass term" Φ^2 will be generated through the standard fermion loop diagram, but since Φ has scaling dimension 2, this mass term will be irrelevant. Hence the edge state of a $3d$ TI is stable even at the bulk quantum critical point where the time-reversal symmetry is spontaneously broken, and the properties of the edge states (such as electron Green's function) should be identical to the edge state of TI in the infrared. To make the coupling g relevant, the quantum critical modes also need to localize on the boundary, which is one of the situations studied in Ref. [89].

Edge states of bosonic SPT states

The situation of bosonic SPT phases can be much more interesting. The bosonic SPT state can only exist in strongly interacting systems. We use the prototype $3d$ bosonic

SPT phase with $(\mathrm{U}(1)\times\mathrm{U}(1))\times Z_2^T$ symmetry as an example, since this phase can be viewed as the parent state of many $3d$ bosonic SPT phases by breaking the symmetry down to its subgroups, without fully trivializing the SPT phase. The topological feature of this phase can be conveniently captured by the following nonlinear sigma model in the $(3+1)d$ bulk [77, 90]:

$$\mathcal{S}=\int d^3xd\tau\ \frac{1}{g}(\partial\boldsymbol{n})^2+\frac{\mathrm{i}2\pi}{\Omega_4}\epsilon_{abcde}n^a\partial_x n^b\partial_y n^c\partial_z n^d\partial_\tau n^e, \tag{2.26}$$

where $\boldsymbol{n}$ is a five component vector field with unit length, and Ω_4 is the volume of the four dimension sphere with unit radius. (n_1,n_2), and (n_3,n_4) transform as a vector under the two U(1) symmetries respectively, and the Z_2^T changes the sign of all components of the vector $\boldsymbol{n}$. The nonlinear sigma model Eq. 2.26 is invariant under all the transformations.

The $2d$ edge state of this SPT phase can be described by the following $(2+1)d$ action:

$$\begin{aligned}\mathcal{S} &= \int d^2xd\tau\sum_{\alpha=1,2}|(\partial-\mathrm{i}a)z_\alpha|^2+r|z_\alpha|^2+u|z_\alpha|^4\\ &+ \frac{1}{e^2}(\mathrm{d}a)^2,\end{aligned} \tag{2.27}$$

where a_μ is a noncompact U(1) gauge field. The theory Eq. 2.27 is referred to as the "easy-plane noncompact CP^1" (EP-NCCP^1) model. We are most interested in the point $r=0$. The term $\sum_\alpha r|z_\alpha|^2$ would be forbidden if there is an extra Z_2 self-dual symmetry that exchanges the two U(1) symmetries [91], while without the self-duality symmetry r needs to be tuned to zero, and the point $r=0$ becomes the transition point between two ordered phases that spontaneously breaks the two U(1) symmetries respectively [15, 16]. At $r=0$, starting with the UV fixed point with noninteracting z_α and a_μ, both u and e are expected (though not proven) to flow to a fixed point with $u=u_*$, $e=e_*$.

The putative conformal field theory at $r = 0$ and its fate under coupling to the boundary fluctuations (boundary modes) of the bulk quantum critical points is the goal of our study in this section. As was discussed in previous literatures, it is expected that there is an emergent O(4) symmetry in Eq. 2.27 at $r = 0$, when we fully explore all the duality features of Eq. 2.27 [91, 78, 79, 92, 80, 81, 22]. In the EP-NCCP^1 action, the following operators form a vector under O(4):

$$(n_1, n_2, n_3, n_4) \sim (z^\dagger \sigma^1 z,\ z^\dagger \sigma^2 z,\ \mathrm{Re}[\mathcal{M}_a],\ \mathrm{Im}[\mathcal{M}_a]), \tag{2.28}$$

where $\mathcal{M}_a$ is the monopole operator (the operator that annihilates a quantized flux of a_μ). In the equation above, (n_1, n_2) and (n_3, n_4) form vectors under the two U(1) symmetries respectively. The emergent O(4) includes the self-dual Z_2 symmetry of the EP-NCCP^1, *i.e.* the operation that exchanges the two U(1) symmetries.

Now we consider the $3d$ bulk quantum phase transition between the SPT phase and the ordered phases that break part of the defining symmetries of the SPT phase. We first consider two order parameters: ϕ_0, ϕ_3. ϕ_0 is the order parameter that corresponds to the self-dual Z_2 symmetry; and ϕ_3 is a singlet under the emergent SO(4) but odd under the improper rotation of the emergent O(4), and also odd under Z_2^T. Again we view our system as a two layer structure: layer-1 is a SPT phase with solid edge states described by Eq. 2.27; layer-2 is a topological-trivial system that undergoes the transition of condensation of either ϕ_0 or ϕ_3. Both order parameters have an ordinary mean field like transition in the bulk of layer-2. Again at the boundary, both order parameters will have very different scalings from the bulk. We assume that system under study fills the entire semi-infinite space at $z < 0$, then at the boundary plane $z = 0$, the most natural boundary condition is that $\phi_0(z \geq 0) = \phi_3(z \geq 0) = 0$, hence all order parameters near but inside the bulk should be replaced by the following representations: $\Phi_0 \sim \partial_z \phi_0$,

$\Phi_3 \sim \partial_z \phi_3$. Both order parameters have scaling dimensions 2 at the $(2+1)d$ boundary of layer-2.

Now we couple Φ_0 and Φ_3 to the edge states of layer-1. The coupling will take the following form:

$$\mathcal{L}_{c0} = \sum_{\alpha} g_0 \Phi_0 |z_\alpha|^2, \quad \mathcal{L}_{c3} = g_3 \Phi_3 z^\dagger \sigma^3 z. \tag{2.29}$$

The RG flow of coupling constants $g_{0,3}$ can be systematically evaluated in certain large$-N$ generalization of the action in Eq. 2.27:

$$\mathcal{S} \;=\; \int d^2x d\tau \sum_{\alpha=1,2} \sum_{j=1}^{N/2} |(\partial - \mathrm{i}a) z_{j,\alpha}|^2 + u(\sum_j |z_{j,\alpha}|^2)^2. \tag{2.30}$$

The large$-N$ generalization facilitate calculations of the RG flow, but the down side is that the duality structure and emergent symmetries no longer exist for $N > 2$. In the large$-N$ limit of Eq. 2.30, the scaling dimension of the operators under study is

$$N \to +\infty : \quad [z^\dagger \sigma^3 z] = [|z|^2] = 2. \tag{2.31}$$

In the equation above, each operator has a sum of index j, which was not written explicitly. Apparently coupling constants $g_{0,3}$ are both irrelevant with large$-N$ due to the weakened boundary correlation of Φ_0 and Φ_3.

We are seeking for more interesting scenarios when the boundary is driven to a new fixed point due to the bulk quantum criticality. For this purpose we consider another order parameter $\vec{\phi}$ which transforms as a vector under one of the two U(1) symmetries. Here we no longer assume the Z_2 self-dual symmetry on the lattice scale. Again at the boundary $\vec{\phi}$ should be replaced by $\vec{\Phi} \sim \partial_z \vec{\phi}$. At the $2d$ boundary, the coupling between

$\vec{\Phi}$ and the edge state of layer-2 reads

$$\mathcal{L}_{cv} = g_v \left(\Phi_1 z^\dagger \sigma^1 z + \Phi_2 z^\dagger \sigma^2 z \right). \tag{2.32}$$

In the large$-N$ limit of Eq. 2.30, the scaling dimension of the operators under study is

$$N \to +\infty : \quad [z^\dagger \sigma^1 z] = [z^\dagger \sigma^2 z] = 1. \tag{2.33}$$

Hence g_v is marginal in the large$-N$ limit, and there is a chance that g_v could drive the system to a new fixed point with $1/N$ corrections.

We introduce the following action in order to compute the RG flow of g_v with finite but large N:

$$\begin{aligned} \mathcal{S} &= \int d^2x d\tau \sum_{\alpha=1,2} \sum_{j=1}^{N/2} |(\partial - \mathrm{i}a) z_{j,\alpha}|^2 + \mathrm{i}\lambda_+ |z_{j,\alpha}|^2 \\ &+ \mathrm{i}\lambda_- z_j^\dagger \sigma^3 z_j + \mathrm{i} g_v \vec{\Phi} \cdot z_j^\dagger \vec{\sigma} z_j + \frac{1}{2} \vec{\Phi} \cdot \frac{1}{|\partial|} \vec{\Phi}. \end{aligned} \tag{2.34}$$

The $\lambda_\pm$ are two Hubbard-Stratonovich (HS) fields introduced for the standard $1/N$ calculations [93, 94]. The scaling of $|z|^2$ and $z^\dagger \sigma^3 z$ in Eq. 2.30 are replaced by the HS fields λ_+, λ_- in the new action Eq. 4.20 respectively. A coefficient "i" is introduced in the definition of g_v by redefining $\Phi \to \mathrm{i}\Phi$ for convenience of calculation.

The schematic beta function of g_v reads

$$\frac{dg_v}{d\ln l} = (1 - \Delta_v) g_v - B g_v^3 + O(v^5). \tag{2.35}$$

Δ_v is the scaling dimension of $z_j^\dagger \vec{\sigma} z_j$ in the large$-N$ generalization of the EP-NCCP^1

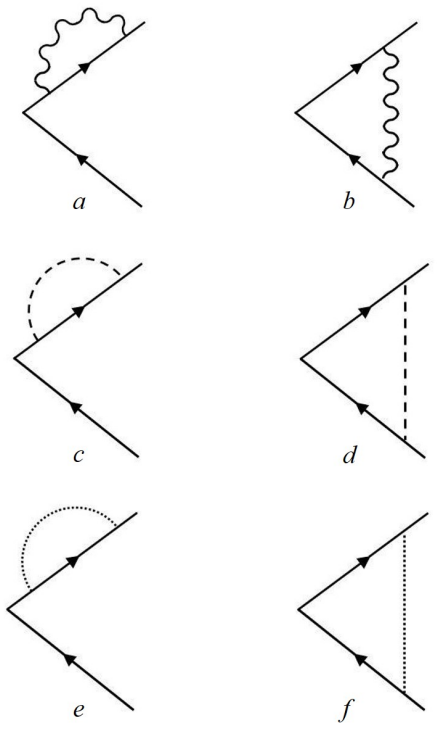

Figure 2.4: (a, b) the $1/N$ contribution to $z^\dagger \sigma^{1,2} z$ and $\bar{\psi}\tau^{1,2}\psi$ from the gauge field fluctuation, the solid lines represent either the propagator of z_α or ψ_α, the wavy line represents the propagator of the photon; (c, d) the $1/N$ contribution to $z^\dagger \vec{\sigma} z$ from $\lambda_\pm$ in Eq. 4.20; (e, f) the contribution to B in Eq. 2.35.

model Eq. 2.30, with $\vec{\sigma} = (\sigma^1, \sigma^2)$. The standard $1/N$ calculation leads to

$$\Delta_v = 1 - \frac{56}{3\pi^2 N} + O(\frac{1}{N^2}). \tag{2.36}$$

The $1/N$ correction of Δ_v comes from diagram Fig. 2.4$(a-d)$, where the wavy line is the gauge boson propagator, and the dashed line represents propagators of both $\lambda_\pm$. The first term of Eq. 2.36 implies that g_v is indeed weakly relevant with finite but large$-N$.

The constant B in the beta function arises from the operator product expansion of the coupling term Eq. 2.32, which is equivalent to the diagrams Fig. 2.4e, f. This computation leads to $B = 1/(3\pi^2)$. The two diagrams in Fig. 2.5 which are also at g_v^3 order cancel each other for arbitrary gauge choices. Similar two-loop diagrams at the

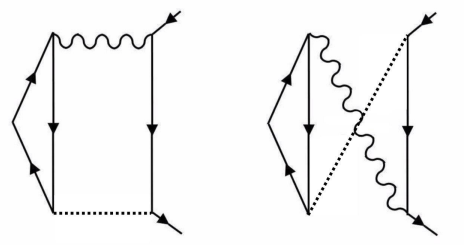

Figure 2.5: The two diagrams at g_v^3 order which cancel each other for arbitrary gauge choices.

same order of $1/N$ do not enter the RG equation due to lack of logarithmic contribution, as was explained in Ref. [94]. $\vec{\Phi}$ does not receive a wave function renormalization due to the singular form of its action. Hence with finite but large$-N$, g_v indeed flows to a new fixed point:

$$g_{v*}^2 = \frac{56}{N} + O(\frac{1}{N^2}). \tag{2.37}$$

We stress that this result is drawn from a controlled calculation and it is valid to the leading order of $1/N$.

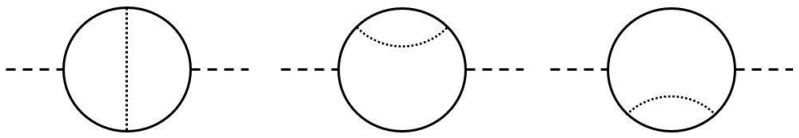

Figure 2.6: The g_v^2 diagrams that contributes to the scaling dimension of $[\lambda_+]$. Here the solid line represents the propagator of $z_{j,\alpha}$, the dotted line represents the vector operator $\vec{\Phi}$, and the dashed line represents λ_+.

As we explained before, the point $r = 0$ is a direct transition between two ordered phases that spontaneously break the two U(1) symmetries. This transition will be driven to a new fixed point by coupling to the boundary fluctuations of bulk critical points as we demonstrated above. At this new fixed point, the critical exponent ν follows from the

relation

$$\nu^{-1} = 3 - [\lambda_+]. \tag{2.38}$$

To evaluate the scaling dimension $[\lambda_+]$ we have to incorporate the contributions of g_v^2 from the diagrams shown in Fig. 2.6, and combined with $1/N$ calculations performed previously [95, 94]. Then in the end we obtain

$$\begin{aligned} \nu_*^{-1} &= 1 + \frac{160}{3\pi^2 N} + \frac{4g_{v*}^2}{3\pi^2} + O(\frac{1}{N^2}) \\ &= 1 + \frac{128}{\pi^2 N} + O(\frac{1}{N^2}). \end{aligned} \tag{2.39}$$

Again, there are other loop diagrams which appear to be at the same order of $1/N$ but do not make any logarithmic contributions [94].

2.2.3 Interface States Embedded in $3d$ bulk

Interface states of noninteracting electron systems

In previous examples we studied topological edge states at the boundary of a $3d$ system. In this section we will consider the $2d$ states localized at an interface ($z = 0$) in a $3d$ space, when the entire $3d$ bulk (for both $z > 0$ and $z < 0$ semi-infinite spaces) undergoes a phase transition simultaneously. Without fine-tuning, we need to assume an extra reflection symmetry $z \to -z$ that connects the two sides of the interface, which guarantees a simultaneous phase transition in the entire system. In this case there is no physical reason to impose the strong boundary condition at the interface embedded in the $3d$ space, hence the quantum critical modes at the interface follow the ordinary bulk scalings, instead of the weakened correlation of boundary CFT.

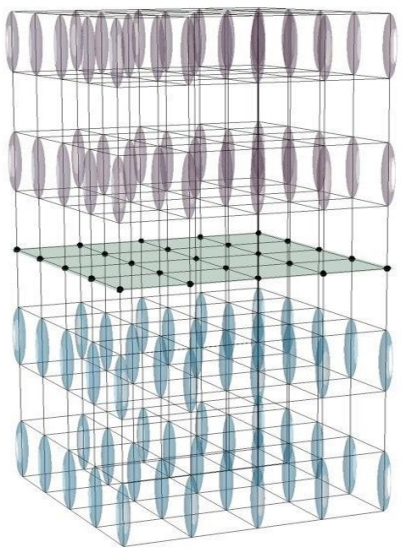

Figure 2.7: We consider a SU(N) antiferromagnet with self-conjugate representation on each site. The system forms a background VBS pattern, with opposite dimerizations between semi-infinite spaces $z > 0$ and $z < 0$. There is a $2d$ antiferromagnet localized at the interface $z = 0$, and the entire bulk can undergo phase transition simultaneously due to the mirror (reflection) symmetry that connects the two sides of the domain wall.

Again we will consider free fermion systems first. Let us first recall that the AIII class TI has a $\mathbb{Z}$ classification which is characterized by a topological index n_T. n_T will appear as the coefficient of the electromagnetic response of the TI: $\mathcal{L} \sim i\pi n_T \mathbf{E} \cdot \mathbf{B}$. n_T must change sign under spatial reflection transformation $\mathcal{M}_z : z \to -z$. To construct the desired system, we assume the semi-infinite space $z < 0$ is occupied with the AIII class TI with Hamiltonian $\hat{H}$, whose topological index is n_T; and its "reflection conjugate" $\mathcal{M}_z^{-1} \hat{H} \mathcal{M}_z$ fills the semi-infinite space $z > 0$. Then there are $N_f = 2n_T$ flavors of massless Dirac fermions localized at the $2d$ plane $z = 0$, which are still protected by time-reversal symmetry. Now we assume the entire bulk undergoes a quantum phase transition with a spontaneous time-reversal symmetry breaking, whose order parameter couples to the

domain wall Dirac fermions as

$$\begin{aligned} \mathcal{S} &= \int d^2x d\tau \sum_{\alpha=1}^{N_f} \bar{\psi}_\alpha \gamma_\mu \partial_\mu \psi_\alpha + g\phi\bar{\psi}_\alpha\psi_\alpha \\ &+ \frac{1}{2}\phi(-\partial^2)^{1/2}\phi. \end{aligned} \tag{2.40}$$

The last term in the action is still defined in the $(2+1)d$ interface, and it reproduces the correlation of ϕ in the bulk: $\langle\phi(0)\phi(r)\rangle \sim 1/r^2$. We stress that, since now the order parameter resides in the entire bulk, ϕ no longer obeys the boundary scaling as we discussed in previous examples. A negative boson mass term $-r\phi^2$ can be generated through the standard fermion mass loop diagram, hence we need to tune an extra term at the interface to make sure the mass term of ϕ vanishes.

In this case the coupling constant g is a marginal perturbation based on simple power-counting. But g will flow under renormalization group (RG) with loop corrections in Fig. 2.4(e, f):

$$\beta(g) = \frac{dg}{d\ln l} = -\frac{2}{3\pi^2}g^3 + O(g^5). \tag{2.41}$$

Hence even in this case, the coupling between the domain wall states and the bulk quantum critical modes is perturbatively marginally irrelevant.

So far we have assumed that the velocity of the interface state is identical with the bulk. Now let us tune the velocity of the domain wall Dirac fermions slightly different, which can be captured by the following term in the Lagrangian:

$$\sum_\alpha \delta\bar{\psi}_\alpha(\gamma^1\partial_x + \gamma^2\partial_y - 2\gamma^3\partial_3)\psi_\alpha. \tag{2.42}$$

δ defined above is an eigenvector under the leading order RG flow. With the loop dia-

grams in Fig. 2.8, we obtain the leading order beta function of δ:

$$\beta(\delta) = \frac{d\delta}{d\ln l} = -\frac{1}{5\pi^2} g^2 \delta. \tag{2.43}$$

Together with $\beta(g)$, the velocity anisotropy is also perturbatively irrelevant.

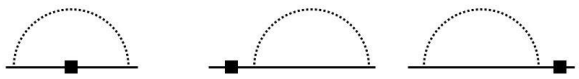

Figure 2.8: The Feynman diagrams that renormalizes the extra velocity δ in Eq. 2.42. The box represents the vertex δ, and all three diagrams contributes to the fermion self-energy and renormalize δ.

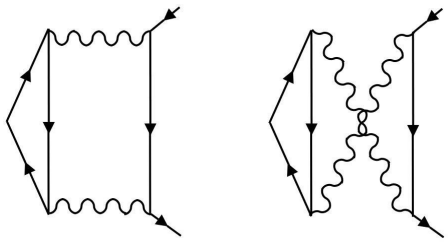

Figure 2.9: The extra diagrams that contribute to the scaling dimension of $\sum_\alpha \bar{\psi}_\alpha \psi_\alpha$ at the leading order of $1/N_f$ in QED_3. Again the wavy lines are photon propagators.

Interface states of quantum antiferromagnet

We now consider a SU(N) quantum antiferromagnet on a tetragonal lattice with a self-conjugate representation on each site (we assume N is an even integer). With large$-N$, an antiferromagentic Heisenberg SU(N) model has a dimerized ground state [96, 97] where the two SU(N) spins on two nearest neighbor sites form a spin singlet (valence bond). We consider the following background configuration of valence bond solid (VBS): the spins form VBS along the $\hat{z}$ direction which spontaneously break the translation symmetry, while there is a domain wall between two opposite dimerizations at the $2d$ XY plane $z = 0$, namely $z = 0$ is still a mirror plane of the system (Fig. 2.7). In each $1d$ chain

along the $\hat{z}$ direction, there is a dangling self-conjugate SU(N) spin localized on the site at the domain wall. Hence the $2d$ domain wall is effectively a SU(N) antiferromagnet on a square lattice.

One state of SU(N) antiferromagnet which is the "parent" state of many orders and topological orders on the square lattice, is the gapless $\pi-$flux U(1) spin liquid [98, 99]. At low energy this spin liquid is described by the following action of $(2+1)d$ quantum electrodynamics (QED_3):

$$\mathcal{S} = \int d^2x d\tau \sum_{\alpha=1}^{N_f} \bar{\psi}_\alpha \gamma_\mu (\partial_\mu - \mathrm{i}a_\mu)\psi_\alpha + \cdots \tag{2.44}$$

ψ_α is $N_f = 2N$ flavors of $2-$component Dirac fermions, and they are the low energy Dirac fermion modes of the slave fermion $f_{j,\alpha}$ defined as $\hat{S}_j^b = f_{j,\alpha}^\dagger T_{\alpha\beta}^b f_{j,\beta}$, T^b with $b = 1 \cdots N^2 - 1$ are the fundamental representation of the SU(N) Lie Algebra. Besides the spin components, there is an extra two dimensional internal space which corresponds to two Dirac points in the Brillouin zone. There is an emergent SU(N_f) flavor symmetry in QED_3 which includes both the SU(N) spin symmetry and discrete lattice symmetry.

It is known that when N_f is greater than a critical integer, the QED_3 is a conformal field theory (CFT). We will consider the fate of this CFT when the three dimensional bulk is driven to a quantum phase transition. We will first consider a disorder-to-order quantum phase transition, where the ordered phase spontaneously breaks the time-reversal and parity symmetry of the XY plane. Notice that due to the reflection symmetry $z \to -z$ of the background VBS configuration, the two sides of the domain wall will reach the quantum critical point simultaneously. The bulk transition is still described by Eq. 2.23. When we couple the Ising order parameter ϕ to the domain wall QED_3, the

total $(2+1)d$ action reads

$$\begin{aligned} \mathcal{S} &= \int d^2x d\tau \sum_{\alpha=1}^{N_f} \bar{\psi}_\alpha \gamma_\mu (\partial_\mu - \mathrm{i}a_\mu)\psi_\alpha \\ &+ g\phi\bar{\psi}_\alpha\psi_\alpha + \frac{1}{2}\phi(-\partial^2)^{1/2}\phi. \end{aligned} \tag{2.45}$$

If the gauge field fluctuation is ignored, or equivalently in the large$-N_f$ limit, the scaling dimension of $\bar{\psi}\psi$ is $[\bar{\psi}\psi] = 2$, and hence the scaling dimension of g is $[g] = 0$, *i.e.* g is a marginal perturbation. The $1/N_f$ correction to the RG flow arises from the Feynman diagrams (Fig. 2.4(a,b) and Fig. 2.9) which involves one or two photon propagators:

$$G^a_{\mu\nu}(\vec{p}) = \frac{16}{N_f p}\left(\delta_{\mu\nu} - \frac{p_\mu p_\nu}{p^2}\right). \tag{2.46}$$

Again in this case the fermions will generate a mass term for the order parameter at the interface, which we need to tune to zero. At the leading order of $1/N_f$ the corrected beta function for g reads

$$\beta(g) = \frac{dg}{d\ln l} = -\frac{128}{3\pi^2 N_f}g - \frac{2}{3\pi^2}g^3 + O(g^3). \tag{2.47}$$

But this beta function does not lead to a new unitary fixed point other than the decoupled fixed point $g = 0$. Hence in this case the domain wall state is decoupled from the bulk quantum critical modes in the infrared limit.

A more interesting scenario is when the bulk undergoes a transition which spontaneously breaks the translation and C_4 rotation symmetry by developing an extra VBS order within the XY plane. The inplane VBS order parameters are $V_x \sim \bar{\psi}\tau^1\psi$, and $V_y \sim \bar{\psi}\tau^2\psi$, where $\tau^{1,2}$ are the Pauli matrices operating in the Dirac valley space. The

coupling between the VBS order parameter and the domain wall QED_3 reads

$$\mathcal{S}_c = \int d^2x d\tau \; g\left(\phi^* \bar{\psi}\tau^- \psi + \phi \bar{\psi}\tau^+ \psi\right) + \phi^*(-\partial^2)^{1/2}\phi. \tag{2.48}$$

Here $\tau^{\pm} = (\tau^1 \pm \mathrm{i}\tau^2)/2$. The scaling dimension of the VBS order parameter at the QED_3 fixed point has been computed previously [99, 100, 101]: $[\bar{\psi}\tau^a\psi] = 2 - 64/(3\pi^2 N_f)$, and the beta function of g to the leading order of $1/N_f$ reads

$$\beta(g) = \frac{64}{3\pi^2 N_f} g - \frac{1}{6\pi^2} g^3 + O(g^3). \tag{2.49}$$

In the large$-N_f$ limit, the coupling g is marginally irrelevant; but with finite and large$-N_f$, g is weakly relevant at the noninteracting fixed point, and it will flow to an interacting fixed point

$$g_*^2 = \frac{128}{N_f} + O(\frac{1}{N_f^2}). \tag{2.50}$$

This new fixed point will break the emergent SU(N_f) flavor symmetry down to SU(N) $\times$ $U(1)$ symmetry, where U(1) corresponds to the rotation of the Dirac valley space. The following gauge invariant operators receive different corrections to their scaling dimensions from coupling to the bulk quantum critical modes:

$$\begin{aligned}
[\bar{\psi}\psi] &= 2 + \frac{128}{3\pi^2 N_f} + \frac{2}{3\pi^2} g_*^2 + O(\frac{1}{N_f^2}); \\
[\bar{\psi}T^b\psi] &= 2 - \frac{64}{3\pi^2 N_f} + \frac{2}{3\pi^2} g_*^2 + O(\frac{1}{N_f^2}); \\
[\bar{\psi}\tau^3\psi] &= 2 - \frac{64}{3\pi^2 N_f} - \frac{1}{3\pi^2} g_*^2 + O(\frac{1}{N_f^2});
\end{aligned}$$

$$[\bar{\psi}\tau^{1,2}\psi] = 2 - \frac{64}{3\pi^2 N_f} + \frac{1}{6\pi^2} g_*^2. \tag{2.51}$$

The operators $\bar{\psi}\tau^{1,2}\psi$ have exactly scaling dimension 2, the Feynman diagram contributions from Fig. 2.4 cancel each other for operator $\bar{\psi}\tau^{1,2}\psi$ as they should. Notice that the last three operators in Eq. 2.51 should have the same scaling dimension in the original QED_3 fixed point due to the large $SU(N_f)$ flavor symmetry, but at this new fixed point they will acquire different corrections.

Another interesting scenario is that the bulk is at a critical point whose order parameter couples to the Ising like operator $\bar{\psi}\tau^3\psi$, which breaks the inplane parity but preserves the time-reversal:

$$\mathcal{S}_c = \int d^2x d\tau \; g\phi\bar{\psi}\tau^3\psi + \frac{1}{2}\phi(-\partial^2)^{1/2}\phi. \tag{2.52}$$

The microsopic representation of the operator $\bar{\psi}\tau^3\psi$ can be found in Ref. [99]. The beta function of the coupling g reads

$$\beta(g) = \frac{64}{3\pi^2 N_f} g - \frac{2}{3\pi^2} g^3 + O(g^3), \tag{2.53}$$

and once again there is new stable fixed point $g_*^2 = 32/N_f + O(1/N_f^2)$. And at this fixed point,

$$\begin{aligned}
[\bar{\psi}\psi] &= 2 + \frac{128}{3\pi^2 N_f} + \frac{2}{3\pi^2} g_*^2 + O(\frac{1}{N_f^2}); \\
[\bar{\psi}T^b\psi] &= 2 - \frac{64}{3\pi^2 N_f} + \frac{2}{3\pi^2} g_*^2 + O(\frac{1}{N_f^2}); \\
[\bar{\psi}\tau^{1,2}\psi] &= 2 - \frac{64}{3\pi^2 N_f} - \frac{1}{3\pi^2} g_*^2 + O(\frac{1}{N_f^2});
\end{aligned}$$

$$[\bar{\psi}\tau^3\psi] \;=\; 2 - \frac{64}{3\pi^2 N_f} + \frac{2}{3\pi^2} g_*^2. \tag{2.54}$$

The domain wall state considered here is formally equivalent to the boundary state of a $3d$ bosonic SPT state with $\mathrm{pSU}(N) \times \mathrm{U}(1)$ symmetry, which can also be embedded to the $3d$ SPT with $\mathrm{pSU}(N_f)$ symmetry discussed in Ref. [102]. This SPT state can be constructed as follows: we first break the U(1) symmetry in the $3d$ bulk by driving the bulk $z < 0$ into a superfluid phase, and then decorate the vortex loop of the superfluid phase with a $1d$ Haldane phase with $\mathrm{pSU}(N)$ symmetry [103, 104, 105, 106]. Eventually we proliferate the decorated vortex loops to restore all the symmetries in the bulk. A $1d$ $\mathrm{pSU}(N)$ Haldane phase can be constructed as a spin-chain with a $\mathrm{pSU}(N)$ spin on each site, and there is a dangling self-conjugate representation of $\mathrm{SU}(N)$ on each end of the chain. And this dangling spin will also exist in the U(1) vortex at the boundary of the $\mathrm{pSU}(N) \times \mathrm{U}(1)$ SPT state. Notice that the self-conjugate representation of $\mathrm{SU}(N)$ is a projective representation of $\mathrm{pSU}(N)$.

2.2.4 Discussion

In this section we systematically studied the interplay of two different nontrivial boundary effects: the $2d$ edge states of $3d$ symmetry protected topological states, and the boundary fluctuations of $3d$ bulk quantum phase transitions. New fixed points were identified through generic field theory descriptions of these systems and controlled calculations. We then generalized our study to the $2d$ states localized at the interface embedded in the $3d$ bulk.

The last case studied in Eq. 2.53, 2.54 is special when $N_f = 2$, and when the gauge field is noncompact. This is the theory that has been shown to be dual to the EP-NCCP^1 model [92, 81] studied in Eq. 2.27, the operator $\sum_\alpha r|z_\alpha|^2$ is dual to $r\bar{\psi}\tau^3\psi$, and both

theories are self-dual. By coupling the operator $\bar{\psi}\tau^3\psi$ to the bulk critical modes (rather than the boundary fluctuations of the bulk critical points), we have shown that this $(2+1)d$ theory is driven to a new fixed point, and the self-duality structure still holds. The self-duality transformation of Eq. 2.27 now is combined with the Ising symmetry of the order parameter ϕ. However, the O(4) emergent symmetry no longer exists at this new fixed point, due to the nonzero fixed point of g in Eq. 2.52.

The methodology used in this section can have many potential extensions. We can apply the same field theory and RG calculation to the $1d$ boundary of $2d$ SPT states (for instance the AKLT state), which was studied through exactly soluble lattice Hamiltonians [83] and also numerical methods [86, 87, 88]. Also, $1d$ defect in a $3d$ topological state can also have gapless modes [107, 108], it would be interesting to investigate the fate of a $1d$ defect embedded in a $3d$ bulk at the bulk quantum phase transition. Defects of free or weakly interacting fermionic topological insulator and topological superconductor coupled with bulk critical modes was studied in Ref. [89], but we expect the defect of an intrinsic strongly interacting topological state can lead to much richer physics. Last but not least, the "higher order topological insulator" has nontrivial modes localized at the corner instead of the boundary of the system [109]. The coupling between the bulk quantum critical points and corner topological modes is also worth exploration.

2.3 Continuous Néel-VBS Quantum Phase Transition in Non-Local one-dimensional systems with SO(3) Symmetry

Our understanding of one dimensional ($1d$) quantum many-body systems with local Hamiltonians is far more complete compared with higher dimensional systems, since

many powerful analytical methods such as Bethe ansatz [110], Virasoro algebra [111], etc. are applicable only to $1d$ systems (or $(1+1)d$ space-time). We also understand that $1d$ systems have many unique features that are fundamentally different from higher dimensions. For example, with local Hamiltonians, generally there can not be spontaneous continuous symmetry breaking in $(1+1)d$ even at zero temperature (with exceptions of the scenarios when a fully polarized ferromagnet is the exact ground state), the closest one can possibly get is a quasi-long range power-law correlation of order parameters that transform nontrivially under a continuous symmetry. There is also no topological order in $1d$ systems analogous to fractional quantum Hall states which have a gap and simultaneously ground state topological degeneracy [42]. This means that many phenomena that are found in higher dimensions do not occur in $1d$ systems.

To seek for richer physics in one dimensional systems, we need to explore beyond the restriction of local Hamiltonians. One way to get around this restriction is to consider $1d$ systems at the boundary of a $2d$ systems, and drive the $2d$ bulk to a quantum phase transition. The physics becomes especially interesting when the disordered phase in the phase diagram of the $2d$ bulk is a symmetry protected topological (SPT) phase, which already has topologically protected $1d$ edge state. The interplay between the topological edge state and gapless quantum critical modes can lead to very nontrivial physics, which has been studied through numerical methods recently [112, 113, 87, 88]. One can also directly turn on nonlocal spatial interaction in a $1d$ Hamiltonian. $1d$ quantum spin chains with nonlocal spatial interactions have also been studied recently, and very intriguing physics was found [114, 115]. We will discuss the results of these numerical works later in this section.

In this section we investigate the $2d$ SPT state protected by symmetry $\mathrm{SO}(3) \times G$, where $\mathrm{SO}(3)$ is the ordinary spin symmetry, while G is a discrete symmetry, which could be an onsite unitary Z_2 symmetry, or an anti-unitary time-reversal Z_2^T. G can also be a

lattice symmetry such as translation by one lattice constant. For example, when G is the translation along the $\hat{x}$ axis (T_x), this state can be realized as the Affleck-Kennedy-Lieb-Tasaki (AKLT) state of the spin-2 system on a $2d$ square lattice [116]. In the example of spin-2 AKLT state, there is a chain of dangling spin-1/2 at the boundary of the system, as long as the boundary is along the $\hat{x}$ axis and preserves the translation symmetry T_x. The nature of the SPT states, and the Lieb-Shultz-Mattis (LSM) theorem [117, 118, 119] guarantee that this boundary system cannot be trivially gapped, *i.e.* it must be either gapless, or gapped but degenerate (For a closed $1d$ system without $0d$ boundaries, a generic ground state degeneracy can only originate from spontaneous discrete symmetry breaking [42]). In this section we will take the AKLT state as an example, but our results can be straightforwardly generalized to other discrete symmetries G.

Our study will mainly focus on the $1d$ boundary of strongly interacting $2d$ bosonic SPT phases, using a controlled renormalization group method. We would like to mention that previous literature has discussed the coupling between quantum criticality and topologically localized gapless states in various fermionic topological insulators [89]; other approaches such as constructing soluble models and various numerical methods have also been used to study edge states of interacting SPT states at a bulk quantum criticality [83, 84, 85]. Our main finding is that there is a generic continuous quantum phase transition between a long range antiferromagnetic Néel order which spontaneously breaks the SO(3) spin symmetry, and a valence bond solid state, at the $1d$ boundary of an AKLT state that couples to the bulk quantum critical modes. The bulk quantum critical modes effectively yield nonlocal interactions at the $1d$ boundary, which makes the long range Néel order possible.

In principle the $1d$ boundary of this AKLT state should be effectively described by

an extended Heisenberg model

$$H = \sum_j J\vec{S}_j \cdot \vec{S}_{j+1} + \cdots \tag{2.55}$$

where $\vec{S}_j$ is the spin-1/2 operator, and the ellipsis includes other possible terms allowed by $\mathrm{SO}(3) \times T_x$. The ground state of Eq. 2.55 depends on the entire lattice Hamiltonian. But a useful starting point of analyzing this boundary system is the $\mathrm{SU}(2)_1$ conformal field theory (CFT) described by the following Hamiltonian in the infrared limit:

$$H_0 = \int dx \, \frac{1}{3 \cdot 2\pi} \left(\vec{J}_L \cdot \vec{J}_L + \vec{J}_R \cdot \vec{J}_R \right). \tag{2.56}$$

The $\mathrm{SU}(2)_1$ CFT has a larger symmetry than the lattice Hamiltonian Eq. 2.56, since $\vec{J}_L$ and $\vec{J}_R$ generate the $\mathrm{SU}(2)_{L,R}$ symmetries for the left and right chiral modes respectively. The relation between the microscopic operator $\vec{S}$ and the low energy field is [120]

$$\vec{S}(x) \sim \frac{1}{2\pi} \left(\vec{J}_L(x) + \vec{J}_R(x) \right) + (-1)^x \vec{n}(x), \tag{2.57}$$

where $\vec{n}(x)$ is the Néel order parameter at the boundary. $\vec{J}_{L,R}$ both have scaling dimension $+1$ at the $\mathrm{SU}(2)_1$ CFT fixed point, while $\vec{n}(x)$ has scaling dimension $1/2$ at the $\mathrm{SU}(2)_1$ CFT.

The diagonal SU(2) symmetry (simultaneous SU(2) rotation between the left and right modes) corresponds to the original SO(3) spin symmetry on the lattice scale. And because the lattice Hamiltonian has a lower symmetry than the infrared theory Eq. 2.56, another term is allowed in the low energy Hamiltonian:

$$H_1 = \int dx \, \lambda \vec{J}_L \cdot \vec{J}_R. \tag{2.58}$$

Since $\vec{J}_{L,R}$ have scaling dimension +1, power-counting indicates the coefficient λ has scaling dimension 0. Depending on the sign of λ, this term can be either marginally relevant or marginally irrelevant. When λ is negative and marginally irrelevant the system flows back to the $\mathrm{SU}(2)_1$ CFT with an enlarged $\mathrm{SU}(2)_L \times \mathrm{SU}(2)_R$ symmetry. When this term is positive and marginally relevant, it will flow to infinite (nonperturbative) and generate a mass gap, which based on the nature of the SPT phase would imply that the system spontaneously breaks the discrete symmetry G. For example, when this system is realized as the AKLT state, and G is the translation T_x, the LSM theorem demands that when the boundary of the system generates a mass gap, it spontaneously breaks the translation symmetry and develops a nonzero expectation value of a dimerized valence bond solid (VBS) order: $v \sim (-1)^j \vec{S}_j \cdot \vec{S}_{j+1}$. As a side-note, we emphasize that the state we are studying here is different from the SO(3) or SU(2) SPT state defined through the group cohomology of SO(3) or SU(2) [43, 44, 121], since in those states the symmetry acts chirally, *i.e.* it only acts on either the left or right modes. While in our case the spin symmetry acts on both the left and right modes of the $1d$ boundary, and another discrete symmetry such as translation is demanded.

Our goal is to study the edge states when the bulk undergoes a disorder-order quantum phase transition, and the disordered phase of the bulk phase diagram is the AKLT state. The quantum critical fluctuation in the bulk may affect the edge of the AKLT state. To study the interplay between the topologically protected edge states, and the quantum critical modes, we adopt the "two layer" picture used in Ref. [122]: in layer-1, the system remains a gapped AKLT state in the bulk with solid edge states described by Eq. 2.55 and Eq. 2.56; in layer-2 the system undergoes a phase transition between an ordinary *trivial* disordered phase and an ordered phase. These two systems are glued together at the boundary. We have used the common wisdom that the transition between the SPT phase and the ordered phase is generically in the same universality class as the

transition between an ordinary disordered phase and an ordered phase [1]. We will discuss two kinds of ordered phases: an SO(3) antiferromagnetic order, and an Ising-like VBS order that spontaneously breaks T_x, assuming the boundary is at $y = 0$. In the bulk the two disorder-order transitions under discussion correspond to the three dimensional ($3D$) SO(3) and Ising Wilson-Fisher transitions respectively, which can be studied through a standard $\epsilon = 4 - D$ expansion, where $D = 2 + 1$ is the space-time dimension in the bulk. We only extend the bulk dimensionality of layer-2 to $3 - \epsilon$ spatial dimensions, while the layer-1 still has a two-dimensional bulk and one-dimensional boundary.

We denote the bulk SO(3) antiferromagnetic order parameter, and the Ising-VBS order parameter in layer-2 as $\vec{\phi}$ and ϕ respectively, which should couple to the Néel order parameter $\vec{n}$ and the VBS order parameter v at the boundary theory of layer-1, and this coupling could lead to new physics in the infrared. However, $\vec{\phi}$ and ϕ do not directly couple to $\vec{n}$ and v due to the boundary condition of the Wilson-Fisher fixed point. Assuming the boundary of the $2d$ system is at $y = 0$, the most natural boundary condition for fields $\vec{\phi}, \phi$ would be $\vec{\phi}(y = 0) = \phi(y = 0) = 0$ [2]. Then the leading nonvanishing boundary fields with the same quantum number as $\vec{\phi}$ and ϕ are $\vec{\Phi} \sim \partial_y \vec{\phi}$ and $\Phi \sim \partial_y \phi$ [24].

The SO(3) order parameter $\vec{\phi}$ and the Ising order parameter ϕ will not become critical simultaneously without fine-tuning, but they can be treated in the same framework. The boundary quantum critical modes $\vec{\Phi}$ and Φ couple to the fields at the boundary of layer-1

[1] This statement can be inferred based on the observation that, the topological effects of many of the SPT states can be captured by a nonlinear Sigma model plus a topological $\Theta-$term at $\Theta = 2\pi$ [77, 102]. The $\Theta = 2\pi$ topological term reduces precisely to a boundary term, and we do not expect this topological term to change the bulk universality class.

[2] This boundary condition corresponds to the "ordinary transition" in the standard boundary criticality literatures; other possibilities can also occur such as special and extraordinary boundary transitions [24].

through the following terms in the action

$$\begin{aligned}\mathcal{S} &= \int d^2\mathbf{x}\ g_n\vec{\Phi}(\mathbf{x})\cdot\vec{n}(\mathbf{x}) + g_v\Phi(\mathbf{x})v(\mathbf{x}) \\ &+ \int d^2\mathbf{x}d^2\mathbf{x}'\ \frac{1}{2}\Phi^a(\mathbf{x})C_n^{-1}(\mathbf{x},\mathbf{x}')_{ab}\Phi^b(\mathbf{x}') \\ &+ \int d^2\mathbf{x}d^2\mathbf{x}'\ \frac{1}{2}\Phi(\mathbf{x})C_v^{-1}(\mathbf{x},\mathbf{x}')\Phi(\mathbf{x}'),\end{aligned} \tag{2.59}$$

where $\mathbf{x} = (x,\tau)$ is the space-time coordinate. $C_n(\mathbf{x},\mathbf{x}')_{ab}$ and $C_v(\mathbf{x},\mathbf{x}')$ are the normalized correlation functions of Φ^a and Φ at the boundary:

$$\begin{aligned}C_n(\mathbf{x},0)_{ab} &= \langle\Phi^a(x,\tau)\Phi^b(0,0)\rangle = \frac{\delta_{ab}}{(x^2+\tau^2)^{3/2-\epsilon_n}}, \\ C_v(\mathbf{x},0) &= \langle\Phi(x,\tau)\Phi(0,0)\rangle = \frac{1}{(x^2+\tau^2)^{3/2-\epsilon_v}}.\end{aligned} \tag{2.60}$$

The scaling dimension of $\vec{\Phi}$ and Φ is $\Delta_n = D/2-\epsilon_n+O(\epsilon^2)$ and $\Delta_v = D/2-\epsilon_v+O(\epsilon^2)$, where $D=3$ is the bulk space-time dimension. $\epsilon_{n/v}$ can be computed again through the $\epsilon = (4-D)$ expansion, following the calculation of boundary criticality of the Wilson-Fisher fixed points [24, 27, 26, 55, 31]: for an O(N) Wilson-Fisher fixed point in the bulk, the scaling dimension of the boundary modes of the order parameter is

$$\Delta_{\mathrm{O}(N)} = \frac{D}{2} - \frac{N+2}{2(N+8)}\epsilon + O(\epsilon^2). \tag{2.61}$$

In our case $\epsilon_{n/v} = \epsilon(N+2)/(2(N+8))$ with $N=3,1$ respectively. We again stress that the ϵ dimensionality was introduced for layer-2 only. The effective action of $\vec{\Phi}$ and Φ in Eq. 2.59 already received leading order correction from the $\epsilon-$expansion due to the self-interaction of the bulk critical modes. These effective actions can in principle receive

further corrections from the g_v and g_n couplings with the boundary fields $\vec{n}$ and v, but this correction should be at least at the order of g_n^2, g_v^2, which will be at higher order of $\epsilon-$expansion. As we can see later, the main physics we will discuss is at the vicinity of a fixed point where $g_n, g_v \sim \epsilon$.

Eq. 2.56, 2.58, 2.59 together can be viewed as an effective non-local $1d$ theory, and this theory will be the starting point of our discussion hereafter. Considering the fact that the scaling dimension of both the Néel and VBS order parameter at the $\mathrm{SU}(2)_1$ CFT is 1/2, to the leading order of ϵ expansion, the scaling dimensions of the coupling constants must be

$$\Delta_{g_n} = \epsilon_n + O(\epsilon^2), \quad \Delta_{g_v} = \epsilon_v + O(\epsilon^2)$$

$$\epsilon_n = \frac{5}{22}\epsilon, \quad \epsilon_v = \frac{1}{6}\epsilon. \tag{2.62}$$

$g_{n/v}$ are hence weakly relevant assuming a small parameter ϵ. Hence the $\mathrm{SU}(2)_1$ CFT at the boundary of the AKLT state will be unstable against coupling to the quantum critical modes, while fortunately due to the weak relevance of the coupling constants, this effect can be studied perturbatively.

To proceed we need to compute the coupled renormalization group (RG) flow of λ and $g_{n/v}$ in Eq. 2.58 and Eq. 2.59. The RG equations can be derived based on the following operator product expansion (OPE):

$$J_L^a(z) n^b(w,\bar{w}) \sim \frac{1}{2}\frac{1}{z-w}\left(\mathrm{i}\delta_{ab} v(w,\bar{w}) + \mathrm{i}\epsilon_{abc} n^c(w,\bar{w})\right),$$

$$J_R^a(\bar{z}) n^b(w,\bar{w}) \sim \frac{1}{2}\frac{1}{\bar{z}-\bar{w}}\left(-\mathrm{i}\delta_{ab} v(w,\bar{w}) + \mathrm{i}\epsilon_{abc} n^c(w,\bar{w})\right),$$

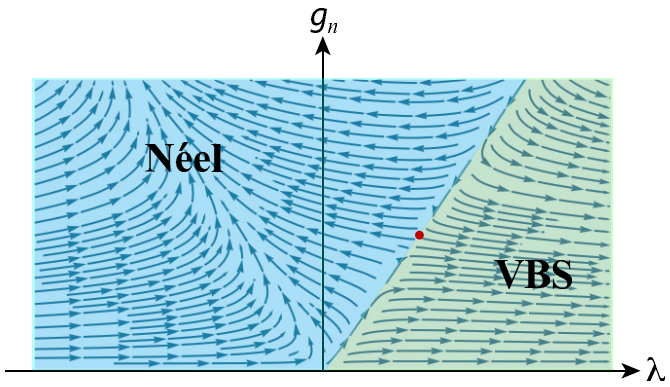

Figure 2.10: The coupled RG flow of λ and g_n based on Eq. 2.65. A new fixed point $(\lambda^*, g_n^*) = (\frac{2\epsilon_n}{\pi}, \frac{4\epsilon_n}{\pi})$ is found, which separates two phases: the phase where $\lambda \to +\infty$ is the VBS phase, and the phase with $(\lambda, g_n) \to (-\infty, +\infty)$ is the long range Néel order at the $1d$ boundary. But on the Néel order side of the phase diagram, the RG flow is complicated and nonmonotonic, hence it may take a long RG scale, or a large system size to finally reveal the true long range order.

$$J_L^a(z)v(w,\bar{w}) \sim -\frac{1}{2}\frac{\mathrm{i}}{z-w}n^a(w,\bar{w}),$$

$$J_R^a(\bar{z})v(w,\bar{w}) \sim \frac{1}{2}\frac{\mathrm{i}}{\bar{z}-\bar{w}}n^a(w,\bar{w}).$$

$$\left(\sum_a n^a(z,\bar{z})\Phi^a(z,\bar{z})\right)\left(\sum_b n^b(w,\bar{w})\Phi^b(w,\bar{w})\right)$$

$$\sim \frac{3}{2}\frac{1}{|z-w|^4} + \frac{1}{2}\frac{1}{|z-w|^2}\sum_{a=1,2,3} J_L^a(w)J_R^a(\bar{w}),$$

$$+ \frac{3}{4}\frac{1}{(\bar{z}-\bar{w})^2}T_L(w) + \frac{3}{4}\frac{1}{(z-w)^2}T_R(\bar{w}) + ...,$$

$$(v(z,\bar{z})\Phi(z,\bar{z}))\,(v(w,\bar{w})\Phi(w,\bar{w}))$$

$$\sim \frac{1}{2}\frac{1}{|z-w|^4} - \frac{1}{2}\frac{1}{|z-w|^2}\sum_{a=1,2,3} J_L^a(w)J_R^a(\bar{w})$$

$$+\frac{1}{4}\frac{1}{(\bar{z}-\bar{w})^2}T_L(w)+\frac{1}{4}\frac{1}{(z-w)^2}T_R(\bar{w})+...,$$

$$\left(\sum_{a=1,2,3}J_L^a(z)J_R^a(\bar{z})\right)\left(\sum_{b=1,2,3}J_L^b(w)J_R^b(\bar{w})\right)$$
$$\sim\frac{3}{4}\frac{1}{|z-w|^4}-\frac{2}{|z-w|^2}\sum_{a=1,2,3}J_L^a(w)J_R^a(\bar{w})$$
$$+\frac{3}{2}\frac{1}{(\bar{z}-\bar{w})^2}T_L(w)+\frac{3}{2}\frac{1}{(z-w)^2}T_R(\bar{w})+... \tag{2.63}$$

In these equations, z and w are the chiral coordinates ($z=\tau+\mathrm{i}x$); and the ellipsis contains less singular terms of the OPEs. The fields $T_{L/R}$ are the energy-momentum tensor of the left and right movers, which are given via the Suguwara construction by $T_L=\frac{1}{3}\sum_a :J_L^aJ_L^a:$ and $T_R=\frac{1}{3}\sum_a :J_R^aJ_R^a:$. Notice the form of energy-momentum tensors is similar to the Hamiltonian Eq. 2.56 but with an extra factor of 2π. The OPEs above involving the fields Φ^a and Φ are derived to the leading order of $\epsilon_{n/v}$.

These OPEs are sufficient to derive the desired RG equations to the second order of the coupling constants. For example, using the first two lines of Eq. 2.63, we can derive another set of secondary OPEs:

$$\left(\sum_{a=1,2,3}J_L^a(z)J_R^a(\bar{z})\right)\left(\sum_b n^b(w,\bar{w})\Phi^b(w,\bar{w})\right)$$
$$\sim\frac{1}{4}\frac{1}{|z-w|^2}\left(\sum_b n^b(w,\bar{w})\Phi^b(w,\bar{w})\right),$$

$$\left(\sum_{a=1,2,3} J_L^a(z) J_R^a(\bar{z})\right) (v(w,\bar{w})\Phi(w,\bar{w}))$$

$$\sim -\frac{3}{4}\frac{1}{|z-w|^2}\left(v(w,\bar{w})\Phi(w,\bar{w})\right). \tag{2.64}$$

The coupled RG equations (beta functions) for λ and $g_{n/v}$ then read

$$\begin{aligned}
\beta(\lambda) = \frac{d\lambda}{d\ln l} &= 2\pi\lambda^2 - \frac{\pi}{2}g_n^2 + \frac{\pi}{2}g_v^2, \\
\beta(g_n) = \frac{dg_n}{d\ln l} &= \epsilon_n g_n - \frac{\pi}{2}\lambda g_n, \\
\beta(g_v) = \frac{dg_v}{d\ln l} &= \epsilon_v g_v + \frac{3\pi}{2}\lambda g_v.
\end{aligned} \tag{2.65}$$

These RG equations are valid as long as we restrict our analysis to the parameter region with $\lambda, g_n, g_v \sim \epsilon$, since every term in the RG equations Eq. 2.65 would be at the same order of ϵ^2.

As we explained before, there is no general reason for $\vec{\phi}, \phi$ to become critical simultaneously in the bulk. Hence let us ignore the Φ field first, and consider the coupled RG equation for λ, g_n only. If there is no bulk quantum critical modes, an initial positive value $\lambda = \lambda_0$ will be marginally relevant, and open up an energy gap when it flows to positive infinite. According to the LSM theorem, and the nature of the SPT state, this $1d$ boundary cannot be trivially gapped, hence a nonperturbative positive λ would drive the system into an SO(3) invariant VBS state with spontaneous symmetry breaking of translation symmetry T_x. But by coupling to the boundary modes $\vec{\Phi}$ of quantum critical fluctuation, the beta functions have an new unstable fixed point at

$$(\lambda^*, g_n^*) = \left(\frac{2\epsilon_n}{\pi},\ \frac{4\epsilon_n}{\pi}\right). \tag{2.66}$$

The two eigenvectors of RG flow expanded at the new fixed point have scaling dimensions $(8.9\epsilon_n, -0.89\epsilon_n)$.

Of course the RG analysis above is only at the leading nontrivial order of $\epsilon-$expansion, and at this order of accuracy, no other fixed point is found in the phase diagram. The new fixed point found above separates two phases: phase I where λ flows to positive infinity, and phase II where λ and g_n flow to negative and positive infinity respectively. Then both phases no longer have scaling invariance, so both phases should have certain long range order considering the fact that there is no topological order in one dimension [42]. Phase I with $\lambda \to +\infty$ is the dimerized VBS phase as we discussed before; phase II with $(\lambda, g_n) \to (-\infty, +\infty)$ should be a Néel ordered phase, *i.e.* the $1d$ boundary can develop the Néel order before the bulk, even though the bulk is still at a quantum critical point. A negative λ would enhance the correlation of the Néel order parameter, and after integrating out $\vec{\Phi}$, a long range interaction proportional g^2 would be generated between the Néel order parameters. Hence the infrared limits $\lambda \to -\infty$ and $g \to +\infty$ of phase II both favor the long range Néel order.

The correlation length critical exponent ν of this Néel-VBS transition is $\nu \sim 1/(8.9\epsilon_n)$. At the transition point $(\lambda^*, g_n^*) = (2\epsilon_n/\pi, 4\epsilon_n/\pi)$, the scaling dimensions of the Néel and VBS order parameters can again be computed to the leading order of $\epsilon-$expansion:

$$\begin{aligned} \Delta_{\vec{n}} &= \frac{1}{2} + \frac{\pi\lambda^*}{2} = \frac{1}{2} + \epsilon_n, \\ \Delta_v &= \frac{1}{2} - \frac{3\pi\lambda^*}{2} = \frac{1}{2} - 3\epsilon_n. \end{aligned} \tag{2.67}$$

One can see that compared with the $\mathrm{SU}(2)_1$ CFT, the Néel order correlation is suppressed while the VBS order correlation is enhanced at the new transition fixed point, since $\lambda^* > 0$. This also implies that this Néel-VBS transition has no enlarged symmetry of

$\mathrm{SU}(2)_L \times \mathrm{SU}(2)_R$. An enlarged $\mathrm{SU}(2)_L \times \mathrm{SU}(2)_R \sim \mathrm{SO}(4)$ symmetry would guarantee that the Néel and VBS order parameters have the same scaling dimension, because $(\vec{n}, v)$ transform as a vector under SO(4). Many previous studies suggest that at an unconventional quantum critical point between two phases with different spontaneous symmetry breaking, an enlarged emergent symmetry in the infrared is often expected due to a series of dualities [78, 80, 79, 81, 92, 22, 123]. But in our current case we expect the infrared symmetry at the Néel-VBS transition is still the microscopic symmetry $\mathrm{SO}(3) \times G$.

As we mentioned before, suppose we integrate out the field $\vec{\Phi}$ in Eq. 2.59, a long range interaction in space-time will be generated between the Néel order parameter. The scenario is similar to the spin-1/2 chain with a long range spin-spin interaction, the only difference is that in the latter case the long range interaction is instantaneous and only nonlocal in space. Recently a direct transition between the Néel and VBS order was found in a spin-1/2 chain with nonlocal two-spin interaction and local four-spin interaction [114, 115]. It was found numerically that at the direct Néel-VBS transition the scaling dimension of the Néel order parameter is greater than the VBS order parameter, which is fundamentally different from the $\mathrm{SU}(2)_1$ CFT, but consistent with our RG calculations Eq. 4.9. We also note that a previous RG analysis was performed for $1d$ spin-1/2 system with an instantaneous nonlocal spin interaction, but the Néel-VBS transition was not found therein. Instead the previous analysis identified a transition between the true long range Néel order and a quasi-long range order at the parameter region $\epsilon_n < 0$ and $\lambda < 0$ with our notation [124].

So far we have assumed that the fields $\vec{n}, v$ and $\vec{\Phi}, \Phi$ have the same velocity in our effective $1d$ theory Eq. 2.59, hence the theory we considered so far has a Lorentz invariance. We can also turn on a weak velocity difference between these two sets of fields, and analyze how it flows under RG. This velocity anisotropy corresponds to modifying

the correlation function of $\vec{\Phi}$:

$$C_n(\mathbf{x},0)_{ab} = \langle \Phi^a(x,\tau)\Phi^b(0,0)\rangle$$

$$= \frac{\delta_{ab}}{\left((1-\frac{\delta v}{2})^2 x^2 + (1+\frac{\delta v}{2})^2\tau^2\right)^{3/2}}. \tag{2.68}$$

Here we have assumed that the velocity of $\vec{\Phi}$ exceeds the velocity of $\vec{n}$ by a factor of $(1+\delta v)$ (to the first order of δv). We have taken $\epsilon_n = 0$ for the leading order calculation. δv can flow under RG as it is the "seed" for velocity difference. Based on symmetry, the RG flow of δv should look like

$$\frac{d\delta v}{d\ln l} = -\alpha g_n^2 \delta v. \tag{2.69}$$

And eventually we will plug in the fixed point value of $g_n = g_n^*$. Based on previous experience, at an interacting fixed point, a weak velocity anisotropy is often irrelevant [99, 125], since intuitively in the infrared all the interacting modes are expected to have the same velocity. Hence we expect $\alpha > 0$, *i.e.* a weak velocity difference between the boundary and bulk will be irrelevant at the Néel-VBS transition fixed point.

To evaluate α, we expand the correlation function of $\vec{\Phi}$ to the leading order of δv:

$$C_n(\mathbf{x},0) = \frac{1}{|z|^3} - \frac{3}{2}\frac{\delta v}{|z|^5}\frac{z^2+\bar{z}^2}{2} + O(\delta v^2) \tag{2.70}$$

Using the OPEs in Eq. 2.64, the second order perturabtion of g_n would generate the following term:

$$-\frac{1}{2}\, g_n^2 \left(\sum_a n^a(z,\bar{z})\Phi^a(z,\bar{z})\right)\left(\sum_b n^b(w,\bar{w})\Phi^b(w,\bar{w})\right)$$

$$\sim -\frac{3g_n^2}{4|z-w|^4} - g_n^2\frac{1}{4}\frac{1}{|z-w|^2}\sum_{a=1,2,3} J_L^a(w)J_R^a(\bar{w})$$

$$+ g_n^2\delta v\frac{9}{32}\frac{1}{|z-w|^2}\left(T_L(w)+T_R(\bar{w})\right)+\cdots \tag{2.71}$$

Here we only kept the terms that will lead to nonzero effect under real space RG. The last term in Eq. 2.71 would contribute a renormalization (or acceleration) for the velocity of $\vec{n}$. Under rescaling, the ratio between the two velocities reduces by a factor:

$$1+\delta v \to \frac{1+\delta v}{1+g_n^2\delta v\frac{9\pi^2}{8}\ln l}, \tag{2.72}$$

which leads to the RG equation for δv:

$$\frac{d\delta v}{d\ln l} = -\frac{9\pi^2}{8}(g_n^*)^2\delta v, \tag{2.73}$$

which confirms our expectation that δv is an irrelevant perturbation at the Néel-VBS transition fixed point.

Suppose we start with $\delta v > 0$, namely the velocity of $\vec{n}$ is smaller than $\vec{\Phi}$, the velocity of $\vec{n}$ will increase under RG. This means that in this case the system will qualitatively behave like $z < 1$, where z is the dynamic critical exponent (not to confuse with the chiral coordinate). On the contrary, if we start with $\delta v < 0$, the velocity of $\vec{n}$ would decrease under RG, which means that effectively $z > 1$. The former scenario is analogous to a spin chain with instantaneous spatial nonlocal interaction [115], which is equivalent to taking the velocity of the effective action of $\vec{\Phi}$ and Φ to infinity in our effective $1d$ theory Eq. 2.59. Although our calculation is for $\delta v > 0$, rather than taking the velocity in the $\vec{\Phi}$ action to be infinity, the "acceleration" of the modes derived here (including $z < 0$) is qualitatively consistent with what was observed in Ref. [115] at the Néel-VBS transition

in a spin-1/2 chain with nonlocal spatial interactions.

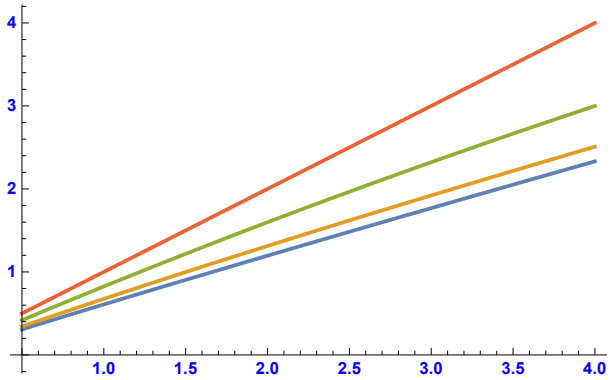

Figure 2.11: The plot of $\ln[3\pi G_n(\mathbf{k})(1 + A(g_n^{*\prime})^2)]$ against $\ln[1/|\mathbf{k}|]$, where $G_n(\mathbf{k})$ is given by Eq. 2.74. From top to bottom, $A(g_n^{*\prime})^2 = 0, 1/2, 2$, and 5.

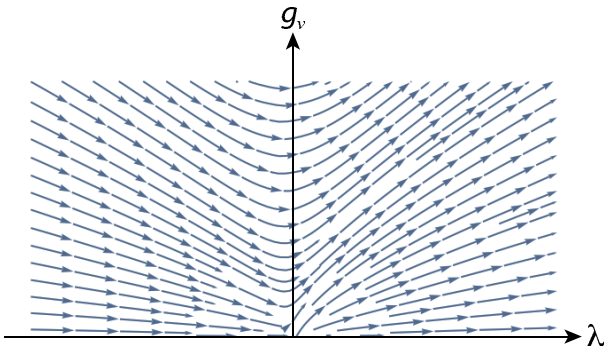

Figure 2.12: The RG flow of (λ, g_v). As long as the initial value g_v is nonzero, both parameters will flow to positive infinity, which implies that the boundary will likely develop the Ising-VBS order before the bulk.

In the phase diagram Fig. 2.10, on the side of the Néel order, the path of the RG flow towards the long range order can be complicated. It may take a long RG scale and hence large system size to reveal the true long range order. For example, on part of the phase diagram, λ changes its sign and eventually flow away to the negative nonperturbative regime. While λ changes sign, g_n first decreases its magnitude from the initial value g_0, then after reaching its minimum $g_n^{*\prime}$ along the RG flow, g_n keeps increasing and eventually become nonperturbative. Hence it is possible that for a relatively large intermediate scale, the system behaves like $g_n \sim g_n^{*\prime}$. The effect of this nonmonotonic RG flow can be

illustrated by a simple perturbation theory to the correlation function of the Néel order parameter:

$$\begin{aligned} & G_n(\mathbf{x}) = \langle \vec{n}(\mathbf{x}) \cdot \vec{n}(0) \rangle \\ \sim \quad & \frac{3}{2}\frac{1}{|\mathbf{x}|} + \frac{3}{4}\int d^2\mathbf{x}_1 d^2\mathbf{x}_2 \frac{(g_n^{*\prime})^2}{|\mathbf{x}-\mathbf{x}_1||\mathbf{x}_1-\mathbf{x}_2|^{3-2\epsilon_n}|\mathbf{x}_2|} \\ + \quad & O(g_n^{*\prime})^4 + \cdots . \end{aligned} \tag{2.74}$$

Hence $G_n(\mathbf{k})$ in the momentum-frequency space $\mathbf{k} = (k, \omega)$ reads

$$G_n(\mathbf{k}) \sim \frac{1}{G^{(0)}(\mathbf{k})^{-1} - \Sigma(\mathbf{k})}, \tag{2.75}$$

where $G^{(0)}(\mathbf{k}) = 3\pi/|\mathbf{k}|$, $\Sigma(\mathbf{k}) = -A(g_n^{*\prime})^2|\mathbf{k}|^{1-2\epsilon_n}/(3\pi)$, and $A > 0$ for $0 < \epsilon_n < 1/2$. The system will have enhanced spin-spin correlation function compared with the $\mathrm{SU}(2)_1$ CFT of the spin-1/2 chain, as was observed in numerical simulations [112, 87, 88]. The mixture of the two terms in $G^{-1}(\mathbf{k})$ may yield results that appear to be power-law correlation with different scaling dimensions, which is illustrated in Fig. 2.11, where we have fixed $\epsilon_n = 5/22\epsilon$ but chosen different $g_n^{*\prime}$. This nonuniversal power-law like scaling of spin correlation was also observed in recent numerics concerning the edge states of the AKLT state during a bulk phase transition [87, 88].

Now we briefly consider the situation when the bulk undergoes a disorder-order quantum phase transition between the AKLT state and the Ising like VBS order, which is described by order parameter ϕ. The boundary mode of ϕ is $\Phi \sim \partial_y \phi$, and it couples to the VBS order parameter v at the boundary CFT. In this case, the coupled RG flow of λ and g_v in Eq. 2.59 is relatively simple: as long as we start with nonzero (λ_0, g_{v0}),

both g_v and λ quite generally flow to positive infinity, which corresponds to a nonzero long range order of v. Hence the $1d$ boundary of the system should develop the Ising-VBS order before the bulk. when the bulk is tuned closer and closer to a VBS (Ising) transition, the boundary will go through a transition between the gapless $SU(2)_1$ CFT state to a VBS phase, before the bulk actually hits criticality. This boundary transition should be in the same universality class as the transition from an $SU(2)_1$ CFT to a VBS phase in a purely one-dimensional spin-1/2 chain with both nearest and next nearest neighbor Heisenberg interactions (see, for example, Ref. [126] for the one-dimensional transition). We note that this transition is not an ordinary $1+1d$ Ising transition and, hence, is different from the "extraordinary transition" studied in the standard boundary criticality literature. But if we start with a negative initial value λ_0, it may take a long RG time before the coupling constants become positive and nonperturbative. Hence the VBS order parameter may still appear to have quasi long range correlation for a finite system.

In conclusion, we have found that there can be a direct continuous quantum phase transition between the long range antiferromagnetic Néel order, and the VBS order, in an effective $1d$ spin-1/2 system with nonlocal interactions (Eq. 2.59). Due to the nonlocality of the model, even in a $1d$ system with a continuous SO(3) spin symmetry there can be a long range Néel order. Within the accuracy of our method, the effective spin-1/2 system Eq. 2.59 arises from coupling the $1d$ boundary of a $2d$ SPT phase to bulk quantum critical modes. Our results were drawn from a controlled renormalization group study, and the critical exponents extracted (including the anomalous dimensions of order parameters and the dynamical exponent) are qualitatively consistent with the Néel-VBS transition found numerically in recent simulation of a spin-1/2 chain with spatially instantaneous nonlocal interactions [114, 115]. If a $1d$ system has local interactions only, there can only be spontaneous discrete symmetry breaking. Previous numerical and analytical

works [127, 128, 129] have studied the analogue of deconfined quantum critical point between two phases that spontaneously break different discrete symmetries.

Chapter 3

Interactions between exotic criticalities and Fermi surface

3.1 Non-Landau Quantum Phase Transitions and nearly-Marginal non-Fermi Liquid

3.1.1 Introduction

In the past few decades, a consensus has been gradually reached that quantum many-body physics with strong quantum entanglement can be much richer than classical physics driven by thermal fluctuations [130, 131]. Classical phase transitions usually happen between a disordered phase with high symmetries, and an ordered phase which spontaneously breaks such symmetries. Typical classical phase transitions can be well described by the Landau's paradigm, but the Landau's paradigm may or may not apply to quantum phase transitions that happen at zero temperature. Generally speaking, the Landau's formalism can only describe the quantum phase transition between a direct-product quantum disordered state and a spontaneous symmetry breaking state; but it

can no longer describe the quantum phase transition between two states when at least one of the states cannot be adiabatically connected to a direct product states, *i.e.* when this state is a topological order [95]; nor can the Landau's paradigm describe generic continuous quantum phase transitions between states with different spontaneous symmetry breakings [15, 16, 123].

Phenomenologically, in contrast with the ordinary Landau's transitions, non-Landau transitions often have a large anomalous dimension of order parameters, due to fractionalization or deconfinement of the order parameter [49, 50, 51, 52]. The ordinary Wilson-Fisher (WF) fixed point in $(2+1)d$ space-time (or three dimensional classical space) has very small anomalous dimensions [59], meaning that the Wilson-Fisher fixed point is not far from the mean field theory. In particular, in the large$-N$ limit, the anomalous dimension of the vector order parameter of the O(N) Wilson-Fisher fixed point is $\eta \sim 0$; while the CP^{N-1} model, the theory that describes a class of non-Landau quantum phase transition [15, 16], has $\eta \sim 1$ in the large-N limit [93]. Numerically it was also confirmed that the quantum phase transition between the Z_2 topological order and the superfluid phase has $\eta \sim 1.5$ [45, 46], as was predicted theoretically. The large anomalous dimension has been used as a strong signature when searching for unconventional QCPs numerically.

In this section we propose that the unique physics described above about the unconventional QCPs with strong fractionalization can be used to construct another broadly observed phenomenon beyond the classic Landau's theory: the non-Fermi liquid whose fermion self-energy scales $\Sigma_f(\mathrm{i}\omega) \sim \mathrm{isgn}(\omega)|\omega|^\alpha$ with $\alpha < 1$. When $\alpha = 1$, this non-fermi liquid is referred to as marginal fermi liquid [132]. Signature of marginal fermi liquid and nearly-marginal fermi liquid have been observed rather broadly in various materials [133, 134, 135]. In this section we will focus on the non-Fermi liquid that is "nearly-marginal", meaning α is close to 1.

We assume that there exists a field $\mathcal{O}(\boldsymbol{x}, \tau)$ in the unconventional QCP that carries zero momentum, and it couples to the fermi surface in the standard way: $\int d^2x d\tau \; g\psi^\dagger T\psi\mathcal{O}$, where T is a flavor matrix of the fermion. We assume that we first solve (or approximately solve) the bosonic part of the theory, *i.e.* the strongly interacting QCP without coupling to the fermi surface, and calculate the anomalous dimension η at the QCP:

$$\langle \mathcal{O}(\boldsymbol{q}, \omega)\mathcal{O}(-\boldsymbol{q}, -\omega)\rangle \sim \frac{1}{\Omega^{2-\eta}} \tag{3.1}$$

where $\Omega \sim \sqrt{v^2\boldsymbol{q}^2 + \omega^2}$. Then the fermion self-energy, the quantity of central interest to us, is computed perturbatively with the boson-fermion coupling g.

When the anomalous dimension η is close to 1, we can take $\eta = 1 - \epsilon$ with small ϵ. Ref. [36, 136, 37] developed a formalism for the boson-fermion coupled theory with an expansion of ϵ, though eventually one needs to extrapolate the calculation to $\epsilon = 1$ for the problems studied therein [36, 136, 37], and the convergence of the $\epsilon-$expansion at $\epsilon = 1$ is unknown, *i.e.* even if we start with a weak boson-fermion coupling, it would become nonperturbative under renormalization group (RG). But we will demonstrate in the next section that in the cases that we are interested in, ϵ is naturally small when η is close to 1, due to the fractionalized nature of many unconventional QCPs. To the leading nontrivial order, our problem can be naturally studied by the previously proposed perturbative formalism with small ϵ.

Here we stress that our goal is to construct a scenario in which a non-Fermi liquid state within an energy window can be constructed using a controlled method. Recently many works have taken a similar spirit, and various non-Fermi liquid states especially a state that mimics the strange metal were constructed by deforming the soluble Sachdev-Ye-Kitaev (SYK) and related models [137, 138, 139, 140, 141]. Then within the energy window where the deformation remains perturbative, the system resembles the non-Fermi

liquid [142, 143, 144, 145, 146, 147]. Our current section also starts with (approximately) soluble strongly interacting bosonic systems (in the sense that the gauge invariant order parameters in these systems are bosonic), and then we turn on perturbation, which in our case is the boson-fermion coupling. We will demonstrate that a non-Fermi liquid can be constructed based on the unique nature of the strongly interacting bosonic system.

3.1.2 Expansion of ϵ

A controlled reliable study of the non-Fermi liquid problem is generally considered as a very challenging problem, one example of the difficulties was discussed in Ref. [148]. Over the years various approximation methods were proposed. We begin by reviewing the $\epsilon-$expansion developed in Ref. [36, 136, 37], and demonstrate how perturbation of ϵ is naturally justified for some unconventional QCPs. It is often convenient to study interacting fermions with finite density by expanding at one patch of the Fermi surface. The low-energy theory of the fermions expanded at one patch of the fermi surface is

$$\mathcal{L}_f = \psi^\dagger \left(\xi \partial_\tau - \mathrm{i} v_F \partial_x - \kappa \partial_y^2 \right) \psi, \tag{3.2}$$

where x is perpendicular to the fermion surface and y is the tangent direction. The initial value of ξ is $\xi_0 = 1$, and it will be renormalized by the fermion self-energy. Our main goal is to evaluate the fermion self-energy to the leading nontrivial order of the boson-fermion coupling. We will show that this is equivalent to the leading nontrivial order of $\epsilon = 1 - \eta$. At this order of expansion of ϵ, for our purpose it is sufficient to consider a simple "effective action" of $\mathcal{O}(\boldsymbol{x}, \tau)$:

$$\mathcal{S}_{eff} \sim \int d^2x d\tau \ \mathcal{O}(\boldsymbol{x}, \tau)(-\partial_\tau^2 - v^2 \boldsymbol{\nabla}^2)^{1-\frac{\eta}{2}} \mathcal{O}(\boldsymbol{x}, \tau) \tag{3.3}$$

which will reproduce the correlation function of $\mathcal{O}(\boldsymbol{x},\tau)$, assuming we have fully solved the interacting bosonic system first.

When the boson-fermion coupling is zero, i.e., $g = 0$, the system is at a Gaussian fixed point with the following scaling dimensions of spacetime coordinates and fields

$$[\tau] = -2, \quad [x] = -2, \quad [y] = -1,$$

$$[\psi(\boldsymbol{x},\tau)] = \frac{3}{2}, \quad [\mathcal{O}(\boldsymbol{x},\tau)] = \frac{3}{2} + \frac{\eta}{2} = 2 - \frac{\epsilon}{2}. \tag{3.4}$$

We then turn on the boson-fermion interaction

$$\int d^2x d\tau \; g\psi^\dagger T\psi\mathcal{O} \tag{3.5}$$

and consider the perturbative RG at the Gaussian fixed point. We find that the scaling dimension of g is $[g] = \epsilon/2$, hence it is weakly relevant if ϵ is naturally small, and it may flow to a weakly coupled new fixed point in the infrared which facilitates perturbative calculations with expansion of ϵ. Indeed, the beta function of g^2 at the leading order of ϵ was derived in Ref. [36, 136, 37]:

$$\frac{dg^2}{d\log b} = \frac{\epsilon}{2}g^2 - \Upsilon g^4. \tag{3.6}$$

Thus there is a fixed point at weak coupling $g_*^2 = \epsilon/(2\Upsilon)$, where the parameter $\Upsilon \sim 1/(4\pi^2 v_F v)$.

Under the rescaling $x' = xb^{-1}$, namely after integrating out the short scale degrees of freedom, the fermion acquires a one-loop self-energy

$$\delta\Sigma_f(\mathrm{i}\omega,\boldsymbol{p}) \sim g^2 \int d\nu d\boldsymbol{q} \langle \mathcal{O}^*_{\boldsymbol{q},\nu}\mathcal{O}_{\boldsymbol{q},\nu}\rangle G_f(\mathrm{i}\omega + \mathrm{i}\nu, \boldsymbol{q}+\boldsymbol{p})$$

$$\sim g^2 \int d\nu dq_x \int_{\frac{\Lambda}{\sqrt{b}}}^{\Lambda} dq_y \frac{1}{\left|v^2 q_x^2 + v^2 q_y^2 + \omega^2\right|^{\frac{1+\epsilon}{2}}}$$

$$\times \frac{1}{\mathrm{i}\left(\omega+\nu\right) - v_F\left(p_x+q_x\right) - \kappa\left(p_y+q_y\right)^2}. \tag{3.7}$$

In the boson correlation function, $v^2 q_x^2$ and ω^2 are irrelevant compared with $v^2 q_y^2$, hence we first integrate over q_x, and the fermion propagator contributes a factor $\mathrm{sgn}\left(\omega+\nu\right)\mathrm{i}/(2v_F)$. We then perform the ν integral and finally integrate q_y over the momentum shell $\Lambda b^{-1/2} < |q_y| < \Lambda$. The last integral is evaluated at $\epsilon = 0$, which is valid at the leading order perturbation of ϵ. This procedure leads to

$$\delta\Sigma_f\left(\mathrm{i}\omega, \boldsymbol{p}\right) = -\mathrm{i}\omega g^2 \Upsilon \log b + O\left(\epsilon^2\right). \tag{3.8}$$

Combining the calculations above, at the fixed point g_*^2, the renormalized $\mathrm{i}\xi(\omega)\omega$ in the Fermion Green's function reads

$$\mathrm{i}\xi(\omega)\omega \sim -\mathrm{i}\mathrm{sgn}\left(\omega\right)|\omega|^{1-\epsilon/2}. \tag{3.9}$$

The fermion self-energy, hence the decay rate of the fermion, scales in the same way as Eq. 3.9. The calculation above gives a nearly-marginal non-Fermi liquid behavior for small but finite ϵ. For small η such as the cases in the Wilson-Fisher fixed points, the calculation of the scaling of fermion self-energy is not reliable with the leading order expansion of ϵ described above.

Here we stress that, our main purpose is to compute $\mathrm{i}\xi(\omega)\omega$, or the fermion self-energy to the leading order of boson-fermion coupling $g_*^2 \sim \epsilon$, assuming a weak initial coupling g. At higher order expansion of the boson-fermion coupling, corrections to the boson field

self-energy (for example the standard RPA diagram) from the boson-fermion coupling needs to be considered. The RPA diagram is proportional to $\mathcal{L}_{\rm RPA} \sim |\mathcal{O}_{\omega,\boldsymbol{q}}|^2 g^2 |\omega|/(v_F \kappa q)$. Several parameters can be tuned, including the weak coupling fixed point value of g_*^2, to make this term weak enough to allow an energy window where the calculations in this section apply. At the elementary level, we need the terms in Eq. 4.8 to dominate the RPA effect $|\mathcal{O}_{\omega,\boldsymbol{q}}|^2 g^2 |\omega|/(v_F \kappa q)$. A field $\mathcal{O}$ at momentum $\boldsymbol{q}$ should correspond to energy scale $\omega \sim vq$. For Eq. 4.8 at $\eta = 1$ to dominate the RPA effect, we need $q > g^2/(v_F\kappa)$, or $\omega > g^2 v/(v_F \kappa)$. If we start with a weak initial bare coupling constant g_0, and also $\epsilon \ll 1$ hence the fixed point value of g_* is also perturbative, there is a sufficiently large energy window for our result. Tuning the parameter v/v_F and κ can further expand the energy window. A full analysis of the term $\mathcal{L}_{\rm RPA} \sim |\mathcal{O}_{\omega,\boldsymbol{q}}|^2 g^2 |\omega|/(v_F \kappa q)$ in the bosonic sector of the theory in the infrared limit requires more detailed analysis because $\mathcal{O}_{\omega,\boldsymbol{q}}$ is a composite operator in the field theories discussed in the next section.

3.1.3 Candidate unconventional QCPs

(1) Bosonic-QED-Chern-Simons theory

In the following we will discuss candidate QCPs which suffice the desired condition $\eta \sim 1$, or $\epsilon \ll 1$. When we study the pure bosonic sector of the theory, we ignore the coupling to the fermions, assuming the boson-fermion coupling is weak, which is self-consistent with the conclusion in the previous review section that the boson-fermion interaction will flow to a weakly coupled fixed point $g_*^2 \sim \epsilon$. As we stated in the previous section, we will start with a weak boson-fermion coupling g, and eventually we only compute the fermion self-energy to the leading nontrivial order of the fixed point $g_*^2 \sim \epsilon$. In the purely bosonic theory, the scaling of the space-time has the standard Lorentz invariance. To avoid confusion, we use "[ ]" to represent scaling dimensions under the scaling

Eq. 4.9 of the one-patch theory in the previous section, and "{ }" represent the scaling dimension in the Lorentz invariant purely bosonic theory. At a QCP, multiple operators will become "critical", namely multiple operators can have power-law correlation. We will demand that the operator with the strongest correlation (smallest scaling dimension) satisfy the desired condition, since this is the operator that provides the strongest scattering with the electrons.

We consider $(2+1)d$ bosonic quantum electrodynamics (QED) with N flavors of bosons coupled to a noncompact U(1) gauge field with a Chern-Simons term:

$$\begin{aligned}\mathcal{L}_{\text{bQED}} &= \sum_{\alpha=1}^{2}\sum_{a=1}^{N/2}|(\partial_\mu - \mathrm{i}b_\mu)z_{\alpha,a}|^2 + r(z^\dagger_{\alpha,a}z_{\alpha,a}) \\ &+ u(\sum_{\alpha,a}|z_{\alpha,a}|^2)^2 + u'\sum_{\alpha=1}^{2}(\sum_{a=1}^{N/2}|z_{\alpha,a}|^2)^2 \\ &+ \frac{\mathrm{i}kN}{4\pi}b\wedge db. \end{aligned} \tag{3.10}$$

The following operators are gauge invariant composite fields, which we assume are all at zero momentum:

$$\mathcal{O}_0 = \sum_{\alpha=1}^{2}\sum_{a=1}^{N/2} z^\dagger_{\alpha,a}z_{\alpha,a}, \quad \mathcal{O}_{1,3} = \sum_{a=1}^{N/2} z^\dagger_a \sigma^{1,3} z_a. \tag{3.11}$$

Potential applications of this field theory to strongly correlated systems will be discussed later.

To compute their scaling dimensions, we introduce two Hubbard-Stratonovich(HS) fields to decouple the quartic potentials:

$$\mathcal{L}'_{\text{bQED}} = \sum_{\alpha=1}^{2}\sum_{a=1}^{N/2}|(\partial_\mu - \mathrm{i}b_\mu)z_{\alpha,a}|^2 + r(z^\dagger_{\alpha,a}z_{\alpha,a})$$

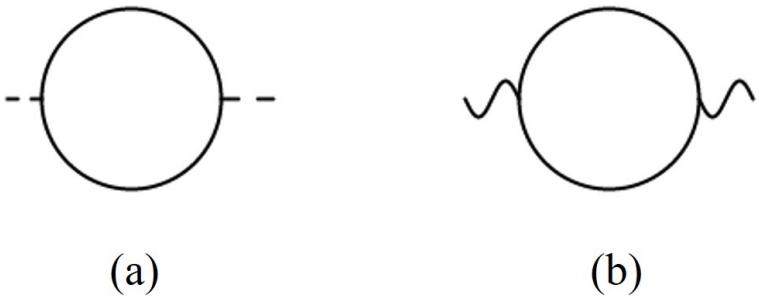

Figure 3.1: The self-energy of field σ_+ and gauge field b_μ in the large$-N$ limit.

$$+ \quad \mathrm{i}\sigma_+\mathcal{O}_0 + \mathrm{i}\sigma_-\mathcal{O}_3 + \frac{1}{2u'+4u}\sigma_+^2 + \frac{1}{2u'}\sigma_-^2$$

$$+ \quad \frac{\mathrm{i}kN}{4\pi} b \wedge db. \tag{3.12}$$

We will consider the following two scenarios: (1) $u' \to 0, u > 0$, where σ_- is fully suppressed and the system has a full $\mathrm{SU}(N) \times \mathrm{U}(1)_T$ symmetry, where the $\mathrm{U}(1)_T$ is the "topological symmetry" that corresponds to the conservation of the gauge flux; and (2) $u, u' > 0$ when the $\mathrm{SU}(N)$ symmetry is broken down to $\mathrm{SU}(N/2) \times \mathrm{SU}(N/2) \times \mathrm{U}(1) \rtimes Z_2$, where the $\mathrm{U}(1) \rtimes Z_2$ is the symmetry within the Pauli matrix space in Eq. 3.11.

In scenario (1) with a full $\mathrm{SU}(N)$ symmetry, at the critical point $r = 0$, the field σ_+ acquires a self-energy in the large$-N$ limit

$$\Sigma_{\sigma_+}(p) = N \int \frac{d^3q}{(2\pi)^3} \frac{1}{q^2(q+p)^2} = \frac{N}{8p}. \tag{3.13}$$

Hence the propagator of field σ_+ in the large$-N$ limit reads

$$G_{\sigma_+}(p) = 1/\Sigma_{\sigma_+} = \frac{8p}{N}. \tag{3.14}$$

Similarly, for the gauge field, the self-energy in the large$-N$ limit is

$$\begin{aligned}\Sigma_{b,\mu\nu}(p) &= -N\int\frac{d^3q}{(2\pi)^3}\frac{(2q+p)_\mu(2q+p)_\nu}{q^2(q+p)^2}\\ &= \frac{N}{16p}(p^2\delta_{\mu\nu}-p_\mu p_\nu).\end{aligned} \tag{3.15}$$

When combined with the Chern-Simons term, in the Landau gauge, the gauge field has the following large$-N$ propagator [95]

$$G_{b,\mu\nu}(p)=\frac{1}{Np}\left(F\left(\delta_{\mu\nu}-\frac{p_\mu p_\nu}{p^2}\right)+H\frac{\epsilon_{\mu\nu\rho}p^\rho}{p}\right), \tag{3.16}$$

where

$$F=\frac{16\pi^2}{\pi^2+64k^2},\quad H=-\frac{128\pi k}{\pi^2+64k^2}. \tag{3.17}$$

After introducing the HS fields, the scaling dimension of the composite operator $\mathcal{O}_0$ of the original field theory Eq. 3.10 is "transferred" to the scaling dimension of the HS fields σ_+. To the order of $O(1/N)$, the Feynman diagrams in Fig. 3.2 contribute to the σ_+ self energy, which was computed in Ref. [95].

But it is evident that in the large$-N$ limit, the scaling dimension of σ_+ (and the scaling dimension of operator $\mathcal{O}_0$ of the original field theory Eq. 3.10) is $\lim_{N\to\infty}\{\mathcal{O}_0\}=2$, hence it does not meet the desired condition. When $\mathcal{O}_0$ couples to the Fermi surface, the boson-fermion coupling will be irrelevant in the one patch theory discussed in the previous section according to the scaling of space-time Eq. 4.9.

The scaling dimension of $\sigma_{1,3}$ equal to each other with a full SU(N) symmetry, and unlike $\mathcal{O}_0$, they have scaling dimension 1 in the large$-N$ limit. The $1/N$ corrections to their anomalous dimensions come from diagram $(a)-(d)$ in Fig. 3.2, or equivalently

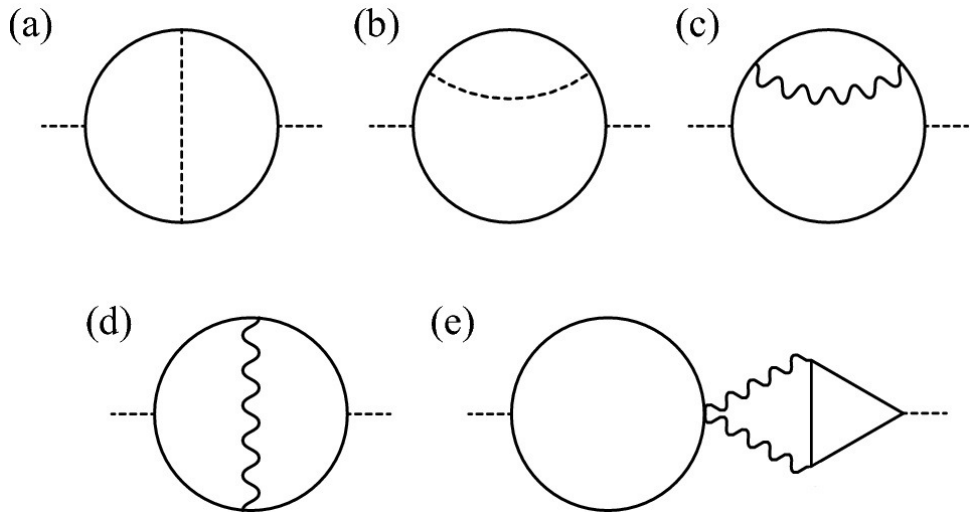

Figure 3.2: In scenario (1), diagrams $(a)-(e)$ contribute to the anomalous dimension of $\mathcal{O}_0$ in Eq. 3.10 or equivalently σ_+ in Eq. 3.12; while only diagrams $(a)-(d)$ contribute to the anomalous dimension of $\mathcal{O}_{1,3}$. The solid line represents the propagator of $z_{\alpha,a}$, the dashed and wavy lines represent the large$-N$ propagators of σ_+ and b_μ respectively.

through the standard momentum shell RG:

$$\{\mathcal{O}_{1,3}\} = 1 + \frac{16}{3\pi^2 N} - \frac{4}{3\pi^2 N} F. \tag{3.18}$$

Ref. [93] and references therein have computed scaling dimensions of gauge invariant operators for theories with matter fields coupled with a U(1) gauge field, without a Chern-Simons term. Our result is consistent with these previous references, since $\lim_{k\to 0}\{\mathcal{O}_{1,3}\} = 1 - 16/(\pi^2 N)$, which is the result of the CP^{N-1} model with a noncompact gauge field. Also, in the limit of $k \to +\infty$, our result is consistent with Ref. [93] when the fermion component is taken to be infinity, since both limits suppress the gauge field fluctuation completely. In general operators $\mathcal{O}_{1,3}$ have stronger correlations than $\mathcal{O}_0$, hence they will make stronger contributions to scattering when coupled with the fermi surface. As an

example, the anomalous dimension of $\mathcal{O}_{1,3}$ with $k = 1/2$ reads

$$\eta_{1,3} \sim 1 - \frac{0.57}{N}, \tag{3.19}$$

which is reasonably close to 1 even for the most physically relevant case with $N = 2$.

In scenario (2) we should keep both σ_+ and σ_- in the calculation, and both $\sigma_\pm$ (operator $\mathcal{O}_0$ and $\mathcal{O}_3$ in theory Eq. 3.10) have scaling dimension 2 in the large$-N$ limit [94]. Now $\mathcal{O}_1$ has the strongest correlation, and at the order of $O(1/N)$, its scaling dimension reads:

$$\{\mathcal{O}_1\} \;=\; 1 + \frac{8}{3\pi^2 N} - \frac{4}{3\pi^2 N} F. \tag{3.20}$$

When $k = 1$, its anomalous dimension reads

$$\eta_1 \sim 1 - \frac{0.037}{N}, \tag{3.21}$$

which is always very close to 1. Using the formalism reviewed in the previous section, by coupling to $\mathcal{O}_1$, the fermion self-energy would scale as $\Sigma_f\left(\mathrm{i}\omega, \boldsymbol{p}\right) \sim -\mathrm{isgn}\left(\omega\right)|\omega|^{0.99}$ for $N = 2$.

The field theory Eq. 3.10 describes a quantum phase transition from a topological order with Abelian anyons to an ordered phase that spontaneously breaks the global flavor symmetry. The flavor symmetry can be either a full $\mathrm{SU}(N)$ symmetry (scenario *1*) or $\mathrm{SU}(N/2) \times \mathrm{SU}(N/2) \times \mathrm{U}(1) \rtimes Z_2$ (scenario *2*). So far we have assumed that the gauge invariant $\mathcal{O}_{1,3}$ have zero momentum, hence they cannot be the ordinary antiferromagnetic Néel order parameter. They must be translational invariant order parameters with nontrivial representation under the internal symmetry group, for example they could be the quantum spin Hall order parameter for $N = 2$.

The topological order described by the Chern-Simons theory with $N = 2$, $k = 1$ is the most studied state in condensed matter theory. This topological order is the $U(1)_2$ or equivalently the $SU(2)_1$ topological order with semionic anyons. It is the most natural topological order that can be constructed from the slave particle formalism [149]. And recently it was conjectured that this topological order is also related to the parent state of the cuprates high temperature superconductor [150] motivated by the giant thermal Hall signal observed [151].

Another interesting scenario is when $N = 2$, $k = 0$ and $u > 0$. In this case Eq. 3.10 is the same field theory as the easy-plane deconfined QCP between the inplane antiferromagnetic Néel order and the valence bond solid state on the square lattice. Recent numerical studies have shown that this quantum phase transition may be continuous, and the scaling dimension of both $\mathcal{O}_0$ and $\mathcal{O}_3$ are fairly close to 1 based on numerical results [52, 152]. It has been proposed that this field theory is self-dual [91], and it is dual to the transition between the bosonic symmetry protected topological (SPT) phase and the trivial phase [81, 92], which is directly describe by a noncompact QED with $N = 2$ flavors of Dirac fermion matter fields [153, 154]. The tuning parameter for this topological transition is instead coupled to $\mathcal{O}_3$. Hence this SPT-trivial transition is also a candidate quantum phase transition which meets the desired criterion proposed in this section that leads to a nearly-marginal fermi liquid. But in these cases there are other fields (for example the inplane Néel order parameter) with smaller scaling dimensions, and we need to assume that these operators carry finite lattice momentum hence couple to the Fermi surface differently.

(2) Gross-Neveu-Yukawa QCP

Another candidate QCP that likely suffices the desired condition $\eta \sim 1$ is the Gross-

Neveu-Yukawa QCP with $N-$flavors of Dirac fermion:

$$\begin{aligned} \mathcal{L}_{\text{GNY}} &= \sum_{a=1}^{N} \bar{\chi}_a \gamma_\mu \partial_\mu \chi_a + g\phi \bar{\chi}_a \chi_a \\ &+ (\partial\phi)^2 + r\phi^2 + u\phi^4. \end{aligned} \tag{3.22}$$

At the critical point $r = 0$, both u and g flows to a fixed point. In our context, the QCP describes a bosonic or spin system, hence χ is viewed as a fermionic slave particle of spin, *i.e.* the spinon, and we assume that χ is coupled to a Z_2 gauge field, namely the system is a Z_2 spin liquid with fermionic spinons. But the dynamical Z_2 gauge field does not lead to extra singular corrections to low energy correlation functions of gauge invariant operators, hence the universality class of Eq. 3.22 is still identical to the Gross-Neveu-Yukawa (GNY) theory, as long as we only focus on gauge invariant operators.

The GNY QCP can still be solved in the large$-N$ limit, and the cases with finite N can approached through a $1/N$ expansion. At the GNY QCP coupled with a Z_2 gauge field, the gauge invariant operator with the lowest scaling dimension is ϕ, and its scaling dimension can be found in Ref. [155] and references therein:

$$\{\phi\} \sim 1 - \frac{16}{3\pi^2 N}. \tag{3.23}$$

Other gauge invariant operators such as $\bar{\chi} T \chi$ with a SU(N) matrix T have much larger scaling dimension at the GNY QCP, for example $\{\bar{\chi} T \chi\} = 2$ in the large$-N$ limit. If we replace the Z_2 gauge field by a U(1) gauge field, the U(1) gauge fluctuation will enhance the correlation of ϕ, hence increases $\epsilon = 1 - \eta$ compared with the situation with only a Z_2 gauge field. Hence a GNY QCP with a U(1) gauge field is less desirable according to our criterion.

The GNY QCP coupled with a Z_2 gauge field can be realized in various lattice model Hamiltonians for quantum antiferromagnet. For example, for SU(M) spin systems on the triangular lattice with a self-conjugate representation on each site, using the fermionic spinon formalism, when there is a $\pi-$flux through half of the triangles, there are $N = 2M$ components of Dirac fermions at low energy [156]. SU(M) quantum magnet may be realized in transition metal oxides with orbital degeneracies [157, 158, 159], and also cold atom systems with large hyperfine spins [160, 161, 162, 163]. Recently it was also proposed that an approximate SU(4) quantum antiferromagnet can be realized in some of the recently discovered Moiré systems [164, 165, 166], and a SU(4) quantum antiferromagnet on the triangular lattice may realize the Z_2-gauged GNY QCP with $N = 8$ (with lower spatial symmetry compared with SU(2) systems as was pointed out in Ref. [167]). On the other hand, a SU(M) spin systems on the honeycomb lattice can potentially realize the GNY QCP with $N = 2M$ (with zero flux through the hexagon) or $N = 4M$ (with $\pi-$flux through the hexagon).

The operator ϕ is odd under time-reversal and spatial reflection, hence physically ϕ corresponds to the spin chirality order. Hence the Z_2-gauged GNY QCP is a quantum phase transition between a massless spin liquid and a chiral spin liquid.

Non-Fermi liquid is often observed only at a finite temperature/energy window in experiments. At the infrared limit, the non-Fermi liquid is usually preempted by other instabilities, for example a dome of superconductor [168, 169, 170]. In Ref. [168] the instability of non-Fermi liquid towards the superconductor dome was systematically studied in the framework of the $\epsilon-$expansion. According to Ref. [168], when $\mathcal{O}$ is an order parameter at zero momentum, at $\epsilon = 0$ the superconductor instability will occur at an exponentially suppressed temperature/energy scale $\Delta_{\rm sc} \sim \Lambda_\omega \exp(-A/|g_0|)$, where g_0 is the bare boson-fermion coupling constant. In our case the estimate of the superconductor instability is complicated by the fact that $\mathcal{O}$ is a composite field, but the qualitative

exponentially-suppressed form of $\Delta_{\rm sc}$ is not expected to change because g is still at most a marginally relevant coupling. When $\epsilon = 0$, the imaginary part of the fermi self-energy (the inverse of quasi-particle life-time) scales linearly with ω. Because the bare electron dispersion has no imaginary part at all, the imaginary part of the self-energy should be much easier to observe compared with the real part, assuming other scattering mechanisms of the fermions are weak enough. The scaling behavior of the fermion self-energy is also observable numerically like Ref. [171]. This linear scaling behavior of the imaginary part of self-energy is observable for fermionic excitations at energy scale $\omega > \Delta_{\rm sc}$, . Hence above the superconductor energy scale $\Delta_{\rm sc}$, the non-Fermi liquid behavior is observable. This result should still hold for small enough ϵ. [1]

3.1.4 Conclusion

In this section we proposed a mechanism based on which a nearly marginal non-fermi liquid can be constructed with a controlled method in an energy window. This mechanism demonstrates that two exceptional phenomena beyond the standard Landau's paradigm, *i.e.* the non-Landau quantum phase transitions and the non-fermi liquid may be connected: a non-Landau quantum phase transition can have a large anomalous dimension $\eta \sim 1$, which physically justifies and facilitates a perturbative calculation of the Boson-Fermion coupling fixed point. Several candidate QCPs that suffice this condition were proposed, including topological transitions from Abelian topological orders to an ordered phase, and a Gross-Neveu-Yukawa transition of Z_2 spin liquids.

We would like to compare our construction of non-fermi liquid states and the con-

[1] In Ref. [168], the non-Fermi liquid energy scale $E_{\rm nfl}$ is defined as the energy scale where the fermi velocity v_F is renormalized strongly from its bare value, hence $E_{\rm nfl}$ was defined based on the real part of the fermion self-energy. In other words the $E_{\rm nfl}$ was defined as the scale where the real part of self-energy dominates the bare energy in the Green's function. But since the bare dispersion of fermion is difficult to observe, and the bare fermion energy has no imaginary part at all, we prefer to use the imaginary part of fermion self-energy as a characteristic definition of non-Fermi liquid state.

structions based on the SYK related models. In the constructions based on SYK-like models, the existence of a strange-metal like phase was based on the fact that in the soluble limit, *i.e.* in the SYK model the scaling dimension of fermion is 1/4 (scaling with time only). But since the definition of the electric current operator in these constructions is proportional to the perturbation away from the SYK model, the current-current correlation function and the electrical conductivity is small in the energy window where the construction applies. Recently an improved construction was proposed which can produce the Planckian metal observed in cuprates materials [172]. In our construction, since the boson-fermion coupling will flow to a weakly coupled fixed point, the scattering rate of the fermion due to the boson-fermion coupling is expected to be low. We will further study if a Planckian metal like state can be constructed by developing our current approach. In this future exploration, a mechanism of momentum relaxation, for instance the disorder, or Umklapp process, needs to be introduced.

3.2 Deconfined Quantum Critical Point with Non-locality

A deconfined quantum critical point (DQCP) occurs between two phases that spontaneously break two different symmetries that do not contain each other as a subgroup. The original DQCP was proposed as a direct unfine-tuned continuous quantum phase transition between the collinear Néel and the valence bond solid (VBS) orders on the square lattice [15, 16]. Various analogues of the original DQCP were studied, for example the transition between the superfluid and various density waves of a quantum boson system can be described in a similar framework as that of the DQCP with an easy-plane anisotropy [173, 174]; later the DQCP was also generalized to lattices where the spin

order and VBS order both have different structure from the original DQCP [123]. In all these examples the two ordered phases separated by the DQCP break very different 0-form symmetries; but nowadays one can generalize the notion of DQCP to situations that involve higher-form symmetries. For example a direct transition between a magnetic order and a topological order can be viewed as a DQCP between a phase with spontaneous breaking of a 0-form symmetry and another phase with spontaneous breaking of a (emergent) 1-form symmetry [175, 176, 177, 178, 179, 180, 181, 182, 183, 184]. In the past two decades, a lot of progress has been made towards understanding various aspects of the DQCP, including its connection to mixed 't Hooft anomaly and higher dimensional symmetry protected topological phases [77], as well as a duality web that connects different Lagrangian descriptions of the DQCP [185, 78, 79, 92, 80, 81, 22, 186], etc.

Despite all the theoretical progresses, the nature of the original DQCP proposed on the square lattice has always remained controversial. Very encouraging evidences of DQCP were found in numerics on a $2D$ lattice quantum spin model dubbed the "$J-Q$" model [17, 18], as well as loop models in the $3D$ Euclidean space [187, 188], but numerical simulations have also observed unusual scaling behaviors [19, 20] and other complexities [189]. Recently the DQCP has also been challenged by the "conformal bootstrap" method of analyzing conformal field theories (CFT): the critical exponents obtained from numerical simulations seem incompatible with the bounds given by conformal bootstrap [190, 191]. Though these should not exclude the possibility that the DQCP still exists in other lattice models with critical exponents that are consistent with the conformal bootstrap bounds, a consensus on the nature of the DQCP awaits further efforts.

In this section, rather than trying to address the infrared nature of the original DQCP, we explore a possible continuous quantum phase transition close to the originally pro-

posed DQCP, starting with the transition between the easy-plane Néel order and the VBS order. In particular, we will discuss the effect of nonlocality on DQCP. Nonlocality of a system can directly arise from a long range instantaneous interaction in the Hamiltonian [114, 115], or from coupling to the gapless modes in one higher dimension, when the system is realized at the boundary of a bulk [89, 112, 113, 87, 88, 192, 193, 28, 194, 29, 30, 195]. It was shown that, by coupling to the bulk quantum critical modes, the transition between the Néel and VBS order could be driven to a new fixed point [192, 193]. Nonlocality arising from holography was also explored in Ref. [196].

Here we explore nonlocality arising from a more realistic mechanism. Nonlocality in space-time usually translates to nonanalyticity in the momentum-frequency space. It is well-known that, based on the Hertz-Millis theory [32, 33], by coupling an order parameter ϕ to a Fermi surface, the dynamics of the order parameter acquires a singular contribution in the momentum-frequency space. In particular, when the order parameter carries a finite momentum that connects two "hot spots" of the Fermi surface, after formally integrating out the fermions, the order parameter acquires a singular term $\sim \sum_{\omega,\boldsymbol{q}} |\omega||\phi_{\omega,\boldsymbol{q}}|^2$. Within the framework of the Hertz-Millis theory, this singular term renders the original $\sum_{\omega,\boldsymbol{q}} \omega^2|\phi_{\omega,\boldsymbol{q}}|^2$ term in the Lagrangian irrelevant, and leads to a $z = 2$ Landau-Ginzburg theory of the order parameter ϕ. But the effect of the coupling to the hot spots will be more complex in the case of DQCP, as the physical order parameter ϕ is now a composite operator of the deconfined degrees of freedom at the DQCP. We note that novel physics arising from coupling to a background Fermi surface in a one dimensional setup was explored recently [197].

3.2.1 Easy plane DQCP coupled with hot spots

Let us first inspect the easy-plane DQCP between the inplane Néel order and a VBS order on a square lattice. The order parameters involved in this transition include a two component inplane Néel order (N_x, N_y) at momentum (π, π), and a two component VBS order parameter (V_x, V_y) at momentum $(\pi, 0)$ and $(0, \pi)$ respectively. Since all these order parameters carry a finite momentum, in principle they would acquire a singular term in the form sketched above when the easy-plane DQCP occurs with a background Fermi surface, assuming their momenta connect hot spots of the Fermi surface. The Lagrangian that describes the easy-plane DQCP is an easy-plane CP^1 model, and it is known that this theory enjoys a self-duality [185], *i.e.* the inplane Néel order parameter (N_x, N_y) is a bilinear of the CP^1 field $(N_x, N_y) \sim (z^\dagger \sigma^x z, z^\dagger \sigma^y z)$, and the VBS order parameter along the x and y direction is a bilinear of the *dual* CP^1 field (the vortex of z_1 and z_2 respectively): $(V_x, V_y) \sim (v^\dagger \sigma^x v, v^\dagger \sigma^y v)$. Then after we integrate out the background Fermi surface according to the Hertz-Millis theory, the action that describes the transition becomes

$$\begin{aligned} \mathcal{S} &= \int d^2x d\tau \sum_{\alpha=1,2} |(\partial - \mathrm{i}A) z_\alpha|^2 + r|z_\alpha|^2 + u|z_\alpha|^4 \\ &+ \sum_{\omega, \boldsymbol{q}} \sum_{i=x,y} g|\omega| |(z^\dagger \sigma^i z)_{\omega, \boldsymbol{q}}|^2; \end{aligned} \tag{3.24}$$

and the dual action reads

$$\begin{aligned} \mathcal{S}_d &= \int d^2x d\tau \sum_{\alpha=1,2} |(\partial - \mathrm{i}\tilde{A}) v_\alpha|^2 + \tilde{r}|v_\alpha|^2 + \tilde{u}|v_\alpha|^4 \\ &+ \sum_{\omega, \boldsymbol{q}} \sum_{i=x,y} \tilde{g}|\omega| |(v^\dagger \sigma^i v)_{\omega, \boldsymbol{q}}|^2, \end{aligned} \tag{3.25}$$

where $\tilde{r} = -r$. The actions above will be the starting point of our study; higher order singular terms beyond the Hertz-Millis theory that also arise from integrating out the background fermions will be briefly discussed later. In this section we will show that, although the bare values of g and $\tilde{g}$ can differ, they may actually flow to a fixed point where $g_* = \tilde{g}_*$. Hence this fixed point not only corresponds to a direct inplane Néel-to-VBS transition, our calculation suggests that this new fixed point may still have the self-duality as the originally proposed easy-plane DQCP [185]; but we do not make a statement about the presence of the enlarged emergent O(4) symmetry that can be perceived through the low energy effective nonlinear Sigma model of the easy-plane DQCP [198], as well as the duality web [78, 79, 92, 80, 81, 22, 186].

In order to study the theory Eq. 3.24 in a controllable fashion, we follow the standard procedure (see for example Ref. [93, 94]) by introducing the Hubbard-Stratonovich auxiliary fields λ_α and Φ^i to decompose the two quartic terms of z_α, and consider the following large-N generalization of Eq. 3.24 at the critical point $r = 0$:

$$\begin{aligned} \mathcal{S} &= \int d^2x d\tau \sum_{a=1}^{N} \sum_{\alpha=1,2} |(\partial - \mathrm{i}A) z_{a,\alpha}|^2 + \mathrm{i}\lambda_\alpha |z_{a,\alpha}|^2 \\ &+ \mathrm{i} \sum_{i=x,y} \Phi^i (z_a^\dagger \sigma^i z_a) \end{aligned} \tag{3.26}$$

With large-N, the correlators of the Hubbard-Stratonovich fields, and the gauge field read

$$\langle \lambda_\alpha(\vec{q}) \lambda_{\alpha'}(-\vec{q}) \rangle = \frac{8}{N} |\vec{q}| \delta_{\alpha,\alpha'},$$

$$\langle A_\mu(\vec{q}) A_\nu(-\vec{q}) \rangle = \frac{16}{2N} \left(\frac{\delta_{\mu\nu} - q_\mu q_\nu / q^2}{|q|} \right),$$

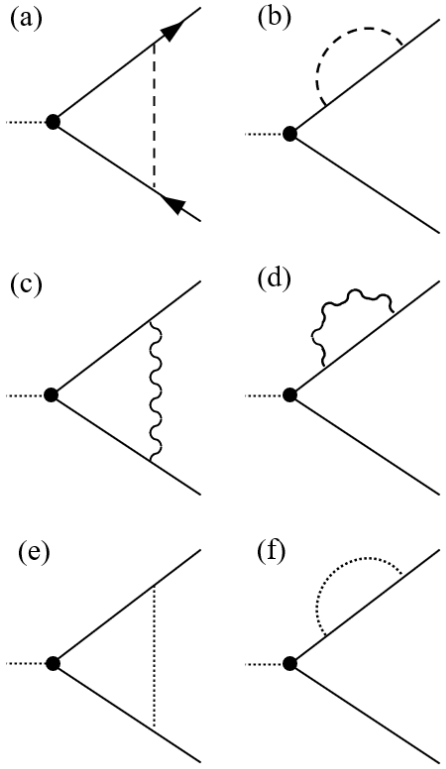

Figure 3.3: One-loop Feymann diagrams that contribute to $\beta(g)$. Here the solid, dashed, dotted and wavy lines represent the correlators of $z_{a,\alpha}$, λ_α, Φ^i and gauge field A_μ, respectively.

$$\langle \Phi^i(\vec{q})\Phi^{i'}(-\vec{q})\rangle = g|\nu|\delta_{i,i'}, \tag{3.27}$$

where $\vec{q} = (\nu, \boldsymbol{q})$. We assume that g is at the order of $1/N$.

We proceed by calculating the renormalization group (RG) flow of g using the momentum-shell RG by integrating out the modes with momentum within $\Lambda/b < |k| < \Lambda$ (the calculations are repeated with the dimensional regularization as well); the most relevant Feynman diagrams are listed in Fig. 3.3. The diagrams (a-d) are the standard contributions to the leading order $1/N$ expansion of the CP^{N-1} model [94]. The key of the calculation is the following: in the large-N limit, the parameter g is exactly marginal, as $z_a^\dagger \sigma^i z_a$ has scaling dimension $[z_a^\dagger \sigma^i z_a] = 1$ for $i = x, y$, while Φ^i has scaling dimension $[\Phi^i] = 2$. With finite N, the scaling dimension of $z_a^\dagger \sigma^i z_a$ receives a negative correction at

the order of $1/N$: $[z_a^\dagger \sigma^i z_a] = 1 - 28/(3\pi^2 N)$, which makes g weakly relevant with large but finite N. Hence the beta function of g should take the form

$$\frac{dg}{d\ln b} = \beta(g) = \frac{56}{3\pi^2 N} g - Cg^2. \tag{3.28}$$

When C is positive and order unity, g will flow to a fixed point at the order of $g_* \sim 1/N$.

Diagram Fig. 3.3(e) and (f) potentially contribute to the coefficient C in the beta function above. Diagram (e) has vanishing contribution at the easy-plane DQCP under consideration right now, due to the matrix identity $\sum_{j=x,y} \sigma^j \sigma^i \sigma^j = 0$ for $i = x, y$. Diagram (f) can be interpreted as the self-energy correction to $z_{a,\alpha}$

$$\begin{aligned} \Sigma(\omega, \boldsymbol{k}) &= \sum_{j=x,y} g\sigma^j \sigma^j \int_{\Lambda/b}^{\Lambda} \frac{d^3q}{(2\pi)^3} \frac{|\nu|}{(q+k)^2} \\ &= g\frac{\omega^2}{2\pi^2} \ln b \times \sigma^0 + \dots . \end{aligned} \tag{3.29}$$

Here $\vec{q} = (\nu, \boldsymbol{q})$, $\vec{k} = (\omega, \boldsymbol{k})$. The ellipses in the equation represent terms which do not contribute at order $\ln b$. This self-energy correction will modify the Gaussian part of the action of $z_{a,\alpha}$ to

$$\mathcal{L} = z_{a,\alpha}^* \left(|\partial_\tau|^{2\left(1 - g/(4\pi^2)\right)} - \partial_x^2 \right) z_{a,\alpha} + \cdots \tag{3.30}$$

This result implies that after coupling to the background Fermi surface, the space-time scaling of the original easy-plane DQCP is modified, which should now be

$$\tau \to b^{-z}\tau, \quad \mathbf{x} \to b^{-1}\mathbf{x}, \tag{3.31}$$

where $z = 1 + \frac{g}{4\pi^2} + O(g^2)$ is the dynamical exponent. Here we remind the readers that,

in the original Hertz-Millis theory, when an order parameter is coupled to hot spots of a Fermi surface, the Gaussian part of the Landau-Ginzburg theory of the order parameter has dynamical exponent $z = 2$. Here although the order parameter is a composite operator of $z_{a,\alpha}$, the dynamical scaling exponent z is still modified due to its coupling to the Fermi surface.

The wave function renormalization in diagram (f) is in fact equivalent to the modification of the space-time scaling, plus a correction to the scaling dimension of $z_{a,\alpha}$: $\Delta[z_{a,\alpha}] = g/(8\pi^2)$. Eventually the beta function of g reads

$$\beta(g) \equiv \frac{dg}{d\ln b} = \left(\frac{56}{3\pi^2 N} - \frac{g}{2\pi^2}\right) g, \tag{3.32}$$

where the first term arises from diagrams (a-d), while the second term is the additional wave-function renormalization from (f) as described above. Indeed, for $g > 0$, the theory flows to a new fixed point $g_* = \frac{112}{3N} + O(\frac{1}{N^2})$. Several two-loop diagrams such as the Aslamazov-Larkin diagrams appear to be also at the $1/N$ order, but careful evaluation shows that these diagrams either do not contribute to the beta function as they do not lead to a logarithmic divergence, or their contributions cancel out with each other [94].

The same calculation applies to $\tilde{g}$ in Eq. 3.25. Hence although the bare values of g and $\tilde{g}$ in Eq. 3.24 and Eq. 3.25 can be different, the RG equations above suggest that they would flow to a fixed point where $g_* = \tilde{g}_*$. Hence our calculation suggests that at this fixed point the self-duality of the original easy-plane DQCP still holds. Another more technical note is that, the VBS order parameter $V_x \sim v^\dagger \sigma^x v$ is also the monopole operator of gauge field A_μ in Eq. 3.24, hence the $\tilde{g}$ term in Eq. 3.25 also corresponds to a correction to the action of the gauge field A_μ. But since we expect $\tilde{g}$ to flow to a fixed point at order $1/N$, at the self-consistent level we can ignore this singular correction and use the gauge field propagator in the large-N limit for our calculation.

At this new RG fixed point, we obtain scaling dimensions for the following operators:

$$[\lambda^+] = 2 - \frac{80}{3\pi^2 N} - \frac{3g_*}{4\pi^2} = 2 - \frac{164}{3\pi^2 N} + O(\frac{1}{N^2}),$$

$$[\lambda^-] = 2 + \frac{16}{3\pi^2 N} + \frac{g_*}{4\pi^2} = 2 + \frac{44}{\pi^2 N} + O(\frac{1}{N^2}),$$

$$[z_a^\dagger \sigma^{x,y} z_a] = 1. \tag{3.33}$$

Here we have defined operators $\lambda^\pm = (\lambda_1 \pm \lambda_2)/2$. Some two-loop diagrams like the ones considered in Ref. [199] contribute to the evaluation of $[\lambda^+]$. The critical exponent ν is inferred from the scaling dimension of λ^+:

$$\nu^{-1} = 2 + z - [\lambda^+] = 1 + \frac{64}{\pi^2 N} + O(\frac{1}{N^2}). \tag{3.34}$$

These standard $1/N$ expansion may not be extremely reliable at the physically relevant case with small N, but the scaling dimensions of $z_a^\dagger \sigma^{x,y} z_a$ should be exactly 1 at $g = g_*$. This is due to the fact that the system remains scaling invariant at the fixed point with nonzero g_*, and the singular frequency dependence $|\omega|$ in Eq. 3.24 cannot be renormalized, then to keep the system scaling invariant the inplane Néel order parameter (N_x, N_y) must have scaling dimension 1 in the Euclidean space-time.

We note that based on the Hertz-Millis theory there is another singular interaction $|\omega||(z^\dagger \sigma^z z)_{\omega,\boldsymbol{q}}|^2$ that would also be generated by coupling the $z-$component of the Néel order to the background Fermi surface, but this term is irrelevant with the large-N generalization of the easy-plane DQCP, as the scaling dimension of $z^\dagger \sigma^z z$ is 2 with large-N.

We would also like to comment on the validity of the Hertz-Millis theory. It was

noted in Ref. [200] that, when we couple an order parameter ϕ to a Fermi surface, besides generating singular terms at the quadratic order of ϕ, similar higher order terms $\sim \phi^n$ with space-time singularity is also generated after integrating out the fermions. It was shown in Ref. [200] that direct power-counting suggests these higher order terms are marginal at the $z = 2$ Gaussian fixed point of the Hertz-Millis theory, hence it is no longer justified to ignore these terms. In fact, in our case, once we identify ϕ as $z^\dagger \sigma^i z$, the higher order terms pointed out in Ref. [200] are still marginal at the new fixed point, since the scaling dimension $[z^\dagger \sigma^i z]$ is precisely 1. But this does not mean that the physics at the new fixed point we derived is not observable. Let us return to the original theory with a bosonic field ϕ coupled with N_F copies of Fermi surfaces:

$$\begin{aligned} \mathcal{L}_{BF} &= \sum_{l=1}^{N_F} f_{l1}^\dagger (\partial_\tau - \mathrm{i}\mathbf{v}_1 \cdot \nabla) f_{l1} + f_{l2}^\dagger (\partial_\tau - \mathrm{i}\mathbf{v}_2 \cdot \nabla) f_{l2} \\ &\quad + u\phi \left[\sum_l (f_{l1}^\dagger T f_{l2} + (1 \leftrightarrow 2)) \right], \end{aligned} \tag{3.35}$$

where $1, 2$ label two points of the Fermi surface connected by the momentum of ϕ, and T is a flavor matrix. The parameter g in Eq. 3.24 is about $g \sim N_F u^2$, and since $g \sim 1/N$, we need $u \sim \sqrt{1/(NN_F)}$. If we fix N, the higher order singular terms considered in Ref. [200] will be at the order of $1/N_F^{n/2-1}$. Hence with large-N_F, although the ultimate fate of these higher order singular terms in the infrared limit is unclear, there could be a large energy window where the physics is controlled by the fixed point g_* derived above.

We can also compute the self-energy of the fermions at the hot spot to the leading nontrivial order of u:

$$\Sigma_F(\omega, \boldsymbol{k}) \sim 2u^2 \sigma^0 \int \frac{d\nu d^2\boldsymbol{q}}{(2\pi)^3} \frac{1}{\mathrm{i}(\omega - \nu) - \mathbf{v}_2 \cdot (\boldsymbol{k} - \boldsymbol{q})}$$

$$\times \quad \frac{1}{(\nu^2+\boldsymbol{q}^2)^{1-\eta/2}}. \tag{3.36}$$

We have taken the correlator of the bosonic field $N_{x,y}(\vec{q}) \sim z^\dagger \sigma^{x,y} z$ to be $1/(\nu^2+\boldsymbol{q}^2)^{1-\eta/2}$, where η is the anomalous dimension of the inplane Néel order parameter $N_{x,y}$ at the purely bosonic easy-plane DQCP. Carrying out the integral, we obtain

$$\Sigma_F(\omega, 0) \sim -\mathrm{i}u^2 \mathrm{sgn}(\omega)|\omega|^\eta \sigma^0. \tag{3.37}$$

Generally we expect the fermions at the hot spots to have non-Fermi liquid like self-energy for a considerable energy window.

3.2.2 SU(2) invariant DQCP coupled with hot spots

Here we briefly discuss the SU(2)-invariant DQCP coupled to a background Fermi surface, which can be studied in the same way as the easy-plane case. Here we only need one Hubbard-Stratonovich field λ^+ to decompose the quartic term, and we obtain the following large-N theory at the critical point:

$$\begin{aligned} \mathcal{S} &= \int d^2x d\tau \sum_{a=1}^{N} \sum_{\alpha=1,2} |(\partial - \mathrm{i}A) z_{a,\alpha}|^2 + \mathrm{i}\lambda^+ |z_{a,\alpha}|^2 \\ &+ \mathrm{i} \sum_{i=x,y,z} \Phi^i (z_a^\dagger \sigma^i z_a). \end{aligned} \tag{3.38}$$

Now the Fermi surfaces are coupled to all three components of the Néel order parameter $\vec{N} = z^\dagger \vec{\sigma} z$. The new dynamic exponent is now $z = 1 + \frac{3g}{8\pi^2} + O(g^2)$, and the beta function of g is

$$\beta(g) \equiv \frac{dg}{d\ln b} = \frac{16}{\pi^2 N} g - \frac{g^2}{4\pi^2}. \tag{3.39}$$

If $g > 0$, the theory flows to a new RG fixed point at $g_* = \frac{64}{N}$. At the new RG fixed point, we have the following scaling dimensions

$$[\lambda^+] = 2 - \frac{24}{\pi^2 N} - \frac{9g_*}{8\pi^2} = 2 - \frac{96}{\pi^2 N} + O(\frac{1}{N^2}),$$

$$[z_a^\dagger \sigma^{x,y,z} z_a] = 1, \tag{3.40}$$

and the critical exponent

$$\nu^{-1} = 2 + z - [\lambda^+] = 1 + \frac{120}{\pi^2 N} + O(\frac{1}{N^2}). \tag{3.41}$$

Again, the Néel order parameter has scaling dimension $[\vec{N}] = 1$ exactly at the new fixed point. Though it is not so convenient to directly compute the RG flow of the singular term of the VBS order parameter due to the lack of a dual Lagrangian for the SU(2) invariant DQCP, we expect the scaling dimension of the VBS order parameter should also be 1 at the new fixed point. To elaborate, the VBS order parameter V_x, V_y should still acquire a singular term $V_x|\partial_\tau|V_x + (x \to y)$ from coupling to the Fermi surface. This term is singular (nonanalytic) in the frequency space, and also long range in the temporal direction. The form of the singular term $|\partial_\tau|$ cannot be renormalized under RG. And if this term flows to a fixed point, this term $V_x|\partial_\tau|V_x + (x \to y)$ remains scaling invariant at the fixed point, hence the VBS order parameter V^x should have precisely scaling dimension 1.

Ref. [16] pointed out that at the DQCP there are two length scales, one for the correlation length ξ of the order parameter N_x, the other is the thickness of the VBS domain wall (ξ_{VBS}). In our system these two length scales still exit, and the relation between these two length scale should be similar to what was pointed out in Ref. [16]:

$\xi_{\text{VBS}} \sim \xi f(\lambda \xi^{d+z-\Delta})$, where λ is the strength of the four-fold monopole operator of the gauge field that is the minimal topological defect allowed by symmetry on a square lattice, and Δ is the scaling dimension of the four-fold monopole, which we assume is greater than $d + z$ (which means that the four-fold monopole is irrelevant at the DQCP). z is the dynamical exponent computed in this section. Following the discussions in Ref. [16], one can further infer that $\xi_{\text{VBS}} \sim \xi^{(\Delta - z)/2}$ close to the DQCP. Since we expect Δ to be greater than $2 + z$, ξ_{VBS} diverges faster than ξ near the DQCP.

The quantum critical modes at the new fixed point with $z > 1$ will make a contribution $C \sim T^{2/z}$ to the specific heat, which is different from ordinary $(2 + 1)d$ QCP with $z = 1$. But the background Fermi surface would contribute a specific heat linear with temperature T, hence we expect that the contribution from the quantum critical modes will be overshadowed by the background Fermi surface.

3.2.3 Discussion

In this section we discussed the fate of the DQCP when it occurs with a background Fermi surface. We demonstrated that with a large number of copies of Fermi surfaces, there is a substantial energy window where the easy-plane DQCP is controlled by a self-dual fixed point with dynamical exponent $z > 1$. We did not pursue a full renormalization group analysis of the boson-fermion coupled theory, but such analysis like the ones discussed in Ref. [35, 201] when the order parameter ϕ is a composite operator of deconfined degrees of freedom is very much worth studying in the future.

Many insights of the DQCP, including the emergent symmetry, 't Hooft anomaly, as well as possible phase diagram and RG flow, can be gained from the nonlinear sigma model (NLSM) approach that unifies all the order parameters in one action [198, 202, 203, 204, 205, 206, 207]. The very key term in the NLSM is a topological term. The

Néel and VBS order parameters can also be treated on an equal footing in the U(1) and SU(2) spin liquid language [81]. In the future it is also worth to explore the consequence of coupling the DQCP to a Fermi surface using these different formalisms.

Besides the DQCP, our study is also meaningful to the interaction-driven Metal-insulator transition (MIT) where the insulator phase has certain density wave order. The basic formalism of the theory describing this MIT involves introducing bosonic partons that carry the electric charge, and fermionic partons that carry the spin. This MIT is interpreted as a superfluid-to-density wave transition of the charged bosonic parton sector [208, 209] (The "superfluid" phase of the bosonic sector of the phase diagram corresponds to the metallic phase [38]), which is also described by a CP^{N-1} model in which the bosonic matter fields are vortices of the charged bosonic parton. There are multiple components of the vortex fields whose condensate corresponds to the degenerate density wave patterns of the insulator phase. When the density wave order parameter couples to the hot spots of the Fermi surface of the fermionic spinon sector, the same singular terms like the one considered in our current section will arise. Our study indicates that the physics at this MIT could be controlled by a new fixed point with dynamical exponent $z > 1$.

Chapter 4

Field Theoretical Study of Moiré Systems

4.1 Orbital Orders and Possible non-Fermi Liquid in Moiré systems

Systems with Moiré superlattice have surprised the condensed matter community with a plethora of correlated phenomena, supposedly due to the strong Coulomb interaction and the narrowness of the minibands in the Moiré mini Brillouin zone [210, 211, 212, 213, 214, 215, 216]. Correlated insulator at fractional fillings [217, 218], high temperature superconductor (compared with the miniband width) [219, 220, 221, 222, 223, 224, 214, 215, 216], quantum anomalous Hall effect [225, 167, 226, 227], strange metal (non-Fermi liquid) [134, 135], competing orders [228, 229], spin-triplet pairing [214, 215, 216, 230] have all been reported in recent experiments on Moiré systems. Many of these phenomena may have to do with order parameters with nontrivial transformations under spatial symmetries, *i.e.* the orbital orders. For example, the quantum anomalous Hall effect definitely

requires valley polarization because the Chern numbers of two degenerate minibands from two different valleys must cancel each other due to symmetry [225, 167, 226, 227]. Also, strong signature of nematic anisotropy was found in recent experiments on twisted bilayer graphene, in both the superconductor phase and the metallic phase [228, 229]. Mean field analysis of orbital orders in lattice models related to Moiré systems have also been studied [231].

Motivated by the experimental observations, in this section we discuss possible orbital orders in Moiré systems. We will explore novel generic physics at the order-disorder transition of the orbital orders, based on the spatial symmetries of the systems. Three different kinds of orbital orders, *i.e.* (1) the nematic order, (2) valley polarization, and (3) "compass order", which spontaneously break different subgroups of the entire spatial symmetries will be discussed. These orders should be viewed as possible instability of Fermi surface due to interactions. We will focus on the order-disorder quantum phase transition of these order parameters, and especially how the quantum fluctuations of these order parameters may affect the electrons. We demonstrate that, due to the unique symmetry of the systems, the nematic order fluctuation may lead to a special non-Fermi liquid behavior, different from what is usually expected at the quantum critical regime of an orbital order. The interplay between these order parameters allows a very rich phase diagram at zero and finite temperature. Within these three orbital orders, the valley polarization and "compass order" can potentially strongly compete with the superconductor.

4.1.1 Three orbital orders

In all the Moiré systems discovered so far, the most general microscopic symmetry is $C_3 \times \mathcal{T}$, where $\mathcal{T}$ is an effective time-reversal symmetry which is a product between the

ordinary time-reversal and a spin-flipping, hence this effective time-reversal symmetry still holds even with a background Zeeman field (inplane magnetic field). Under this symmetry, the Fermi surface of the miniband emerging from each valley only has a C_3 symmetry, and $\mathcal{T}$ interchanges the two valleys. The dispersion of the minibands from the two valleys satisfy $\varepsilon_1(\vec{k}) = \varepsilon_2(-\vec{k})$, where the subscript is the valley index. Different Moiré systems have different extra symmetries, for example the twisted bilayer graphene (TBG) without alignment with the BN substrate has an inversion symmetry $\mathcal{I}$, while the trilyer graphene and h-BN heterostructure has a reflection symmetry $\mathcal{P}$ [232]. Both $\mathcal{I}$ and $\mathcal{P}$ interchange the two valleys [232, 233, 234]. We assume that the system under study has the symmetry $C_3 \times \mathcal{T} \times \mathcal{I}$. Under these spatial symmetries, the momenta and electron operators transform as

$$\begin{aligned} C_3 \quad &: \quad (k_x + \mathrm{i}k_y) \to e^{\mathrm{i}2\pi/3}(k_x + \mathrm{i}k_y); \\ \\ \mathcal{T} \quad &: \quad c_{a,\vec{k}} \to \tau^1_{ab} c_{b,-\vec{k}}, \quad \mathcal{I} : c_{a,\vec{k}} \to \tau^1_{ab} c_{b,-\vec{k}}, \end{aligned} \tag{4.1}$$

where a, b are the valley indices. In this section we will discuss three different orbital orders, each breaking different subgroups of the entire symmetry $C_3 \times \mathcal{T} \times \mathcal{I}$.

The first orbital order we will consider is the nematic order ϕ, which is a complex scalar order parameter. The microscopic operator of the nematic order parameter in a two dimensional ($2d$) rotational invariant system can be written as [235]

$$\hat{\phi}(\vec{x}) \sim \psi^\dagger(\vec{x})(\partial_x^2 - \partial_y^2 + \mathrm{i}2\partial_x\partial_y)\psi(\vec{x}), \tag{4.2}$$

where $\psi(x)$ is the real space electron operator. $\hat{\phi}$ is an operator with zero or small momentum compared with the Fermi wave vector. In a system with symmetry $C_3 \times \mathcal{T} \times \mathcal{I}$,

the zero momentum nematic operator can be represented as

$$\begin{aligned}\hat{\phi} \sim & \sum_{\vec{k}} c^{\dagger}_{1,\vec{k}} \left(k_x^2 - k_y^2 + 2\mathrm{i}k_x k_y + \alpha(k_x - \mathrm{i}k_y)\right) c_{1,\vec{k}} \\ + & \sum_{\vec{k}} c^{\dagger}_{2,\vec{k}} \left(k_x^2 - k_y^2 + 2\mathrm{i}k_x k_y - \alpha(k_x - \mathrm{i}k_y)\right) c_{2,\vec{k}} \end{aligned} \tag{4.3}$$

with real number α. Since the Fermi surface on each valley only has a C_3 symmetry, the $d_{x^2-y^2} + \mathrm{i}d_{xy}$ order parameter with angular momentum $(+2)$ will mix with a $p_x - \mathrm{i}p_y$ order parameter with angular momentum (-1). The nematic order parameter $\phi \sim \langle\hat{\phi}\rangle$ transforms under the symmetries as

$$C_3 : \phi \to e^{\mathrm{i}2\pi/3}\phi; \quad \mathcal{T} : \phi \to \phi^*, \quad \mathcal{I} : \phi \to \phi. \tag{4.4}$$

A nonzero condensate of ϕ will break the spatial symmetries down to $\mathcal{T}$ and $\mathcal{I}$ only, and in this sense we can still refer to ϕ as a nematic order parameter. Nematic order has been found in many condensed matter systems (for a review see Ref. [236]), and strong signature of the existence of nematic order in both the superconducting phase and the normal metallic phase was recently reported in TBG [228, 229].

The second orbital order we will discuss is the valley polarization Φ, which corresponds to an operator

$$\hat{\Phi} \sim \sum_{\vec{k}} c^{\dagger}_{1,\vec{k}} c_{1,\vec{k}} - c^{\dagger}_{2,\vec{k}} c_{2,\vec{k}}. \tag{4.5}$$

A valley polarization $\Phi \sim \langle\hat{\Phi}\rangle$ is an Ising like order parameter. A nonzero Φ will cause imbalance of the electron density between the two valleys, *i.e.* the electron has higher population at one valley than the other, and it may lead to the quantum anomalous Hall

effect [225, 167, 226, 227]. Φ preserves the C_3 symmetry, but breaks both $\mathcal{T}$ and $\mathcal{I}$.

The last order parameter is the "compass order" which is again a complex scalar order parameter. The microscopic compass order operator is represented as

$$\begin{aligned}\hat{\varphi} \;\sim\; & \sum_{\vec{k}} c^{\dagger}_{1,\vec{k}} \left(k_x^2 - k_y^2 + 2\mathrm{i}k_x k_y + \alpha(k_x - \mathrm{i}k_y)\right) c_{1,\vec{k}} \\ - \; & \sum_{\vec{k}} c^{\dagger}_{2,\vec{k}} \left(k_x^2 - k_y^2 + 2\mathrm{i}k_x k_y - \alpha(k_x - \mathrm{i}k_y)\right) c_{2,\vec{k}}. \end{aligned} \tag{4.6}$$

Under the symmetry actions, the compass order parameter $\varphi \sim \langle\hat{\varphi}\rangle$ transforms as

$$C_3 : \varphi \to e^{\mathrm{i}2\pi/3}\varphi; \;\; \mathcal{T} : \varphi \to -\varphi^*, \;\; \mathcal{I} : \varphi \to -\varphi. \tag{4.7}$$

The symmetry transformation of φ can be viewed as the definition of the order parameter. φ also has the same symmetry transformation as the composite field $\phi\Phi$.

The full symmetry $C_3 \times \mathcal{T} \times \mathcal{I}$ guarantees that, a nonzero nematic order leads to three different degenerate ground states, while a compass order can take six different expectation values with degenerate energy. The compass order and valley polarization both break time-reversal symmetry $\mathcal{T}$, hence both orders can lead to anomalous Hall effect, as was observed in Ref. [226, 227]. Since the nematic order preserves $\mathcal{T}$, a nematic order alone cannot lead to the anomalous Hall signal. But a nematic order breaks the rotation symmetry, hence it directly couples to the background strain of the system.

4.1.2 Order-Disorder Transition of the Nematic Order

Normally when an order parameter with zero or small momentum couples to the Fermi surface, the dynamics of the order parameter is over-damped at low frequency according to the standard Hertz-Millis theory [32, 33]. The nematic order parameter is

slightly more complicated, when coupled to a circular Fermi surface, the dynamics of the nematic order parameter is decomposed into a transverse mode and longitudinal mode, and only the longitudinal mode is over-damped. The separation of the two modes was computed explicitly in Ref. [235], whose physical picture can be understood as following. Consider a general order parameter with a small momentum $\vec{q}$, the over-damping of this mode comes from its coupling with the patch of Fermi surface where the tangential direction is parallel with $\vec{q}$. For a circular Fermi surface, without loss of generality, let us assume $\vec{q} = (q_x, 0)$, then the Fermi patches that cause over-damping locate at $\vec{k}_f \sim \pm\hat{y}$. But $\Im[\phi]$ defined previously has nodes along the $\pm\hat{y}$ direction (rotational invariance guarantees that the "tangential patch" of the Fermi surface coincides with the node of the transverse mode), hence $\Im[\phi]_{\vec{q}}$ with $\vec{q} = (q_x, 0)$ is not over-damped.

But now the symmetry of the system, especially the fact that the $d-$wave order parameter mixes with the $p-$wave order parameter, no longer guarantees that for any small momentum $\vec{q}$ the "tangential patch" of the Fermi surface coincides with the node of the order parameter, hence ϕ is always over-damped, which can be shown with explicit calculations following Ref. [235]. Thus we will start with the following Hertz-Millis type of action for the nematic order parameter ϕ, which is invariant under the symmetry $C_3 \times \mathcal{T} \times \mathcal{I}$:

$$\begin{aligned} \mathcal{S}_b &= \mathcal{S}_0 + \int d^2x d\tau \; u(\phi^3 + \phi^{*3}) + g|\phi|^4, \\ \mathcal{S}_0 &= \sum_{\vec{q},\omega} \phi^*_{\vec{q},\omega} \left(\frac{|\omega|}{q} + q^2 + r \right) \phi_{\vec{q},\omega} \end{aligned} \tag{4.8}$$

For convenience we have written the free part of the action $\mathcal{S}_0$ in the momentum and Matsubara frequency space, but the interaction terms of the action in the Euclidean space-time. Also, since the U(1) rotation of ϕ is in fact a spatial rotation, there should be

coupling between the direction of $\vec{\phi} = (\mathrm{Re}[\phi], \mathrm{Im}[\phi])$ and direction of momentum, which we have ignored for simplicity [1]. Following the standard Hertz-Millis theory [32, 33], the action Eq. 4.8 is scaling invariant if we assign the following scaling dimensions to the parameters and field:

$$[\omega] = 3, \quad [q_x] = [q_y] = 1, \quad [r] = 2,$$

$$[\phi(\vec{x}, \tau)] = \frac{3}{2}, \quad [u] = \frac{1}{2}, \quad [g] = -1. \tag{4.9}$$

At the level of the Hertz-Millis theory, normally the total space-time dimension is greater than the upper critical dimension, hence the self-interaction of the order parameter is usually irrelevant, and the theory will lead to an ordinary mean field transition (for a review see Ref. [133]). However, unlike the ordinary Hertz-Millis theory, in our current case there is an extra symmetry-allowed term $u(\phi^3 + \phi^{*3})$ that is relevant even though the total space-time dimension is $D = d + z = 5$. Thus we need to perform analysis beyond the mean field theory, and explore the possible new physics led by the new term.

The relevant u term breaks the U(1) symmetry of ϕ down to a Z_3 symmetry, which is the symmetry of a three-state clock model [237]. A mean field analysis of such Ginzburg-Landau theory would lead to a first order transition which occurs at $r_c = u^2/g$, but a two dimensional three-state clock model (equivalent to a three-state Potts model) has a continuous transition and can be potentially described by the Ginzburg-Landau theory with a Z_3 anisotropy on a U(1) order parameter [238]. Ref. [239, 240] also presented examples of first order quantum phase transitions at the mean field level (precisely due to a cubic term like our $u-$term in the action) being driven to continuous transitions by

[1] The simplest nonzero term of this type would be $\int d^2x d\tau \phi(\partial_x - \mathrm{i}\partial_y)^2\phi$, which has the same scaling as the rest of the quadratic terms, hence it is not expected to lead to more singular contribution to the physical quantities to be calculated.

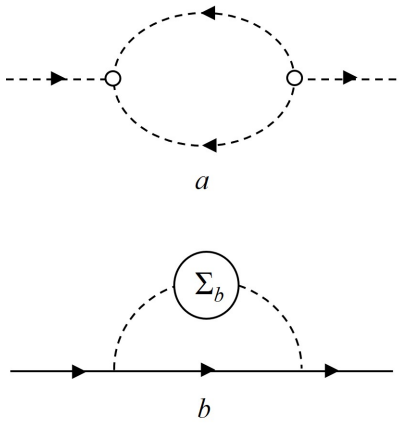

Figure 4.1: a, the one-loop correction to the boson propagator from the u term in Eq. 4.8; b, the one-loop correction (Eq. 4.14) to the fermion propagator through the boson-fermion coupling g' in Eq. 4.12.

fluctuations, especially when the order parameter is coupled to gapless fermions [239], which is analogous to our situation.

Without knowing for sure the true nature of the transition described by Eq. 4.8, at least the scaling analysis in the previous paragraph applies when r is tuned *close to* while *greater than* r_c, and in the energy scale $\omega \gg (u^2/g)^{3/2}$ the order parameter ϕ can always be viewed as a massless scalar field with self-interaction u and g in Eq. 4.8.

If we further assume that $(u^2/g)^{3/2} \ll 1/g^3$ and only look at energy scale $\omega < 1/g^3$, the irrelevant coupling g is renormalized small enough. Hence when the parameters in Eq. 4.8 satisfy $(u^2/g)^{3/2} \ll 1/g^3$, there is a finite energy window $\omega \in \left((u^2/g)^{3/2},\ 1/g^3\right)$ where we can view ϕ as a massless scalar field which interacts with itself mainly through the u term in Eq. 4.8, and the ordinary $|\phi|^4$ interaction is irrelevant and renormalized perturbatively weak. We expect that the action Eq. 4.8 with the relevant interaction u can lead to new universal physics that is beyond the standard Hertz-Millis theory.

Based on Eq. 4.8, if we take into account of the relevant perturbation u, in general

the boson propagator reads

$$\begin{aligned} G_b(\omega,\vec{q}) &= \frac{1}{G_{b0}^{-1}(\omega,\vec{q})+\Sigma_b(\omega,\vec{q})}, \\ G_{b0}^{-1}(\omega,\vec{q}) &= \frac{|\omega|}{q}+q^2. \end{aligned} \tag{4.10}$$

A full reliable analysis of Eq. 4.8 with the relevant perturbation u is difficult, we will first limit our study to the lowest nontrivial order of perturbation of u, later we will discuss other analysis. At the one-loop level (Fig. 4.1a), the boson self-energy $\Sigma_b(\omega,\vec{p})$ reads

$$\begin{aligned} \Sigma_b(\omega,\vec{q}) &\sim u^2\int d^2k d\nu\; G_{b0}(\nu,\vec{k})G_{b0}(\omega+\nu,\vec{q}+\vec{k}), \\ &\sim \text{Const}+Au^2\sqrt{|\omega|^{2/3}+cq^2}+\cdots \end{aligned} \tag{4.11}$$

A and c are both order one constants. The behavior of the boson self-energy is consistent with power-counting of the loop integral, and at low energy it dominates other quadratic terms $\mathcal{S}_0$ in the standard Hertz-Millis theory, due to the fact that u is a relevant perturbation. The cut-off dependent constant can be reabsorbed into r, and the ellipsis includes terms that are less dominant in the infrared [2].

For our purpose we need to analyze the effects of the boson-fermion coupling on the electrons. In the standard Hertz-Millis theory without the relevant u term in the boson action, the one loop self-energy of the electron scales as $\Sigma_f(\omega) \sim \text{isgn}[\omega]|\omega|^{2/3}$. We will analyze how the u term may change the behavior of the fermion self-energy. Following the formalism used in Ref. [36, 136, 37, 148, 34], we expand the system at one patch of the Fermi surface. The "one-patch" theory is a very helpful formalism to

[2]The loop integral is performed numerically, and it fits best with the expression in Eq. 4.11.

systematically evaluate loop diagrams in a boson-fermion coupled theory. This "one-patch theory" breaks the C_3 symmetry, hence the real and imaginary parts of ϕ are no longer degenerate. Since we are most interested in the scaling behavior of the Fermion self-energy, we will consider a one component boson field with the dressed propagator and self-energy given by Eq. 4.11. The one-patch theory reads

$$\begin{aligned} \mathcal{S}_{bf} &= \sum_{\omega,\vec{k}} \psi^{\dagger}_{\omega,\vec{k}}(\mathrm{i}\omega - v_f k_x - v k_y^2)\psi_{\omega,\vec{k}} \\ &+ \mathcal{S}_0 + \sum_{\omega,\vec{q}} \Sigma_b(\omega,\vec{q})|\phi_{\omega,\vec{q}}|^2 \\ &+ \int d^2x d\tau \; g'\phi\psi^{\dagger}\psi, \end{aligned} \tag{4.12}$$

Where $\mathcal{S}_0$ is given by Eq. 4.8, and $\Sigma_b(\omega,\vec{q})$ given by Eq. 4.11.

For this "one-patch" boson-fermion coupled theory we need to use a different assignment of scaling dimensions, which was introduced in Ref. [36, 136, 37, 148, 34] for a better controlled analysis of the boson-fermion coupled theory. In order to avoid confusion, we use "[ ]" to denote the scaling dimension of the original pure boson theory Eq. 4.8, but "{ }" to denote the scaling dimension of the "one-patch" boson-fermion coupled theory:

$$\{\omega\} = 3, \quad \{k_x\} = 2, \quad \{k_y\} = 1,$$

$$\{\phi(\vec{x},\tau)\} = \frac{5}{2}, \quad \{\psi\} = 2, \quad \{g'\} = -\frac{1}{2}. \tag{4.13}$$

Under the new scaling relation Eq. 4.13, $\mathcal{S}_0$ becomes irrelevant compared with $\Sigma_b(\omega,\vec{q})$ in Eq. 4.11. We will first ignore the irrelevant term $\mathcal{S}_0$ completely (which will be revisited later) to reveal the main effect of the new $u-$term in Eq. 4.8. The one-loop fermion

self-energy (Fig. 4.1*b*) reads

$$\begin{aligned}\Sigma_f(\omega) &\sim \int d^2k d\nu\ G_{f0}(\nu,\vec{k})G_b(\omega+\nu,\vec{k}) \\ &\sim \int d^2k d\nu \frac{1}{\mathrm{i}\nu - v_f k_x - v k_y^2}\frac{1}{\sqrt{|\omega+\nu|^{2/3}+ck^2}} \\ &\sim \mathrm{i}\omega \log\left(\frac{\Lambda}{|\omega|}\right). \end{aligned} \tag{4.14}$$

This behavior of fermion self-energy is similar to the marginal fermi liquid, and it is consistent with the simple power-counting of the loop integral. The marginal fermi liquid was proposed as a phenomenological theory for the strange metal phase (a non-Fermi liquid phase) of the cuprates high temperature superconductor [132]. A similar strange metal behavior was observed in the TBG [228, 134, 135]. Our goal here is not to directly address the observed strange metal bahavior [3], instead we stress that the electrons at the order-disorder transition of the nematic order in the Moiré systems should behave differently from what is usually expected at a nematic quantum critical point. This difference originates from the unique symmetry of the Moiré systems.

Because g' is an irrelevant perturbation in Eq. 4.12 according to the scaling convention of the "one-patch" theory Eq. 4.13, higher order perturbation of g' in theory Eq. 4.12 is not expected to lead to more dominant correction to the fermion self-energy in the infrared, hence we no long need to worry about the infinite "planar diagram" problem in ordinary cases when an order parameter is coupled with a Fermi surface [148].

The results above are based on the one-loop calculation in the expansion of u, and higher order expansion of u will modify the results in the infrared limit. If eventually

[3] It was suggested that a pure phonon-electron coupling can lead to a linear$-T$ resistivity in Moiré systems [241, 135], but it was argued in Ref. [134] that other mechanisms may be demanded to explain the observed data.

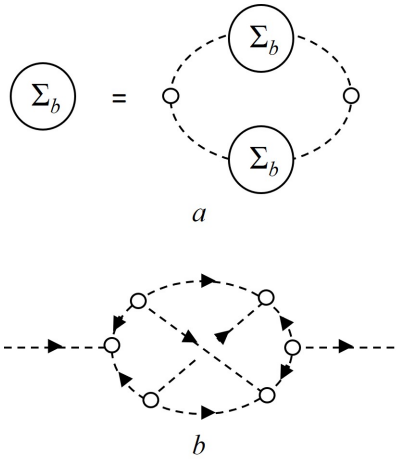

Figure 4.2: a, the schematic representation of the Schwinger-Dyson equation; b, the example of vertex correction that is not summed in the Schwinger-Dyson equation.

the nematic transition is driven continuous by fluctuations as the examples given in Ref. [239, 240], then a full analysis for the infrared limit is desired. Although we cannot completely solve the strongly interacting theory Eq. 4.8 analytically beyond the perturbation expansion, an approximate solution can be obtained through the Schwinger-Dyson (SD) equation, which sums a subset of the Feynman diagrams Fig. 4.2a:

$$\Sigma_b \sim u^2 \int d^2k d\nu \; G_b(\nu, \vec{k}) G_b(\omega + \nu, \vec{q} + \vec{k}),$$

$$G_b^{-1} = G_{b0}^{-1} + \Sigma_b. \tag{4.15}$$

Here we have ignored the vertex correction from the full SD equation (For example, vertex correction Fig. 4.2b). We also take a simple ansatz that at the order-disorder transition the boson self-energy is approximated by the scaling form

$$\Sigma_b(\omega, \vec{q}) \sim u^{2\eta} Q^{2-\eta} \tag{4.16}$$

with anomalous dimension η, where Q is the infrared cut-off that can be taken as

Max$[|\omega|^{1/3}, |\vec{q}|]$. The previous one-loop result simply yields $\eta = 1$. Now the bosonic part of the boson-fermion coupling action Eq. 4.12 is replaced by $\mathcal{S}_b = \mathcal{S}_0 + \sum_{\omega,\vec{p}} \Sigma_b(\omega, \vec{q})|\phi_{\omega,\vec{q}}|^2$. Again, if we tentatively ignore $\mathcal{S}_0$, the scaling of the boson-fermion coupling theory is modified as

$$\{\omega\} = 3, \quad \{k_x\} = 2, \quad \{k_y\} = 1,$$

$$\{\phi(\vec{x}, \tau)\} = \frac{4+\eta}{2}, \quad \{\psi\} = 2, \quad \{g'\} = -\frac{\eta}{2}. \tag{4.17}$$

The one-loop fermion self-energy should then scale as

$$\Sigma_f(\omega) \sim \mathrm{i}\omega|\omega|^{\frac{\eta-1}{3}}. \tag{4.18}$$

As long as $\eta > 0$, the boson-fermion coupling g' in Eq. 4.12 is still irrelevant, hence higher order fermion self-energy diagrams from the boson-fermion coupling theory are not expected to change Eq. 4.18 in the infrared.

The solution of the approximate SD equation would yield $\eta = 1/3$, which will lead to a non-fermi liquid behavior that is in-between the standard Hertz-Millis theory and also the marginal fermi liquid. After we convert the Matsubara frequency to real frequency, the imaginary part of the fermion self-energy (inverse of the fermion life-time) is a very characteristic property of the non-Fermi liquid. And the analysis above suggests that the imaginary part of fermion self-energy should scale as $\mathrm{Im}(\Sigma_f) \sim \mathrm{sgn}(\omega)|\omega|^\beta$ with $2/3 < \beta < 1$.

If eventually the transition in Eq. 4.8 is driven continuous by fluctuation (like the examples given in Ref. [239, 240]), then the field ϕ is indeed massless even in the infrared limit at the transition. Then the difference of our results described above from the stan-

dard Hertz-Millis theory should be obvious in the infrared limit. But even if the transition is first order at $r_c = u^2/g$, as we discussed previously, when the parameters in Eq. 4.8 satisfy $(u^2/g)^{3/2} \ll 1/g^3$, at least there is a finite energy window $|\omega| \in \left((u^2/g)^{3/2},\ 1/g^3\right)$ where ϕ can be viewed as a massless scalar field with strong self-interaction mainly through the u term, while other interactions in Eq. 4.8 can be ignored. In this case, the calculations in this section were simplified by assuming that the boson self-energy Σ_b dominates the other quadratic term, *i.e.* $\mathcal{S}_0$ in Eq. 4.8, because $\mathcal{S}_0$ is irrelevant compared with Σ_b. But in the finite energy window described above, since we are not in the infrared limit, one should keep a nonzero $\mathcal{S}_0$ together with Σ_b in the calculation of the fermion self-energy. Then the loop integral in the evaluation of $\Sigma_f(\omega)$ is more complicated. The fermion self-energy is no longer a simple scaling form $\mathrm{Im}(\Sigma_f) \sim \mathrm{sgn}(\omega)|\omega|^\beta$ with a constant exponent β. Instead, the exponent β is expected to increase from the standard Hertz-Millis result $\beta = 2/3$ while decreasing ω, *i.e.* in other words the system should crossover back to the standard Hertz-Millis result at higher energy scale. We have numerically calculated the fermion self-energy by keeping a nonzero $\mathcal{S}_0$ in the bosonic theory, and confirmed this expectation of crossover.

Recently the standard result of the fermion self-energy scaling of the Hertz-Millis theory was confirmed in numerical simulation [171] on nematic transitions on a square lattice. We expect that our qualitative prediction of the fermion self-energy under the symmetry of the Moiré systems can also be seen in future numerical simulations.

4.1.3 Valley Polarization and Compass order

The effective theory of the valley polarization order Φ and compass order φ are more conventional Hertz-Millis theories whose analysis can be quoted from Ref. [133]. A cubic self-interaction term is not allowed for either order parameters. But the symmetry

transformation of the compass order φ allows a term

$$u_6(\varphi^6 + \varphi^{*6}) \tag{4.19}$$

in the Ginzburg-Landau-Hertz-Millis theory of φ, which is irrelevant in the infrared at the total space-time dimension $D = 5$. The three order parameters are coupled together in the effective theory, and the lowest order symmetry-allowed couplings are:

$$\begin{aligned} \mathcal{L}_{mix} &= \cdots + r_\phi|\phi^2| + r_\varphi|\varphi|^2 + r_\Phi|\Phi|^2 \\ &+ v_1(\Phi\phi\varphi^* + h.c.) + v_2(\Phi\varphi^3 + h.c.) \\ &+ v_3\Phi^2|\phi|^2 + v_4\Phi^2|\varphi|^2. \end{aligned} \tag{4.20}$$

A full exploration of the multi-dimensional parameter space will lead to a very complex and rich phase diagram. The specific values of the parameters in Eq. 4.20 depend heavily on the microscopic physics of the system.

Recently evidence of strain that breaks the C_3 rotation symmetry has been reported in Moiré systems [242], and the strain can potentially strongly affect the band structure [243]. With a background strain field, the nematic order parameter ϕ acquires a nonzero expectation value, and hence Φ and φ become the same order parameter through the coupling v_1 in $\mathcal{L}_{mix}$.

At finite temperature, the nematic order and valley polarization will go through continuous transitions which correspond to the three-state potts and Ising conformal field theory with central charges 4/5 and 1/2 respectively. While if we start with a zero temperature compass order, the finite temperature physics can be mapped to a

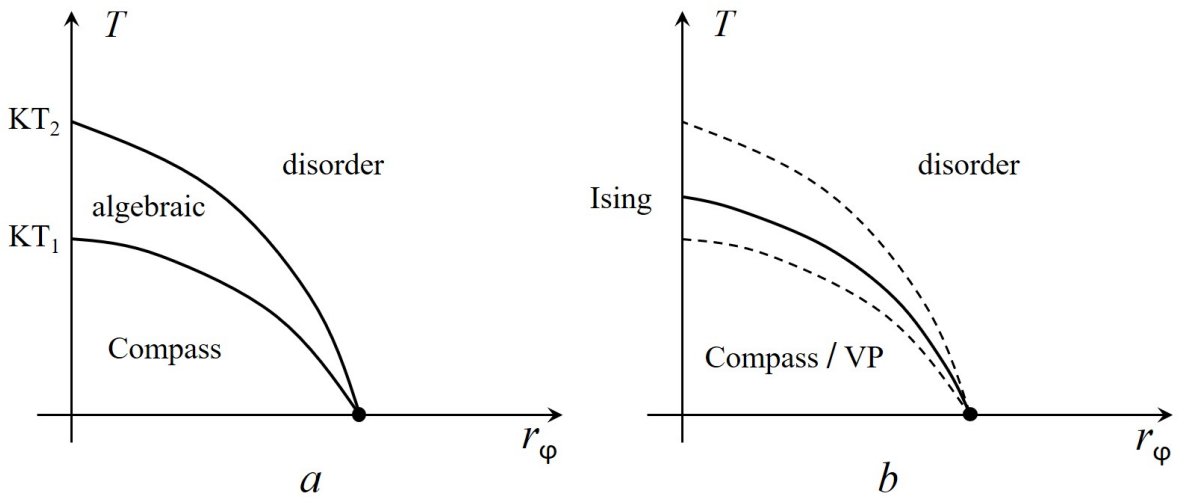

Figure 4.3: a, the phase diagram when there is a compass order at zero temperature, there are two consecutive Kosterlitz-Thouless transitions at finite temperatures and an algebraic phase in between; b, once there is a background strain in the system, the compass order is identical to the valley polarization (VP) order, and hence there is only one Ising transition at finite temperature.

six-state clock model due to the u_6 term mentioned previously in the Ginzburg-Landau theory of the compass order. In this case while raising temperature the system will undergo two consecutive continuous Kosterlitz-Thouless transitions with an algebraic quasi-long range order in between. Within the algebraic phase, the scaling dimension of the compass order parameter $[\varphi]$ is temperature dependent, and $1/18 < [\varphi] < 1/8$. The nematic order parameter $\phi \sim \varphi^{*2}$ and valley polarization $\Phi \sim \varphi^3 + \varphi^{*3}$ also have power-law correlation function in the algebraic phase, and their scaling dimensions are $[\phi] = 4[\varphi]$, and $[\Phi] = 9[\varphi]$. Hence even a weak background strain which pins ϕ is always a relevant perturbation in the algebraic phase, and will collapse the two Kosterlitz-Thouless transitions of φ into a single Ising transition of Φ.

Signature of a hidden order which strongly competes with superconductor was observed experimentally [228, 229]. Within the three orbital orders that we have discussed in this section, the valley polarization and compass order both obviously compete with

the superconductor. The reason is that both these two order parameters break $\mathcal{T}$ and $\mathcal{I}$, hence break the degeneracy between electrons at $\vec{k}$ and $-\vec{k}$ (the C_3 symmetry alone does not protect this degeneracy), hence a nonzero Φ or φ makes it difficult to form zero momentum Cooper pair. Indeed, experiments so far have not found superconductivity near the quantum anomalous Hall state in Moiré systems which at least require either valley polarization or the compass order. We stress that the competing order mentioned here does not necessarily mean it is the nature of the correlated insulator observed experimentally.

4.1.4 Final remarks

In this section we studied three different orbital orders that may occur in Moiré systems. We demonstrate that at the order-disorder transition of the nematic order parameter (one of the three orbital orders), a special non-Fermi liquid behavior is expected in a finite energy window, due to the symmetry of the system. We focused on the metallic phase at the disorder-order transition of the orbital order, since experimentally a nematic metallic phase was observed [229] above the nematic superconducting phase. Since the three different orbital orders can interact with each other in the effective theory and lead to a complex and rich phase diagram, depending on the parameters the Moiré systems under different conditions may display different orbital orders. We demonstrate that the effective theory for the nematic order is beyond the standard Hertz-Millis theory. Numerical methods such as Ref. [244, 245, 246, 171] are demanded to verify the results in the current section.

We focused on the generic field theory analysis of the phase transitions of the orbital orders, based on the symmetry of the system. The parameters of the field theory can be estimated through a calculation based on the lattice models, but this estimate depends

on the microscopic details of the systems, and it may vary strongly between different systems. For example, the parameter u stems from the C_3 symmetry of the Fermi surface at each valley, and its value depends on the extent of the C_3 deformation from the ordinary circular Fermi surface, which likely strongly depends on the microscopic model as well as the charge density. Due to the complexity and subtlety of the microscopic analysis, we plan to leave it to future studies. In the future we will also pursue a proper generalized renormalization group expansion such as Ref. [36, 136, 37], as well as analysis of the stability of the nematic order transition towards other orders such as superconductivity [168, 169, 170, 247] in Moiré systems.

4.2 Interaction driven Metal-Insulator Transition with Charge Fractionalization

4.2.1 Introduction

Many correlated phenomena have been observed in graphene-based moiré systems, such as high temperature superconductivity (compared with the bandwidth of the moiré bands), correlated insulators [248, 249, 250, 251, 252, 224, 253, 254, 255], and the strange metal phase [256, 135], etc. The most fundamental reason for the emergence of these correlated physics is that the slow modulating moiré potential leads to very narrow bandwidths [257, 258]. Great theoretical interests and efforts have been devoted to the graphene based moiré systems [259, 260, 261, 262, 263, 264, 265, 266, 267, 268, 225, 269, 270, 271, 272, 273, 274, 275]. But the theoretical description and understanding of the graphene based moiré systems may be complicated by the fact that in the noninteracting limit the moiré mini bands can have various types of either robust or fragile nontrivial topologies [276, 277, 278, 279, 280, 281, 282, 283, 284, 285], although the exact role of

the band topology to the interacting physics at fractional filling is not entirely clear. Hence similar narrow band systems with trivial band topology and unambiguous concise theoretical framework would be highly desirable. It was proposed that much of the correlated physics of the transition metal dichalcogenide (TMD) moiré heterostructure can be captured by an extended Hubbard model with an effective spin-1/2 electron on a triangular moiré lattice [286]

$$H = \sum_{\boldsymbol{r},\boldsymbol{r}',\alpha} -t_{\boldsymbol{r},\boldsymbol{r}'} c^{\dagger}_{\boldsymbol{r},\alpha} c_{\boldsymbol{r}',\alpha} + H.c. + \sum_{\boldsymbol{r}} U n_{\boldsymbol{r},\uparrow} n_{\boldsymbol{r},\downarrow} + \cdots \tag{4.21}$$

The electron operator $c_{\boldsymbol{r},\alpha}$ is constructed by states within a topologically trivial moiré mini band. Due to the strong spin-orbit coupling, the spin and valley degrees of freedom are locked with each other in the TMD moiré system. We will use $\alpha = \uparrow, \downarrow$ or $1, 2$ to denote two spin or equivalently two valley flavors. When a moiré band is partially filled, the correlated physics within the partially filled moiré mini bands may be well described by Eq. 4.21, which only contains half of the degrees of freedom of a mini band in a graphene based moiré system. The ellipsis in Eq. 4.21 can include further neighbor hopping, "spin-orbit" coupling terms allowed by symmetry [287], and further neighbor interaction. Note the "spin-orbit" coupling here refers to the hopping terms in Eq. 4.21 that depend on the spin index α and should not be confused with the bare spin-orbit coupling within the TMD system before the moiré superlattice is imposed. The TMD moiré systems are hence considered as a simulator for the extended Hubbard model on a triangular lattice [288].

Like the graphene-based moiré systems, the TMD moiré heterostructure is a platform for many correlated physics. This section mainly concerns the metal-insulator transition (MIT) driven by interaction. The MIT of the Hubbard model on a triangular lattice has attracted much numerical efforts recently [289, 290]. The symmetry of the TMD moiré

heterostructure is different from the simplest version of the Hubbard model, hence even richer physics can happen in the system. Continuous MIT has been reported at half-filling of the moiré bands (electron filling $\nu = 1/2$, or one electron per moiré unit cell on average) in the TMD moiré system [39, 40]. The experimental tuning parameter of the MIT in the TMD heterostructure is the displacement field, i.e. an out-of-plane electric field, which tunes the width of the mini moiré bands, and hence the ratio between the kinetic and interaction energies in the effective Hubbard model. Correlated insulators have also been observed at various other fractional electron fillings, though the nature of the MITs at these fractional fillings have not been thoroughly inspected experimentally [291, 292, 293, 294]. In this section we will mainly focus on $\nu = 1/2$, but other fractional fillings will also be briefly discussed.

The nature of an interaction driven MIT depends on the nature of the insulator phase near the MIT. The Hubbard model on the triangular lattice has one site per unit cell, which based on the generalized Lieb-Shultz-Matthis theorem [117, 119] demands that the insulator phase at half-filling should not be a trivial incompressible (gapped) state which preserves the translation symmetry. If the insulator phase has a semiclassical spin order that breaks the translation symmetry, the evolution between the metal and insulator could involve two transitions: at the first transition a semiclassical spin order develops, which reduces the Fermi surface to several Fermi pockets; and at the second transition the size of the Fermi pockets shrink to zero, and the system enters an insulator phase. A more interesting scenario of the MIT only involves one single transition [295, 296, 297], but then the insulator phase is not a semiclassical spin order, instead it is a spin liquid state with a spinon Fermi surface. An intuitive picture for this transition is that, at the MIT, the charge degrees of freedom are gapped, but the spins still behave as if there is a "ghost" Fermi surface. The spinon Fermi surface can lead to the Friedel oscillation just like the metal phase [298]. The structure of the Fermi surface does not change drastically

across the transition.

In a purely two dimensional system, conductivity (or resistivity) is a dimensionless quantity, hence it can take universal value at the order of e^2/h (or h/e^2) in various scenarios. For example, the Hall conductivity of the quantum Hall state is precisely $\sigma_H = \nu e^2/h$; the conductivity (or resistivity) at a $(2+1)d$ quantum critical point also takes a universal value at the order of e^2/h (or h/e^2) [299]. One central prediction given by the theory above for interaction driven continuous MIT is that, there is a universal resistivity jump at the order of $\sim h/e^2$ at the MIT compared with the metal phase; and the critical resistivity at the MIT should also be close to the order of h/e^2 (we will review these predictions in the next section). In this section we will argue that the current experimental observations suggest that the nature of the MIT in $MoTe_2/WSe_2$ moiré superlattice without twisting [39] is beyond the previous theory [295, 296, 297], and we propose an alternative candidate theory of MIT with further charge fractionalizations. We will discuss how the alternative theory can potentially address the experimental puzzles, and more predictions based on our theory will be made. Our assumption is that the MIT in this system is indeed driven by electron-electron interaction (as was suggested by Ref. [39]); If the disorder plays the dominant role in this system, the MIT may be described by the picture discussed in Ref. [300].

The section is organized as follows: In section 4.2.2 we introduce an alternative parton construction for systems described by the extended Hubbard model with a spin-orbit coupling, which naturally leads to charge fractionalization at the interaction-driven MIT even at half-filling; we also give an intuitive argument of physical effects caused by charge fractionalization at the MIT. In section 4.2.3, we will discuss the theory for MIT when the insulating phase spontaneously breaks the translation symmetry. Section 4.2.4 studies the theory of MIT when the insulating phase has different types of topological orders. In section 4.2.5 we discuss various experimental predictions based on our theory,

for the MIT and also the phases nearby. We present the details of our theory in the appendix, including the projective symmetry group, field theories, and calculation of DC resistivity, etc.

4.2.2 Two Parton constructions

The previous theory for the interaction-driven continuous MIT for correlated electrons on frustrated lattices was based on a parton construction. The parton construction splits the quantum number of an electron into a bosonic parton which carries the electric charge, and a fermionic parton which carries the spin. In the current section we compare two different parton constructions:

$$\text{I} : c_{\boldsymbol{r},\alpha} = b_{\boldsymbol{r}} f_{\boldsymbol{r},\alpha}, \quad \text{II} : c_{\boldsymbol{r},\alpha} = b_{\boldsymbol{r},\alpha} f_{\boldsymbol{r},\alpha}. \tag{4.22}$$

In parton construction-I only one species of charged bosonic parton b is introduced for electrons with both spin/valley flavors; while in parton construction-II a separate charged bosonic parton b_α is introduced for each spin/valley flavor. As we will see later, the two different parton constructions will lead to very different observable effects. The construction-I is the standard starting point of the theory of MIT that was used in previous literature [295, 296, 297]; construction-II is usually unfavorable for systems with a full spin SU(2) invariance, because the parton construction itself breaks the spin rotation symmetry. But the construction-II is a legitimate parton construction for the system under study, whose band structure in general does not have full rotation symmetry between the two spin/valley flavors.

The time-reversal symmetry of the microscopic TMD system relates the two spin/valley flavors. But it is not enough to guarantee a full SU(2) rotation symmetry between the two flavors. In fact, since the two flavors can be tied to the two valleys of the TMD

material, the trigonal warping of the TMD bands, which takes *opposite* signs for the two different valleys, can lead to the breaking of such an SU(2) rotation symmetry. To estimate the trigonal warping effect in the Hubbard model, one can compare the k^2 term and the $k_x^3 - 2k_x k_y^2$ term in the electron dispersion of one of the two layers in the heterostructure expanded at one valley. Then the relative strength of the trigonal warping compared to the SU(2)-invariant hopping in Eq. 4.21 is given by the ratio between the lattice constant of the original TMD material and that of the morié superlattice. In addition, the natural microscopic origin of the interactions in the Hamiltonian Eq. 4.21 is the Coulomb interaction between the electrons. The Coulomb interaction when projected to the low-energy bands relevant to the moiré-scale physics is expected to contain SU(2)-breaking interaction terms. The momentum conservation only guarantees the valley U(1) symmetry. Assuming the unscreened Coulomb interaction between electrons before the projection to the low-energy bands, further neighbor interaction will appear in the extended Hubbard model. The relative strength of the SU(2)-breaking interaction terms obtained from the projection compared to the SU(2)-invariant interactions can again be estimated by the ratio between the lattice constant of the original TMD material and the moiré superlattice, as the Fourier transform of unscreened Coulomb interaction in $2d$ space is $V_q \sim 1/q$.

The most important difference between these two parton theories resides in the filling of the bosonic partons. Since each bosonic parton carries the same electric charge as an electron, the total number of bosonic partons should equal to the number of electrons. Hence at electron filling ν (meaning 2ν electrons per unit cell), the filling factor of boson b in construction-I is $\nu_b = 2\nu$, i.e. 2ν bosonic parton per unit cell; in construction-II the filling factor of boson b_α has filling factor $\nu_b^\alpha = \nu$ for each spin/valley flavor. Hence even with one electron per site (half-filing or $\nu = 1/2$ of the extended Hubbard model), the bosonic parton in construction-II is already at half filling for each spin/valley flavor.

The half-filling will lead to nontrivial features inside the Mott insulator phase, as well as at the MIT. Another more theoretical difference is that, in construction-I there is one dynamical emergent U(1) gauge field a_μ which couples to both b and f_α; while in construction-II there are two dynamical U(1) gauge fields $a_{\alpha,\mu}$, one for each spin/valley flavor.

In construction-I, the bosonic parton b is at integer filling, and the MIT is naturally interpreted as a superfluid to Mott insulator (SF-MI) transition of boson b. At the MIT, using the Ioffe-Larkin rule [301], the DC resistivity of system is $\rho = \rho_b + \rho_f$, where ρ_b and ρ_f are the resistivity contributed by the bosonic and fermionic partons respectively. ρ_f caused by disorder or interaction such as the Umklapp process is a smooth function of the tuning parameter, the drastic change of ρ across the MIT arises from ρ_b. In the metal phase, i.e. the "superfluid phase" of b, ρ_b is zero, and the total resistivity is just given by ρ_f. Also, in the superfluid phase of b, the U(1) gauge field a_μ that couples to both b and f_α is rendered massive due to the Higgs mechanism caused by the condensate of b. In the insulator phase, ρ_b and ρ are both infinity, and the system enters a spin liquid phase with a spinon Fermi surface of f_α that couples to the dynamical U(1) gauge field a_μ. The MIT which corresponds to the condensation of b belongs to the 3D XY universality class. The dynamical gauge field a_μ is argued to be irrelevant at the transition due to the overdamping of the gauge field that arises from the spinon Fermi surface [296, 297], and hence does not change the universality class of the SF-MI transition of b.

In parton construction-I, at the MIT the bosonic parton contribution to the resistivity ρ_b is given by $\rho_b = Rh/e^2$, where R is an order-1 universal constant. In the order of limit $T \to 0$ before $\omega \to 0$, R is associated to the 3D XY universality class [302], because the gauge field a_μ is irrelevant as mentioned above. This universal conductivity at the 3D XY transition has been studied through various analytical and numerical methods [299, 303, 304, 305, 306, 307, 308, 309, 310]. At finite T and zero frequency,

the gauge field a_μ can potentially enhance the value R to $R' > R$, based on a large-**N** calculation in Ref. [311] (**N** is different from N in this section). The evaluation in Ref. [311] gave $R' \sim 7.92$, while we evaluate the same quantity to be $R' \sim 7.44$. Hence the prediction of the construction-I is that, the DC resistivity of the system right at the MIT has a universal jump compared with the resistivity at the metallic phase close to the MIT [296, 297], i.e. $\Delta\rho = \rho_b = R'h/e^2$. With moderate disorder, at the MIT ρ_b of the bosonic parton is supposed to dominate the resistivity ρ_f of the fermionic parton f_α, hence the total resistivity $\rho = \rho_b + \rho_f$ should be close to ρ_b.

In the experiment on the $MoTe_2/WSe_2$ moiré superlattice, it was reported that disorder in the system is playing a perturbative role, and the continuous MIT is mainly driven by the interaction [39]. However, the reported resistivity ρ increases rapidly with the tuning parameter (the displacement field) near the MIT. The bare value of ρ near and at the MIT is significantly greater than h/e^2 (and significantly larger than the computed value of $\rho_b \sim R'h/e^2$ mentioned above), and it is clearly beyond the Mott-Ioffe-Regel limit, i.e. the system near and at the MIT is a very "bad metal" [312, 313]. This suggests that the MIT is not a simple SF-MI transition of b, or in other words b should be "much less conductive" compared with what was predicted in construction-I considered in previous literature. We will demonstrate that construction-II can potentially address the large resistivity at the MIT. The most basic picture is that, since b_1 and b_2 are both at half-filling, the LSM theorem [117, 119] dictates that the Mott insulator phase of each flavor of boson cannot be a trivial insulator, namely the Mott insulator must either be a density wave that spontaneously breaks the translation symmetry, or have topological order. In either case, the MIT is not a simple 3D XY transition, and the most prominent feature of the transition is that, the bosonic parton number (or the electric charge) must further fractionalize.

The MIT with charge fractionalization will be discussed in detail in the next section

using the dual vortex formalism, but the consequence of this charge fractionalization can be understood from a rather intuitive picture. Suppose b fractionalizes into N parts at the MIT, meaning the charge carriers at the MIT have charge $e_* = e/N$, then each charge carrier will approximately contribute a resistivity at the order of $h/e_*^2 \sim N^2 h/e^2$ at the MIT; and if there are in total N_b species of the fractionalized charge carriers, at the MIT the bosonic parton will approximately contribute resistivity

$$\rho_b \sim \frac{N^2 h}{N_b e^2}. \tag{4.23}$$

There is a factor of N_b in the denominator because intuitively the total conductivity of b will be a sum of the conductivity of each species of fractionalized charge carriers, i.e. $\sigma_b = \sum_{j=1}^{N_b} \sigma_j$, in the unit of e^2/h (a more rigorous rule of combining transport from different partons will be discussed later). Hence when $N^2/N_b > 1$, the construction-II with inevitable charge fractionalization can serve as a natural explanation for the large ρ at the MIT, and it will also predict a large jump of resistivity $\Delta\rho$ at the MIT.

4.2.3 Mott insulator with translation symmetry breaking

General Formalism

In this section we will discuss the MIT following the parton construction-II discussed in the previous section. The MIT is still interpreted as the SF-MI transition of both spin/valley flavors of the bosonic parton b_α, although as we discussed previously the insulator cannot be a trivial incompressible state of b_α. In the superfluid phase of b_α, both U(1) gauge fields $a_{1,\mu}$ and $a_{2,\mu}$ that couple to the two flavors of partons are gapped out by the Higgs mechanism, and the system enters a metal phase of the electrons; b_1 and b_2 must undergo the SF-MI transition simultaneously, since the time-reversal or spatial

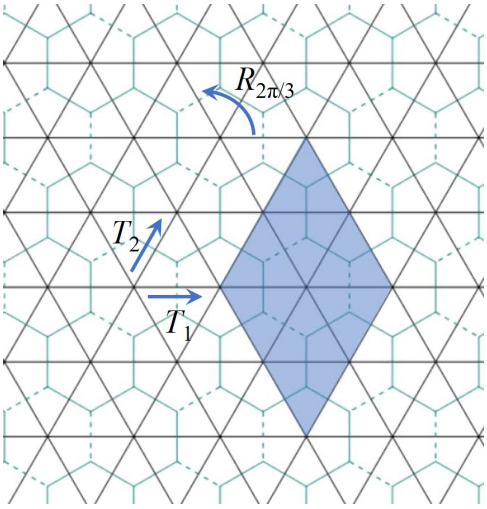

Figure 4.4: The triangular moiré lattice, and its dual honeycomb lattice. In the parton construction-II, the bosonic parton b_α is at half-filling for each spin/valley flavors, which becomes a $\pi-$flux of the dual gauge field A_μ through the hexagon of the dual honeycomb lattice. Hence the vortex ψ defined on the dual honeycomb lattice does not have a uniform hopping amplitude, the dashed links on the dual honeycomb lattice have negative hopping amplitudes. The symmetry of the lattice will be realized as a projective symmetry group. There are eight dual sites per unit cell (shaded area) in this gauge choice. At each spin/valley flavor, there are translation symmetries $T_{1,2}$, a rotation symmetry $R_{\frac{2\pi}{3}}$, and a product of reflection $P_x(x \to -x)$ and time-reversal $\mathcal{T}$. We also argue that P_y is a symmetry of the system as long as there is no valley mixing; and the six-fold rotation $R_{\pi/3}$ becomes a good approximate symmetry of the Hubbard model in the case of long moiré lattice constant.

reflection symmetries both interchange the two flavors of partons due to the spin-valley locking.

The dual vortex theory [314, 315, 316] is the most convenient formalism that describes a transition between a superfluid and a nontrivial insulator of a boson at fractional filling. If we start with a boson b, after the boson-vortex duality, a vortex of the superfluid phase of b becomes a point particle that couples to a dynamical U(1) gauge field A_μ, which is the dual of the Goldstone mode of the superfluid (not to be confused with the U(1) gauge field a_μ mentioned before that couples to the bosonic parton b). In the dual picture, the superfluid phase of b (which corresponds to the metal phase of the electron) is the insulator phase of the vortex field; while the Mott insulator phase of b corresponds to

the condensate of the vortices, which "Higgses" the U(1) gauge field A_μ, and drives the boson b into a gapped insulator phase. If at low energy there is only one component of vortex field with gauge charge 1 under A_μ (which corresponds to integer filling of boson b), the insulator phase of b is a trivial insulator without any further symmetry breaking or topological order; if there are more than one component of the vortex fields at low energy, or if the vortex field carries multiple gauge charges of A_μ, the insulator must be of nontrivial nature.

For example, when b has a fractional filling $\nu_b = 1/q$ with integer q, Ref. [317, 174] studied the quantum phase transition between the bosonic SF and various MIs with commensurate density waves which spontaneously break the translation symmetry but have no topological order. The study is naturally generalized to filling factor $\nu_b = p/q$ with coprime integers (p, q). We can use this formalism in our system. Hereafter we focus on one spin/valley flavor α, and the index α will be hidden for conciseness. In this case the theory for the SF-MI transition at one spin/valley flavor is:

$$\begin{aligned} \mathcal{L}^{(1)} &= \sum_{j=0}^{N-1}(|(\partial_\mu - \mathrm{i}A_\mu)\psi_j|^2 + r|\psi_j|^2) + u(\sum_{j=0}^{N-1}|\psi_j|^2)^2 \\ &\quad + \frac{\mathrm{i}}{2\pi}A \wedge d(a + eA_{\mathrm{ext}}) + \cdots \end{aligned} \tag{4.24}$$

Here ψ_j with $j \in \{0, \cdots N-1\}$ are N flavors of vortex fields of the boson b at low energy, and A_μ is the dual gauge field of boson b: $\frac{1}{2\pi}dA = J_b$, where J_b is the current of boson b. a_μ is the gauge field that couples to both b and f, and A_{ext} is the external electromagnetic field. The reason there are N flavors of the vortex field is that, the vortex which is defined on a dual honeycomb lattice will view the partially filled boson density as a fractional background flux of the dual gauge field A_μ through each hexagon, and the band structure of the vortex will have multiple minima in the momentum space.

The degeneracy of the multiple minima is protected by the symmetry of the triangular lattice. ψ_j transforms as a representation of the projective symmetry group (PSG) of the lattice. Notice that since Eq. 4.24 describes one of the two spin/valley flavors, the PSG that constrains Eq. 4.24 should include translation, and $2\pi/3$ rotation of the lattice ($R_{\frac{2\pi}{3}}$). There is another more subtle symmetry $P_x\mathcal{T}$ for each spin/valley flavor of the boson and vortex fields. P_x that takes $x \to -x$, and time-reversal $\mathcal{T}$ both exchange the two spin/valley indices, but their product will act on the same spin/valley species, and part of its role is to take momentum k_y to $-k_y$.

In the appendix we will argue that P_y which takes y to $-y$ within each valley is also a good symmetry of the system, as long as valley mixing is negligible. One consequence of the P_y symmetry is that the expectation value of gauge flux da can be set to zero for the theory Eq. 4.24, or equivalently the P_y symmetry ensures that the "chemical potential" term $\psi_j^*\partial_\tau\psi_j$ does not appear in Eq. 4.24, as P_y transforms a vortex to anti-vortex: $\psi_a \to U_{ab}\psi_b^*$. Also, with long moiré lattice constant, the trigonal warping $k_x^3 - 3k_xk_y^2$ in each valley of the original BZ of the system becomes less important compared with the leading order quadratic dispersion expanded at each valley, hence the six-fold rotation $R_{\pi/3}$ becomes a good approximate symmetry of the effective Hubbard model with long moiré lattice constant.

The theory in Eq. 4.24 also has an emergent particle-hole symmetry. The simplest choice of the particle-hole symmetry is $\psi_a \to U_{ab}\psi_b^*$, $A \to -A$, $a \to -a$ and $A_{\text{ext}} \to -A_{\text{ext}}$. Although we used the same transformation matrix U_{ab} as P_y, this emergent particle-hole symmetry is different from P_y as it does not involve any spatial transformations. Note that any (spatially uniform) P_y-symmetric terms involving only the "matter fields" ψ_j must also preserve this emergent particle-hole symmetry. Another potentially relevant particle-hole-symmetry-breaking perturbation that needs to be examined is given by the finite density of the fluxes dA. dA is tied to the physical U(1) charge density (compared

to the charge density set by the fixed electron filling $\nu = 1/2$) and hence should have a vanishing spatial average. At the SF-MI transition point, the translation symmetry of the theory Eq. 4.24 and the fact that dA has a vanishing spatial average guarantee that dA has a vanishing expectation value everywhere, which respects the particle-hole symmetry. Therefore, the particle-hole symmetry is a valid emergent symmetry at the SF-MI critical point described by Eq. 4.24. The same argument would also conclude the emergent particle-hole symmetry at the ordinary SF-MI transition in the Bose-Hubbard model.

For parton construction-II, when the electron has filling $\nu = 1/2$, both b_1 and b_2 are at filling $\nu_b^\alpha = 1/2$. For each flavor of b_α, the formalism in Ref. [174] would lead to a dual vortex theory with $N = 4$ components of vortex fields, i.e. there are four degenerate minima of the vortex band structure in the momentum space for each spin/valley index. This calculation is analogous to the frustrated Ising model on the honeycomb lattice [318, 319]. Using the gauge choice of Fig. 4.4, the four minima are located at the K and K' points of the reduced Brillouin zone (BZ), with two fold degeneracy at each point.

From $N = 4$ to "$N = \infty$"

Ref. [174] considered a specific band structure of the vortex, which only involved the nearest neighbor hopping of vortices on the dual honeycomb lattice. But there is no fundamental reason that further neighbor hopping of vortices should be excluded. Indeed, once we take into account of further neighbor hopping, the dual vortex theory has a much richer possibility. We have explored the phase diagram of the dual vortex theory up to seventh neighbor hopping, and we obtained the phase diagram in Fig. 4.5*a*. Further neighbor hopping of the vortex field can modify the band structure, and lead to $N = 6$ or $N = 12$ components of vortex fields by choosing different hopping amplitudes. The $N = 6$ minima are located at three inequivalent M points of the reduced BZ (Fig. 4.5),

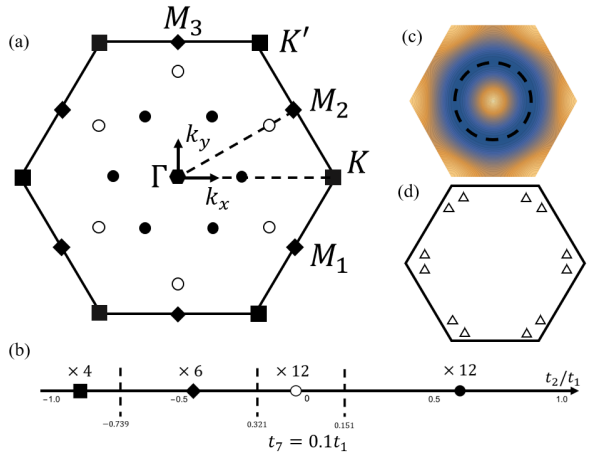

Figure 4.5: (a) The minima of the vortex band structure. With nearest neighbor vortex hopping on Fig. 4.4, the minima locate at the K and K' points of the Brillouin zone, each K point has two fold degeneracy; with further neighbor hoppings, the minima can shift to the three M points, still with two fold degeneracy at each M point. (b) The phase diagram of vortex modes with seventh neighbor hopping $t_7 = 0.1t_1$, and by tuning t_2 there are two regions in the phase diagram with $N = 12$ vortex modes at low energy. The 12 vortex modes are located either on the lines between Γ and K/K' or Γ and M. (c) With only t_1 and t_2, there is a large region of the phase diagram where there is a ring degeneracy of the vortex band structure. (d) All the symmetries (including approximate symmetries) of the system can protect up to 24 degenerate vortex modes, which locate at 12 incommensurate momenta in the BZ.

each M point again has two-fold degeneracy. The two-fold degeneracy at each M point is protected by the translation symmetry of the triangular moiré lattice only, which is required by the LSM theorem. The shift of the vortex field minima from the K points to M points is similar to what was discussed in the context of frustrated quantum Ising models with further neighbor couplings [320, 321]. With symmetries $T_{1,2}$, $R_{\frac{2\pi}{3}}$ and $P_x\mathcal{T}$ at each spin/valley flavor, the degeneracy of the $N = 6$ minima at the M points are protected.

There are two regions in the phase diagram in Fig. 4.5*b* with $N = 12$ modes of vortex, two at each momentum. The six incommensurate momenta at the minima of the vortex band structure can be located either on the lines between Γ and K/K' or Γ and M. With the $R_{\pi/3}$ symmetry that becomes a good approximate symmetry with long moiré lattice

constant, the degeneracy of the $N = 12$ vortex modes is protected. In principle, all the symmetries together including $R_{\pi/3}$ can protect up to $N = 24$ degenerate minima, as shown in Fig. 4.5*d*.

For a theory with N components of vortex fields, the electric charge carried by the boson b will fractionalize. Under the boson-vortex duality $\frac{1}{2\pi}dA = J_b$, the boson number of b becomes the flux number of the dual gauge field A_μ. The gauge flux of A_μ is trapped at the vortex core of each field ψ_j (we denote the vortex of ψ_j as φ_j). With N components of the vortex fields, the vortex of each ψ_j field will carry $1/N$ flux quantum of the gauge field A_μ, hence the charge e_* of each fractionalized charge carrier should be e/N at the MIT. And there are in total $N_b = 2N$ species of the charge carriers (the factor of 2 comes from the two spin/valley flavors).

With just t_1 and t_2 (first and second neighbor vortex hopping), there is a large region of the parameter space where the minima of the vortex band structure form a ring. This one dimensional ring degeneracy is not protected by the symmetry of the system, but its effect may still be observable for a finite energy range. A ring degeneracy is analogous to $N = \infty$ in Eq. 4.24. Condensed matter systems with a ring degeneracy have attracted considerable interests [322, 323, 324, 325]. By integrating out the vortices with ring degeneracy, a "mass term" for the transverse component of A_μ is generated in the infrared limit [325] (in the limit of momentum goes to zero before frequency), meaning the fluctuation of A_μ is highly suppressed, which is consistent with the intuition of $N = \infty$.

The ellipsis in Eq. 4.24 includes other terms allowed by the PSG of the triangular lattice, but break the enlarged flavor symmetry of the CP^{N-1} model field theory. More details about PSG, extra terms in the Lagrangian, coupling to fermionic parton f_α [326], and the possible valence bond solid orders with $N = 6$ will be discussed in appendix A and B. The exact fate of the critical theory in the infrared is complicated by these extra

perturbations. It was shown previously that nonlocal interactions can drive a transition to a new fixed point [89, 192, 193], and here nonlocal interactions arise from coupling to the fermionic partons [326]. Hence the transition may eventually flow to a CFT different from the CP^{N-1} theory in Eq. 4.24, or be driven to a first order transition eventually. But as long as the first order nature is not strong, the charge fractionalization and large resistivity to be discussed in the next subsection is expected to hold at least for a considerable energy/temperature window.

So far we have not paid much attention to the dynamical gauge fields a_μ in parton construction-I or $a_{\alpha,\mu}$ in construction-II shared by the bosonic and fermionic partons, as the gauge coupling between b (b_α) and the gauge field is irrelevant at the MIT with a background spinon Fermi surface. Here we briefly discuss the fate of the spinon Fermi surface in the insulator phase. When the bosonic parton b is gapped, the theory of spinon Fermi surface coupled with the dynamical U(1) gauge field is a problem that has attracted a great deal of theoretical efforts [327, 328, 329, 330, 331, 332, 333]. These studies mostly rely on a "patch" theory approximation of the problem, which zooms in one or two patches of the Fermi surface. Then an interacting fixed point with a nonzero gauge coupling is found in the IR limit based on various analytical perturbative expansion methods.

Previous studies have also shown that the non-Fermi liquid obtained through coupling a Fermi surface to a dynamical bosonic field can be instable against BCS pairing of fermions [334, 335, 336, 337, 338, 339, 340]. If there is only one flavor of U(1) gauge field, the low energy interacting fixed point is expected to be robust against this pairing instability, because the U(1) gauge field leads to repulsive interaction between the spinons. However, when there are two flavors of U(1) gauge fields [340, 341], like the case in our parton construction-II, the two U(1) gauge fields can lead to interflavor spinon pairing instability. This interflavor pairing can still happen at the MIT. But depending on the

microscopic parameters this instability can happen at rather low energy scale.

Resistivity at the MIT

For low frequency and temperature, the resistivity of a system is usually written as $\rho(x)$ with $x = \omega/T$. The DC conductivity at zero temperature corresponds to $x = 0$, i.e. the limit $\omega \to 0$ before $T \to 0$. As we have mentioned, the interaction driven MIT has a jump of resistivity at the MIT compared with the metal phase near MIT, and this jump is given by the resistivity ρ_b of the bosonic parton b_α. For a bosonic system with an emergent particle-hole symmetry in the infrared, $\rho_b(x)$ with $x = 0$ or $x = \infty$ have attracted most studies. In general both $\rho_b(0)$ and $\rho_b(\infty)$ should be universal numbers at the order of $\sim h/e^2$. The reason $\rho_b(0)$ could be finite even without considering disorder and Umklapp process is that, with an emergent particle-hole symmetry in the infrared discussed in the previous subsection, there is zero overlap between the electric current and the conserved momentum density (extra subtleties about this from hydrodynamics will be discussed in section VI). The universal $\rho_b(0)$ was evaluated in Ref. [311] for the interaction-driven MIT without charge fractionalization. The calculation therein was based on Boltzmann equation in a theoretical large$-\mathbf{N}$ limit and eventually $\mathbf{N}$ was taken to 1 (we remind the readers that the $\mathbf{N}$ introduced in Ref. [311] was for technical reasons, it is not to be confused with N used in this section).

We have generalized the computation in Ref. [311] to our case with $N-$components of vortex fields and charge fractionalization. To proceed with the computation we need to turn on "easy plane" anisotropy to Eq. 4.24 and perform duality to the basis of fractional charge carriers φ_j (Eq. A.29). The φ_j will be coupled to multiple gauge fields which are the dual of the ψ_j fields. Eventually the total resistivity $\rho_b(0)$ is obtained through a

generalized Ioffe-Larkin rule, which combines the resistivity of each parton φ_j into ρ_b:

$$\rho_b = \frac{\hbar}{e^2}\left(\sum_{j=0}^{N-1}\rho_{b,j}\right). \tag{4.25}$$

$\rho_{b,j}$ is the resistivity of each charge carrier φ_j when its charge is taken to be 1. The detail of the computation is presented in the appendix, and we summarize the results here. For N flavors of vortices in Eq. 4.24, the resistivity $\rho_b(0)$ at the MIT roughly increases linearly with N, as was expected through the intuitive argument we gave before:

$$\rho_b(0) = \Delta\rho = \left(R^{(0)} + R^{(1)}(N-1)\right)\frac{h}{e^2}, \tag{4.26}$$

where $R^{(0)} \sim 3.62$, $R^{(1)} \sim 1.68$. We would like to compare our prediction with the previous theory of MIT without charge fractionalization. In the previous theory, the DC resistivity jump is evaluated to be $\Delta\rho \sim 7.92h/e^2$ [311] (we reproduced this calculation and our result at $N = N_b = 1$ is $7.44h/e^2$). Eq. 4.23 suggests that when $N \geq 4$, the resistivity jump in our case is indeed larger than that predicted by the previous theory of MIT.

We would also like to discuss the AC resistivity $\rho_b(\infty)$. One way to evaluate $\rho_b(\infty)$ is to again start with Eq. A.29, and follow the same strategy as the calculation of the DC resistivity. According to the generalized Ioffe-Larkin rule, the AC resistivity contributed by *each valley* is given by

$$\rho_b = N\frac{1}{\sigma_\varphi}\frac{\hbar}{e^2}, \quad \sigma_\varphi = \lim_{\omega\to 0}\frac{1}{\mathrm{i}\omega}\langle J^\varphi_\omega J^\varphi_{-\omega}\rangle_{\vec{p}=0}, \tag{4.27}$$

where $J^\varphi = \mathrm{i}\varphi_j^*\nabla\varphi_j + h.c.$ is the current of the charge carrier φ_j. With the theoretical large-$\mathbf{N}$ limit mentioned above, the effects of all the dynamical gauge fields are sup-

pressed, and φ_j will contribute conductivity $\sigma_\varphi(\infty) = \frac{1}{16}$ (contrary to DC transport, $\sigma_\varphi(\infty)$ does not need collisions; the effects of dynamical gauge fields can be included through the $1/\mathbf{N}$ expansion). Eventually one would obtain resistivity from each valley

$$\rho_b = \frac{8N}{\pi}\frac{h}{e^2}, \tag{4.28}$$

the final resistivity of the system is half of Eq. 4.28 due to the two spin/valley flavors. With $N = 1$, the transition should belong to the ordinary 3D XY universality class, and the value given by Eq. 4.28 is not far from what was obtained through more sophisticated methods (see for instance Ref. [305, 304, 306], $\rho_b \sim 2.8h/e^2$). This should not be surprising as the 3D XY universality class can be obtained perturbatively from the free boson theory. In our current case with charge fractionalization, with $N \geq 4$, the total AC resistivity which is half of the value in Eq. 4.28 is larger than the universal resistivity at the 3D XY transition.

Another way to evaluate the resistivity of Eq. 4.24 is by integrating out ψ_j from Eq. 4.24, and an effective Lagrangian for A_μ is generated

$$\mathcal{L} = \sum_{p_\mu} \frac{Np}{16}\left(\delta_{\mu\nu} - \frac{p_\mu p_\nu}{p^2}\right) A_\mu(p)A_\nu(-p). \tag{4.29}$$

This effective action is supposed to be accurate in the limit of $N \to \infty$. The electric current carried by b is $J^b = \frac{e}{2\pi}dA$, hence the current-current correlation can be extracted from the photon Green's function based on the effective action Eq. 4.29:

$$\rho_{b,N\to\infty} = \frac{\pi N}{8}\frac{h}{e^2}. \tag{4.30}$$

Again the final resistivity of the system is half of Eq. 4.30 due to the two spin/valley flavors. The evaluation Eq. 4.30 is still proportional to N just like Eq. 4.28. These two

different evaluations discussed above give different values for $N = N_b = 1$, and compared with the known value of the universal resistivity at the 3D XY transition, the evaluation in Eq. 4.28 is much more favorable, though the evaluation Eq. 4.30 based on Eq. 4.29 is supposed to be accurate with large N.

When there is a ring of degeneracy in the vortex band structure, as we mentioned before the gauge field A_μ will acquire a "mass term" after integrating out ψ_j [325]. In this case the resistivity of the system at the MIT will be infinity, as the dynamics of A_μ is fully suppressed by the mass term in the infrared. One can also integrate out the action of A_μ with the mass term, and verify that the response theory of A_{ext} is no different from that of an insulator in the infrared limit. This is consistent with both Eq. 4.28,4.30 by naively taking N to infinity. In Ref. [325] when the boson field has a ring degeneracy, the phase is identified as a bose metal; this is because in Ref. [325] it is the boson with ring degeneracy that carries charges. But in Eq. 4.24 the electric charge is carried by the flux of A_μ.

4.2.4 Mott insulator with topological order

As we explained in the previous subsection, due to the fractional filling of boson b_α, the vortex dynamics is frustrated by the background fractional flux through the hexagons. To drive the system into an insulator phase, the vortex can either condense at multiple minima in the BZ as was discussed in the previous section, or form a bound state that carries multiple gauge charge of A_μ and become "blind" to the background flux. In parton construction-II, with electron filling $\nu = 1/2$, each flavor of boson is at filling $\nu_b = 1/2$. The double-vortex, i.e. bound state of two vortices, or more generally the bound state of N vortices with even integer N, no longer see the background flux. Hence the N-vortex can condense at zero momentum, and its condensate will drive the system

into a Z_N topological order.

After the boson-vortex duality, the theory for the N-vortex condensation at one of the two spin/valley flavors is

$$\begin{aligned} \mathcal{L}^{(2)} &= |(\partial_\mu - \mathrm{i}NA_\mu)\psi|^2 + r|\psi|^2 + g|\psi|^4 \\ &+ \frac{\mathrm{i}}{2\pi} A \wedge d(a + eA_{\mathrm{ext}}) + \cdots \end{aligned} \tag{4.31}$$

The condensate of ψ will break the U(1) gauge field to a Z_N gauge field, whose deconfined phase has a nontrivial Z_N topological order. In the Z_N topological order as well as at the MIT, the charge carrier is an anyon of the Z_N topological order, and it carries charge $e^* = e/N$. We still label the fractional charge carrier as φ. φ carries charge e/N, and is coupled to a Z_N gauge field originated from the Z_N topological order discussed in the previous paragraph.

In our case, in order to preserve the time-reversal symmetry, both spin/valley flavors should form a Z_N topological order simultaneously. Hence there is one species of φ_α field for each spin/valley flavor. The MIT can equally be described as the condensation of the φ_α field, and since the Z_N gauge field does not lead to singular correction in the infrared, the condensation of φ_α is a 3D XY* transition, and the transition for $N = 2$ was discussed in Ref. [59, 342, 119, 15, 16, 343]. The b_α field is now a composite operator of φ_α. In the condensate of φ_α, the electron operator c_α is related to the fermionic parton operator f_α through $c_\alpha \sim \langle b_\alpha \rangle f_\alpha \sim \langle \varphi_\alpha^N \rangle f_\alpha$. The coupling between the two flavors of φ_α, i.e. the coupling $|\varphi_1|^2|\varphi_2|^2$ is irrelevant at the decoupled 3D XY* transition according to the known critical exponents of the 3D XY* transition. There are also couplings such as $|\varphi_\alpha|^2 f_\alpha^\dagger f_\alpha$ allowed by all the symmetries, but after formally integrating out the fermions, the generated couplings for φ_α is also irrelevant at the two decoupled 3D XY*

universality class. The reason is that after formally integrating out the fermions, terms such as $\frac{|\omega|}{q}|\varphi_\alpha|^2_{\omega,\vec{q}}|\varphi_\beta|^2_{-\omega,-\vec{q}}$ can be generated, but this term is irrelevant knowing that the standard critical exponent $\nu > 2/3$ for the 3D XY* transition.

Following the large$-\mathbf{N}$ calculation discussed before, the DC resistivity jump $\rho_b(0)$ would be $N^2/2$ times that of the previous theory [311], namely

$$\rho_b(0) \sim R^{(2)} N^2 \frac{h}{e^2}, \tag{4.32}$$

where $R^{(2)} = R'/2 \sim 3.7$ based on our evaluation. The AC resistivity jump at the MIT is enhanced by the same factor compared with the previous theory. We also note that the fractional universal conductivity at the transition between the superfluid and a Z_2 topological order was observed numerically in Ref. [343].

Another set of natural topological orders a boson at fractional filling can form are bosonic fractional quantum Hall (bFQH) states which are close analogues to the bosonic Laughlin's wave function. We would like to discuss this possibility as a general exploration, although this state breaks the P_y symmetry (but it still preserves the product $P_x\mathcal{T}$ symmetry). If we interpret the half-filled boson at each site as a quantum spin-1/2 system, this set of states are analogous to a chiral spin liquid [344, 345]. The Chern-Simons theory for this set of states at each valley reads

$$\mathcal{L}_{\rm cs} = -\frac{\mathrm{i}k}{4\pi} A \wedge dA + \frac{\mathrm{i}}{2\pi} A \wedge d(a + A_{\rm ext}), \tag{4.33}$$

with an even integer k and a dynamical Spin$_c$ U(1) gauge field A. The topological order characterized by this theory is the SU$(k)_1$ topological order. Here, the integer k needs to be even so that this theory is compatible with the LSM constraint imposed by the boson filling 1/2 on the lattice [346]. This is because the boson filling 1/2 requires the topological

phase to contain an Abelian anyon that carries a fractional charge 1/2 (modulo integer). There should be one such anyon per unit cell to account for the boson filling 1/2 on the lattice. The fact that such an anyon carries a fractional charge 1/2 implies that this anyon should generate under fusion an Abelian group $\mathbb{Z}_p$ with p an even number. Such a fusion rule is incompatible with any odd value of k. Therefore, k needs to be even in the theory given by Eq. 4.33. The time-reversal of the TMD moiré system demands that the bosonic parton b_α with opposite spin/valley index α forms a pair of time-reversal conjugate bFQH states. Or in other words if we take both spin/valley flavors together, this state is a fractional topological insulator, like the state discussed in Ref. [**?**].

The MIT is now a direct transition between the bFQH state and the superfluid of b_α. When the even integer k is $k = 2n^2$ with odd integer n, there is a natural theory for this direct continuous transition, and its simplest version with $n = 1$ was proposed in Ref. [347]. The transition is a 3D QED with two flavors of Dirac fermions coupled to the dynamical U(1) Spin$_c$ gauge field A_μ (the dual of the Goldstone mode of the boson superfluid) with a Chern-Simons term at level-n^2, and the fermions have gauge charge-n:

$$\begin{aligned} \mathcal{L}^{(3)} &= \sum_{j=1}^{2} \bar{\chi}_j \gamma \cdot (\partial - \mathrm{i}nA)\chi_j + M\bar{\chi}_j\chi_j - \frac{\mathrm{i}n^2}{4\pi} A \wedge dA \\ &+ \frac{\mathrm{i}}{2\pi} A \wedge d(a + eA_{\mathrm{ext}}) + \cdots \end{aligned} \tag{4.34}$$

In this theory, the fact that A is a Spin$_c$ U(1) gauge field and that n is odd guarantee that this theory describes the phases of a boson. A Spin$_c$ connection A_μ means a U(1) gauge field with a "charge-statistics relation": there is no fermionic object that is neutral under A_μ. When A_μ is a Spin$_c$ U(1) gauge field, and n is an odd integer in Eq. 4.34, Eq. 4.34 describes an interacting state of bosons that carries electric charge e. The charge$-e$ object of Eq. 4.34 that is also neutral under A_μ, is a composite of 2π flux of

A_μ and n fermions χ. This composite is a boson as long as n being an odd integer, and this composite should be identified as b_α in Eq. 4.22. The ellipsis in this Lagrangian includes other terms such as the Maxwell term of the gauge field A_μ. Please note that this equation is for one of the two spin/valley flavors of the physical system. The mass M of the Dirac fermions is the tuning parameter of the transition. With one sign of the mass term, after integrating out the Dirac fermions, the Spin_c U(1) gauge field A will acquire a Chern-Simons term at level $-2n^2$, which describes the $\text{SU}(k)_1$ topological order with $k = 2n^2$. With the opposite sign of M, there is no Chern-Simons term of the gauge field A after integrating out the Dirac fermions, and the Maxwell term of the gauge field A is the dual description of the superfluid phase. Hence by tuning M the system undergoes a transition between the $k = 2n^2$ bFQH state and the superfluid state of b (the metal phase of the original electron system).

The translation symmetry of the system actually guarantees that the two flavors of Dirac fermions are degenerate in Eq. 4.34. If these two Dirac fermions are not degenerate, an intermediate topological order is generated by changing the sign of the mass of one of the Dirac fermions in Eq. 4.34. Then after integrating out the fermions, the gauge field A acquires a total CS term with an odd level $-n^2$, which violates the LSM constraint imposed by the boson filling 1/2. Therefore, the masses of the two flavors of the Dirac fermions in Eq. 4.34 should be the same. In fact, for the simplest case with $n = 1$ ($k = 2$), an explicit parton construction of this transition can be given following the strategy in Ref. [347], and the two Dirac fermions in Eq. 4.34 are two Dirac cones of a $\pi-$flux state of χ on the triangular lattice. The degeneracy of these two Dirac fermions is protected by the translation symmetry of the triangular lattice. From the parton formalism one can also see that the boson b is constructed as a product of the two fermions χ_i.

At the transition $M = 0$, though it is difficult to compute the resistivity of Eq. 4.34 exactly, the resistivity $\rho(x)$ should scale as $1/k$ with large $k \sim n^2$, as after integrating

out χ_j the entire effective action of A scales linearly as k. Then after integrating out A, the response theory to A_{ext} is proportional to $1/k$.

4.2.5 Summary of Predictions

So far we have discussed three different kinds of possible Mott insulators at half filling of the extended Hubbard model, based on the parton construction-II: (1) Mott insulators with translation symmetry breaking; (2) a Z_N topological order at each spin/valley flavor with even integer $N \geq 2$; and (3) a pair of conjugate bFQH states at two spin/valley flavors. For all scenarios, we have evaluated the bosonic parton contribution to the resistivity ρ_b at the MIT, which is also the universal jump of resistivity $\Delta\rho$. The predicted resistivity jump for the three scenarios are summarized in the table below.

Nature of Insulator	$\Delta\rho$, or ρ_b
(1) Density wave	$\rho_b(0) \sim (R^{(0)} + R^{(1)}(N-1))\frac{h}{e^2}$
(2) Z_N TO each flavor	$\rho_b(0) = R^{(2)}N^2\frac{h}{e^2}$
(3) Conjugate bFQH	$\rho_b(x) \sim \frac{1}{k}\frac{h}{e^2}$

Another observable effect predicted by the previous theory of interaction-driven MIT is the scaling of quasi-particle weight $\sqrt{Z}$ near the MIT [296, 297], where $\sqrt{Z} \sim r^{\beta_1} \sim |r|^{0.33}$. Our theory also gives a different prediction of the quasi-particle weight compared with the previous theory, and this is most conveniently evaluated for scenario (2). In the metal phase but close to the MIT, the quasi-particle weight scales as

$$\sqrt{Z} \sim \langle \varphi_\alpha^N \rangle \sim |r|^{\beta_N}, \tag{4.35}$$

where $\beta_N = \nu\Delta_N$. $\nu \sim 0.67$ is the standard correlation length exponent at the 3D XY* transition (it is the same as the 3D XY transition) and Δ_N is the scaling dimension of φ^N

at the 3D XY transition. These exponents can be extracted from numerical simulation on the 3D XY and XY* transitions. For example, when $N = 2$, β_2 should be close to 0.8 [59, 342, 348], hence $\sqrt{Z} \sim |r|^{0.8}$. The scaling of quasi-particle weight can be checked in future experiments through the measurement of local density of states of electrons.

For scenario (1), i.e. where the insulator has translation symmetry breaking, the scaling of quasiparticle weight can be estimated with large-N in Eq. 4.24. The boson creation operator $b^\dagger$ is a monopole operator of A_μ which creates a 2π gauge flux. With large-N in Eq. 4.24 the monopole operator has scaling dimension proportional to N [349, 350], hence the critical exponent β in the quasiparticle weight $\sqrt{Z} \sim |r|^\beta$ is expected to be proportional to N. The similar evaluation applies to Eq. 4.34, and the creation operator $b^\dagger$ has a scaling dimension proportional to k, which is also proportional to $\sqrt{Z}$.

As we explained, our theory provides a natural explanation of the anomalously large resistivity at the MIT. Another qualitative experimental feature reported in Ref. [39] is that, the resistivity drops rapidly as a function of temperature at the MIT where the charge gap vanishes. Our theory also provides a natural explanation for the temperature dependence of the critical resistivity. At zero temperature the bosonic chargeon parton b fractionalizes into multiple partons with smaller charges, and these partons will couple to extra gauge fields. These extra gauge fields will all confine at finite temperature. Hence at finite temperature, there is a crossover from transport with fractionalized charge to unfractionalized charge, which will cause a significant drop of resistivity with increasing temperature.

In the following paragraphs we discuss physics in phases near the MIT, based on our theory. These analysis can distinguish the three possible scenarios discussed to this point. Let us first discuss the insulator phase at fixed electron filling $\nu = 1/2$. The scenario (3) describes a topological order that is essentially a topological fractional quantum spin Hall insulator, hence this insulator phase, if does exists, must have nonchiral gapless

modes localized at the boundary of the system. This nonchiral edge gapless modes should lead to similar experimental phenomena as the experiments on quantum spin Hall insulator [351]; but rather than edge conductance $2e^2/h$, the edge conductance of the fractional quantum spin Hall insulator should be $2e^2/(kh)$, which is twice of the edge conductance of the bFQH state with CS level-k. Also, the edge conductance should be suppressed by external magnetic field, also analogous to what was observed in Ref. [351].

The insulating phase of scenario (1) and scenario (2) also lead to distinctive predictions. In scenario (1), the electric charges are only deconfined at the MIT, but still confined in the insulating phase, which has no topological order. Hence the charge deconfinement of scenario (1) is analogous to the original deconfined quantum critical point discussed in Ref. [15, 16]. The confinement of fractional charges in scenario (1) happens even at zero temperature in the insulating phase. However, in scenario (2), the insulator phase has a Z_N topological order that supports deconfined fractional charge at zero temperature even in the insulator phase. While at finite temperature, the Z_N gauge field will lead to confinement of fractional charges with confinement length $\xi \sim \exp(c\Delta_m/T)$, where Δ_m is the gap of the fractionalized Z_N gauge fluxes, which is an anyon with nontrivial statistics with the fractional charges. If we look at the insulator phase close to the MIT, the gap of the fractional charge, i.e. the $e-$anyon of the Z_N topological order is suppsosed to be smaller than Δ_m, as the MIT corresponds to the condensation of the $e-$anyon, hence at very low temperature the thermally activated $e-$anyon has a much smaller distance l_e with each other compared with ξ. Then at low but finite temperature the transport is governed by charge carriers with gap Δ_e and charge $e_* = e/N$. The gap Δ_e can be extracted from fitting the low temperature transport data versus temperature. However, if one measures the tunnelling gap through tunnelling spectroscopy, since the external device can only inject a single electron which fractionalizes into multiple $e-$anyons, the tunneling gap should be approximately $N\Delta_e$. This contrast between

tunneling gap and the thermally activated transport gap happens in scenario (2) but not scenario (1).

We also consider the metallic phase next to the insulator after charge doping, and we will see the scenario (2) also leads to very nontrivial predictions due to the deconfined nature of the Z_N topological order. In scenario (2), after some charge doping, we expect a metallic state with charge fractionalization at low temperature. The bosonic charge carriers are coupled to the Z_N gauge field as well as the U(1) gauge field a_μ that are shared with the fermionic partons f_α. When the temperature is increased, the Z_N gauge field will confine, and due to the time-reversal symmetry, the confine-deconfine crossover should happen for both spin/valley flavors simultaneously. In the following, we shall only focus on one spin/valley. According to the Ioffe-Larkin composition rule, the total resistivity is composed of contributions from both bosonic and fermionic partons $\rho = \sigma^{-1} = \sigma_b^{-1} + \sigma_f^{-1}$. Let us assume the resistivity of both the bosonic and fermionic sectors are dominated by the scattering with the gauge field a_μ (this of course assumes that the momentum of the gauge field a_μ can relax through other mechanism such as disorder). This scattering mechanism was first evaluated in Ref. [352]. The gauge-field propagator can be written as $D(\omega, \boldsymbol{q})^{-1} = i\gamma\omega/q + \chi_d q^2$, where the ω/q term is due to the Landau damping from the fermi-surface, and the "diamagnetic" χ_d is roughly a constant within the temperature window of interest. The scattering rate can then be estimated using the imaginary part of the boson/fermion self-energy:

$$\mathrm{Im}\Sigma_{b,f}(\omega, \boldsymbol{k}) = \int_0^\infty d\omega' \int \frac{d^2\boldsymbol{k}'}{(2\pi)^2}(1 + n_b(\omega'))(1 \pm n_{b,f}(\omega_{\boldsymbol{k}'}))$$
$$\frac{(k_\alpha + k'_\alpha)(k_\beta + k'_\beta)}{2m_{b,f}} \frac{\delta_{\alpha\beta} - q_\alpha q_\beta}{\boldsymbol{q}^2} \delta(\omega - \omega_{\boldsymbol{k}'} - \omega')\mathrm{Im}D(\omega', \boldsymbol{q}),$$

where $\boldsymbol{q} = \boldsymbol{k}' - \boldsymbol{k}$, $n_{b,f}(\omega)$ denotes the Bose-Einstein (Fermi-Dirac) distribution function, and $m_{b,f}$ is the boson/fermion mass. We must stress that the expression of $\Sigma_{b,f}$ is valid

for partons with gauge charge-1. When the Z_N gauge field is deconfined, each boson carries the gauge charge-$1/N$ of the gauge field a_μ, and therefore there is an additional factor $1/N^2$ in the self-energy. The integral was evaluated in Ref. [352], and the time-scale responsible for transport has an extra factor proportional to q^2 in the integral. After taking these into account, we obtain the "transport" scattering rate for boson/fermion

$$\frac{1}{\tau_f} \sim T^{4/3}, \qquad \frac{1}{\tau_b} \approx \frac{k_B T}{m_b \chi_d}. \tag{4.36}$$

Comparing $1/\tau_b$ and $1/\tau_f$, we can see that the resistivity is dominated by the boson-gauge scattering at low temperature, and the bosonic partons are in a disordered phase rather than a quasi long range order at finite temperature due to their coupling to the dynamical gauge field a_μ. We take the Drude formula for the dilute Bose gas that we use to model the bosonic partons at finite temperature:

$$\rho \sim \frac{m_b}{n_* e_*^2} \frac{1}{\tau_b} \sim \frac{g_*^2}{n_* e_*^2} \frac{k_B T}{\chi_d}, \tag{4.37}$$

where $e_* = e/N$ and $g_* = 1/N$ denote the electric and gauge charges of bosons, and $n_* e_*$ is the doped physical electric charge density. Here, we have assumed that the resistivity ρ is dominated by the boson contribution because $(i.)$ the scattering rate of the boson is bigger compared to the fermions at low temperature as shown in Eq. 4.36, and $(ii.)$ the bosons have much lower density at low charge doping compared to the fermions which already has finite fermi surface at zero charge doping. In the following discussion, we will work under these assumptions at least up to the temperature scale T_c around which the Z_N gauge becomes fully confined.

The Z_N gauge field is fully confined when ξ is at the same order as the lattice constant; *i.e.* $T > T_c \sim \Delta_m$. Here we assume that the gauge field a_μ that is coupled to the fermionic

parton is less prone to confinement due to its coupling to the large density of gapless fermoins. Above T_c, the charge carriers in the system carry charge-e. The equation above still hold with the substitutions $e_* \to e = Ne_*, g_* \to g = Ng_*, n_* \to n = n_*/N$. We expect there is a crossover from the deconfined value of resistivity $\rho(T \sim 0)$ to the confined value $\rho(T \geq T_c)$:

$$\frac{(d\rho/dT)_{T\geq T_c}}{(d\rho/dT)_{T\sim 0}} \sim N, \tag{4.38}$$

This is an observable effect of scenario (2) that can be experimentally verified. Note that the crossover caused by confinement at the metallic phase is different from the critical point of the MIT; as transport at the critical point originates from rather different physics; for example both particles and holes will contribute to the charge transport at the critical point [**?**].

Contrary to the Ioffe-Larkin rule, the total thermal conductivity of the system is a sum of the contribution from the bosonic parton, fermionic parton, and also the gauge boson. With low charge doping away from $\nu = 1/2$, we expect the fermionic partons dominates the thermal transport according to Ref. [353]: $\kappa_f \sim T^{1/3}$. As we discussed above, in scenario (2) the low-temperature charge transport is dominated by the boson contribution $\sigma_b \sim 1/T$, while the thermal transport is dominated by the fermion contribution $\kappa_f \sim T^{1/3}$. Due to the crossover of charge transport at finite temperature caused by the confinement of the Z_N gauge field in scenario (2), there is also an observable prediction one can make for the Lorentz number $L = \kappa/(T\sigma) \approx \kappa_f/(T\sigma_b)$:

$$\frac{(L/T^{1/3})_{T\geq T_c}}{(L/T^{1/3})_{T\sim 0}} \sim N. \tag{4.39}$$

4.2.6 Summary, Discussion, and Other fractional fillings

In this section we proposed a theory for a potentially continuous metal-insulator transition for the extended Hubbard model on the triangular lattice at half-filling (one electron per unit cell). The extended Hubbard model is simulated by the TMD moiré systems. We introduce a different parton construction from the previous literature, which leads to a series of observable predictions. We demonstrated that our theory is more favorable given the current experiments on the heterobilayer TMD moiré systems. Although our theory was motivated by the recent experiments on $MoTe_2/WSe_2$ moiré superlattice [39], we envision our theory can have broad application given the recent rapid progresses in synthesizing pure two dimensional systems.

The moiré potential in the $MoTe_2/WSe_2$ moiré superlattice with no twisting is formed due to the mismatch of the lattice constants of the two layers. There is another experiment on MIT in twisted WSe_2 [40]. The situation in twisted WSe_2 seems rather different from $MoTe_2/WSe_2$ moiré superlattice. Inside the "insulator phase", the resistivity $\rho(T)$ at some displacement fields first increases with decreasing temperature, and eventually the plot seems to saturate at a finite value, which is much lower than the resistivity observed in the $MoTe_2/WSe_2$ moiré superlattice near the MIT. Hence the MIT of twisted WSe_2 could be of a different nature, between the metallic phase and the insulator phase, there could be an intermediate phase with an order at nonzero momentum and reduced size of electron Fermi pockets.

Correlated insulators at other fractional fillings $\nu = p/q$ have been reported in various TMD moiré systems [291, 292, 293, 294]. Although the nature of the MIT at these fillings has not been looked into carefully, here we briefly discuss the theory for the possible continuous MIT at general fractional filling $\nu = p/q$. As long as $q > 2$, even for parton construction-I, the bosonic parton b will have fractional filling, and hence the insulator

phase of b cannot be a trivial incompressible state without translation symmetry breaking or topological order. Here we would like to acknowledge that charge fractionalization for interacting electron system at fractional electron number per unit cell was discussed in previous literature [354], using similar formalism as the parton construction-I. At electron filling $\nu = 1/q$, the boson filling $\nu_b = 2/q$; if we only consider nearest neighbor hopping of the vortex, the insulator has commensurate density wave that spontaneously breaks the translation symmetry, and the MIT is described by Eq. 4.24 with $N = q$ for odd integer q; $N = q/2$ for $q = 4k + 2$; and $N = q$ for $q = 4k$. The electron charge will further fractionalize at the continuous MIT. In parton construction-I, there are in total N species of the charge carriers each carrying electric charge $e^* = e/N$. Hence the estimate of ρ_b is $\rho_b \sim Nh/e^2$.

For parton construction-II, with electron filling $\nu = 1/q$, the boson filling for each spin/valley flavor is $\nu_b = 1/q$. Again, if only nearest neighbor hopping of the vortices is considered, the MIT is described by Eq. 4.24 with $N = q$ for odd integer q; $N = 2q$ for even integer q. The field theory describing the MIT is two copies of Eq. 4.24: ψ_j, A_μ and a_μ should all carry a spin index α. There are in total $N_b = 2N$ species of the charge carriers each carrying electric charge $e^* = e/N$. Hence the estimate of ρ_b is $\rho_b \sim Nh/(2e^2)$. If we consider further neighbor hopping like section 4.2.3, the charge carriers may carry even smaller fractional charge, and hence larger ρ_b.

Here, we would like to discuss some subtlety regarding the conductivity σ_b of the bosonic parton. In a generic theory with momentum conservation, one expects a finite overlap between the electric current and the conversed momentum. Such a finite overlap would lead to a Drude peak in the (optical) conductivity (see Ref. [**?**] for a review) $\sigma(\omega) = \sigma_Q + \mathcal{D}\left(\frac{i}{\omega} + \delta(\omega)\right)$ where $\mathcal{D} > 0$ is the Drude weight and ω is the frequency. In a theory with an exact particle-hole symmetry, this overlap between the electric current and momentum is strictly zero and, consequently, the Drude weight $\mathcal{D}$ vanishes. In the MIT

considered in this section and previous literature such as Ref. [295, 296, 311], the theories that govern the bosonic partons all have an emergent particle-hole symmetry. This emergent particle-hole symmetry is expected to produce a Drude weight that vanishes at zero temperature, namely $\mathcal{D} \to 0$ as $T \to 0$. If there is a finite momentum relaxation time τ_p induced by for example disorder, the Drude peak should take the form $\frac{\mathcal{D}}{\tau_p^{-1} - i\omega}$ and should be viewed as an extra correction, when we take $\omega \to 0$, to the bosonic parton DC conductivity σ_b calculated for the MIT. Since $\mathcal{D}$ vanishes as $T \to 0$ due to the emergent particle-hole symmetry, the DC limit, i.e. $\omega \to 0$, of the Drude peak becomes a small correction to the bosonic parton DC conductivity σ_b at low temperature.

There is another subtlety associated with the bosonic parton conductivity due to extra hydrodynamical corrections and the purely two dimensional nature of the system. It was known (see, for example, Ref. [355] for a review) that, when momentum is strictly conversed, even in the presence of particle-hole symmetry, hydrodynamical fluctuations lead to a logarithmic correction to the optical conductivity that scale as $\log(\tau_{\text{th}}\omega)$. Here, τ_{th} is the time scale of local thermalization [356] and can be estimated as $\sim T^{-1}$. This hydrodynamical correction to the conductivity diverges in the DC limit. This divergence is due to the long-lived hydrodynamical mode associated with the conserved momentum. As we mentioned before, in real systems disorder and Umklapp process always induce a finite momentum relaxation time τ_p. The diverging hydrodynamical correction is only valid when $\tau_p \gg \tau_{\text{th}} \sim T^{-1}$, meaning momentum is strictly conserved over the thermalization time scale, where the hydrodynamical description becomes applicable. When the temperature T is low compared to τ_p^{-1}, hydrodynamical corrections are cut-off by τ_p^{-1} and are again expected to be small corrections to the bosonic parton conductivity calculated in the rest parts of this section. In fact the divergent hydrodynamical correction may be already cut-off at a higher temperature scale that is favorable to us, as the crossover scale is suppressed by a large factor depending on the dimensionless entropy density of

the system [356].

We would like to stress that the optical conductivity $\sigma(\infty)$ which is much easier to evaluate theoretically (see section.III for an example) is free of these subtleties, and we encourage future experiments to measure the optical conductivity at the MIT as well.

In recent years very impressive progresses have been made on numerically simulating interacting fermionic systems (for examples see Ref. [357, 358, 359, 360]). It is conceivable that an extended Hubbard model with spin-orbit coupling can be constructed on the triangular lattice, and by changing the parameter (for example the strength of the spin-orbit coupling), two types of interaction-driven MIT may be realized, one described by the original theory [295, 297], the other described by our current theory. Predictions made in these two theories, such as different universality classes and transport properties at the MIT, different scalings of quasiparticle weight, and the existence of the spinon Fermi surface in the insulator phase, can potentially be directly tested through various numerical methods on the extended Hubbard model. We will leave this to future exploration.

Chapter 5

Green's function Zero and Symmetric Mass Generation

5.1 Introduction

Short range interactions can modify the classification of topological superconductors (TSC) and topological insulators (TI) in the classic "ten-fold way" table for free electrons [67, 68, 69]. The most prominent feature of a TSC or a TI is at its boundary, i.e in the noninteracting limit, the boundary of a TSC or TI should be gapless unless the boundary breaks the defining symmetry of the system. A short range interaction can enrich the phenomena at the boundary of a TSC and TI: it can drive the boundary into a spontaneous symmetry breaking phase, or a gapped topological phase which preserves all the symmetries [361, 362, 363, 364]. But it has also been realized that, a short range interaction may trivialize some of the TSCs and TIs, in the sense that short range interaction can "trivially" gap out the boundary of some TSCs and TIs without breaking any symmetry or leading to any ground state degeneracy. The first $1d$ example of this interaction-trivialized TSC was found in Ref. [365, 366], and soon other examples were

found in all dimensions [367, 368, 369, 363, 370, 371, 372, 373, 374, 375], For example, now it is known that 16 copies of the TSC ^{3}He-B phase is trivialized by interaction, hence although this TSC in the noninteracting limit has a $\mathbb{Z}$ classification, under interaction ^{3}He-B has a $\mathbb{Z}_{16}$ classification [363, 370].

Interaction trivialized TSC and TI has a deep relation with another phenomenon called "symmetric mass generation" (SMG). In the noninteracting limit the boundary of a $(d+1)$-dimensional TSC is described by a d-dimensional gapless Majorana fermion (or chiral Majorana fermion depending on the dimensionality), which carries with it certain 't Hooft anomaly of the defining symmetries of the TSC. A mass term of the boundary fermion will explicitly break the symmetry, and hence is prohibited to exist. When interaction reduces the classification of a TSC from $\mathbb{Z}$ to $\mathbb{Z}_N$, it means that for N copies of the d-dimensional Majorana fermions, it is possible to generate a gap through interaction without any degeneracy at the d-dimensional boundary, and the expectation value of any fermion bilinear mass operator is zero. The mechanism of SMG is in stark contrast with the ordinary mass generation of a Dirac or Majorana fermion (the well-known Gross-Neveu-Yukawa-Higgs mechanism [376]), which is caused by the condensation of a boson that couples to the fermion bilinear mass term. The condensation of the boson will break the symmetry of the system, and lead to a nonzero expectation value of a fermion mass term. The SMG has attracted broad attentions from both the condensed matter [377, 378, 379, 380] and high energy communities [381, 382, 383, 384, 385, 386, 387, 388] in the last few years, partly motivated by the observation that the SMG mechanism may be related to the lattice regularization of chiral gauge theories such as the Grand Unified Theories [389, 390, 391, 392, 393, 394, 395, 396].

A natural question one may ask is that, after the interaction "trivializes" the system, or after the SMG, is there still any remaining trace of the nontrivial topology of the original noninteracting system? Or for a system with a fully gapped spectrum, how do we

know the gap originates from the mechanism of SMG? The two most important features of TSCs or TIs are their stable boundary states, and the unavoidable bulk topological phase transition from the trivial insulator. When a TSC or TI is trivialized by interaction, both features mentioned above no longer robustly hold. It has been proposed before that strongly interacting TIs and TSCs may have a close relation with the zero of fermion Green's functions [397, 398, 377, 399, 400, 385, 379, 380]. In this work we use the general "decorated defect" construction of symmetry protected topological (SPT) states [401], and map the computation of the fermion Green's function to a problem of single particle path integral. Our method demonstrates in arbitrary dimensions the existence of fermion Green's function zero, after the interaction trivializes the TSC and TI, i.e. after the symmetric mass generation. One of the previous arguments (which will be reviewed later) for the existence of the Green's function zero relies on the quantized topological number defined with fermion Green's function in the momentum space. Our method can be generalized to the cases without translation symmetry, where a momentum space is no longer meaningful.

5.2 Green's function "zero" from decorated defects

Intuitively the decorated defect construction of a SPT state follows three steps: (1) one starts with a bosonic system with certain symmetry G, and drive the bosonic system into an ordered state with spontaneous symmetry breaking of the symmetry G, which allows topological defects; (2) decorate the topological defects with a lower dimensional SPT state, and (3) eventually proliferate the defects to restore the symmetry G. This decorated defect construction was originally designed for bosonic SPT states [401], but it also applies to fermionic TSCs and TIs. For example, the $2d$ TSC with the $Z_2 \times Z_2^T$ symmetry ($p \pm \mathrm{i}p$ TSC) can be constructed by decorating the Z_2 domain wall with a

$1d$ TSC with the time-reversal (Z_2^T) symmetry (the $1d$ BDI class TSC or the so called Kitaev's chain); The $3d$ TSC (or TI) of the AIII class can be constructed by decorating a U(1) vortex line with the Kitaev's chain.

We will start with the example of $2d$ TSC with $Z_2 \times Z_2^T$ symmetry, and first compute the fermion Green's function at the $1d$ boundary of the system. Consider a $2d$ Ising magnet in a ferromagnetic phase (SSB of the Z_2 spin symmetry). We perform the "decorated domain wall" construction by decorating each Ising domain wall with a $1d$ Kitaev chain with time-reversal symmetry Z_2^T. The parameters of the Hamiltonian are then tuned to proliferate these decorated domain walls. When a $1d$ Z_2 domain wall meets (or intersect) with the $1d$ boundary of the system, the domain wall becomes a $0d$ object decorated with Majorana zero modes coming from the boundary of the Kitaev's chain. These Majorana zero modes transform under the time-reversal Z_2^T as $\gamma_a \to \gamma_a$, hence any Hermitian fermion bilinear operator $\mathrm{i}\gamma_a\gamma_b$ would break the time-reversal symmetry and hence prohibited. For decoration number $\nu = 8$, with a proper flavor symmetry between the Majorana fermion operators γ_a, the interaction will induce a many-body symmetric gap between the Majorana modes, and drive the fermion Green's function at each $0d$ intersection to the following form [400, 377]:

$$G_{ab}(\mathrm{i}\omega) \sim \frac{\mathrm{i}\omega\delta_{ab}}{(\mathrm{i}\omega)^2 - m^2}, \tag{5.1}$$

in which m is proportional to the strength of the fermion interaction. There is a uniform gap energy scale in the Green's function, as long as the eight Majorana fermion operators γ_a form an irreducible representation of the flavor symmetry, such as a spinor representation of SO(7) or SO(5). G_{ab} approaches zero when $\omega \to 0$. Notice that this Green's function takes a different form from a free massive $0d$ fermion, where a mass term would explicitly break the time-reversal.

After being gapped by interaction through the SMG, in the Euclidean time the Majorana modes (MM) Green's function reads

$$G_{ab}(\tau) = G_{\mathrm{MM}}(\tau)\delta_{ab} \sim \mathrm{sgn}(\tau)e^{-m|\tau|}\delta_{ab}. \tag{5.2}$$

Our goal is to compute the fermion Green's function after the proliferation of Ising domain wall. To do this we map the computation of the Green's function to the following Feynmann path-integral problem in the $(1+1)d$ space-time, and the different choice of path $x(\tau)$ physically represents the fluctuation of the domain wall configuration:

$$G_{ab}(\beta, x) = \delta_{ab}G(\beta, x),$$

$$G(\beta, x) \sim \mathrm{sgn}(\beta) \int D[x(\tau)] \prod_{i=1}^{N} G_0(\delta\tau, \delta x_i)\rho(\delta\tau, \delta x_i), \tag{5.3}$$

Where $\delta x_i = x_i - x_{i-1}$. Here we have inserted $N-1$ intermediate steps between the starting point $(\tau = 0, x_0 = 0)$ and the end point $(\tau = \beta, x_N = x)$. x_i is the spatial coordinate along the $1d$ boundary space with lattice constant a (Fig. 5.1). $\delta\tau = \frac{|\beta|}{N}$ is the time interval for each intermediate step.

The physical picture behind Eq. 5.3 is shown in Fig. 5.1. $D[x(\tau)] \sim \prod_{i=1}^{N-1}(dx_i/a)$ is the integral measure of Feynmann path integral, which should arise from summing over x_i along the $1d$ space with lattice constant a: $\sum_x f(x) = \frac{1}{a}\int dx f(x)$. $G_0(\delta\tau, \delta x) = e^{-m\sqrt{\delta\tau^2+\delta x^2}}$ is the intermediate step short range propagation of the MM, inherited from Eq. 5.2. Here we take the simplest possible form of $G_0(\delta\tau, \delta x)$ as a generalization of Eq. 5.2, which has a Lorentz invariance between $\delta\tau$ and δx. $\rho(\delta\tau, \delta x_i)$ with $\delta x_i = x_i - x_{i-1}$ is an extra factor to control the fluctuation between intermediate steps, whose form depends on the microscopic details of domain wall proliferation. We will first consider

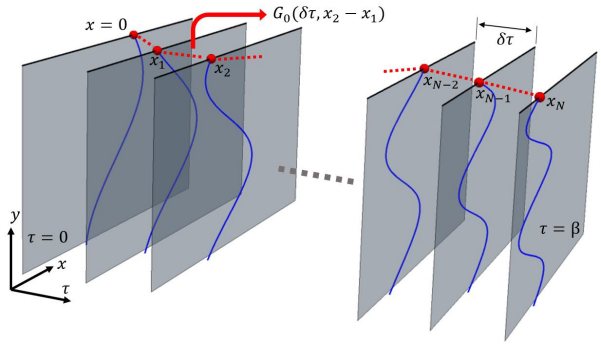

Figure 5.1: Physical picture of the path integral in Eq. 5.3. Here each plane represents the 2d bulk at an intermediate time, the solid lines are the decorated domain walls, the circles are gapped Majorana modes at the boundary. The Majorana modes are connected by dashed lines, which stand for the local Green's function $G_0(\delta\tau, x_i - x_{i-1})$.

the simplest scenario with $\rho(\delta\tau, \delta x_i) = 1$.

A direct path integral of Eq. 5.3 is a bit awkward. We could change the variables inside each Green's function using the following trick:

$$\begin{aligned} G(\beta, x) &= \mathrm{sgn}(\beta) \int D[x(\tau)] \prod_{i=1}^{N} \frac{d\lambda_i d\phi_i}{2\pi} \prod_{j=1}^{N} G_0(\delta\tau, \phi_j) \\ &\times \exp\left(i \sum_{k=1}^{N} \lambda_k (x_k - x_{k-1} - \phi_k) \right). \end{aligned} \tag{5.4}$$

Here we introduced two sets of auxiliary variables: λ_i are Lagrangian multipliers; ϕ_i substitute the coordinate differences. Now we can integrate out $x(\tau)$ first, which generates a product of delta functions $\prod_{i=2}^{N} \delta(\lambda_i - \lambda_{i-1})$, i.e. all λ_i should equal. Then we can further integrate out λ_i,

$$\begin{aligned} G(\beta, x) &= \mathrm{sgn}(\beta) \left(\frac{1}{a}\right)^{N-1} \int \prod_{i=1}^{N} d\phi_i G_0(\delta\tau, \phi_i) \\ &\times \delta(x - \sum_{k=1}^{N} \phi_k). \end{aligned} \tag{5.5}$$

Now we can perform a Fourier transformation of the spatial coordinate x, and

$$\begin{aligned} G(\beta,k) &\sim \frac{1}{a}\int dx\ e^{\mathrm{i}kx}G(\beta,x) \\ &= \mathrm{sgn}(\beta)\left(\frac{1}{a}\int d\phi\ e^{\mathrm{i}k\phi}G_0(\delta\tau,\phi)\right)^{\frac{|\beta|}{\delta\tau}}. \end{aligned} \tag{5.6}$$

Here we have replace all N in the expression by $|\beta|/\delta\tau$, and view $\delta\tau$ as an independent variable, unrelated to β. $G(\beta,k)$ takes an exponential form just like $G_{\mathrm{MM}}(\tau)$, and this comparison allows us to define an effective mass gap for $G(\beta,k)$ as follows

$$\begin{aligned} m'(k) &\equiv -\frac{\ln\left(\frac{1}{a}\int d\phi\ e^{\mathrm{i}k\phi}G_0(\delta\tau,\phi)\right)}{\delta\tau} \\ &= -\frac{\ln\left(\frac{2m\delta\tau}{a\sqrt{m^2+k^2}}K_1(\delta\tau\sqrt{m^2+k^2})\right)}{\delta\tau}, \end{aligned} \tag{5.7}$$

so that $G(\beta,k)\sim \mathrm{sgn}(\beta)e^{-m'(k)|\beta|}$. $K_1(x)$ is the modified Bessel function of the second kind.

With large m or k, the effective mass $m'(k)$ is proportional to $m'(k)\sim\sqrt{m^2+k^2}$. Hence with large m,k in the momentum and Matsubara frequency space, the fermion Green's function takes the approximate form

$$G(\mathrm{i}\omega,k)\sim\frac{\mathrm{i}\omega}{\omega^2+m^2+k^2}. \tag{5.8}$$

This form of Green's function after SMG is consistent with the fermion Green's functions obtained in different models [377, 400, 385, 379, 380], after taking the trace of the Green's functions in these literature, since in our formalism there is a single component of Majorana fermion in the Dirac space. As long as $m'(k)>0$, i.e. the fermion Green's function decays exponentially in the long time limit, the Fourier transformation of the

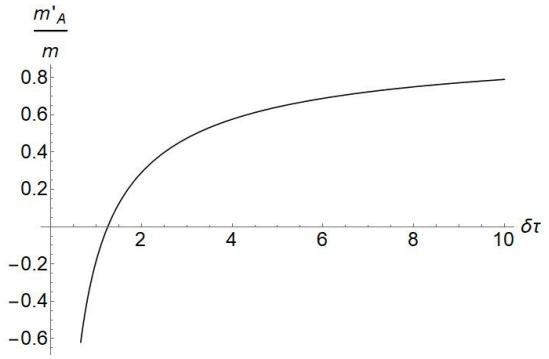

Figure 5.2: Effective mass gap ratio $m'(0)/m$ as a function of $\delta\tau$. The sign of $m'(0)$ changes from positive to negative while decreasing $\delta\tau$, suggesting a phase transition caused by domain wall fluctuation. Here we set $m = a = 1$.

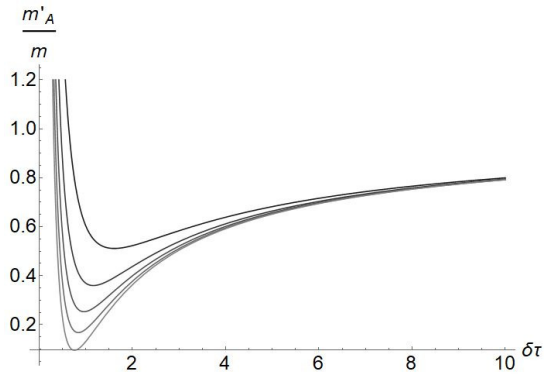

Figure 5.3: Effective mass ratio versus $\delta\tau$ for different control parameter A with $m = a = 1$. From top to bottom $A = 1, 2, \cdots 5$.

Green's function to the Matsubara frequency space will have zero at $\omega = 0$.

The ratio between effective mass gap $m'(0)$ and m as a function of $\delta\tau$ is shown in Fig. 5.2, in which we set $m = a = 1$. When $\delta\tau \ll a$ (meaning there are many intervals in the path integral), the effective mass m' becomes negative, this means that in the long time limit the Green's function of the Majorana fermion no longer exponentially decays. The sign change of m' signals a phase transition, which is caused by increased steps of intervals, or physically stronger fluctuation of the domain wall.

Now we turn on the control function $\rho(\delta\tau, \delta x_i)$ in the Green's function path integral. For example, we can turn on a Gaussian control function of the fluctuation of the domain

wall: $\rho_A(\delta\tau, \delta x_i) = \exp(-(\delta x_i/\delta\tau)^2/A)$, It is not hard to see, from Eqs. 5.4 to 5.7, that adding such control factor will not alter the exponential form of the outcome, while the effective mass gap now reads

$$m'_A = -\frac{\ln\left(\frac{1}{a}\int d\phi\ G_0(\delta\tau, \phi)e^{-\phi^2/(A\delta\tau^2)}\right)}{\delta\tau}. \tag{5.9}$$

Results of numerical integral of ϕ with different A are plotted in Fig. 5.3. Again all m'_A approaches to m when $\delta\tau \to \infty$. And as expected, smaller A will lead to a larger m', because a smaller A suppresses proliferation of the domain walls more strongly.

5.3 Higher spatial dimensions

"Decorated defect construction" of TSCs and TIs, or more generally SPT states can be generalized to higher dimension. As we mentioned in the introduction, the $3d$ TI in the AIII class can be constructed by starting with a superfluid with spontaneous U(1) symmetry breaking in the $3d$ bulk, then decorate each vortex line with a Kitaev's chain, and eventually proliferate the vortex line to restore the U(1) symmetry in the bulk. A $4d$ TSC with SO(3) and time-reversal symmetry can be constructed in a similar way: in the $4d$ space, the hedgehog monopole of a SO(3) vector order parameter is a line defect; one can start with an ordered phase with a SO(3) vector order parameter, and decorate the hedgehog monopole line with a $1d$ Kitaev's chain, and then eventually proliferate the monopole line.

In general one can start with a $d-$dimensional system with symmetry group G (for example SO$(d-1)$) that allows one dimensional topological defect line. In this case each defect line could be decorated with Kitaev chains, and when these line defects are proliferated we again presumably obtain gapped TSC with symmetry $G \times Z_2^T$. When

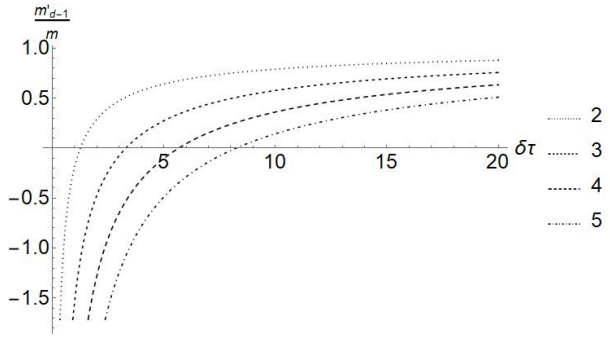

Figure 5.4: m'_{d-1}/m as functions of $\delta\tau$ with $m = a = 1$. From top to bottom $d = 2, 3, 4, 5$.

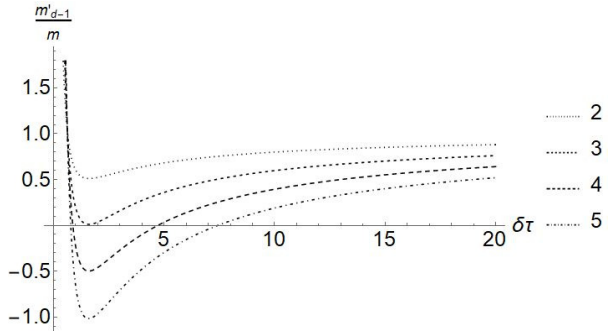

Figure 5.5: m'_{d-1}/m under Gaussian control function as functions of $\delta\tau$, with $m = a = 1$, $d = 2$ to 5 and $A = 1$.

the decorated line defects meet the $(d-1)-$dimensional boundary, the $0d$ intersection is decorated with Majorana zero modes. When eight copies of Kitaev's chains are decorated on the $1d$ defect line, the Majorana modes at the intersection is gapped by interaction through the SMG mechanism, and their Green's function is given by Eq. 5.1.

Once we proliferate the defects, the fermion Green's function at the $(d-1)-$dimensional boundary can still reduce to a path integral problem:

$$G^{(d-1)}(\beta, \mathbf{x}) = \mathrm{sgn}(\beta) \int D[\mathbf{x}(\tau)] \prod_{i=1}^{N} G_0^{(d-1)}(\delta\tau, \delta\mathbf{x}_i)$$

$$\times \rho(\delta\tau, \delta\mathbf{x}_i) \tag{5.10}$$

where $\delta\mathbf{x}_i = \mathbf{x}_i - \mathbf{x}_{i-1}$, and $\mathbf{x}_i$ are intermediate positions at the $d-1$ dimensional boundary

(with $\mathbf{x}_0 = 0$ and $\mathbf{x}_N = \mathbf{x}$) and $G_0^{(d-1)}(\delta\tau, \delta\mathbf{x}_i) = \exp\left(-m\sqrt{\delta\tau^2 + \delta\mathbf{x}_i^2}\right)$ is the simplest extension of Eq. 5.1 to $(d-1)-$dimensional space. The same trick of variable substitution applies here:

$$\begin{aligned} G^{(d-1)}(\beta, \mathbf{x}) &= \mathrm{sgn}(\beta) \int D[\mathbf{x}(\tau)] \prod_{i=1}^{N} \frac{d\vec{\lambda}_i d\vec{\phi}_i}{(2\pi)^{d-1}} \\ &\times G_0^{(d-1)}(\delta\tau, \vec{\phi}_i)\rho(\vec{\phi}_i) \exp\left(i \sum_{k=1}^{N} \vec{\lambda}_k \cdot (\mathbf{x}_k - \mathbf{x}_{k-1} - \vec{\phi}_k)\right). \end{aligned} \tag{5.11}$$

Again, integrating out $\mathbf{x}(t)$ and $\vec{\lambda}_i$ leaves us with a single constraint $\delta^{(d)}(\mathbf{x} - \sum_{i=1}^{N} \vec{\phi}_i)$. After integrating over $\mathbf{x}$, we are left with $\int d\mathbf{x} G^{(d-1)}(\beta, \mathbf{x}) \propto \mathrm{sgn}(\beta) e^{-m'_{d-1}|\beta|}$, in which

$$\begin{aligned} m'_{d-1} \equiv &- \frac{1}{\delta\tau} \ln\left\{\left(\frac{1}{a}\right)^{d-1} \int d^{d-1}\vec{\phi} \right. \\ &\left. \times G_0^{(d-1)}(\delta\tau, \vec{\phi})\rho(\vec{\phi})\right\} \\ = &- \frac{\ln\left(\frac{ma}{\pi}\left(\frac{2\pi\delta\tau}{ma^2}\right)^{\frac{d}{2}} K_{d/2}(m\delta\tau)\right)}{\delta\tau} (\text{for } \rho(\vec{\phi}) = 1) \end{aligned} \tag{5.12}$$

is the new effective mass gap. The ratios between m'_{d-1} and m is plotted in Fig. 5.4, and we can see from the plot that increasing spatial dimension makes the effective mass gap smaller, indicating that fluctuation is stronger for higher dimensions. Indeed, for higher dimensions there is more space for the proliferation of path $\mathbf{x}(\tau)$. When the Gaussian control function $\rho_A(\delta\tau, \delta\mathbf{x}_i) = \exp(-(\delta\mathbf{x}_i/\delta\tau)^2/A)$ is turned on, the stronger fluctuation for higher dimensions makes the Gaussian suppression less effective (see Fig. 5.5). Nevertheless, for nonzero A, m'_{d-1} can still be positive (and hence there is a zero in the Green's function) for a broad range of parameters.

5.4 Scenarios without Translation symmetry

One of the previous observations and arguments for the existence of fermion Green's function zero, is based on the quantized topological number for TSC and TI defined with the fermion Green's function [397, 398]. A typical topological number can be defined in the Matsubara frequency and momentum space of the Euclidean space-time fermion Green's function [402, 403, 404, 405, 406]: $n \sim \int d\omega d^d k \ \mathrm{tr}[B(G^{-1}\partial G) \wedge (G^{-1}\partial G) \cdots]$, where G is the matrix of the fermion Green's function, and B is a matrix in the flavor space. The number n must be a quantized integer mathematically, and it can only change when the Green's function has singularity.

The number n can change through two types of "transitions". The first type of transition is a physical transition where $G^{-1}(\mathrm{i}\omega = 0)$ vanishing to zero at certain momentum, i.e. the fermions become gapless. In this case the physical topological transition coincides with the transition of the topological number. However, one can easily notice that in the definition of n, G^{-1} and G are on an equal footing, hence theoretically the topological number mentioned above can also change when $G(\mathrm{i}\omega = 0) = 0$, i.e. when the Green's function has a zero. Hence when the TSC or TI is trivialized by the interaction, although there is no unavoidable phase transition between the TSC (or TI) and a trivial insulator, the topological number n still has to change discontinuously somewhere in the phase diagram, and since there is no real physical transition, the number n has to change through zero of the Green's function.

This argument for Green's function zeros relies on the quantized topological number in the momentum space, hence it requires the translation symmetry. But none of the TSC and TI in the "ten-fold way" classification requires translation symmetry, hence it is natural to ask whether the Green's function zeros persist when the translation symmetry is broken. Normally the translation symmetry breaking is caused by disorder,

i.e. a random potential energy. But a fermion bilinear potential term $i\gamma_a\gamma_b$ breaks the time-reversal symmetry of the decorated Kitaev's chain. Hence the most natural translation symmetry breaking perturbation that can be turned on in the system, is a spatial dependent random four-fermion interaction, *i.e.* a randomized $m(x)$ in Eq. 5.2, Eq. 5.3.

Now Eq. 5.3 is modified to

$$G(\beta, x) = \mathrm{sgn}(\beta) \int D[x(\tau)] e^{\sum_{i=1}^{N} -m(x_i)\sqrt{\delta\tau^2+\delta x_i^2}} \rho_A(\delta\tau, \delta x_i). \tag{5.13}$$

$m(x_i)$ is a space-dependent but time-independent function. In principle $m(x_i)$ could be any function of space. Here we focus on the situation when $m(x_i) = m + \delta m(x_i)$, where m is a positive constant, while $\delta m(x_i)$ is random function of space with zero mean and Gaussian distribution. After disorder average, the expression for the Green's function is

$$\begin{aligned}\overline{G(\beta)} = \quad & \mathrm{sgn}(\beta) \int D[x(\tau)] \\ & \times e^{\sum_{i=1}^{N} -m\sqrt{\delta\tau^2+\delta x_i^2}+\sum_{j,k}\Delta\delta(x_j-x_k)\sqrt{\delta\tau^2+\delta x_j^2}\sqrt{\delta\tau^2+\delta x_k^2}} \times \rho_A(\delta\tau, \delta x_i).\end{aligned} \tag{5.14}$$

Δ is given by the Gaussian distribution of $\delta m(x_i)$:

$$\overline{\delta m(x_j)\ \delta m(x_k)} \sim \Delta\delta(x_j - x_k). \tag{5.15}$$

The delta function $\delta(x_j - x_k)$ is only nonzero when $x_j = x_k$. This condition automatically satisfies when $j = k$, but may still happen when $j \neq k$, meaning the path $x(\tau)$ returns to the same spatial location at different time instances. We first consider the

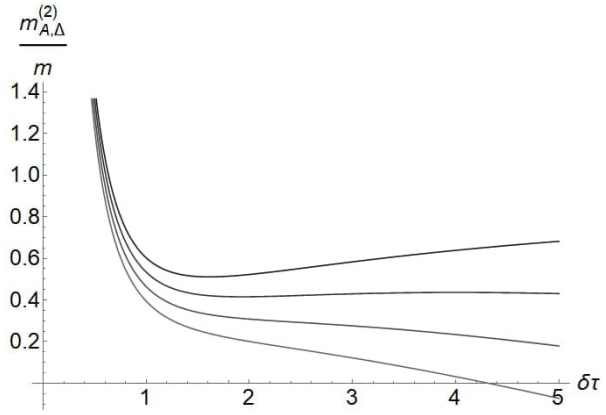

Figure 5.6: Effective mass gaps $m^{(2)}_{A,\Delta}$ for the lowest order of disorder averaged Green's function $\overline{G(\beta)}_0$ as functions of $\delta\tau$. Here we set $m = a = A = 1$, $\Delta = 0$, 0.05, 0.1, 0.15 from the top to bottom.

contribution from disorder average when $j = k$:

$$\begin{aligned}\overline{G(\beta)}_0 &= \mathrm{sgn}(\beta)\int D[x(\tau)]e^{\sum_{i=1}^{N} -m\sqrt{\delta\tau^2+\delta x_i^2}+\sum_i \Delta(\delta\tau^2+\delta x_i^2)}\rho_A(\delta\tau,\delta x_i).\\ &= \mathrm{sgn}(\beta)\exp\left(-\beta(m'_{\tilde{A}}-\Delta\delta\tau)\right). \qquad (5.16)\end{aligned}$$

Here $m'_{\tilde{A}}$ with $\tilde{A} = \frac{A}{1-A\Delta}$ is the effective mass gap defined in Eq. 5.9 with a new Gaussian control parameter $\tilde{A} = \frac{A}{1-A\Delta}$. Thus $\overline{G(\beta)}_0$ behaves identically to the previously computed Gaussian suppressed Green's function, albeit with a slower decaying rate, $m^{(2)}_{A,\Delta} \equiv m'_{\tilde{A}} - \Delta\delta\tau$. The effect of disorder on the effective mass $m^{(2)}_{A,\Delta}$ is plotted in Fig. 5.6.

For the contribution from $j \neq k$ (we assume that $j < k$ hereafter), we can expand the Green's function into powers of Δ. The first order of this expansion is

$$\begin{aligned}\overline{G(\beta)}_1 &\equiv \Delta\mathrm{sgn}(\beta)e^{\beta\Delta\delta\tau}\sum_{j\neq k}\int D[x(\tau)]e^{\sum_{i=1}^{N} -m\sqrt{\delta\tau^2+\delta x_i^2}}\\ &\times \sum_{j\neq k}\delta(x_j-x_k)\sqrt{\delta\tau^2+\delta x_j^2}\sqrt{\delta\tau^2+\delta x_k^2}\end{aligned}$$

$$\times \quad \prod_{i=1}^{N} \rho_{\tilde{A}}(\delta\tau, \delta x_i). \tag{5.17}$$

Again using the previous variable substitution, we obtain

$$\begin{aligned}
\overline{G(\beta)}_1 &= \Delta \mathrm{sgn}(\beta) e^{\beta\Delta\delta\tau} \sum_{j\neq k} \int D[x(\tau)] \prod_{i=1}^{N} \frac{d\lambda_i d\phi_i}{2\pi} \\
&\times \quad e^{-\sum_i m\sqrt{\delta\tau^2+\phi_i^2} - \mathrm{i}\lambda_i(x_i - x_{i-1} - \phi_i)} \delta(x_j - x_k) \\
&\times \quad \sqrt{\delta\tau^2+\phi_j^2}\sqrt{\delta\tau^2+\phi_k^2} \prod_{i=1}^{N} \rho_{\tilde{A}}(\delta\tau, \phi_i).
\end{aligned} \tag{5.18}$$

Integrating over all x_i and x_0, we obtain the product of a series of delta functions

$$\begin{aligned}
&\prod_{i=1}^{j-1} \delta(\lambda_i - \lambda_{i+1}) \prod_{i=j+1}^{k-1} \delta(\lambda_i - \lambda_{i+1}) \prod_{i=k+1}^{N-1} \delta(\lambda_i - \lambda_{i+1}) \\
\times \quad &\delta(\lambda_N)\delta(\lambda_k - \lambda_{k+1} + \lambda_j - \lambda_{j+1}).
\end{aligned} \tag{5.19}$$

For example $\delta(\lambda_N)$ comes from $\int dx_N$. Integrating out other x_i will enforce $\lambda_i = 0$ for all $i > k$; $\lambda_i = \lambda_1$ for all $i \leq j$; and $\lambda_i = \lambda_k$ for all $j < i \leq k$. The final delta function above thus also enforces $\lambda_i = \lambda_1 = 0$ with all $i \leq j$. Notice that λ_k is unconstrained here, because $\delta(x_j - x_k)$ effectively removes one δ function constraint for λ_i's. So we are left with the a single integral of $\lambda_k \equiv \lambda$, and the result is

$$\begin{aligned}
\overline{G(\beta)}_1 &= 2\Delta \mathrm{sgn}(\beta) e^{\beta\Delta\delta\tau} \sum_{j<k} (\tilde{G}_\Delta(0))^{N-(k-j)-1} \partial_m \tilde{G}_\Delta(0) \\
&\times \quad \int d\lambda (\tilde{G}_\Delta(\lambda))^{k-j-1} \partial_m \tilde{G}_\Delta(\lambda)
\end{aligned}$$

$$= \overline{G(\beta)}_0 \times 2\Delta \frac{\partial_m \tilde{G}_\Delta(0)}{\tilde{G}_\Delta(0)} \sum_{h=1}^{N-1} (N-h)$$

$$\times \int d\lambda \left(\frac{\tilde{G}_\Delta(\lambda)}{\tilde{G}_\Delta(0)} \right)^{h-1} \frac{\partial_m \tilde{G}_\Delta(\lambda)}{\tilde{G}_\Delta(0)}. \tag{5.20}$$

Here $\tilde{G}_\Delta(\lambda) = \int \frac{d\phi}{a} e^{\mathrm{i}\lambda\phi - m\sqrt{\delta\tau^2+\phi^2}} \rho_{\tilde{A}}(\delta\tau, \phi)$.

Numerical integration of λ in the expression above shows that the ratio between the first two orders of the Δ expansion, i.e. $\overline{G(\beta)}_1 / \overline{G(\beta)}_0$ approaches $\beta^{3/2}$ for large β (see Fig. 5.7). Thus at large β the overall behavior of the first order term in the Δ expansion still exponentially decays with β. The behavior of large β can be understood in the following way: The integral of $\tilde{G}_\Delta(\lambda)$ can be approximated by replacing $\sqrt{\delta\tau^2+\phi^2}$ by $\delta\tau + |\phi|$ in the exponent, which means $\frac{\tilde{G}_\Delta(\lambda)}{\tilde{G}_\Delta(0)}$ and $\frac{\partial_m \tilde{G}_\Delta(\lambda)}{\tilde{G}_\Delta(0)}$ behaves approximately as $e^{-\frac{A}{4(1-A\Delta)}\lambda^2}$. The λ integral gives a $\frac{1}{\sqrt{h}}$ factor in each term of the summation of Eq. 5.20. Eventually $\overline{G(\beta)}_1 / \overline{G(\beta)}_0$ is evaluated as

$$\sum_{h=1}^{N} \frac{N-h}{\sqrt{h}} \sim \int_0^\beta dx \frac{\beta - x}{\sqrt{x}} \sim \beta^{3/2}. \tag{5.21}$$

And as long as the overall behavior of $\overline{G(\beta)}$ decays exponentially with β, the Fourier transformation of $\overline{G(\beta)}$ has a zero at $\omega = 0$.

At higher dimensions, it is less likely for $\mathbf{x}_j = \mathbf{x}_k$ at $j \neq k$, i.e. it is less likely for a path $\mathbf{x}(\tau)$ to return to exactly the same spatial location at two different time instances. Hence we expect that for higher spatial dimensions the zeroth order $\overline{G(\beta)}_0$ in the formulation above should be even more accurate.

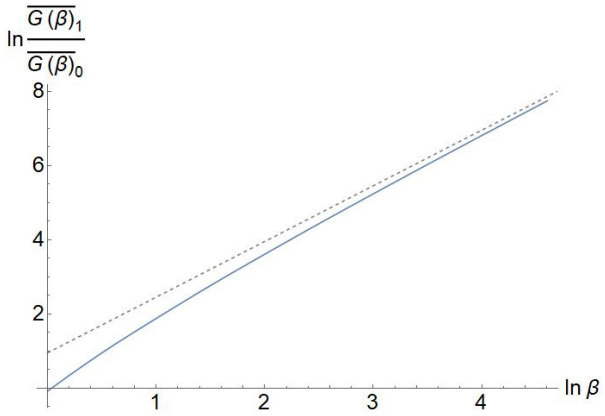

Figure 5.7: Log-log plot of numerical integration of $\overline{G(\beta)}_1/\overline{G(\beta)}_0$. Here we set $m = a = A = 1$, $\delta\tau = 0.3$ and $\Delta = 0.1$. The dashed line is a guide to the eye with slope 3/2.

5.5 The "avoided" topological transition in the bulk

As we discussed in the introduction, besides the nontrivial boundary state, there is another prominent feature of a TI and TSC: there must be an unavoidable bulk topological transition between the TI or TSC and the trivial insulator when tuning the parameter of the bulk Hamiltonian. However, once the TI or TSC is trivialized by interaction, not only can the boundary state be trivially gapped, the bulk topological transition also becomes avoidable [365, 366]: there is an adiabatic path in the phase diagram connecting the original TI (or TSC) phase and the original trivial insulator phase without closing the gap at all. In this case the original topological transition is also called "unnecessary transition" [407, 408]. In fact there is a close relation between the boundary state and the bulk topological transition. The simplest model to visualize such relation is the Chalker-Coddington model [409, 410], which was first developed for the integer quantum Hall transition. This boundary-bulk relation can be made much more general for strongly interacting symmetry protected topological states [411]. In general the bulk topological transition between the trivial phase and the SPT phase can be viewed as growing islands of the SPT phase inside a trivial phase, and the unavoidable topological transition orig-

inates from the nontrivial interface states between the trivial and SPT phases. When the interfaces percolate, the bulk is at the topological transition. Using this picture, our real-space calculation for Green's function in the previous sections for a $d-$dimensional boundary, also applies to the avoided bulk topological transition at $d-$dimensions.

5.6 Summary

In this chapter we demonstrate the existence of the Green's function zero as a remaining trace of nontrivial topology, after the system acquires a fully gapped spectrum after the mechanism of symmetric mass generation. Our method mostly relies on the real space decorated defect construction of the SPT states, and it does not require spatial symmetries such as translation.

Appendix A

Appendix

A.1 Appendix to Section 4.2

A.1.1 Field theories for $N = 6$ and $N = 12$ of scenario (1)

In the next section we will derive the projective symmetry group transformation for the low energy vortex modes of scenario (1). For $N = 6$, with symmetries $R_{2\pi/3}$, translation, $P_x\mathcal{T}$, and P_y, the PSG-invariant interactions between the vortex fields ψ_a beyond Eq. 4.24 take the following form:

$$\begin{aligned}\mathcal{L}^{(1)\prime}[\psi_a] =& u_1 \sum_{a=0}^{2}(|\psi_{2a}|^2 + |\psi_{2a+1}|^2)^2 + u_2 \left(\sum_{a=0}^{5}|\psi_a|^2\right)^2 \\ &+ v_1 \left(\sum_{a=0}^{5}\psi_a^2\right)\left(\sum_{a=0}^{5}(\psi_a^*)^2\right) + v_2 \sum_{a=0}^{2}(\psi_{2a}^2 + \psi_{2a+1}^2)((\psi_{2a}^*)^2 + (\psi_{2a+1}^*)^2) \\ &+ w_1 \sum_{a=0}^{2}(|\psi_{2a}|^2 - |\psi_{2a+1}|^2)(\psi_{2a+2}\psi_{2a+3}^* + \psi_{2a+2}^*\psi_{2a+3}) \\ &+ w_2 \left\{\sum_{a=0}^{2}(\psi_{2a}^2 - \psi_{2a+1}^2)\psi_{2a+2}^*\psi_{2a+3}^* + c.c.\right\} + \dots\end{aligned} \tag{A.1}$$

Here the dots stand for terms higher than the quartic order. The parameters $\{u_1, u_2, v_1, v_2, w_1, w_2\}$ in (A.1) are all real, and the index a for ψ_a is regarded as cyclic modulo 6.

In addition to the quartic terms, the gauge invariant density wave order parameter can couple to the Fermi surface of the fermionic partons, and quartic terms of ψ_a with singularity in the frequency space can be generated as was pointed out by Ref. [326], such as $|\omega||S_{\omega,q}|^2$, where $S_{\omega,q}$ is a bilinear of ψ_a. This coupling only arises for scenario (1). For scenario (2) discussed in the main text, the 3D XY* fixed point should be stable against symmetry allowed perturbations; the field theory Eq. 4.34 is also stable against coupling to the fermionic parton Fermi surface.

Although we do not aim to give a full discussion of the fate of the infrared limit of scenario (1), in the current section we establish the formalism for this problem that one can use in the future. As we explained in the previous paragraph, after integrating out the fermion that is connected by the finite momentum of the density wave order parameter, a term is generated $\sim |\omega||S_{\omega,q}|^2$, where $S = \psi^\dagger T \psi$ and T is an $N \times N$ matrix. One can introduce a new field Φ through the Hubbard-Stratonovich transformation, and ψ_a will interact with the Φ field [412]. We start with the first line of Eq. A.1. The field theory Eq. 4.24 with u_1 and u_2 in Eq. A.1 can be reformulated by introducing multiple Lagrange multipliers λ_i:

$$\begin{aligned}
\mathcal{L}^{(1)} &= \sum_{a=0}^{N-1} |(\partial - \mathrm{i}A)\psi_a|^2 + \mathrm{i}\sum_{i=1}^{N_1} \lambda_i \left(\sum_{\tau=1}^{N_2} |\psi_{\tau,i}|^2 \right) + \mathrm{i}\Phi \psi^\dagger T \psi; \\
&\langle \lambda_i(\vec{q}) \lambda_{i'}(-\vec{q}) \rangle = \frac{8}{N_2} |q| \delta_{i,i'}, \\
&\langle A_\mu(\vec{q}) A_\nu(-\vec{q}) \rangle = \frac{16}{N} \left(\frac{\delta_{\mu\nu} - q_\mu q_\nu / q^2}{|q|} \right), \\
&\langle \Phi(\vec{q}) \Phi(-\vec{q}) \rangle = g|\omega|.
\end{aligned} \tag{A.2}$$

Here $N = N_1 N_2$, and for the real system with $N = 6$, $N_1 = 3$ and $N_2 = 2$. Introducing λ_i for each index i physically means that we are investigating the theory near the point with a SU(N_2) symmetry for each index i, rather than the original CP^{N-1} theory with a large SU(N) flavor symmetry. This is analogous to the "easy-plane bosonic QED_3" considered in Ref. [94]. The actions of λ_i and the transverse component of gauge field A are generated by integrating out the fields ψ_a. One possible way to proceed with the calculation is that, we can fix N_1, and take $1/N_2$ as a small parameter. When g is the same order of $1/N_2$, the interaction between ψ_a and the Φ field will lead to the contribution comparable with that arising from coupling to λ_i and A. The calculation would be analogous to the one formulated in Ref. [193], where the nonlocal interaction on top of a bosonic QED flows to a new fixed point. One can evaluate the scaling behaviors (such as relevance/irrelevance in the IR) of the v and w terms in the second and third lines in Eq. A.2 at this new fixed point. By exploring the parameter space of g, $1/N_2$, and different choice of matrix T, it is possible to identify a finite region where Eq. A.2 corresponds to a stable fixed point where the v and w terms in Eq. A.1 are irrelevant.

The same strategy can be applied to the situation with $N = 12$. With long moiré lattice constants, the 6-fold rotation $R_{\pi/3}$ also becomes a good approximate symmetry. Together with $R_{\pi/3}$, the quartic terms in the field theory for $N = 12$ (please refer to the phase diagram in Fig. 4.5) are:

$$\begin{aligned}
\mathcal{L}^{(1)\prime}[\psi_{\sigma,\tau,i}] &= u_1 \sum_{\sigma,i} \left(\sum_{\tau} |\psi_{\sigma,\tau,i}|^2 \right)^2 + u_2 \left(\sum_{\sigma\tau i} |\psi_{\sigma\tau i}|^2 \right)^2 \\
&+ v_1 \sum_{\sigma,i\neq i'} \left(\sum_{\tau} |\psi_{\sigma,\tau,i}|^2 \right) \left(\sum_{\tau'} |\psi_{\sigma,\tau',i'}|^2 \right) + v_2 \sum_{i} \left(\sum_{\tau} |\psi_{+,\tau,i}|^2 \right) \left(\sum_{\tau'} |\psi_{-,\tau',i}|^2 \right) \\
&+ w_1 \left| \sum_{i,\tau} \psi_{+,\tau,i} \psi_{-,\tau,i} \right|^2 + \mathrm{i} w_2 \left(\sum_{i,\tau,\tau'} \psi^*_{+,\tau,i+1} \psi^*_{-,\tau,i+1} \psi_{+,\tau',i} \psi_{-,\tau',i} - h.c. \right)
\end{aligned} \tag{A.3}$$

Here the 12 modes are labelled by $\psi_{\sigma,\tau,i}$ in which $\tau = \pm$ labels two degenerate modes at the same momentum, $\sigma = \pm$ labels two sets of momenta that are each connected by $R_{2\pi/3}$, and $i = 0, 1, 2 \mod 3$ labels these three momenta within each set.

We can again start with the first line of Eq. A.3, and introduce Lagrange multiplier $\lambda_{\sigma,i}$ which couples to the ψ_a fields as $\sum_{\tau=1}^{N_2} \lambda_{\sigma,i}|\psi_{\sigma,\tau,i}|^2$. Notice that we have generalized τ to $1 \cdots N_2$. Then the Hubbard-Stratonovich transformation can introduce new fields that couple to ψ_a to account for the singular terms generated through interacting with the Fermi surface. A combined perturbation theory of $1/N_2$ and g can again determine the relevance/irrelevance of the second and third lines of Eq. A.3. In particular, the two terms in the second line of Eq. A.3 are indeed irrelevant with large-N_2, as the scaling dimension of $\sum_\tau |\psi_{\sigma,\tau,i}|^2$ is 2 with large-N_2.

A.1.2 The PSG transformation for $N = 6$ in scenario (1)

Under the boson-vortex duality, the dual vortex theory on the hexagonal lattice takes the form

$$H = \sum_{\langle ij \rangle} -t_{ij}\phi_i^* \phi_j + H'_\phi + V_\phi + \ldots, \quad t_{ij} = te^{-\mathrm{i}A_{ij}} \tag{A.4}$$

Here H'_ϕ describes hopping terms between further neighbors. The potential V_ϕ includes a quadratic term $\sum_i r|\phi_i|^2$ which tunes through the phase transition.

When t_{ij} is nonzero only for nearest neighbor links on the dual honeycomb lattice, and it takes positive sign on the solid links and negative sign on the dashed links in Fig. 4.4 due to the π flux of A_μ through each hexagon, there are four minima of the vortex band structure in the Brillouin zone (Fig. 4.5). We label the four minimum modes from 0 to 3, each have momentum (k_x, k_y)

$$\mathbf{Q}_{0,1} = \mathbf{K} = \left(\frac{2\pi}{3\sqrt{3}}, 0\right), \quad \mathbf{Q}_{2,3} = \mathbf{K}' = \left(\frac{\pi}{3\sqrt{3}}, \frac{\pi}{3}\right). \tag{A.5}$$

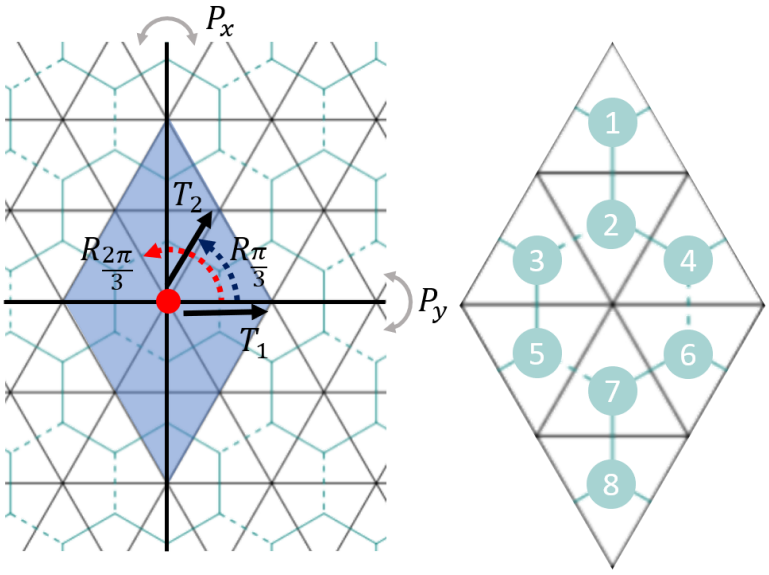

Figure A.1: Crystal symmetry of the triangular lattice, the nearest neighbor hopping amplitudes of the vortices, and the unit cell after taking into account of the sign of t_{ij}.

With further neighbor vortex hopping (please refer to the phase diagram in Fig. 4.5), the minima of the vortex band structure can shift to the M points, similar to Ref. [320]. When the degenerate minima are shifted to the M points (Fig. 4.5), the six corresponding momenta are

$$\mathbf{Q}_{0,1} = \left(\frac{\pi}{2\sqrt{3}}, -\frac{\pi}{6}\right), \ \mathbf{Q}_{2,3} = \left(\frac{\pi}{2\sqrt{3}}, \frac{\pi}{6}\right), \ \mathbf{Q}_{4,5} = \left(0, \frac{\pi}{3}\right). \tag{A.6}$$

Similar to the four minima case, the vortex field can be expanded using these six modes as

$$\phi_{n,\mathbf{r}} \sim \sum_{a=0}^{5} \psi_a v_{a,n} e^{\mathrm{i}\mathbf{Q}_a \cdot \mathbf{r}}. \tag{A.7}$$

The coefficients $v_{a,n}$ are solved from the band structure.

The symmetries of the theory for one single valley must include translation T_1, T_2, three-fold rotation $R_{2\pi/3}$, $P_x\mathcal{T}$. These transformations do not mix the two valleys. In the following we derive the PSG matrices of these symmetries. We first need the form of

the transformations when acting on the 8 sites in each unit cell:

$$T_{1,2}(\phi_{n,\mathbf{k}}) = \sum_m (t_{1,2})_{nm}\phi_{m,\mathbf{k}},\ t_1 = \begin{pmatrix} 0 & 0 & 0 & 0 & 0 & 0 & 1 & 0 \\ 0 & 0 & 0 & 0 & 0 & 0 & 0 & 1 \\ 0 & 0 & 0 & -1 & 0 & 0 & 0 & 0 \\ 0 & 0 & 1 & 0 & 0 & 0 & 0 & 0 \\ 0 & 0 & 0 & 0 & 0 & 1 & 0 & 0 \\ 0 & 0 & 0 & 0 & -1 & 0 & 0 & 0 \\ -1 & 0 & 0 & 0 & 0 & 0 & 0 & 0 \\ 0 & -1 & 0 & 0 & 0 & 0 & 0 & 0 \end{pmatrix}, \tag{A.8}$$

$$t_2 = \begin{pmatrix} 0 & 0 & 1 & 0 & 0 & 0 & 0 & 0 \\ 0 & 0 & 0 & 0 & 1 & 0 & 0 & 0 \\ -1 & 0 & 0 & 0 & 0 & 0 & 0 & 0 \\ 0 & 0 & 0 & 0 & 0 & 0 & -1 & 0 \\ 0 & -1 & 0 & 0 & 0 & 0 & 0 & 0 \\ 0 & 0 & 0 & 0 & 0 & 0 & 0 & 1 \\ 0 & 0 & 0 & 1 & 0 & 0 & 0 & 0 \\ 0 & 0 & 0 & 0 & 0 & -1 & 0 & 0 \end{pmatrix} \tag{A.9}$$

$$R_{2\pi/3}(\phi_{n,\mathbf{k}}) = (r_{\pi/3})_{nm}\phi_{m,R_{2\pi/3}\mathbf{k}},\ r_{2\pi/3} = \begin{pmatrix} 1 & 0 & 0 & 0 & 0 & 0 & 0 & 0 \\ 0 & 0 & 0 & 0 & 1 & 0 & 0 & 0 \\ 0 & 0 & 0 & 0 & 0 & 0 & 1 & 0 \\ 0 & 0 & 1 & 0 & 0 & 0 & 0 & 0 \\ 0 & 0 & 0 & 0 & 0 & 1 & 0 & 0 \\ 0 & 1 & 0 & 0 & 0 & 0 & 0 & 0 \\ 0 & 0 & 0 & 1 & 0 & 0 & 0 & 0 \\ 0 & 0 & 0 & 0 & 0 & 0 & 0 & 1 \end{pmatrix}, \tag{A.10}$$

$$P_x\mathcal{T}(\phi_{n,\mathbf{k}}) = (p_x t)_{nm}\phi_{m,-P_x\mathbf{k}},\ (p_x t)_{ab} = \begin{pmatrix} 1 & 0 & 0 & 0 & 0 & 0 & 0 & 0 \\ 0 & 1 & 0 & 0 & 0 & 0 & 0 & 0 \\ 0 & 0 & 0 & -1 & 0 & 0 & 0 & 0 \\ 0 & 0 & -1 & 0 & 0 & 0 & 0 & 0 \\ 0 & 0 & 0 & 0 & 0 & 1 & 0 & 0 \\ 0 & 0 & 0 & 0 & 1 & 0 & 0 & 0 \\ 0 & 0 & 0 & 0 & 0 & 0 & -1 & 0 \\ 0 & 0 & 0 & 0 & 0 & 0 & 0 & -1 \end{pmatrix}, \tag{A.11}$$

Besides these symmetries, here we argue that, if the system does have an effective Hubbard model description with two local Wannier orbitals per unit cell (one for each valley), P_y is also a good symmetry of the Hubbard model, as long as the valley mixing is negligible, which is a justified assumption with long wavelength moiré potential modulation. Let us first assume there is no valley mixing, then for each valley the band structure of the moiré mini band is described by a tight binding model with one orbital per site on the moiré triangular lattice. The hopping amplitude $t(\theta)$ along angle θ must

satisfy the following relations based on the explicit $P_x\mathcal{T}$ and translation symmetry:

$$t(\theta) = t^*(\pi - \theta), \quad t^*(\theta) = t(\pi + \theta), \tag{A.12}$$

we can easily show that $t(\theta) = t(-\theta)$, namely the system should have a P_y symmetry.

However, when there is valley mixing, t becomes a 2×2 matrix with off-diagonal terms that mix two valleys. A 2×2 hopping matrix t should satisfy four symmetries, P_x, $\mathcal{T}$, translation, and $R_{2\pi/3}$ rotation. A natural choice of P_x and $\mathcal{T}$ on t is

$$P_x : t(\theta) \to \sigma^x t(\pi - \theta)\sigma^x; \quad \mathcal{T} : t(\theta) \to (\mathrm{i}\sigma^y)t^*(-\mathrm{i}\sigma^y); \tag{A.13}$$

and the translation symmetry plus hermicity demands $t^\dagger(\theta) = t(\pi + \theta)$. P_y does not change the valley indices; if P_y takes $t(\theta)$ to $t(-\theta)$, there exists a valley mixing term $t(\theta) \sim \mathrm{i}\sigma^x \sin(3\theta)$ that preserves all the symmetries mentioned above, but breaks P_y; while if P_y takes $t(\theta)$ to $\sigma^z t(-\theta)\sigma^z$ this term becomes $t(\theta) \sim \mathrm{i}\sigma^y \cos(3\theta)$.

P_y acts on the ϕ bosons as

$$P_y(\phi_{n,\mathbf{k}}) = (p_y)_{nm}\phi^*_{m,-P_y\mathbf{k}}, \ (p_y)_{ab} = \begin{pmatrix} 0 & 0 & 0 & 0 & 0 & 0 & 0 & 1 \\ 0 & 0 & 0 & 0 & 0 & 0 & 1 & 0 \\ 0 & 0 & 0 & 0 & 1 & 0 & 0 & 0 \\ 0 & 0 & 0 & 0 & 0 & 1 & 0 & 0 \\ 0 & 0 & 1 & 0 & 0 & 0 & 0 & 0 \\ 0 & 0 & 0 & 1 & 0 & 0 & 0 & 0 \\ 0 & 1 & 0 & 0 & 0 & 0 & 0 & 0 \\ 1 & 0 & 0 & 0 & 0 & 0 & 0 & 0 \end{pmatrix}. \tag{A.14}$$

Furthermore, in the case with long moiré lattice constant, we additionally have the

six-fold rotation $R_{\pi/3}$

$$R_{\pi/3}(\phi_{n,\mathbf{k}}) = (r_{\pi/3})_{nm}\phi_{m,R_{\pi/3}\mathbf{k}},\ (r_{\pi/3})_{ab} = \begin{pmatrix} 0 & 0 & 0 & 0 & 0 & 0 & 0 & -1 \\ 0 & 0 & -1 & 0 & 0 & 0 & 0 & 0 \\ 0 & 0 & 0 & 0 & 1 & 0 & 0 & 0 \\ 0 & 1 & 0 & 0 & 0 & 0 & 0 & 0 \\ 0 & 0 & 0 & 0 & 0 & 0 & -1 & 0 \\ 0 & 0 & 0 & -1 & 0 & 0 & 0 & 0 \\ 0 & 0 & 0 & 0 & 0 & 1 & 0 & 0 \\ 1 & 0 & 0 & 0 & 0 & 0 & 0 & 0 \end{pmatrix}. \quad \text{(A.15)}$$

In the position space, the transformation rules can be summarized as

$$G(\phi_{n,\mathbf{r}}) = \sum_{m=1}^{8} g_{n,m}\phi_{m,\mathbf{r}'_m} \quad \text{(A.16)}$$

in which $\mathbf{r}'_m$ is the center of the unit cell of field ϕ_m which is obtained by certain site in the original unit cell (centered at $\mathbf{r}$) after transformation under symmetry operation G. For example, under T_1, $\mathbf{r}'_7 = \mathbf{r}'_8 = \mathbf{r} + 2\mathbf{a}_2$, because sites 1 and 2 at unit cell $\mathbf{r}$ are transformed into sites 7 and 8 in the nearby enlarged unit cell which is centered at $\mathbf{r} + 2\mathbf{a}_2$. In general, we can write the transformation as $\mathbf{r}'_m = G\mathbf{r} + \vec{\Delta}_{G,m}$, in which $\vec{\Delta}_{G,m}$ is a constant that does not depend on $\mathbf{r}$, and $G\mathbf{r}$ is the coordinate of the center of the unit cell after spacial symmetry G.

Now we plug in the low energy expansions of $\phi_{n_\mathbf{k}}$ around the minima into the equation, which yields

$$\sum_{a=0}^{N-1} G(\psi_a)v_{a,n}e^{\mathrm{i}\mathbf{Q}_a\cdot\mathbf{r}} = \sum_{a=0}^{N-1}\sum_{m=1}^{8} \psi_a g_{nm} v_{m,a} e^{\mathrm{i}\mathbf{Q}_a\cdot\mathbf{r}'_m}. \quad \text{(A.17)}$$

The relation can be viewed as a vector identity with n being the vector index on both

sides. Because all the vectors $v_{a,n}(a = 0, \ldots, N-1)$ are orthogonal to each other, we can multiply the conjugated vector $v^*_{b,n}$ on both sides and sum over n:

$$G(\psi_b)e^{\mathrm{i}\mathbf{Q}_b\cdot\mathbf{r}} = \sum_{a=0}^{N-1}\sum_{m,n=1}^{8} \psi_a v^*_{b,n} g_{n,m} v_{a,m} e^{\mathrm{i}\mathbf{Q}_a\cdot\mathbf{r}'_m}. \tag{A.18}$$

For this equation to hold for all $\mathbf{r}$, the RHS needs to have the same momentum. This requires $\mathbf{Q}_b = G^{-1}\mathbf{Q}_a$, which can only be satisfied by two possible choices of a (recall that in the convention of eight-site unit cell, each momentum $\mathbf{Q}_a$ always has two fold degeneracy for all N), denoted by a_1 and a_2. Thus we eventually have

$$G(\psi_b) = \sum_{m,n=1}^{8} v^\dagger_{b,n} g_{nm} v_{a_1,m} e^{\mathrm{i}\mathbf{Q}_{a_1}\cdot\vec{\Delta}_{G,m}} \times \psi_{a_1} + \sum_{m,n=1}^{8} v^\dagger_{b,n} g_{nm} v_{a_2,m} e^{\mathrm{i}\mathbf{Q}_{a_2}\cdot\vec{\Delta}_{G,m}} \times \psi_{a_2} \tag{A.19}$$

The final results can be organized into $N \times N$ matrices. For $N = 6$, the transformations read

$$T_{1,2}(\psi_a) = (\mathfrak{t}_{1,2})_{ab}\psi_b,\ (\mathfrak{t}_1)_{ab} = \begin{pmatrix} -1 & 0 & 0 & 0 & 0 & 0 \\ 0 & 1 & 0 & 0 & 0 & 0 \\ 0 & 0 & 0 & 1 & 0 & 0 \\ 0 & 0 & 1 & 0 & 0 & 0 \\ 0 & 0 & 0 & 0 & 0 & 1 \\ 0 & 0 & 0 & 0 & -1 & 0 \end{pmatrix},\ (\mathfrak{t}_2)_{ab} = \begin{pmatrix} 0 & 1 & 0 & 0 & 0 & 0 \\ -1 & 0 & 0 & 0 & 0 & 0 \\ 0 & 0 & 1 & 0 & 0 & 0 \\ 0 & 0 & 0 & -1 & 0 & 0 \\ 0 & 0 & 0 & 0 & 0 & -1 \\ 0 & 0 & 0 & 0 & -1 & 0 \end{pmatrix}, \tag{A.20}$$

$$R_{2\pi/3}(\psi_a) = (\mathfrak{R}_{2\pi/3})_{ab}\psi_b,\ (\mathfrak{R}_{2\pi/3})_{ab} = \begin{pmatrix} 0 & 0 & 0 & 0 & 1 & 0 \\ 0 & 0 & 0 & 0 & 0 & 1 \\ -1 & 0 & 0 & 0 & 0 & 0 \\ 0 & -1 & 0 & 0 & 0 & 0 \\ 0 & 0 & 1 & 0 & 0 & 0 \\ 0 & 0 & 0 & 1 & 0 & 0 \end{pmatrix}, \tag{A.21}$$

$$P_x\mathcal{T}(\psi_a) = (\mathfrak{P}_x\mathfrak{T})_{ab}\psi_b,\ (\mathfrak{P}_x\mathfrak{T})_{ab} = \frac{1}{\sqrt{2}}\begin{pmatrix} 0 & 0 & 1 & -1 & 0 & 0 \\ 0 & 0 & -1 & -1 & 0 & 0 \\ 1 & -1 & 0 & 0 & 0 & 0 \\ -1 & -1 & 0 & 0 & 0 & 0 \\ 0 & 0 & 0 & 0 & 1 & -1 \\ 0 & 0 & 0 & 0 & -1 & -1 \end{pmatrix}. \tag{A.22}$$

$$P_y(\psi_a) = (\mathfrak{P}_y)_{ab}\psi_b^*,\ (\mathfrak{P}_y)_{ab} = \frac{1}{\sqrt{2}}\begin{pmatrix} 0 & 0 & 1 & 1 & 0 & 0 \\ 0 & 0 & 1 & -1 & 0 & 0 \\ 1 & 1 & 0 & 0 & 0 & 0 \\ 1 & -1 & 0 & 0 & 0 & 0 \\ 0 & 0 & 0 & 0 & 1 & 1 \\ 0 & 0 & 0 & 0 & 1 & -1 \end{pmatrix}. \tag{A.23}$$

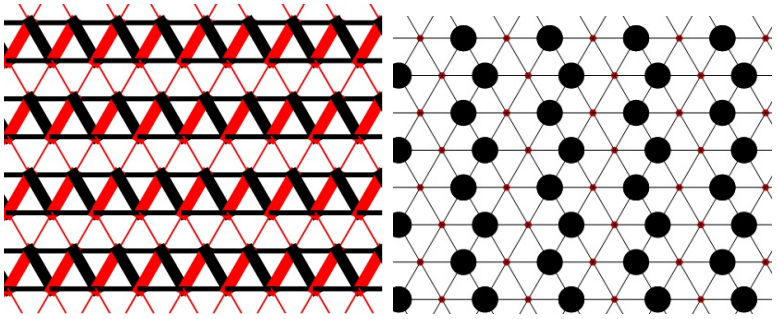

Figure A.2: Some possible density wave patterns of the original boson that correspond to different condensate of ψ_a with $a = 0, \cdots 5$. The left and right patterns correspond to $\vec{\Psi} \sim (1, 0, 0, 0, 0, 0)$ and $\vec{\Psi} \sim (0, 1/\sqrt{2}, 1/2, -1/2, 0, 0)$ respectively.

$$R_{\pi/3}(\psi_a) = (\mathfrak{R}_{\pi/3})_{ab}\psi_b, \ (\mathfrak{R}_{\pi/3})_{ab} = \begin{pmatrix} 0 & 0 & 0 & -1 & 0 & 0 \\ 0 & 0 & 1 & 0 & 0 & 0 \\ 0 & 0 & 0 & 0 & 0 & 1 \\ 0 & 0 & 0 & 0 & -1 & 0 \\ 0 & 1 & 0 & 0 & 0 & 0 \\ -1 & 0 & 0 & 0 & 0 & 0 \end{pmatrix}. \tag{A.24}$$

Deep inside the vortex condensate phase with $r \ll 0$ in equation Eq. 4.24, the vector $\vec{\Psi} = (\psi_0, \psi_1, \psi_2, \psi_3, \psi_4, \psi_5)$ can have different condensates depending on the parameters in Eq. A.1. Without loss of generality we set $\sum_{a=0}^{5} |\psi_a|^2 = 1$. The two figures in Eq. A.2 illustrate the density waves of the bosonic parton centered at the bonds and the sites on the moiré triangular lattice that correspond to two different possible condensates of $\vec{\Psi}$. The density on the bond l is inferred from $t_{ij}\langle\phi_i^*\phi_j\rangle$, with ij being the link on the dual honeycomb lattice that is dual to l, and t_{ij} takes the sign according to the gauge convention of Fig. 4.4. The operator $t_{ij}\langle\phi_i^*\phi_j\rangle$ is the energy density in terms of vortex fields, and the modulation of this operator should correspond to the valence bond solid of the original bosonic parton. We also consider an operator centered on site p of the original lattice (plaquette of the dual lattice): $\sum_{\langle ij\rangle\in p} t_{ij}\langle\phi_i^*\phi_j\rangle$, with the summation over

the links that surround the plaquette p on the dual honeycomb lattice, whose center hosts the site p of the original moiré triangular lattice. In both cases, $\langle \phi_i^* \phi_j \rangle$ is evaluated using Eq. A.7 and the value of $\vec{\Psi}$ which minimizes the quartic energy. The left pattern in Eq. A.2 is a rather common valence bond solid configuration for either spin-1/2 system or hard core boson on the triangular lattice. If one started with the construction-I of the parton construction, the discussion in this section corresponds to the original electron system with an average 1/2 electron per unit cell (the filling considered in Ref. [292]); while for construction-II, the discussion here applies to one electron per unit cell, and the analysis in this section corresponds to one of the two spin/valley flavors of the system.

A.1.3 Dual of the vortex theory

Here we derive the Lagrangian written in terms of the fractionally charged bosonic partons for scenario (1). We start with Eq. 4.24 in this section:

$$\mathcal{L}^{(1)} = \sum_{j=0}^{N-1} |(\partial_\mu - \mathrm{i}A_\mu)\psi_j|^2 + r|\psi_j|^2 + \frac{\mathrm{i}}{2\pi} A \wedge d(a + eA_{\mathrm{ext}}) + \cdots \tag{A.25}$$

To facilitate the calculation of the DC resistivity which will be discussed in the next subsection, we need to "dual back" to the charge-carriers, which requires deforming Eq. A.25 with an easy-plane anisotropy $\sum_j |\psi_j|^4$. The bosonic fractional charge carriers φ_j are the vortices of the vortex fields ψ_j. We first take the standard duality for ψ_j, and Eq. A.25 becomes:

$$\mathcal{L}^{(1)} = \sum_{j=0}^{N-1} |(\partial - \mathrm{i}\tilde{A}_j)\varphi_j|^2 + \tilde{r}|\varphi_j|^2 + \frac{\mathrm{i}}{2\pi} \tilde{A}_j \wedge dA + \frac{\mathrm{i}}{2\pi} A \wedge d(a + eA_{\mathrm{ext}}) + \cdots \tag{A.26}$$

The basic duality relation is that the current of ψ_j, *i.e.* $J_{\psi_j} \sim d\tilde{A}_j$. Now integrating out A would lead to the following constraint for the rest of the gauge fields:

$$\sum_j \tilde{A}_j - a - eA_{\text{ext}} = 0. \tag{A.27}$$

From this constraint we can take $\tilde{A}_j$ as

$$\tilde{A}_j = \tilde{a}_j + \frac{1}{N}a + \frac{e}{N}A_{\text{ext}}, \quad \sum_j \tilde{a}_j = 0. \tag{A.28}$$

Hence the dual of the dual theory becomes

$$\mathcal{L}^{(1)} = \sum_{j=0}^{N-1} |(\partial - \mathrm{i}\tilde{a}_j - \mathrm{i}\frac{1}{N}a - \mathrm{i}\frac{e}{N}A_{\text{ext}})\varphi_j|^2 + \tilde{r}|\varphi_j|^2 + \cdots . \tag{A.29}$$

The gauge fields $\tilde{a}_j$ are still subject to the constraint $\sum_j \tilde{a}_j = 0$. φ_j carries e/N charge of external EM gauge field; it also carries charge $1/N$ of gauge field a which is shared with the fermionic parton f_α.

For scenario (2) the theory in terms of fractional parton φ is much simpler: there is only one flavor of φ for each valley, and there is no extra continuous gauge fields $\tilde{a}$ besides gauge field a: Following the calculation in Ref. [311], one can generalize this one flavor of φ in each valley to an $\mathbf{N}$ component of bosons:

$$\mathcal{L}^{(2)} = \sum_{l=1}^{\mathbf{N}} |(\partial - \mathrm{i}\frac{1}{N}a - \mathrm{i}\frac{e}{N}A_{\text{ext}})\varphi^l|^2 + \mathrm{i}\lambda|\varphi^l|^2 + \cdots \tag{A.30}$$

and the bosons will scatter with both gauge field a and field λ which is introduced as a Lagrange multiplier. The fact that φ^l carries charge $1/N$ of gauge field a does not change the scattering rate through the large-$\mathbf{N}$ calculation, as the gauge charge cancels out in the calculation of scattering rate through the large-$\mathbf{N}$ approach. Compared with

scenario (2), in scenario (1) the parton φ_j is also coupled to extra gauge fields $\tilde{a}_j$, which will lead to extra scattering to the charge carriers.

When computing the resistivity, especially the DC resistivity of scenario (1), we also rely on a large$-\mathbf{N}$ generalization, namely we need to introduce an extra $l = 1 \cdots \mathbf{N}$ index for each component of fractional charge field: φ_j^l.

A.1.4 DC resistivity jump in scenario (1)

In this section we present a detailed computation of the DC resistivity jump in the scenario (1) of MIT, i.e. the scenario when the insulator has a density wave. We start with Eq. A.29. The resistivity jump at the MIT is given by the universal resistivity of the bosonic sector of the system ρ_b at the MIT. First of all, one can prove a generalized Ioffe-Larkin rule, which combines the resistivity of each parton φ_j into ρ_b:

$$\rho_b = \frac{\hbar}{e^2} \left(\sum_{j=0}^{N-1} \rho_{b,j} \right), \tag{A.31}$$

where $\rho_{b,j}$ is the resistivity of each parton φ_j, when the charge of φ_j is taken to be 1. This generalized Ioffe-Larkin rule can be proven by formally integrating out φ_j, gauge fields $\tilde{a}_j$ and a from Eq. A.29, and eventually arriving at a response function of A_{ext}. At each level of the path integral, we keep a quadratic form of the action, i.e. the random phase approximation. This Ioffe-Larkin rule is independent of the assignment of electric charges on each parton.

To compute ρ_b, we formulate the quantum Boltzmann equation (QBE) for the φ_j fields of a given valley. The computation follows that for ρ_b at the MIT without charge fractionalization [311], where the gauge field dynamics needs to be modified due to the charge fractionalization, which we explain in detail below for comparison. Note that ρ_b can be finite without momentum relaxation due to the emergent particle-hole symmetry.

Furthermore, the two-in two-out scatterings among the φ_j fields are enough to relax the current and generate finite DC resistivity. For simplicity, we consider the scattering between the φ_j and emergent gauge fields in Eq. (A.29), where the gauge fields are in thermal equilibrium and their dynamics is acquired due to the coupling with the matter fields φ_j and f. Here, we argue that treating the gauge fields as in thermal equilibrium is a legitimate approximation. First, the gauge field a couples to the spinon field f, which is sensitive to impurities and relaxes momentum fast. Second, diagrammatically, the two-in two-out scatterings between the φ_j fields that give finite DC resistivity can be captured by the φ_j scattering with the emergent gauge fields.

To simplify the computation of the gauge field dynamics, it is convenient to express Eq. A.29 in terms of the gauge field $\tilde{A}_j$ (Eq. A.27), together with the effective action for the spinon field, the dual theory reads

$$\mathcal{L}^{(1)} = \sum_{j=0}^{N-1} |(\partial - \mathrm{i}\tilde{A}_j)\varphi_j|^2 + \tilde{r}|\varphi_j|^2 + \tag{A.32}$$

$$\bar{f}\left(\partial_\tau - \mu - \mathrm{i}\sum_{j=0}^{N-1}\tilde{A}_{j,0} + \mathrm{i}eA_{\mathrm{ext},0} + \frac{1}{2m}(\nabla - \mathrm{i}\sum_{j=0}^{N-1}\tilde{\boldsymbol{A}}_j + \mathrm{i}e\boldsymbol{A}_{\mathrm{ext}})^2\right) f + \cdots . \tag{A.33}$$

Integrating out φ_j and f fields, the gauge field propagators read

$$D_{ij}^{(\tilde{A})} = -\mathrm{i}\langle \mathrm{T}_t \tilde{A}_i \tilde{A}_j\rangle = \begin{cases} \frac{\Pi_b^J + (N-1)\Pi_f^J}{(\Pi_b^J)^2 + N\Pi_b^J\Pi_f^J} & \text{if } i = j \\ \frac{-\Pi_f^J}{(\Pi_b^J)^2 + N\Pi_b^J\Pi_f} & \text{if } i \neq j \end{cases}, \tag{A.34}$$

where Π_b^J, Π_f^J is the current-current correlation function for φ_j and f fields, respectively.

For a controlled systematic calculation of transport, we introduce a large number of (complex) rotor and spinon flavors $\mathbf{N}$ with the constraint $\sum_{l=1}^{\mathbf{N}} |\varphi_j^l|^2 = 1$ for all $j = 0, 1, ..., N-1$, and only the $l = 1$ component couples to A_{ext}. The $\mathbf{N} = 1$ limit will be

taken at the end. The effective action for the extended model becomes

$$\mathcal{L} = \sum_{j=0}^{N-1} \left(\sum_{l=1}^{\mathbf{N}} |(\partial - \mathrm{i}\tilde{A}_j)\varphi_j^l|^2 + \mathrm{i}\lambda_j (\sum_{l=1}^{\mathbf{N}} |\varphi_j^l|^2 - 1) + \frac{1}{2g^2}(\epsilon_{\mu\nu\lambda}\partial_\nu \tilde{A}_{j,\lambda})^2 \right) + \sum_{l=1}^{\mathbf{N}} \bar{f}_l \left(\partial_\tau - \mu - \mathrm{i}\sum_{j=0}^{N-1} \tilde{A}_{j,0} + \mathrm{i}eA_{\mathrm{ext},0}\delta_{l,1} + \frac{1}{2m}(\nabla - \mathrm{i}\sum_{j=0}^{N-1} \tilde{\boldsymbol{A}}_j + \mathrm{i}e\boldsymbol{A}_{\mathrm{ext}}\delta_{l,1})^2 \right) f_l + \cdots . \tag{A.35}$$

Using the Fourier expansion for the electrically charged rotor $\varphi_j^{l=1}$ in terms of the holons (+) and doublons (-),

$$\varphi_j^{l=1} = \int_{\boldsymbol{k}} \alpha_{+,j}(t,\boldsymbol{k}) e^{\mathrm{i}\boldsymbol{k}\cdot\boldsymbol{x}} + \alpha_{-,j}(t,\boldsymbol{k}) e^{-\mathrm{i}\boldsymbol{k}\cdot\boldsymbol{x}}, \tag{A.36}$$

the conductivity $\sigma_{b,j} = \rho_{b,j}^{-1}$ can be obtained as

$$\sigma_{b,j} = \langle J_{x,j}\rangle / E_x, \quad \langle J_{x,j}\rangle = \int_{\boldsymbol{k}} \sum_{s=\pm} s\frac{\boldsymbol{k}}{\epsilon_{\boldsymbol{k}}} f_{s,j}(t,\boldsymbol{k}), \tag{A.37}$$

where we define the distribution for holon ($s = +$) and doublon ($s = -$) as $f_{s,j} = \langle \alpha_{s,j}^\dagger(t,\boldsymbol{k})\alpha_{s,j}(t,\boldsymbol{k})\rangle$, and they satisfy the QBE as

$$(\partial_t + s\boldsymbol{E}\cdot\partial_{\boldsymbol{k}}) f_{s,j}(t,\boldsymbol{k}) = \frac{1}{2\mathbf{N}}(I_{\lambda_j}[f_{\pm,j}] + I_{\tilde{A}_j}[f_{\pm,j}]). \tag{A.38}$$

Note that the gauge choice in Eq. A.33 ensures that $f_{s,j}$ are decoupled and equal for different j within the approximation that $\tilde{A}_j$ is in thermal equilibrium, so the subindex j will be dropped unless there is ambiguity. The RHS of Eq. A.38 reads

$$\begin{aligned}\text{RHS} = \frac{1}{2\mathbf{N}}\int_0^\infty \frac{\mathrm{d}\Omega}{\pi}\int \frac{\mathrm{d}^2\boldsymbol{q}}{(2\pi)^2}\{\tau_\lambda \Im D^{(\lambda)}(\Omega,\boldsymbol{q}) + \tau_{\tilde{A}}\Im D_{ii}^{(\tilde{A})}(\Omega,\boldsymbol{q})\}\\ \times\{\frac{2\pi\delta(\epsilon_{\boldsymbol{k}}-\epsilon_{\boldsymbol{k}+\boldsymbol{q}}+\Omega)}{4\epsilon_{\boldsymbol{k}}\epsilon_{\boldsymbol{k}+\boldsymbol{q}}}[f_s(t,\boldsymbol{k})(1+f_s(t,\boldsymbol{k}+\boldsymbol{q}))n_{\boldsymbol{q}}(\Omega)-(1+f_s(t,\boldsymbol{k}))f_s(t,\boldsymbol{k}+\boldsymbol{q})(1+n_{\boldsymbol{q}}(\Omega))]\\ +\frac{2\pi\delta(\epsilon_{\boldsymbol{k}}-\epsilon_{\boldsymbol{k}+\boldsymbol{q}}-\Omega)}{4\epsilon_{\boldsymbol{k}}\epsilon_{\boldsymbol{k}+\boldsymbol{q}}}[f_s(t,\boldsymbol{k})(1+f_s(t,\boldsymbol{k}+\boldsymbol{q}))(1+n_{\boldsymbol{q}}(\Omega))-(1+f_s(t,\boldsymbol{k}))f_s(t,\boldsymbol{k}+\boldsymbol{q})n_{\boldsymbol{q}}(\Omega)]\\ +\frac{2\pi\delta(-\epsilon_{\boldsymbol{k}}-\epsilon_{\boldsymbol{k}+\boldsymbol{q}}+\Omega)}{4\epsilon_{\boldsymbol{k}}\epsilon_{\boldsymbol{k}+\boldsymbol{q}}}[f_s(t,\boldsymbol{k})f_s(t,\boldsymbol{k}+\boldsymbol{q})(1+n_{\boldsymbol{q}}(\Omega))-(1+f_s(t,\boldsymbol{k}))(1+f_s(t,\boldsymbol{k}+\boldsymbol{q}))n_{\boldsymbol{q}}(\Omega)]\},\end{aligned} \tag{A.39}$$

where $\tau_\lambda = -1$ and $\tau_{\tilde{A}} = (2\boldsymbol{k}\times\hat{\boldsymbol{q}})^2$ come from the bare vertex functions.

N	1	2	3	4	5	6	...	∞
$\sigma_{b,j}(e^2/\hbar)$	0.021	0.029	0.034	0.036	0.038	0.039		0.047
$\rho_b(h/e^2)$	3.72	5.41	7.09	8.76	10.44	12.11		$(3.62+1.68(N-1))$

Table A.1: Rotor conductivity ($\sigma_{b,j}$) and resistivity jump ρ_b at the MIT with fractionally charged bosonic parton $e_* = e/N$.

$\Im D^{(\lambda)}, \Im D^{(\tilde{A})}$ physically denote the density of states of the emergent fields that scatter with φ, which are broad in the $(\Omega,\boldsymbol{q})$ space due to the couplings with the φ fields. Below, we ignore the bare dynamics. $D^{(\lambda),(\tilde{A})}$ in the large-$\mathbf{N}$ limit reads

$$\begin{aligned}D^{(\lambda)}(\Omega,\boldsymbol{q}) &= \frac{1}{\Pi_b},\\ D_{ii}^{(\tilde{A})}(\Omega,\boldsymbol{q}) &= \frac{\Pi_b^J+(N-1)\Pi_f^J}{(\Pi_b^J)^2+N\Pi_b^J\Pi_f^J} = \frac{N-1}{N}\frac{1}{\Pi_b^J}+\frac{1}{N}\frac{1}{\Pi_b^J+N\Pi_f^J},\end{aligned} \tag{A.40}$$

where $D_{ii}^{(\tilde{A})}$ reduces to the MIT without charge fractionalization as discussed in Ref. [311] when $N=1$. For $N>1$, as only the linear combination of $\tilde{A}_j$, i.e. $\sum_{j=0}^{N-1}\tilde{A}_j$ couples to the spinon field f and is Landau damped, there is a factor $\frac{1}{N}$ for the Landau damped component of the gauge field propagator $D_{ii}^{(\tilde{A})}$, which may also be understood as the a

component of gauge field in Eq. (A.29). The rest part is not Landau damped, and is determined solely by Π_b^J. Note that as $\Im\Pi_f^J \gg \Im\Pi_b^J$ in the limit $\mu \gg T$, the Landau damped component can be approximated as $\frac{1}{N}\frac{1}{\Pi_b^J + N\Pi_f^J} \approx \frac{1}{N}\frac{1}{\Pi_b^J(\Omega=0,\boldsymbol{q}) + N\Pi_f^J(\Omega,\boldsymbol{q})}$, and be treated in the same way as Ref. [311] for the gauge field a. On the other hand, the first term in $D_{ii}^{(\tilde{A})}$ should be determined for generic $\Omega, \boldsymbol{q}$. Using the standard expression for polarizations Π,

$$\begin{aligned}
\Pi_b(\Omega,\boldsymbol{q}) &= \frac{T}{2}\sum_m \int_{\boldsymbol{k}} \tau_\lambda \frac{1}{(\nu_m+\Omega_n)^2+\epsilon_{\boldsymbol{k}+\boldsymbol{q}}^2}\frac{1}{\nu_m^2+\epsilon_{\boldsymbol{k}}^2}\Big|_{\mathrm{i}\Omega_n\to\Omega+\mathrm{i}\delta} \\
\Pi_b^J(\Omega,\boldsymbol{q}) &= \frac{T}{2}\sum_m \int_{\boldsymbol{k}} \tau_{\tilde{A}} \frac{1}{(\nu_m+\Omega_n)^2+\epsilon_{\boldsymbol{k}+\boldsymbol{q}}^2}\frac{1}{\nu_m^2+\epsilon_{\boldsymbol{k}}^2}\Big|_{\mathrm{i}\Omega_n\to\Omega+\mathrm{i}\delta} \\
\Pi_f^J(\Omega,\boldsymbol{q}) &= -\frac{T}{2}\sum_m \int_{\boldsymbol{k}} \frac{(2\boldsymbol{k}\times\hat{\boldsymbol{q}})^2}{(2m)^2}\frac{1}{\mathrm{i}(\omega_m+\Omega_n)-\xi_{\boldsymbol{k}+\boldsymbol{q}}}\frac{1}{\mathrm{i}\omega_m-\xi_{\boldsymbol{k}}}\Big|_{\mathrm{i}\Omega_n\to\Omega+\mathrm{i}\delta},
\end{aligned} \tag{A.41}$$

Eq. (A.38) can be solved self-consistently. In Tab. A.1, we show $\sigma_{b,j}$ and the final resistivity $\rho_b = (N\sigma_{b,j}^{-1})/2$ at different N, again the factor of $1/2$ arises from the two spin/valley flavors. ρ_b increases roughly linearly with N, and the fit of the data points at different N gives

$$\rho_b = \left(R^{(0)} + R^{(1)}(N-1)\right)\frac{h}{e^2} = (3.62 + 1.68(N-1))\,\frac{h}{e^2}. \tag{A.42}$$

Bibliography

[1] Yichen Xu, Xiao-Chuan Wu, Mengxing Ye, Zhu-Xi Luo, Chao-Ming Jian, and Cenke Xu. Interaction-driven metal-insulator transition with charge fractionalization. *Physical Review X*, 12(2):021067, 2022.

[2] Yichen Xu, Xiao-Chuan Wu, and Cenke Xu. Deconfined quantum critical point with nonlocality. *Phys. Rev. B*, 106:155131, Oct 2022.

[3] Xiao-Chuan Wu, Yichen Xu, Mengxing Ye, Zhu-Xi Luo, and Cenke Xu. A construction of exotic metallic states. In *A Festschrift in Honor of the CN Yang Centenary: Scientific Papers*, pages 517–533. World Scientific, 2022.

[4] Yichen Xu and Cenke Xu. Green's function zero and symmetric mass generation. *arXiv preprint arXiv:2103.15865*, 2021.

[5] Chao-Ming Jian, Xiao-Chuan Wu, Yichen Xu, and Cenke Xu. Physics of symmetry protected topological phases involving higher symmetries and its applications. *Physical Review B*, 103(6):064426, 2021.

[6] Chao-Ming Jian, Yichen Xu, Xiao-Chuan Wu, and Cenke Xu. Continuous néel-vbs quantum phase transition in non-local one-dimensional systems with $so(3)$ symmetry. *SciPost Physics*, 10(2):033, 2021.

[7] Yichen Xu, Hao Geng, Xiao-Chuan Wu, Chao-Ming Jian, and Cenke Xu. Non-landau quantum phase transitions and nearly-marginal non-fermi liquid. *Journal of Statistical Mechanics: Theory and Experiment*, 2020(7):073102, 2020.

[8] Yichen Xu, Xiao-Chuan Wu, Chao-Ming Jian, and Cenke Xu. Orbital order and possible non-fermi liquid in moiré systems. *Physical Review B*, 101(20):205426, 2020.

[9] Yichen Xu, Xiao-Chuan Wu, Chao-Ming Jian, and Cenke Xu. Topological edge and interface states at bulk disorder-to-order quantum critical points. *Physical Review B*, 101(18):184419, 2020.

[10] Xiao-Chuan Wu, Yichen Xu, Hao Geng, Chao-Ming Jian, and Cenke Xu. Boundary criticality of topological quantum phase transitions in two-dimensional systems. *Physical Review B*, 101(17):174406, 2020.

[11] Xiao-Chuan Wu, Yichen Xu, Chao-Ming Jian, and Cenke Xu. Interacting valley chern insulator and its topological imprint on moiré superconductors. *Physical Review B*, 100(15):155138, 2019.

[12] Subir Sachdev. Quantum phase transitions. *Physics world*, 12(4):33, 1999.

[13] Subir Sachdev. *Quantum Phase Transitions*. Cambridge University Press, 2011.

[14] Eduardo Fradkin. *Field theories of condensed matter physics*. Cambridge University Press, 2013.

[15] T. Senthil, Ashvin Vishwanath, Leon Balents, Subir Sachdev, and M. P. A. Fisher. *Science*, 303:1490, 2004.

[16] T. Senthil, Leon Balents, Subir Sachdev, Ashvin Vishwanath, and Matthew P. A. Fisher. Quantum criticality beyond the landau-ginzburg-wilson paradigm. *Phys. Rev. B*, 70:144407, Oct 2004.

[17] Anders W. Sandvik. Evidence for deconfined quantum criticality in a two-dimensional heisenberg model with four-spin interactions. *Phys. Rev. Lett.*, 98:227202, Jun 2007.

[18] Roger G. Melko and Ribhu K. Kaul. Scaling in the fan of an unconventional quantum critical point. *Phys. Rev. Lett.*, 100:017203, Jan 2008.

[19] Anders W. Sandvik. Continuous quantum phase transition between an antiferromagnet and a valence-bond solid in two dimensions: Evidence for logarithmic corrections to scaling. *Phys. Rev. Lett.*, 104:177201, Apr 2010.

[20] Hui Shao, Wenan Guo, and Anders W. Sandvik. Quantum criticality with two length scales. *Science*, 352(6282):213–216, apr 2016.

[21] Todadri Senthil, Leon Balents, Subir Sachdev, Ashvin Vishwanath, and Matthew PA Fisher. Deconfined criticality critically defined. *Journal of the Physical Society of Japan*, 74(Suppl):1–9, 2005.

[22] T. Senthil, Dam Thanh Son, Chong Wang, and Cenke Xu. Duality between (2+1)d quantum critical points. *Physics Reports*, 827:1 – 48, 2019. Duality between (2+1)d quantum critical points.

[23] Chong Wang, Adam Nahum, Max A Metlitski, Cenke Xu, and T Senthil. Deconfined quantum critical points: symmetries and dualities. *Physical Review X*, 7(3):031051, 2017.

[24] John Cardy. *Scaling and Renormalization in Statistical Physics*. Cambridge Lecture Notes in Physics, 1996.

[25] John L. Cardy. Conformal invariance and surface critical behavior. *Nuclear Physics B*, 240(4):514 – 532, 1984.

[26] H. W. Diehl and S. Dietrich. Field-theoretical approach to static critical phenomena in semi-infinite systems. *Zeitschrift für Physik B Condensed Matter*, 42(1):65–86, Mar 1981.

[27] S. Dietrich and H. W. Diehl. The effects of surfaces on dynamic critical behavior. *Zeitschrift für Physik B Condensed Matter*, 51(4):343–354, Dec 1983.

[28] Max A. Metlitski. Boundary criticality of the O(N) model in d = 3 critically revisited. *SciPost Phys.*, 12:131, 2022.

[29] Francesco Parisen Toldin. Boundary critical behavior of the three-dimensional heisenberg universality class. *Phys. Rev. Lett.*, 126:135701, Mar 2021.

[30] Francesco Parisen Toldin and Max A. Metlitski. Boundary criticality of the 3d o(n) model: From normal to extraordinary. *Phys. Rev. Lett.*, 128:215701, May 2022.

[31] H. W. Diehl. The theory of boundary critical phenomena. *International Journal of Modern Physics B*, 11(30):3503–3523, 1997.

[32] John A. Hertz. Quantum critical phenomena. *Phys. Rev. B*, 14:1165–1184, Aug 1976.

[33] A. J. Millis. Effect of a nonzero temperature on quantum critical points in itinerant fermion systems. *Phys. Rev. B*, 48:7183–7196, Sep 1993.

[34] Max A. Metlitski and Subir Sachdev. Quantum phase transitions of metals in two spatial dimensions. i. ising-nematic order. *Phys. Rev. B*, 82:075127, Aug 2010.

[35] Max A. Metlitski and Subir Sachdev. Quantum phase transitions of metals in two spatial dimensions. ii. spin density wave order. *Phys. Rev. B*, 82:075128, Aug 2010.

[36] Chetan Nayak and Frank Wilczek. Non-fermi liquid fixed point in 2 + 1 dimensions. *Nuclear Physics B*, 417(3):359 – 373, 1994.

[37] David F. Mross, John McGreevy, Hong Liu, and T. Senthil. Controlled expansion for certain non-fermi-liquid metals. *Phys. Rev. B*, 82:045121, Jul 2010.

[38] T. Senthil. Theory of a continuous mott transition in two dimensions. *Phys. Rev. B*, 78:045109, Jul 2008.

[39] Tingxin Li, Shengwei Jiang, Lizhong Li, Yang Zhang, Kaifei Kang, Jiacheng Zhu, Kenji Watanabe, Takashi Taniguchi, Debanjan Chowdhury, Liang Fu, Jie Shan, and Kin Fai Mak. Continuous mott transition in semiconductor moiré superlattices. *2103.09779*, 2021.

[40] Augusto Ghiotto, En-Min Shih, Giancarlo S. S. G. Pereira, Daniel A. Rhodes, Bumho Kim, Jiawei Zang, Andrew J. Millis, Kenji Watanabe, Takashi Taniguchi, James C. Hone, Lei Wang, Cory R. Dean, and Abhay N. Pasupathy. Quantum criticality in twisted transition metal dichalcogenides. *2103.09796*, 2021.

[41] XIAO-GANG WEN. Theory of the edge states in fractional quantum hall effects. *International Journal of Modern Physics B*, 06(10):1711–1762, 1992.

[42] Xiao-Gang Wen. Choreographed entanglement dances: Topological states of quantum matter. *Science*, 363(6429), 2019.

[43] Xie Chen, Zheng-Cheng Gu, Zheng-Xin Liu, and Xiao-Gang Wen. *Phys. Rev. B*, 87:155114, 2013.

[44] Xie Chen, Zheng-Cheng Gu, Zheng-Xin Liu, and Xiao-Gang Wen. *Science*, 338:1604, 2012.

[45] Sergei V. Isakov, Matthew B. Hastings, and Roger G. Melko. *Nature Physics*, 7:772, 2011.

[46] Sergei V. Isakov, Matthew B. Hastings, and Roger G. Melko. *Science*, 335:193, 2012.

[47] Andrey V. Chubukov, Subir Sachdev, and T. Senthil. Quantum phase transitions in frustrated quantum antiferromagnets. *Nuclear Physics B*, 426(3):601 – 643, 1994.

[48] Cenke Xu. Unconventional quantum critical points. *International Journal of Modern Physics B*, 26(18):1230007, 2012.

[49] Anders W. Sandvik. Evidence for deconfined quantum criticality in a two-dimensional heisenberg model with four-spin interactions. *Phys. Rev. Lett.*, 98:227202, Jun 2007.

[50] Hui Shao, Wenan Guo, and Anders W. Sandvik. Quantum criticality with two length scales. *Science*, 352(6282):213–216, 2016.

[51] Roger G. Melko and Ribhu K. Kaul. Scaling in the fan of an unconventional quantum critical point. *Phys. Rev. Lett.*, 100:017203, Jan 2008.

[52] Yan Qi Qin, Yuan-Yao He, Yi-Zhuang You, Zhong-Yi Lu, Arnab Sen, Anders W. Sandvik, Cenke Xu, and Zi Yang Meng. Duality between the deconfined quantum-critical point and the bosonic topological transition. *Phys. Rev. X*, 7:031052, Sep 2017.

[53] Andre K Geim and Irina V Grigorieva. Van der waals heterostructures. *Nature*, 499(7459):419–425, 2013.

[54] John L. Cardy and Eliezer Rabinovici. *Nucl. Phys. B*, 205:1, 1982.

[55] J Reeve and A J Guttmann. Renormalisation group calculations of the critical exponents of the n-vector model with a free surface. *Journal of Physics A: Mathematical and General*, 14(12):3357–3366, dec 1981.

[56] N. Read and Subir Sachdev. Large-n expansion for frustrated quantum antiferromagnets. *Phys. Rev. Lett.*, 66:1773–1776, Apr 1991.

[57] Subir Sachdev and Nick Read. Large n expansion for frustrated and doped quantum antiferromagnets. *International Journal of Modern Physics B*, 5(01n02):219–249, 1991.

[58] Congjun Wu, Jiang-ping Hu, and Shou-cheng Zhang. Exact so(5) symmetry in the spin-3/2 fermionic system. *Phys. Rev. Lett.*, 91:186402, Oct 2003.

[59] Pasquale Calabrese, Andrea Pelissetto, and Ettore Vicari. *arXiv:cond-mat/0306273*, 2003.

[60] Eduardo Fradkin and Leonard Susskind. Order and disorder in gauge systems and magnets. *Phys. Rev. D*, 17:2637–2658, May 1978.

[61] Long Zhang and Fa Wang. Unconventional surface critical behavior induced by a quantum phase transition from the two-dimensional affleck-kennedy-lieb-tasaki phase to a néel-ordered phase. *Phys. Rev. Lett.*, 118:087201, Feb 2017.

[62] Thomas Scaffidi, Daniel E. Parker, and Romain Vasseur. Gapless symmetry-protected topological order. *Phys. Rev. X*, 7:041048, Nov 2017.

[63] C. L. Kane and E. J. Mele. Quantum spin hall effect in graphene. *Physical Review Letter*, 95:226801, 2005.

[64] C. L. Kane and E. J. Mele. Z_2 topological order and the quantum spin hall effect. *Physical Review Letter*, 95:146802, 2005.

[65] Liang Fu, C. L. Kane, and E. J. Mele. *Phys. Rev. Lett.*, 98:106803, 2008.

[66] J. E. Moore and L. Balents. Topological invariants of time-reversal-invariant band structures. *Phys. Rev. B*, 75:121306(R), 2007.

[67] Andreas P. Schnyder, Shinsei Ryu, Akira Furusaki, and Andreas W. W. Ludwig. *AIP Conf. Proc.*, 1134:10, 2009.

[68] Shinsei Ryu, Andreas Schnyder, Akira Furusaki, and Andreas Ludwig. *New J. Phys.*, 12:065010, 2010.

[69] A. Kitaev. *AIP Conf. Proc*, 1134:22, 2009.

[70] Lukasz Fidkowski, Xie Chen, and Ashvin Vishwanath. *Phys. Rev. X*, 3:041016, 2013.

[71] Xie Chen, Lukasz Fidkowski, and Ashvin Vishwanath. *Phys. Rev. B*, 89:165132, 2014.

[72] Parsa Bonderson, Chetan Nayak, and Xiao-Liang Qi. *J. Stat. Mech.*, page P09016, 2013.

[73] Chong Wang, Andrew C. Potter, and T. Senthil. *Phys. Rev. B*, 88:115137, 2013.

[74] Max A. Metlitski, C. L. Kane, and Matthew P. A. Fisher. *arXiv:1306.3286*, 2013.

[75] Chong Wang and T. Senthil. *Phys. Rev. B*, 87:235122, 2013.

[76] Meng Cheng, Michael Zaletel, Maissam Barkeshli, Ashvin Vishwanath, and Parsa Bonderson. Translational symmetry and microscopic constraints on symmetry-enriched topological phases: A view from the surface. *Phys. Rev. X*, 6:041068, Dec 2016.

[77] Ashvin Vishwanath and T. Senthil. Physics of three-dimensional bosonic topological insulators: Surface-deconfined criticality and quantized magnetoelectric effect. *Phys. Rev. X*, 3:011016, Feb 2013.

[78] Cenke Xu and Yi-Zhuang You. Self-dual quantum electrodynamics as boundary state of the three-dimensional bosonic topological insulator. *Phys. Rev. B*, 92:220416, Dec 2015.

[79] David F. Mross, Jason Alicea, and Olexei I. Motrunich. Explicit derivation of duality between a free dirac cone and quantum electrodynamics in (2+1) dimensions. *Phys. Rev. Lett.*, 117:016802, Jun 2016.

[80] Po-Shen Hsin and Nathan Seiberg. Level/rank duality and chern-simons-matter theories. *Journal of High Energy Physics*, 2016(9):95, 2016.

[81] Chong Wang, Adam Nahum, Max A. Metlitski, Cenke Xu, and T. Senthil. Deconfined quantum critical points: Symmetries and dualities. *Phys. Rev. X*, 7:031051, Sep 2017.

[82] Nathan Seiberg, T. Senthil, Chong Wang, and Edward Witten. A duality web in 2+1 dimensions and condensed matter physics. *Annals of Physics*, 374:395 – 433, 2016.

[83] Thomas Scaffidi, Daniel E. Parker, and Romain Vasseur. Gapless symmetry-protected topological order. *Phys. Rev. X*, 7:041048, Nov 2017.

[84] Ruben Verresen, Nick G. Jones, and Frank Pollmann. Topology and edge modes in quantum critical chains. *Phys. Rev. Lett.*, 120:057001, Jan 2018.

[85] Ruben Verresen, Ryan Thorngren, Nick G. Jones, and Frank Pollmann. Gapless topological phases and symmetry-enriched quantum criticality. *arXiv e-prints*, page arXiv:1905.06969, May 2019.

[86] Guo-Yi Zhu, Tao Xiang, and Guang-Ming Zhang. *arXiv:1806.07535*, 2018.

[87] Lukas Weber, Francesco Parisen Toldin, and Stefan Wessel. Nonordinary edge criticality of two-dimensional quantum critical magnets. *Phys. Rev. B*, 98:140403, Oct 2018.

[88] Lukas Weber and Stefan Wessel. Nonordinary criticality at the edges of planar spin-1 heisenberg antiferromagnets. *Phys. Rev. B*, 100:054437, Aug 2019.

[89] Tarun Grover and Ashvin Vishwanath. Quantum Criticality in Topological Insulators and Superconductors: Emergence of Strongly Coupled Majoranas and Supersymmetry. *arXiv e-prints*, page arXiv:1206.1332, June 2012.

[90] Zhen Bi, Alex Rasmussen, Kevin Slagle, and Cenke Xu. Classification and description of bosonic symmetry protected topological phases with semiclassical nonlinear sigma models. *Phys. Rev. B*, 91:134404, Apr 2015.

[91] Olexei I. Motrunich and Ashvin Vishwanath. *Phys. Rev. B*, 70:075104, 2004.

[92] Andrew C. Potter, Chong Wang, Max A. Metlitski, and Ashvin Vishwanath. Realizing topological surface states in a lower-dimensional flat band. *Phys. Rev. B*, 96:235114, Dec 2017.

[93] Ribhu K. Kaul and Subir Sachdev. Quantum criticality of u(1) gauge theories with fermionic and bosonic matter in two spatial dimensions. *Phys. Rev. B*, 77:155105, Apr 2008.

[94] Sergio Benvenuti and Hrachya Khachatryan. Easy-plane qed3's in the large nf limit. *Journal of High Energy Physics*, 2019(5):214, May 2019.

[95] Xiao-Gang Wen and Yong-Shi Wu. Transitions between the quantum hall states and insulators induced by periodic potentials. *Phys. Rev. Lett.*, 70:1501–1504, Mar 1993.

[96] Daniel S. Rokhsar. Quadratic quantum antiferromagnets in the fermionic large-n limit. *Phys. Rev. B*, 42:2526–2531, Aug 1990.

[97] N. Read and Subir Sachdev. Some features of the phase diagram of the square lattice su(n) antiferromagnet. *Nuclear Physics B*, 316(3):609 – 640, 1989.

[98] Ian Affleck and J. Brad Marston. Large-n limit of the heisenberg-hubbard model: Implications for high-T_c superconductors. *Phys. Rev. B*, 37:3774–3777, Mar 1988.

[99] Michael Hermele, T. Senthil, and Matthew P. A. Fisher. *Phys. Rev. B*, 72:104404, 2005.

[100] Walter Rantner and Xiao-Gang Wen. Electron spectral function and algebraic spin liquid for the normal state of underdoped high T_c superconductors. *Phys. Rev. Lett.*, 86:3871–3874, Apr 2001.

[101] Cenke Xu and Subir Sachdev. Square-lattice algebraic spin liquid with so(5) symmetry. *Phys. Rev. Lett.*, 100:137201, Apr 2008.

[102] Cenke Xu. *Phys. Rev. B*, 87:144421, 2013.

[103] H. Nonne, M. Moliner, S. Capponi, P. Lecheminant, and K. Totsuka. Symmetry-protected topological phases of alkaline-earth cold fermionic atoms in one dimension. *EPL (Europhysics Letters)*, 102(3):37008, 2013.

[104] V. Bois, S. Capponi, P. Lecheminant, M. Moliner, and K. Totsuka. Phase diagrams of one-dimensional half-filled two-orbital SU(n) cold fermion systems. *Phys. Rev. B*, 91:075121, Feb 2015.

[105] S. Capponi, P. Lecheminant, and K. Totsuka. Phases of one-dimensional su() cold atomic fermi gasesâfrom molecular luttinger liquids to topological phases. *Annals of Physics*, 367:50 – 95, 2016.

[106] Kasper Duivenvoorden and Thomas Quella. Topological phases of spin chains. *Phys. Rev. B*, 87:125145, Mar 2013.

[107] Ying Ran, Yi Zhang, and Ashvin Vishwanath. *Nature Physics*, 5:298, 2009.

[108] Jeffrey C. Y. Teo and C. L. Kane. Topological defects and gapless modes in insulators and superconductors. *Phys. Rev. B*, 82:115120, Sep 2010.

[109] Wladimir A. Benalcazar, B. Andrei Bernevig, and Taylor L. Hughes. Quantized electric multipole insulators. *Science*, 357(6346):61–66, 2017.

[110] Z. Bethe. *Z. Phy.*, 71:205, 1931.

[111] A.A. Belavin, A.M. Polyakov, and A.B. Zamolodchikov. Infinite conformal symmetry in two-dimensional quantum field theory. *Nuclear Physics B*, 241(2):333 – 380, 1984.

[112] Long Zhang and Fa Wang. Unconventional surface critical behavior induced by a quantum phase transition from the two-dimensional affleck-kennedy-lieb-tasaki phase to a néel-ordered phase. *Phys. Rev. Lett.*, 118:087201, Feb 2017.

[113] Chengxiang Ding, Long Zhang, and Wenan Guo. Engineering surface critical behavior of (2+1)-dimensional o(3) quantum critical points. *Phys. Rev. Lett.*, 120:235701, Jun 2018.

[114] Anders W. Sandvik. Ground states of a frustrated quantum spin chain with long-range interactions. *Phys. Rev. Lett.*, 104:137204, Mar 2010.

[115] Sibin Yang, Dao-Xin Yao, and Anders W. Sandvik. Deconfined quantum criticality in spin-1/2 chains with long-range interactions. *arXiv e-prints*, page arXiv:2001.02821, January 2020.

[116] Ian Affleck, Tom Kennedy, Elliott H. Lieb, and Hal Tasaki. Rigorous results on valence-bond ground states in antiferromagnets. *Phys. Rev. Lett.*, 59:799–802, Aug 1987.

[117] E. H. Lieb, T. D. Schultz, and D. C. Mattis. *Ann. Phys.*, 16:407, 1961.

[118] Masaki Oshikawa. Commensurability, excitation gap, and topology in quantum many-particle systems on a periodic lattice. *Phys. Rev. Lett.*, 84:1535–1538, Feb 2000.

[119] M. B. Hastings. Lieb-schultz-mattis in higher dimensions. *Phys. Rev. B*, 69:104431, Mar 2004.

[120] Oleg A. Starykh and Leon Balents. Dimerized phase and transitions in a spatially anisotropic square lattice antiferromagnet. *Phys. Rev. Lett.*, 93:127202, Sep 2004.

[121] Zheng-Xin Liu and Xiao-Gang Wen. *Phys. Rev. Lett.*, 110:067205, 2013.

[122] Yichen Xu, Xiao-Chuan Wu, Chao-Ming Jian, and Cenke Xu. Topological Edge and Interface states at Bulk disorder-to-order Quantum Critical Points. *arXiv e-prints*, page arXiv:2002.10479, February 2020.

[123] Chao-Ming Jian, Alex Thomson, Alex Rasmussen, Zhen Bi, and Cenke Xu. Deconfined quantum critical point on the triangular lattice. *Phys. Rev. B*, 97:195115, May 2018.

[124] Nicolas Laflorencie, Ian Affleck, and Mona Berciu. *Journal of Statistical Mechanics: Theory and Experiment*, 2005(12):P12001–P12001, dec 2005.

[125] Sung-Sik Lee. Emergence of supersymmetry at a critical point of a lattice model. *Phys. Rev. B*, 76:075103, Aug 2007.

[126] Alexei M. Tsvelik Alexander O. Gogolin, Alexander A. Nersesyan. *Bosonization and Strongly Correlated Systems*. Cambridge University Press, 2004.

[127] Anders W. Sandvik, Leon Balents, and David K. Campbell. Ground state phases of the half-filled one-dimensional extended hubbard model. *Phys. Rev. Lett.*, 92:236401, Jun 2004.

[128] Brenden Roberts, Shenghan Jiang, and Olexei I. Motrunich. Deconfined quantum critical point in one dimension. *Phys. Rev. B*, 99:165143, Apr 2019.

[129] Shenghan Jiang and Olexei Motrunich. Ising ferromagnet to valence bond solid transition in a one-dimensional spin chain: Analogies to deconfined quantum critical points. *Phys. Rev. B*, 99:075103, Feb 2019.

[130] X. G. WEN. Topological orders in rigid states. *International Journal of Modern Physics B*, 04(02):239–271, 1990.

[131] Xiao-Gang Wen. Choreographed entanglement dances: Topological states of quantum matter. *Science*, 363(6429), 2019.

[132] C. M. Varma, P. B. Littlewood, S. Schmitt-Rink, E. Abrahams, and A. E. Ruckenstein. Phenomenology of the normal state of cu-o high-temperature superconductors. *Phys. Rev. Lett.*, 63:1996–1999, Oct 1989.

[133] Hilbert v. Löhneysen, Achim Rosch, Matthias Vojta, and Peter Wölfle. Fermi-liquid instabilities at magnetic quantum phase transitions. *Rev. Mod. Phys.*, 79:1015–1075, Aug 2007.

[134] Yuan Cao, Debanjan Chowdhury, Daniel Rodan-Legrain, Oriol Rubies-Bigordà, Kenji Watanabe, Takashi Taniguchi, T. Senthil, and Pablo Jarillo-Herrero. *arXiv:1901.03710*, 2019.

[135] H. Polshyn, M. Yankowitz, S. Chen, Y. Zhang, K. Watanabe, T. Taniguchi, C. R. Dean, and A. F. Young. *arXiv:1902.00763*, 2019.

[136] Chetan Nayak and Frank Wilczek. Renormalization group approach to low temperature properties of a non-fermi liquid metal. *Nuclear Physics B*, 430(3):534 – 562, 1994.

[137] S. Sachdev and J. Ye. Gapless spin-fluid ground state in a random quantum Heisenberg magnet. *Physical Review Letters*, 70:3339–3342, May 1993.

[138] A. Kitaev. A simple model of quantum holography. http://online.kitp.ucsb.edu/online/entangled15/kitaev/, 2015. Talks at KITP, April 7, 2015 and May 27, 2015.

[139] J. Maldacena and D. Stanford. Remarks on the Sachdev-Ye-Kitaev model. *Phys. Rev. D*, 94(10):106002, November 2016.

[140] E. Witten. An SYK-Like Model Without Disorder. *ArXiv e-prints*, October 2016.

[141] Igor R. Klebanov and Grigory Tarnopolsky. Uncolored random tensors, melon diagrams, and the sachdev-ye-kitaev models. *Phys. Rev. D*, 95:046004, Feb 2017.

[142] Xue-Yang Song, Chao-Ming Jian, and Leon Balents. Strongly correlated metal built from sachdev-ye-kitaev models. *Phys. Rev. Lett.*, 119:216601, Nov 2017.

[143] Aavishkar A. Patel, John McGreevy, Daniel P. Arovas, and Subir Sachdev. Magnetotransport in a model of a disordered strange metal. *Phys. Rev. X*, 8:021049, May 2018.

[144] Aavishkar A. Patel and Subir Sachdev. Critical strange metal from fluctuating gauge fields in a solvable random model. *Phys. Rev. B*, 98:125134, Sep 2018.

[145] Debanjan Chowdhury, Yochai Werman, Erez Berg, and T. Senthil. Translationally invariant non-fermi-liquid metals with critical fermi surfaces: Solvable models. *Phys. Rev. X*, 8:031024, Jul 2018.

[146] Xiaochuan Wu, Xiao Chen, Chao-Ming Jian, Yi-Zhuang You, and Cenke Xu. Candidate theory for the strange metal phase at a finite-energy window. *Phys. Rev. B*, 98:165117, Oct 2018.

[147] Xiao-Chuan Wu, Chao-Ming Jian, and Cenke Xu. Lattice models for non-fermi liquids with tunable transport scalings. *Phys. Rev. B*, 100:075101, Aug 2019.

[148] Sung-Sik Lee. Low-energy effective theory of fermi surface coupled with u(1) gauge field in $2+1$ dimensions. *Phys. Rev. B*, 80:165102, Oct 2009.

[149] Xiao-Gang Wen. *Phys. Rev. B*, 65:165113, 2002.

[150] Rhine Samajdar, Mathias S. Scheurer, Shubhayu Chatterjee, Haoyu Guo, Cenke Xu, and Subir Sachdev. *Nature Physics*, 15:1290, 2019.

[151] G. Grissonnanche, A. Legros, S. Badoux, E. Lefrançois, V. Zatko, M. Lizaire, F. Laliberté, A. Gourgout, J.-S. Zhou, S. Pyon, T. Takayama, H. Takagi, S. Ono, N. Doiron-Leyraud, , and L. Taillefer. *Nature*, 571:376, 2019.

[152] Nikhil Karthik and Rajamani Narayanan. Scale invariance of parity-invariant three-dimensional qed. *Phys. Rev. D*, 94:065026, Sep 2016.

[153] Tarun Grover and Ashvin Vishwanath. Quantum phase transition between integer quantum hall states of bosons. *Phys. Rev. B*, 87:045129, Jan 2013.

[154] Yuan-Ming Lu and Dung-Hai Lee. *arXiv:1210.0909*, 2012.

[155] Rufus Boyack, Ahmed Rayyan, and Joseph Maciejko. Deconfined criticality in the qed_3 gross-neveu-yukawa model: The $1/n$ expansion revisited. *Phys. Rev. B*, 99:195135, May 2019.

[156] Yuan-Ming Lu. Symmetric Z_2 spin liquids and their neighboring phases on triangular lattice. *Phys. Rev. B*, 93:165113, Apr 2016.

[157] Swapan K. Pati, Rajiv R. P. Singh, and Daniel I. Khomskii. Alternating spin and orbital dimerization and spin-gap formation in coupled spin-orbital systems. *Phys. Rev. Lett.*, 81:5406–5409, Dec 1998.

[158] Y. Q. Li, Michael Ma, D. N. Shi, and F. C. Zhang. Su(4) theory for spin systems with orbital degeneracy. *Phys. Rev. Lett.*, 81:3527–3530, Oct 1998.

[159] Y. Tokura and N. Nagaosa. Orbital physics in transition-metal oxides. *Science*, 288(5465):462–468, 2000.

[160] Congjun Wu, Jiang-ping Hu, and Shou-cheng Zhang. Exact so(5) symmetry in the spin-3/2 fermionic system. *Phys. Rev. Lett.*, 91:186402, Oct 2003.

[161] Congjun Wu. Competing orders in one-dimensional spin-3/2 fermionic systems. *Phys. Rev. Lett.*, 95:266404, Dec 2005.

[162] CONGJUN WU. Hidden symmetry and quantum phases in spin-3/2 cold atomic systems. *Modern Physics Letters B*, 20(27):1707–1738, 2006.

[163] A. V. Gorshkov, M. Hermele, V. Gurarie, C. Xu, P. S. Julienne, J. Ye, P. Zoller, E. Demler, M. D. Lukin, and A. M. Rey. *Nature Physics*, 6:289–295, 2009.

[164] Cenke Xu and Leon Balents. Topological superconductivity in twisted multilayer graphene. *Phys. Rev. Lett.*, 121:087001, Aug 2018.

[165] Xiao-Chuan Wu, Anna Keselman, Chao-Ming Jian, Kelly Ann Pawlak, and Cenke Xu. Ferromagnetism and spin-valley liquid states in moiré correlated insulators. *Phys. Rev. B*, 100:024421, Jul 2019.

[166] Constantin Schrade and Liang Fu. Spin-valley density wave in moiré materials. *Phys. Rev. B*, 100:035413, Jul 2019.

[167] Ya-Hui Zhang, Dan Mao, and T. Senthil. Twisted bilayer graphene aligned with hexagonal boron nitride: Anomalous hall effect and a lattice model. *Phys. Rev. Research*, 1:033126, Nov 2019.

[168] Max A. Metlitski, David F. Mross, Subir Sachdev, and T. Senthil. Cooper pairing in non-fermi liquids. *Phys. Rev. B*, 91:115111, Mar 2015.

[169] S. Lederer, Y. Schattner, E. Berg, and S. A. Kivelson. Enhancement of superconductivity near a nematic quantum critical point. *Phys. Rev. Lett.*, 114:097001, Mar 2015.

[170] Jérôme Rech, Catherine Pépin, and Andrey V. Chubukov. Quantum critical behavior in itinerant electron systems: Eliashberg theory and instability of a ferromagnetic quantum critical point. *Phys. Rev. B*, 74:195126, Nov 2006.

[171] Xiao Yan Xu, Avraham Klein, Kai Sun, Andrey V. Chubukov, and Zi Yang Meng. Extracting non-Fermi liquid fermionic self-energy at $T = 0$ from quantum Monte Carlo data. *arXiv e-prints*, page arXiv:2003.11573, March 2020.

[172] Aavishkar A. Patel and Subir Sachdev. Theory of a planckian metal. *Phys. Rev. Lett.*, 123:066601, Aug 2019.

[173] Leon Balents, Lorenz Bartosch, Anton Burkov, Subir Sachdev, and Krishnendu Sengupta. Competing Orders and Non-Landau-Ginzburg-Wilson Criticality in (Bose) Mott Transitions. *Progress of Theoretical Physics Supplement*, 160:314–336, 06 2005.

[174] A. A. Burkov and Leon Balents. Superfluid-insulator transitions on the triangular lattice. *Phys. Rev. B*, 72:134502, Oct 2005.

[175] Zohar Nussinov and Gerardo Ortiz. A symmetry principle for topological quantum order. *Annals of Physics*, 324(5):977–1057, May 2009.

[176] Ofer Aharony, Nathan Seiberg, and Yuji Tachikawa. Reading between the lines of four-dimensional gauge theories. *Journal of High Energy Physics*, 2013(8), Aug 2013.

[177] Sergei Gukov and Anton Kapustin. Topological quantum field theory, nonlocal operators, and gapped phases of gauge theories. 2013.

[178] Anton Kapustin and Ryan Thorngren. Topological field theory on a lattice, discrete theta-angles and confinement. 2013.

[179] Anton Kapustin and Ryan Thorngren. Higher symmetry and gapped phases of gauge theories. 2013.

[180] Anton Kapustin and Nathan Seiberg. Coupling a qft to a tqft and duality. *Journal of High Energy Physics*, 2014(4), Apr 2014.

[181] Davide Gaiotto, Anton Kapustin, Nathan Seiberg, and Brian Willett. Generalized global symmetries. *Journal of High Energy Physics*, 2015(2), Feb 2015.

[182] Po-Shen Hsin, Ho Tat Lam, and Nathan Seiberg. Comments on one-form global symmetries and their gauging in 3d and 4d. *SciPost Physics*, 6(3), Mar 2019.

[183] Nathan Seiberg. Field theories with a vector global symmetry. *SciPost Physics*, 8(4), Apr 2020.

[184] John McGreevy. Generalized symmetries in condensed matter, 2022.

[185] Olexei I. Motrunich and Ashvin Vishwanath. Emergent photons and transitions in the O(3) sigma model with hedgehog suppression. *Phys. Rev. B*, 70:075104, Aug 2004.

[186] Yan Qi Qin, Yuan-Yao He, Yi-Zhuang You, Zhong-Yi Lu, Arnab Sen, Anders W. Sandvik, Cenke Xu, and Zi Yang Meng. Duality between the deconfined quantum-critical point and the bosonic topological transition. *Phys. Rev. X*, 7:031052, Sep 2017.

[187] Adam Nahum, P. Serna, J. T. Chalker, M. Ortuño, and A. M. Somoza. Emergent so(5) symmetry at the néel to valence-bond-solid transition. *Phys. Rev. Lett.*, 115:267203, Dec 2015.

[188] Adam Nahum, J. T. Chalker, P. Serna, M. Ortuño, and A. M. Somoza. Deconfined quantum criticality, scaling violations, and classical loop models. *Phys. Rev. X*, 5:041048, Dec 2015.

[189] Jiarui Zhao, Yan-Cheng Wang, Zheng Yan, Meng Cheng, and Zi Yang Meng. Scaling of entanglement entropy at deconfined quantum criticality. *Phys. Rev. Lett.*, 128:010601, Jan 2022.

[190] Filip Kos, David Poland, David Simmons-Duffin, and Alessandro Vichi. *Journal of High energy Physics*, 1511:106, 2015.

[191] Yu Nakayama and Tomoki Ohtsuki. Necessary condition for emergent symmetry from the conformal bootstrap. *Phys. Rev. Lett.*, 117:131601, Sep 2016.

[192] Yichen Xu, Xiao-Chuan Wu, Chao-Ming Jian, and Cenke Xu. Topological edge and interface states at bulk disorder-to-order quantum critical points. *Phys. Rev. B*, 101:184419, May 2020.

[193] Chao-Ming Jian, Yichen Xu, Xiao-Chuan Wu, and Cenke Xu. Continuous Néel-VBS Quantum Phase Transition in Non-Local one-dimensional systems with SO(3) Symmetry. *SciPost Phys.*, 10:33, 2021.

[194] Shang Liu, Hassan Shapourian, Ashvin Vishwanath, and Max A. Metlitski. Magnetic impurities at quantum critical points: Large-n expansion and connections to symmetry-protected topological states. *Phys. Rev. B*, 104:104201, Sep 2021.

[195] Ruochen Ma, Liujun Zou, and Chong Wang. Edge physics at the deconfined transition between a quantum spin Hall insulator and a superconductor. *SciPost Phys.*, 12:196, 2022.

[196] Gabriele La Nave and Philip W. Phillips. Geodesically complete metrics and boundary non-locality in holography: Consequences for the entanglement entropy. *Phys. Rev. D*, 94:126018, Dec 2016.

[197] Bimla Danu, Matthias Vojta, Tarun Grover, and Fakher F. Assaad. Spin chain on a metallic surface: Dissipation-induced order vs. kondo entanglement, 2022.

[198] T. Senthil and Matthew P. A. Fisher. *Phys. Rev. B*, 74:064405, 2005.

[199] Xiao-Gang Wen and Yong-Shi Wu. Transitions between the quantum hall states and insulators induced by periodic potentials. *Phys. Rev. Lett.*, 70:1501–1504, Mar 1993.

[200] Ar. Abanov and A. Chubukov. Anomalous scaling at the quantum critical point in itinerant antiferromagnets. *Phys. Rev. Lett.*, 93:255702, Dec 2004.

[201] Andres Schlief, Peter Lunts, and Sung-Sik Lee. Exact critical exponents for the antiferromagnetic quantum critical metal in two dimensions. *Phys. Rev. X*, 7:021010, Apr 2017.

[202] Cenke Xu and Andreas W. W. Ludwig. Nonperturbative effects of a topological theta term on principal chiral nonlinear sigma models in $2 + 1$ dimensions. *Phys. Rev. Lett.*, 110:200405, May 2013.

[203] Zhen Bi, Alex Rasmussen, Yoni BenTov, and Cenke Xu. Stable interacting $(2 + 1)$d conformal field theories at the boundary of a class of $(3 + 1)$d symmetry protected topological phases, 2016.

[204] Ruochen Ma and Chong Wang. Theory of deconfined pseudocriticality. *Phys. Rev. B*, 102:020407, Jul 2020.

[205] Adam Nahum. Note on wess-zumino-witten models and quasiuniversality in $2 + 1$ dimensions. *Phys. Rev. B*, 102:201116, Nov 2020.

[206] Zhenjiu Wang, Michael P. Zaletel, Roger S. K. Mong, and Fakher F. Assaad. Phases of the $(2+1)$ dimensional so(5) nonlinear sigma model with topological term. *Phys. Rev. Lett.*, 126:045701, Jan 2021.

[207] Liujun Zou, Yin-Chen He, and Chong Wang. Stiefel liquids: Possible non-lagrangian quantum criticality from intertwined orders. *Phys. Rev. X*, 11:031043, Aug 2021.

[208] Yichen Xu, Xiao-Chuan Wu, Mengxing Ye, Zhu-Xi Luo, Chao-Ming Jian, and Cenke Xu. Interaction-driven metal-insulator transition with charge fractionalization. *Phys. Rev. X*, 12:021067, Jun 2022.

[209] Seth Musser, T. Senthil, and Debanjan Chowdhury. Theory of a continuous bandwidth-tuned wigner-mott transition, 2021.

[210] Rafi Bistritzer and Allan H. MacDonald. Moiré bands in twisted double-layer graphene. *Proceedings of the National Academy of Sciences*, 108(30):12233–12237, 2011.

[211] E. Suárez Morell, J. D. Correa, P. Vargas, M. Pacheco, and Z. Barticevic. Flat bands in slightly twisted bilayer graphene: Tight-binding calculations. *Phys. Rev. B*, 82:121407, Sep 2010.

[212] Shiang Fang and Efthimios Kaxiras. Electronic structure theory of weakly interacting bilayers. *Phys. Rev. B*, 93:235153, Jun 2016.

[213] G. Trambly de Laissardière, D. Mayou, and L. Magaud. Numerical studies of confined states in rotated bilayers of graphene. *Phys. Rev. B*, 86:125413, Sep 2012.

[214] Cheng Shen, Na Li, Shuopei Wang, Yanchong Zhao, Jian Tang, Jieying Liu, Jinpeng Tian, Yanbang Chu, Kenji Watanabe, Takashi Taniguchi, Rong Yang, Zi-Yang Meng, Dongxia Shi, and Guangyu Zhang. *arXiv:1903.06952*, 2019.

[215] Xiaomeng Liu, Zeyu Hao, Eslam Khalaf, Jong Yeon Lee, Kenji Watanabe, Takashi Taniguchi, Ashvin Vishwanath, and Philip Kim. *arXiv:1903.08130*, 2019.

[216] Yuan Cao, Daniel Rodan-Legrain, Oriol Rubies-Bigorda, Jeong Min Park, Kenji Watanabe, Takashi Taniguchi, and Pablo Jarillo-Herrero. *arXiv:1903.08596*, 2019.

[217] Guorui Chen, Lili Jiang, Shuang Wu, Bosai Lv, Hongyuan Li, Kenji Watanabe, Takashi Taniguchi, Zhiwen Shi, Yuanbo Zhang, and Feng Wang. *arXiv:1803.01985*, 2018.

[218] Yuan Cao, Valla Fatemi, Ahmet Demir, Shiang Fang, Spencer L. Tomarken, Jason Y. Luo, J. D. Sanchez-Yamagishi, K. Watanabe, T. Taniguchi, E. Kaxiras, R. C. Ashoori, and P. Jarillo-Herrero. *Nature*, 556:80, 2018.

[219] Yuan Cao, Valla Fatemi, Shiang Fang, Kenji Watanabe, Takashi Taniguchi, Efthimios Kaxiras, and Pablo Jarillo-Herrero. *Nature*, 556:43, 2018.

[220] Matthew Yankowitz, Shaowen Chen, Hryhoriy Polshyn, Yuxuan Zhang, K. Watanabe, T. Taniguchi, David Graf, Andrea F. Young, and Cory R. Dean. Tuning superconductivity in twisted bilayer graphene. *Science*, 363(6431):1059–1064, 2019.

[221] Guorui Chen, Aaron L. Sharpe, Patrick Gallagher, Ilan T. Rosen, Eli Fox, Lili Jiang, Bosai Lyu, Hongyuan Li, Kenji Watanabe, Takashi Taniguchi, Jeil Jung, Zhiwen Shi, David Goldhaber-Gordon, Yuanbo Zhang, and Feng Wang. *arXiv:1901.04621*, 2019.

[222] Aaron L. Sharpe, Eli J. Fox, Arthur W. Barnard, Joe Finney, Kenji Watanabe, Takashi Taniguchi, M. A. Kastner, and David Goldhaber-Gordon. *arXiv:1901.03520*, 2019.

[223] Philip Kim. Ferromagnetic superconductivity in twisted double bilayer graphene. `http://online.kitp.ucsb.edu/online/bands_m19/kim/`, 2019. Talks at KITP, Jan 15, 2019.

[224] Xiaobo Lu, Petr Stepanov, Wei Yang, Ming Xie, Mohammed Ali Aamir, Ipsita Das, Carles Urgell, Kenji Watanabe, Takashi Taniguchi, Guangyu Zhang, Adrian Bachtold, Allan H. MacDonald, and Dmitri K. Efetov. *arXiv:1903.06513*, 2019.

[225] Nick Bultinck, Shubhayu Chatterjee, and Michael P. Zaletel. *arXiv:1901.08110*, 2019.

[226] Guorui Chen, Aaron L. Sharpe, Eli J. Fox, Ya-Hui Zhang, Shaoxin Wang, Lili Jiang, Bosai Lyu, Hongyuan Li, Kenji Watanabe, Takashi Taniguchi, Zhiwen Shi, T. Senthil, David Goldhaber-Gordon, Yuanbo Zhang, and Feng Wang. *arXiv:1905.06535*, 2019.

[227] M. Serlin, C. L. Tschirhart, H. Polshyn, Y. Zhang, J. Zhu, K. Watanabe, T. Taniguchi, and L. Balents abd A. F. Young. *arXiv:1907.00261*, 2019.

[228] Pablo Jarillo-Herrero. Magic Angle Graphene Transport Phenomenology. `http://online.kitp.ucsb.edu/online/bands_m19/jarilloherrero/`, 2019.

[229] Yuan Cao, Daniel Rodan-Legrain, Jeong Min Park, Noah FQ Yuan, Kenji Watanabe, Takashi Taniguchi, Rafael M Fernandes, Liang Fu, and Pablo Jarillo-Herrero. Nematicity and competing orders in superconducting magic-angle graphene. *science*, 372(6539):264–271, 2021.

[230] Jong Yeon Lee, Eslam Khalaf, Shang Liu, Xiaomeng Liu, Zeyu Hao, Philip Kim, and Ashvin Vishwanath. *arXiv:1903.08130*, 2019.

[231] J. F. Dodaro, S. A. Kivelson, Y. Schattner, X. Q. Sun, and C. Wang. Phases of a phenomenological model of twisted bilayer graphene. *Phys. Rev. B*, 98:075154, Aug 2018.

[232] Hoi Chun Po, Liujun Zou, Ashvin Vishwanath, and T. Senthil. Origin of mott insulating behavior and superconductivity in twisted bilayer graphene. *Phys. Rev. X*, 8:031089, Sep 2018.

[233] Liujun Zou, Hoi Chun Po, Ashvin Vishwanath, and T. Senthil. Band structure of twisted bilayer graphene: Emergent symmetries, commensurate approximants, and wannier obstructions. *Phys. Rev. B*, 98:085435, Aug 2018.

[234] Ya-Hui Zhang and T. Senthil. Bridging hubbard model physics and quantum hall physics in trilayer graphene/$h-$BN moiré superlattice. *Phys. Rev. B*, 99:205150, May 2019.

[235] Vadim Oganesyan, Steven A. Kivelson, and Eduardo Fradkin. Quantum theory of a nematic fermi fluid. *Phys. Rev. B*, 64:195109, Oct 2001.

[236] Eduardo Fradkin, Steven A. Kivelson, Michael J. Lawler, James P. Eisenstein, and Andrew P. Mackenzie. Nematic fermi fluids in condensed matter physics. *Annual Review of Condensed Matter Physics*, 1(1):153–178, 2010.

[237] F. Y. Wu. The potts model. *Rev. Mod. Phys.*, 54:235–268, Jan 1982.

[238] F. Fucito and G. Parisi. *J. Phys. A: Math. Gen.*, 14:L507, 1981.

[239] Zi-Xiang Li, Yi-Fan Jiang, Shao-Kai Jian, and Hong Yao. Fermion-induced quantum critical points. *Nature communications*, 8(1):314, 2017.

[240] Zhen Bi, Ethan Lake, and T. Senthil. Landau ordering phase transitions beyond the landau paradigm. *Phys. Rev. Res.*, 2:023031, Apr 2020.

[241] Fengcheng Wu, Euyheon Hwang, and Sankar Das Sarma. Phonon-induced giant linear-in-t resistivity in magic angle twisted bilayer graphene: Ordinary strangeness and exotic superconductivity. *Phys. Rev. B*, 99:165112, Apr 2019.

[242] Yonglong Xie, Biao Lian, Berthold Jäck, Xiaomeng Liu, Cheng-Li Chiu, Kenji Watanabe, Takashi Taniguchi, B. Andrei Bernevig, and Ali Yazdani. *Nature*, 572:101, 2019.

[243] Zhen Bi, Noah F. Q. Yuan, and Liang Fu. Designing flat bands by strain. *Phys. Rev. B*, 100:035448, Jul 2019.

[244] Yoni Schattner, Samuel Lederer, Steven A. Kivelson, and Erez Berg. Ising nematic quantum critical point in a metal: A monte carlo study. *Phys. Rev. X*, 6:031028, Aug 2016.

[245] Samuel Lederer, Yoni Schattner, Erez Berg, and Steven A. Kivelson. Superconductivity and non-fermi liquid behavior near a nematic quantum critical point. *Proceedings of the National Academy of Sciences*, 114(19):4905–4910, 2017.

[246] Xiao Yan Xu, Zi Hong Liu, Gaopei Pan, Yang Qi, Kai Sun, and Zi Yang Meng. *arXiv:1904.07355*, 2019.

[247] Andrey V. Chubukov, Catherine Pépin, and Jerome Rech. Instability of the quantum-critical point of itinerant ferromagnets. *Phys. Rev. Lett.*, 92:147003, Apr 2004.

[248] Yuan Cao, Valla Fatemi, Ahmet Demir, Shiang Fang, Spencer L Tomarken, Jason Y Luo, Javier D Sanchez-Yamagishi, Kenji Watanabe, Takashi Taniguchi, Efthimios Kaxiras, et al. Correlated insulator behaviour at half-filling in magic-angle graphene superlattices. *Nature*, 556(7699):80–84, 2018.

[249] Yuan Cao, Valla Fatemi, Shiang Fang, Kenji Watanabe, Takashi Taniguchi, Efthimios Kaxiras, and Pablo Jarillo-Herrero. Unconventional superconductivity in magic-angle graphene superlattices. *Nature*, 556(7699):43–50, 2018.

[250] Zhong Wang, Xiao-Liang Qi, and Shou-Cheng Zhang. *Phys. Rev. Lett.*, 105:256803, 2010.

[251] Matthew Yankowitz, Shaowen Chen, Hryhoriy Polshyn, Yuxuan Zhang, K Watanabe, T Taniguchi, David Graf, Andrea F Young, and Cory R Dean. Tuning superconductivity in twisted bilayer graphene. *Science*, 363(6431):1059–1064, 2019.

[252] Yu Saito, Jingyuan Ge, Kenji Watanabe, Takashi Taniguchi, and Andrea F Young. Independent superconductors and correlated insulators in twisted bilayer graphene. *Nature Physics*, 16(9):926–930, 2020.

[253] Zhong Wang, Xiao-Liang Qi, and Shou-Cheng Zhang. *Phys. Rev. B*, 85:165126, 2012.

[254] Xiaomeng Liu, Zeyu Hao, Eslam Khalaf, Jong Yeon Lee, Yuval Ronen, Hyobin Yoo, Danial Haei Najafabadi, Kenji Watanabe, Takashi Taniguchi, Ashvin Vishwanath, et al. Tunable spin-polarized correlated states in twisted double bilayer graphene. *Nature*, 583(7815):221–225, 2020.

[255] Yuan Cao, Daniel Rodan-Legrain, Oriol Rubies-Bigorda, Jeong Min Park, Kenji Watanabe, Takashi Taniguchi, and Pablo Jarillo-Herrero. Tunable correlated states and spin-polarized phases in twisted bilayer–bilayer graphene. *Nature*, 583(7815):215–220, 2020.

[256] Yuan Cao, Debanjan Chowdhury, Daniel Rodan-Legrain, Oriol Rubies-Bigorda, Kenji Watanabe, Takashi Taniguchi, T. Senthil, and Pablo Jarillo-Herrero. Strange metal in magic-angle graphene with near planckian dissipation. *Phys. Rev. Lett.*, 124:076801, Feb 2020.

[257] Rafi Bistritzer and Allan H MacDonald. Moiré bands in twisted double-layer graphene. *Proceedings of the National Academy of Sciences*, 108(30):12233–12237, 2011.

[258] J. M. B. Lopes dos Santos, N. M. R. Peres, and A. H. Castro Neto. Continuum model of the twisted graphene bilayer. *Phys. Rev. B*, 86:155449, Oct 2012.

[259] Cenke Xu and Leon Balents. Topological superconductivity in twisted multilayer graphene. *Phys. Rev. Lett.*, 121:087001, Aug 2018.

[260] Noah F. Q. Yuan and Liang Fu. Model for the metal-insulator transition in graphene superlattices and beyond. *Phys. Rev. B*, 98:045103, Jul 2018.

[261] Hiroki Isobe, Noah F. Q. Yuan, and Liang Fu. Unconventional superconductivity and density waves in twisted bilayer graphene. *Phys. Rev. X*, 8:041041, Dec 2018.

[262] Mikito Koshino, Noah F. Q. Yuan, Takashi Koretsune, Masayuki Ochi, Kazuhiko Kuroki, and Liang Fu. Maximally localized wannier orbitals and the extended hubbard model for twisted bilayer graphene. *Phys. Rev. X*, 8:031087, Sep 2018.

[263] Alex Thomson, Shubhayu Chatterjee, Subir Sachdev, and Mathias S. Scheurer. Triangular antiferromagnetism on the honeycomb lattice of twisted bilayer graphene. *Phys. Rev. B*, 98:075109, Aug 2018.

[264] J. F. Dodaro, S. A. Kivelson, Y. Schattner, X. Q. Sun, and C. Wang. Phases of a phenomenological model of twisted bilayer graphene. *Phys. Rev. B*, 98:075154, Aug 2018.

[265] Hoi Chun Po, Liujun Zou, Ashvin Vishwanath, and T. Senthil. Origin of mott insulating behavior and superconductivity in twisted bilayer graphene. *Phys. Rev. X*, 8:031089, Sep 2018.

[266] Jian Kang and Oskar Vafek. Symmetry, maximally localized wannier states, and a low-energy model for twisted bilayer graphene narrow bands. *Phys. Rev. X*, 8:031088, Sep 2018.

[267] Ya-Hui Zhang and T. Senthil. *arXiv:1809.05110*, 2018.

[268] Yi-Zhuang You and Ashvin Vishwanath. Superconductivity from valley fluctuations and approximate so (4) symmetry in a weak coupling theory of twisted bilayer graphene. *npj Quantum Materials*, 4(1):16, 2019.

[269] Nick Bultinck, Shubhayu Chatterjee, and Michael P. Zaletel. Mechanism for anomalous hall ferromagnetism in twisted bilayer graphene. *Phys. Rev. Lett.*, 124:166601, Apr 2020.

[270] Fengcheng Wu and Sankar Das Sarma. *arXiv:1906.07302*, 2019.

[271] Biao Lian, Zhijun Wang, and B. Andrei Bernevig. Twisted bilayer graphene: A phonon-driven superconductor. *Phys. Rev. Lett.*, 122:257002, Jun 2019.

[272] Jong Yeon Lee, Eslam Khalaf, Shang Liu, Xiaomeng Liu, Zeyu Hao, Philip Kim, and Ashvin Vishwanath. Theory of correlated insulating behaviour and spin-triplet superconductivity in twisted double bilayer graphene. *Nature communications*, 10(1):5333, 2019.

[273] Eslam Khalaf, Shubhayu Chatterjee, Nick Bultinck, Michael P Zaletel, and Ashvin Vishwanath. Charged skyrmions and topological origin of superconductivity in magic-angle graphene. *Science advances*, 7(19):eabf5299, 2021.

[274] Yichen Xu, Xiao-Chuan Wu, Chao-Ming Jian, and Cenke Xu. Orbital order and possible non-fermi liquid in moiré systems. *Phys. Rev. B*, 101:205426, May 2020.

[275] Rafael M Fernandes and Jörn WF Venderbos. Nematicity with a twist: Rotational symmetry breaking in a moiré superlattice. *Science Advances*, 6(32):eaba8834, 2020.

[276] Bheema Lingam Chittari, Guorui Chen, Yuanbo Zhang, Feng Wang, and Jeil Jung. Gate-tunable topological flat bands in trilayer graphene boron-nitride moiré superlattices. *Phys. Rev. Lett.*, 122:016401, Jan 2019.

[277] M Serlin, CL Tschirhart, H Polshyn, Y Zhang, J Zhu, K Watanabe, T Taniguchi, L Balents, and AF Young. Intrinsic quantized anomalous hall effect in a moiré heterostructure. *Science*, 367(6480):900–903, 2020.

[278] Ya-Hui Zhang, Dan Mao, Yuan Cao, Pablo Jarillo-Herrero, and T. Senthil. Nearly flat chern bands in moiré superlattices. *Phys. Rev. B*, 99:075127, Feb 2019.

[279] Guorui Chen, Aaron L Sharpe, Eli J Fox, Ya-Hui Zhang, Shaoxin Wang, Lili Jiang, Bosai Lyu, Hongyuan Li, Kenji Watanabe, Takashi Taniguchi, et al. Tunable correlated chern insulator and ferromagnetism in a moiré superlattice. *Nature*, 579(7797):56–61, 2020.

[280] Cécile Repellin and T Senthil. Chern bands of twisted bilayer graphene: Fractional chern insulators and spin phase transition. *Physical Review Research*, 2(2):023238, 2020.

[281] Petr Stepanov, Ming Xie, Takashi Taniguchi, Kenji Watanabe, Xiaobo Lu, Allan H MacDonald, B Andrei Bernevig, and Dmitri K Efetov. Competing zero-field chern insulators in superconducting twisted bilayer graphene. *Physical review letters*, 127(19):197701, 2021.

[282] Shaowen Chen, Minhao He, Ya-Hui Zhang, Valerie Hsieh, Zaiyao Fei, Kenji Watanabe, Takashi Taniguchi, David H Cobden, Xiaodong Xu, Cory R Dean, et al. Electrically tunable correlated and topological states in twisted monolayer–bilayer graphene. *Nature Physics*, 17(3):374–380, 2021.

[283] Andrew T Pierce, Yonglong Xie, Jeong Min Park, Eslam Khalaf, Seung Hwan Lee, Yuan Cao, Daniel E Parker, Patrick R Forrester, Shaowen Chen, Kenji Watanabe, et al. Unconventional sequence of correlated chern insulators in magic-angle twisted bilayer graphene. *Nature Physics*, 17(11):1210–1215, 2021.

[284] Xiao-Chuan Wu, Yichen Xu, Chao-Ming Jian, and Cenke Xu. Interacting valley chern insulator and its topological imprint on moiré superconductors. *Phys. Rev. B*, 100:155138, Oct 2019.

[285] Xiao-Chuan Wu, Yichen Xu, Chao-Ming Jian, and Cenke Xu. Interacting valley chern insulator and its topological imprint on moiré superconductors. *Phys. Rev. B*, 100:155138, Oct 2019.

[286] Fengcheng Wu, Timothy Lovorn, Emanuel Tutuc, and A. H. MacDonald. Hubbard model physics in transition metal dichalcogenide moiré bands. *Phys. Rev. Lett.*, 121:026402, Jul 2018.

[287] Haining Pan, Fengcheng Wu, and Sankar Das Sarma. Band topology, hubbard model, heisenberg model, and dzyaloshinskii-moriya interaction in twisted bilayer wse_2. *Phys. Rev. Research*, 2:033087, Jul 2020.

[288] Yanhao Tang, Lizhong Li, Tingxin Li, Yang Xu, Song Liu, Katayun Barmak, Kenji Watanabe, Takashi Taniguchi, Allan H MacDonald, Jie Shan, and Kin Fai Mak. Wse2/ws2 moiré superlattices: a new hubbard model simulator. *1910.08673*, 2019.

[289] Aaron Szasz, Johannes Motruk, Michael P. Zaletel, and Joel E. Moore. Chiral spin liquid phase of the triangular lattice hubbard model: A density matrix renormalization group study. *Phys. Rev. X*, 10:021042, May 2020.

[290] Aaron Szasz and Johannes Motruk. Phase diagram of the anisotropic triangular lattice hubbard model. *Physical Review B*, 103(23), Jun 2021.

[291] Emma C. Regan, Danqing Wang, Chenhao Jin, M. Iqbal Bakti Utama, Beini Gao, Xin Wei, Sihan Zhao, Wenyu Zhao, Zuocheng Zhang, Kentaro Yumigeta, and et al. Mott and generalized wigner crystal states in wse2/ws2 moiré superlattices. *Nature*, 579(7799):359–363, Mar 2020.

[292] Chenhao Jin, Zui Tao, Tingxin Li, Yang Xu, Yanhao Tang, Jiacheng Zhu, Song Liu, Kenji Watanabe, Takashi Taniguchi, James C. Hone, and et al. Stripe phases in wse2/ws2 moiré superlattices. *Nature Materials*, 20(7):940–944, Mar 2021.

[293] Yang Xu, Song Liu, Daniel A. Rhodes, Kenji Watanabe, Takashi Taniguchi, James Hone, Veit Elser, Kin Fai Mak, and Jie Shan. Correlated insulating states at fractional fillings of moiré superlattices. *Nature*, 587(7833):214–218, Nov 2020.

[294] Xiong Huang, Tianmeng Wang, Shengnan Miao, Chong Wang, Zhipeng Li, Zhen Lian, Takashi Taniguchi, Kenji Watanabe, Satoshi Okamoto, Di Xiao, and et al. Correlated insulating states at fractional fillings of the ws2/wse2 moir¨¦ lattice. *Nature Physics*, 17(6):715–719, Feb 2021.

[295] Sung-Sik Lee and Patrick A. Lee. U(1) gauge theory of the hubbard model: Spin liquid states and possible application to $\kappa-\mathrm{BEDTTTF_2Cu_2CN_3}$. *Phys. Rev. Lett.*, 95:036403, Jul 2005.

[296] T. Senthil. Critical fermi surfaces and non-fermi liquid metals. *Phys. Rev. B*, 78:035103, Jul 2008.

[297] T. Senthil. Theory of a continuous mott transition in two dimensions. *Phys. Rev. B*, 78:045109, Jul 2008.

[298] David F. Mross and T. Senthil. Charge friedel oscillations in a mott insulator. *Phys. Rev. B*, 84:041102, Jul 2011.

[299] Min-Chul Cha, Matthew P. A. Fisher, S. M. Girvin, Mats Wallin, and A. Peter Young. Universal conductivity of two-dimensional films at the superconductor-insulator transition. *Phys. Rev. B*, 44:6883–6902, Oct 1991.

[300] B. Spivak, S. V. Kravchenko, S. A. Kivelson, and X. P. A. Gao. Colloquium: Transport in strongly correlated two dimensional electron fluids. *Rev. Mod. Phys.*, 82:1743–1766, May 2010.

[301] L. B. Ioffe and A. I. Larkin. Gapless fermions and gauge fields in dielectrics. *Phys. Rev. B*, 39:8988–8999, May 1989.

[302] Matthew P. A. Fisher, G. Grinstein, and S. M. Girvin. Presence of quantum diffusion in two dimensions: Universal resistance at the superconductor-insulator transition. *Phys. Rev. Lett.*, 64:587–590, Jan 1990.

[303] Rosario Fazio and Dario Zappalà. ϵ expansion of the conductivity at the superconductor-mott-insulator transition. *Phys. Rev. B*, 53:R8883–R8886, Apr 1996.

[304] Jurij **S**makov and Erik Sørensen. Universal scaling of the conductivity at the superfluid-insulator phase transition. *Phys. Rev. Lett.*, 95:180603, Oct 2005.

[305] William Witczak-Krempa, Erik S. Sorensen, and Subir Sachdev. *Nature Physics*, 10:361, 2014.

[306] Kun Chen, Longxiang Liu, Youjin Deng, Lode Pollet, and Nikolay Prokof'ev. Universal conductivity in a two-dimensional superfluid-to-insulator quantum critical system. *Phys. Rev. Lett.*, 112:030402, Jan 2014.

[307] Shai M. Chester, Walter Landry, Junyu Liu, David Poland, David Simmons-Duffin, Ning Su, and Alessandro Vichi. Carving out ope space and precise o(2) model critical exponents. *Journal of High Energy Physics*, 2020(6):142, Jun 2020.

[308] D. B. Haviland, Y. Liu, and A. M. Goldman. Onset of superconductivity in the two-dimensional limit. *Phys. Rev. Lett.*, 62:2180–2183, May 1989.

[309] Y. Liu, K. A. McGreer, B. Nease, D. B. Haviland, G. Martinez, J. W. Halley, and A. M. Goldman. Scaling of the insulator-to-superconductor transition in ultrathin amorphous bi films. *Phys. Rev. Lett.*, 67:2068–2071, Oct 1991.

[310] S. J. Lee and J. B. Ketterson. Critical sheet resistance for the suppression of superconductivity in thin mo-c films. *Phys. Rev. Lett.*, 64:3078–3081, Jun 1990.

[311] William Witczak-Krempa, Pouyan Ghaemi, T. Senthil, and Yong Baek Kim. Universal transport near a quantum critical mott transition in two dimensions. *Phys. Rev. B*, 86:245102, Dec 2012.

[312] V. J. Emery and S. A. Kivelson. Superconductivity in bad metals. *Phys. Rev. Lett.*, 74:3253–3256, Apr 1995.

[313] N. E. Hussey, K. Takenaka, and H. Takagi. Universality of the mott-ioffe-regel limit in metals. *Philosophical Magazine*, 84(27):2847–2864, 2004.

[314] Michael E Peskin. Mandelstam-'t hooft duality in abelian lattice models. *Annals of Physics*, 113(1):122 – 152, 1978.

[315] C. Dasgupta and B. I. Halperin. *Phys. Rev. Lett.*, 47:1556, 1981.

[316] Matthew P. A. Fisher and D. H. Lee. *Phys. Rev. B*, 39:2758, 1989.

[317] Leon Balents, Lorenz Bartosch, Anton Burkov, Subir Sachdev, and Krishnendu Sengupta. Competing orders and non-landau-ginzburg-wilson criticality in (bose) mott transitions. *Progress of Theoretical Physics Supplement*, 160:314–336, 2005.

[318] R. Moessner and S. L. Sondhi. Ising models of quantum frustration. *Phys. Rev. B*, 63:224401, May 2001.

[319] Cenke Xu and Subir Sachdev. Global phase diagrams of frustrated quantum antiferromagnets in two dimensions: Doubled chern-simons theory. *Phys. Rev. B*, 79:064405, Feb 2009.

[320] Kevin Slagle and Cenke Xu. Quantum phase transition between the Z_2 spin liquid and valence bond crystals on a triangular lattice. *Phys. Rev. B*, 89:104418, Mar 2014.

[321] Cenke Xu and Leon Balents. Quantum phase transitions around the staggered valence-bond solid. *Phys. Rev. B*, 84:014402, Jul 2011.

[322] Cong-Jun Wu, Ian Mondragon-Shem, and Xiang-Fa Zhou. Unconventional bose—einstein condensations from spin-orbit coupling. *Chinese Physics Letters*, 28(9):097102, 2011.

[323] Chunji Wang, Chao Gao, Chao-Ming Jian, and Hui Zhai. Spin-orbit coupled spinor bose-einstein condensates. *Phys. Rev. Lett.*, 105:160403, Oct 2010.

[324] Xiao-Tian Zhang and Gang Chen. Infinity scatter infinity: Infinite critical boson non-fermi liquid. *arXiv preprint arXiv:2102.09272*, 2021.

[325] Ethan Lake, T. Senthil, and Ashvin Vishwanath. Bose-luttinger liquids. *Phys. Rev. B*, 104:014517, Jul 2021.

[326] Seth Musser, T. Senthil, and Debanjan Chowdhury. Theory of a continuous bandwidth-tuned wigner-mott transition, 2021.

[327] Joseph Polchinski. Low-energy dynamics of the spinon-gauge system. *Nuclear Physics B*, 422(3):617 – 633, 1994.

[328] Chetan Nayak and Frank Wilczek. Non-fermi liquid fixed point in $2 + 1$ dimensions. *Nuclear Physics B*, 417(3):359 – 373, 1994.

[329] Chetan Nayak and Frank Wilczek. Renormalization group approach to low temperature properties of a non-fermi liquid metal. *Nuclear Physics B*, 430(3):534 – 562, 1994.

[330] Sung-Sik Lee. Low-energy effective theory of fermi surface coupled with u(1) gauge field in $2 + 1$ dimensions. *Phys. Rev. B*, 80:165102, Oct 2009.

[331] David F. Mross, John McGreevy, Hong Liu, and T. Senthil. Controlled expansion for certain non-fermi-liquid metals. *Phys. Rev. B*, 82:045121, Jul 2010.

[332] Max A. Metlitski and Subir Sachdev. Quantum phase transitions of metals in two spatial dimensions. i. ising-nematic order. *Phys. Rev. B*, 82:075127, Aug 2010.

[333] Max A. Metlitski and Subir Sachdev. Quantum phase transitions of metals in two spatial dimensions. ii. spin density wave order. *Phys. Rev. B*, 82:075128, Aug 2010.

[334] Max A. Metlitski, David F. Mross, Subir Sachdev, and T. Senthil. Cooper pairing in non-fermi liquids. *Phys. Rev. B*, 91:115111, Mar 2015.

[335] Yuxuan Wang and Andrey V. Chubukov. Enhancement of superconductivity at the onset of charge-density-wave order in a metal. *Phys. Rev. B*, 92:125108, Sep 2015.

[336] Ipsita Mandal. Superconducting instability in non-fermi liquids. *Phys. Rev. B*, 94:115138, Sep 2016.

[337] S. Lederer, Y. Schattner, E. Berg, and S. A. Kivelson. Enhancement of superconductivity near a nematic quantum critical point. *Phys. Rev. Lett.*, 114:097001, Mar 2015.

[338] Yuxuan Wang, Artem Abanov, Boris L. Altshuler, Emil A. Yuzbashyan, and Andrey V. Chubukov. Superconductivity near a quantum-critical point: The special role of the first matsubara frequency. *Phys. Rev. Lett.*, 117:157001, Oct 2016.

[339] Samuel Lederer, Yoni Schattner, Erez Berg, and Steven A. Kivelson. Superconductivity and non-fermi liquid behavior near a nematic quantum critical point. *Proceedings of the National Academy of Sciences*, 114(19):4905–4910, 2017.

[340] Liujun Zou and Debanjan Chowdhury. Deconfined metallic quantum criticality: A $u(2)$ gauge-theoretic approach. *Phys. Rev. Research*, 2:023344, Jun 2020.

[341] Ipsita Mandal. Critical fermi surfaces in generic dimensions arising from transverse gauge field interactions. *Phys. Rev. Res.*, 2:043277, Nov 2020.

[342] Sergei V. Isakov, Arun Paramekanti, and Yong Baek Kim. Exotic phase diagram of a cluster charging model of bosons on the kagome lattice. *Phys. Rev. B*, 76:224431, Dec 2007.

[343] Yan-Cheng Wang, Meng Cheng, William Witczak-Krempa, and Zi Yang Meng. Fractionalized conductivity and emergent self-duality near topological phase transitions. *Nature Communications*, 12(1), Sep 2021.

[344] V. Kalmeyer and R. B. Laughlin. Equivalence of the resonating-valence-bond and fractional quantum hall states. *Phys. Rev. Lett.*, 59:2095–2098, Nov 1987.

[345] Vadim Kalmeyer and R. B. Laughlin. Theory of the spin liquid state of the heisenberg antiferromagnet. *Phys. Rev. B*, 39:11879–11899, Jun 1989.

[346] Meng Cheng, Michael Zaletel, Maissam Barkeshli, Ashvin Vishwanath, and Parsa Bonderson. Translational symmetry and microscopic constraints on symmetry-enriched topological phases: A view from the surface. *Phys. Rev. X*, 6:041068, Dec 2016.

[347] S. M. Kravec and John McGreevy. Gauge theory generalization of the fermion doubling theorem. *Physical Review Letters*, 111(16), Oct 2013.

[348] S. V. Isakov, R. G. Melko, and M. B. Hastings. Universal signatures of fractionalized quantum critical points. *Science*, 335(6065):193–195, Jan 2012.

[349] Silviu S. Pufu and Subir Sachdev. Monopoles in 2 + 1-dimensional conformal field theories with global u(1) symmetry. *Journal of High Energy Physics*, 2013(9):127, Sep 2013.

[350] Ethan Dyer, Márk Mezei, Silviu S. Pufu, and Subir Sachdev. Scaling dimensions of monopole operators in the cpnb-1 theory in 2+1 dimensions. *Journal of High Energy Physics*, 2015(6):37, June 2015.

[351] Markus König, Steffen Wiedmann, Christoph Brüne, Andreas Roth, Hartmut Buhmann, Laurens W. Molenkamp, Xiao-Liang Qi, and Shou-Cheng Zhang. Quantum spin hall insulator state in hgte quantum wells. *Science*, 318(5851):766–770, Nov 2007.

[352] Patrick A. Lee and Naoto Nagaosa. Gauge theory of the normal state of high-t_c superconductors. *Phys. Rev. B*, 46:5621–5639, Sep 1992.

[353] Cody P. Nave and Patrick A. Lee. Transport properties of a spinon fermi surface coupled to a u(1) gauge field. *Phys. Rev. B*, 76:235124, Dec 2007.

[354] Gang Chen, Hae-Young Kee, and Yong Baek Kim. Fractionalized charge excitations in a spin liquid on partially filled pyrochlore lattices. *Phys. Rev. Lett.*, 113:197202, Nov 2014.

[355] Pavel Kovtun. Lectures on hydrodynamic fluctuations in relativistic theories. *Journal of Physics A: Mathematical and Theoretical*, 45(47):473001, nov 2012.

[356] Luca V. Delacretaz. Heavy operators and hydrodynamic tails. *SciPost Phys.*, 9:034, 2020.

[357] Yoni Schattner, Samuel Lederer, Steven A. Kivelson, and Erez Berg. Ising nematic quantum critical point in a metal: A monte carlo study. *Phys. Rev. X*, 6:031028, Aug 2016.

[358] Xiao Yan Xu, Kai Sun, Yoni Schattner, Erez Berg, and Zi Yang Meng. Non-fermi liquid at (2 + 1)D ferromagnetic quantum critical point. *Phys. Rev. X*, 7:031058, Sep 2017.

[359] Hong-Chen Jiang and Thomas P Devereaux. Superconductivity in the doped hubbard model and its interplay with next-nearest hopping t. *Science*, 365(6460):1424–1428, 2019.

[360] Aaron Szasz, Johannes Motruk, Michael P. Zaletel, and Joel E. Moore. Chiral spin liquid phase of the triangular lattice hubbard model: A density matrix renormalization group study. *Phys. Rev. X*, 10:021042, May 2020.

[361] Parsa Bonderson, Chetan Nayak, and Xiao-Liang Qi. A time-reversal invariant topological phase at the surface of a 3d topological insulator. *Journal of Statistical Mechanics: Theory and Experiment*, 2013(09):P09016, 2013.

[362] Chong Wang, Andrew C. Potter, and T. Senthil. Gapped symmetry preserving surface state for the electron topological insulator. *Phys. Rev. B*, 88:115137, Sep 2013.

[363] Lukasz Fidkowski, Xie Chen, and Ashvin Vishwanath. Non-abelian topological order on the surface of a 3d topological superconductor from an exactly solved model. *Phys. Rev. X*, 3:041016, Nov 2013.

[364] Max A. Metlitski, C. L. Kane, and Matthew P. A. Fisher. Symmetry-respecting topologically ordered surface phase of three-dimensional electron topological insulators. *Phys. Rev. B*, 92:125111, Sep 2015.

[365] Lukasz Fidkowski and Alexei Kitaev. *Phys. Rev. B*, 81:134509, 2010.

[366] Lukasz Fidkowski and Alexei Kitaev. *Phys. Rev. B*, 83:075103, 2011.

[367] Xiao-Liang Qi. *New J. Phys.*, 15:065002, 2013.

[368] Hong Yao and Shinsei Ryu. *Phys. Rev. B*, 88:064507, 2013.

[369] Shinsei Ryu and Shou-Cheng Zhang. *Phys. Rev. B*, 85:245132, 2012.

[370] Chong Wang and T. Senthil. *Phys. Rev. B*, 89:195124, 2014.

[371] Yi-Zhuang You and Cenke Xu. Symmetry-protected topological states of interacting fermions and bosons. *Phys. Rev. B*, 90:245120, Dec 2014.

[372] Hiroki Isobe and Liang Fu. Theory of interacting topological crystalline insulators. *Phys. Rev. B*, 92:081304, Aug 2015.

[373] Hao Song, Sheng-Jie Huang, Liang Fu, and Michael Hermele. Topological phases protected by point group symmetry. *Phys. Rev. X*, 7:011020, Feb 2017.

[374] Takahiro Morimoto, Akira Furusaki, and Christopher Mudry. Breakdown of the topological classification $\mathbb{Z}$ for gapped phases of noninteracting fermions by quartic interactions. *Phys. Rev. B*, 92:125104, Sep 2015.

[375] Evelyn Tang and Xiao-Gang Wen. Interacting one-dimensional fermionic symmetry-protected topological phases. *Phys. Rev. Lett.*, 109:096403, Aug 2012.

[376] David J. Gross and André Neveu. Dynamical symmetry breaking in asymptotically free field theories. *Phys. Rev. D*, 10:3235–3253, Nov 1974.

[377] Kevin Slagle, Yi-Zhuang You, and Cenke Xu. Exotic quantum phase transitions of strongly interacting topological insulators. *Phys. Rev. B*, 91:115121, Mar 2015.

[378] Yuan-Yao He, Han-Qing Wu, Yi-Zhuang You, Cenke Xu, Zi Yang Meng, and Zhong-Yi Lu. Quantum critical point of dirac fermion mass generation without spontaneous symmetry breaking. *Phys. Rev. B*, 94:241111, Dec 2016.

[379] Yi-Zhuang You, Yin-Chen He, Cenke Xu, and Ashvin Vishwanath. Symmetric fermion mass generation as deconfined quantum criticality. *Phys. Rev. X*, 8:011026, Feb 2018.

[380] Yi-Zhuang You, Yin-Chen He, Ashvin Vishwanath, and Cenke Xu. From bosonic topological transition to symmetric fermion mass generation. *Phys. Rev. B*, 97:125112, Mar 2018.

[381] Venkitesh Ayyar and Shailesh Chandrasekharan. Origin of fermion masses without spontaneous symmetry breaking. *Phys. Rev. D*, 93:081701, Apr 2016.

[382] Simon Catterall. Fermion mass without symmetry breaking. *Journal of High Energy Physics*, 2016(1), Jan 2016.

[383] Venkitesh Ayyar and Shailesh Chandrasekharan. Fermion masses through four-fermion condensates. *Journal of High Energy Physics*, 2016(10), Oct 2016.

[384] Venkitesh Ayyar and Shailesh Chandrasekharan. Massive fermions without fermion bilinear condensates. *Phys. Rev. D*, 91:065035, Mar 2015.

[385] Yoni BenTov. Fermion masses without symmetry breaking in two spacetime dimensions. *Journal of High Energy Physics*, 2015(7), Jul 2015.

[386] Takuya Kanazawa. Chiral symmetry breaking with no bilinear condensate revisited. *Journal of High Energy Physics*, 2015(10), Oct 2015.

[387] Simon Catterall. Chiral lattice theories from staggered fermions, 2020.

[388] Simon Catterall, Goksu Can Toga, and Nouman Butt. Symmetric mass generation for kähler-dirac fermions, 2021.

[389] Xiao-Gang Wen. Classifying gauge anomalies through symmetry-protected trivial orders and classifying gravitational anomalies through topological orders. *Physical Review D*, 88(4), Aug 2013.

[390] Xiao-Gang Wen. A lattice non-perturbative definition of an so (10) chiral gauge theory and its induced standard model. *Chinese Physics Letters*, 30(11):111101, Nov 2013.

[391] Juven Wang and Xiao-Gang Wen. Non-perturbative regularization of 1+1d anomaly-free chiral fermions and bosons: On the equivalence of anomaly matching conditions and boundary gapping rules, 2019.

[392] Yi-Zhuang You, Yoni BenTov, and Cenke Xu. Interacting topological superconductors and possible origin of $16n$ chiral fermions in the standard model, 2014.

[393] Yi-Zhuang You and Cenke Xu. Interacting topological insulator and emergent grand unified theory. *Physical Review B*, 91(12), Mar 2015.

[394] Juven Wang and Xiao-Gang Wen. Solution to the 1+1 dimensional gauged chiral fermion problem. *Physical Review D*, 99(11), Jun 2019.

[395] Juven Wang and Xiao-Gang Wen. Nonperturbative definition of the standard models. *Physical Review Research*, 2(2), Jun 2020.

[396] Shlomo S. Razamat and David Tong. Gapped chiral fermions, 2021.

[397] V. Gurarie. Single-particle green's functions and interacting topological insulators. *Phys. Rev. B*, 83:085426, Feb 2011.

[398] Andrew M. Essin and Victor Gurarie. Bulk-boundary correspondence of topological insulators from their respective green's functions. *Phys. Rev. B*, 84:125132, Sep 2011.

[399] Robert-Jan Slager, Louk Rademaker, Jan Zaanen, and Leon Balents. Impurity-bound states and greens function zeros as local signatures of topology. *Physical Review B*, 92(8), Aug 2015.

[400] Yi-Zhuang You, Zhong Wang, Jeremy Oon, and Cenke Xu. Topological number and fermion green's function for strongly interacting topological superconductors. *Phys. Rev. B*, 90:060502, Aug 2014.

[401] Xie Chen, Yuan-Ming Lu, and Ashvin Vishwanath. *Nature Communications*, 5:3507, 2014.

[402] G E Volovik and V M Yakovenko. Fractional charge, spin and statistics of solitons in superfluid3he film. *Journal of Physics: Condensed Matter*, 1(31):5263–5274, aug 1989.

[403] G. E. Volovik. *The Universe in a Helium Droplet*. Clarendon Press, 2003.

[404] Zhong Wang, Xiao-Liang Qi, and Shou-Cheng Zhang. Topological order parameters for interacting topological insulators. *Phys. Rev. Lett.*, 105:256803, Dec 2010.

[405] Zhong Wang and Shou-Cheng Zhang. Strongly correlated topological superconductors and topological phase transitions via green's function. *Phys. Rev. B*, 86:165116, Oct 2012.

[406] Zhong Wang and Shou-Cheng Zhang. Simplified topological invariants for interacting insulators. *Phys. Rev. X*, 2:031008, Aug 2012.

[407] Zhen Bi and T. Senthil. Adventure in topological phase transitions in 3+1-d: Non-abelian deconfined quantum criticalities and a possible duality. *Physical Review X*, 9(2), May 2019.

[408] Chao-Ming Jian and Cenke Xu. Generic unnecessary quantum critical points with minimal degrees of freedom. *Physical Review B*, 101(3), Jan 2020.

[409] J. T. Chalker and P. D. Coddington. *J. Phys. C*, 21:2665, 1988.

[410] C.-M. Ho and J. T. Chalker. Models for the integer quantum hall effect: The network model, the dirac equation, and a tight-binding hamiltonian. *Phys. Rev. B*, 54:8708–8713, Sep 1996.

[411] Lokman Tsui, Hong-Chen Jiang, Yuan-Ming Lu, and Dung-Hai Lee. Quantum phase transitions between a class of symmetry protected topological states. *Nuclear Physics B*, 896:330C359, Jul 2015.

[412] Ribhu K. Kaul and Subir Sachdev. Quantum criticality of u(1) gauge theories with fermionic and bosonic matter in two spatial dimensions. *Phys. Rev. B*, 77:155105, Apr 2008.